Additives for High Performance Applications

Scrivener Publishing
100 Cummings Center, Suite 541J
Beverly, MA 01915-6106

Publishers at Scrivener
Martin Scrivener(martin@scrivenerpublishing.com)
Phillip Carmical (pcarmical@scrivenerpublishing.com)

Additives for High Performance Applications

Chemistry and Applications

Johannes Karl Fink

WILEY

Co-published by John Wiley & Sons, Inc. Hoboken, New Jersey, and Scrivener Publishing LLC, Beverly, Massachusetts.
Published simultaneously in Canada.

Cover design by Russell Richardson

Library of Congress Cataloging-in-Publication Data:

ISBN 978-1-119-36361-3

Printed in the United States of America

10 9 8 7 6 5 4 3 2 1

Contents

Preface

This book focuses on the chemistry of additives for high performance uses in analytical applications, electrical applications, medical applications, and others, as well as special exemplified uses of these additives.

The text focuses on the literature of the past decade. Beyond education, this book may serve the needs of engineers and specialists who have only a passing knowledge of these issues, but need to know more.

How to Use This Book

Utmost care has been taken to present reliable data. Because of the vast variety of material presented here, however, the text cannot be complete in all aspects, and it is recommended that the reader study the original literature for more complete information.

The reader should be aware that mostly US patents have been cited where available, but not the corresponding equivalent patents of other countries.

For this reason, the author cannot assume responsibility for the completeness, validity or consequences of the use of the material presented here. Every attempt has been made to identify trademarks; however, there were some that the author was unable to locate.

Index

There are four indices: an index of tradenames, an index of acronyms, an index of chemicals, and a general index. In the index of chemicals, compounds that occur extensively, e.g., *acetone*, are not included at every occurrence, but rather when they appear in an important context. When a compound is found in a figure, the entry is marked in boldface letters in the chemical index.

Acknowledgements

I am indebted to our university librarians, Dr. Christian Hasenhüttl, Dr. Johann Delanoy, Franz Jurek, Margit Keshmiri, Dolores Knabl, Friedrich Scheer, Christian Slamenik, Renate Tschabuschnig, and Elisabeth Groß for their support in literature acquisition. In addition, many thanks to the head of my department, Professor Wolfgang Kern, for his interest and permission to prepare this text.

I also want to express my gratitude to all the scientists who have carefully published their results concerning the topics dealt with herein. This book could not have been otherwise compiled.

Last, but not least, I want to thank the publisher, Martin Scrivener, for his abiding interest and help in the preparation of the text. In addition, my thanks go to Jean Markovic, who made the final copyedit with utmost care.

Johannes Fink
Leoben, 6th September 2016

Additives for High Performance Applications: Chemistry and Applications. Johannes Karl Fink.

1

Analysis and Separation Techniques

1.1 High Performance Liquid Chromatography

1.1.1 Ionic Liquids as Mobile Phase Additives

The popularity of ionic liquids has grown in several analytical separation techniques. Thus, the reports concerning the applications of ionic liquids are still increasing. The use of ionic liquids, mainly imidazolium-based, associated with chloride and tetrafluoroborate as mobile phase additives in high performance liquid chromatography (HPLC) has been reviewed (1).

Mostly, ionic liquids just function as salts, but keep several kinds of intermolecular interactions, which are useful for chromatographic separations. Both cation and anion can be adsorbed on the stationary phase, creating a bilayer. This gives rise to hydrophobic, electrostatic and other specific interactions with the stationary phase and solutes, which modify the retention behavior and peak shape (1).

1.1.1.1 Imidazolium Compounds

The beneficial effects of several ionic liquids as mobile phase additives in HPLC using an electrochemical detection for the determination of heterocyclic aromatic amines have been evaluated (2). The tested ionic liquids were 1-butyl-3-methylimidazolium tetrafluoroborate, 1-hexyl-3-methylimidazolium tetrafluoroborate, and

1-methyl-3-octylimidazolium tetrafluoroborate. These compounds are shown in Figure 1.1.

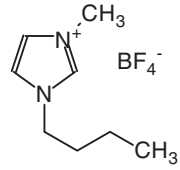

1-Butyl-3-methylimidazolium tetrafluoroborate

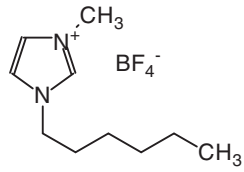

1-Hexyl-3-methylimidazolium tetrafluoroborate

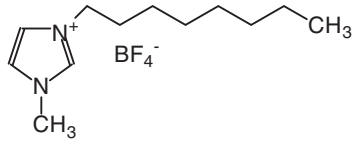

1-Methyl-3-octylimidazolium tetrafluoroborate

Figure 1.1 Ionic liquids.

Several chromatographic parameters have been evaluated in the presence or absence of ionic liquids, or using ammonium acetate as the most common mobile phase additive, with three different C_{18} stationary phases. The effect of the acetonitrile content was also studied. Acetonitrile is shown in Figure 1.2.

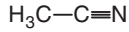

Figure 1.2 Acetonitrile.

Best resolution, lower peak-widths, and lower retention factors were obtained when using ionic liquids rather than ammonium

acetate as mobile phase additives. The best chromatographic conditions were found when using 1-butyl-3-methylimidazolium tetrafluoroborate as the mobile phase additive (2).

1-Butyl-3-methylimidazolium chloride, cf. Figure 1.3, 1-octyl-3-methylimidazolium chloride, and 1-decyl-3-methylimidazolium chloride were used as mobile phase additives in the HPLC to simultaneously separate phenoxy acid herbicides and phenols at neutral pH (3). It was found that when using 1-butyl-3-methylimidazolium chloride, a good baseline separation and good chromatograms for all the acid compounds were obtained on a normal reversed phase C_{18} column.

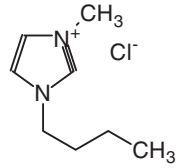

Figure 1.3 1-Butyl-3-methylimidazolium chloride.

The retention time of the target acid compounds was shortened with the increase of the alkyl chain length and the concentrations of ionic liquids, probably due to the delocalization of the positive charge on the imidazolium cation, the repulsion between chlorine ions of ionic liquids and the acid compounds, as well as the stereohindrance effect (3).

Extraction of Sudan Dyes. Sudan dyes are typically used as coloring additives in the manufacturing of wax, textile, and floor and shoe polishes (4, 5). Sudan I has been classified as a category 3 carcinogen by the International Agency for Research on Cancer (IARC). Also, Para Red could be a genotoxic carcinogen (6). The structures of the coloring additives are shown in Figure 1.4. The chemical names of the dyes are summarized in Table 1.1.

A method for the analysis of such dyes has been developed. The method is based on coupling of ionic liquid-based extraction with HPLC. In this way, Sudan dyes and Para Red in chili powder, chili oil, and food additive samples can be found.

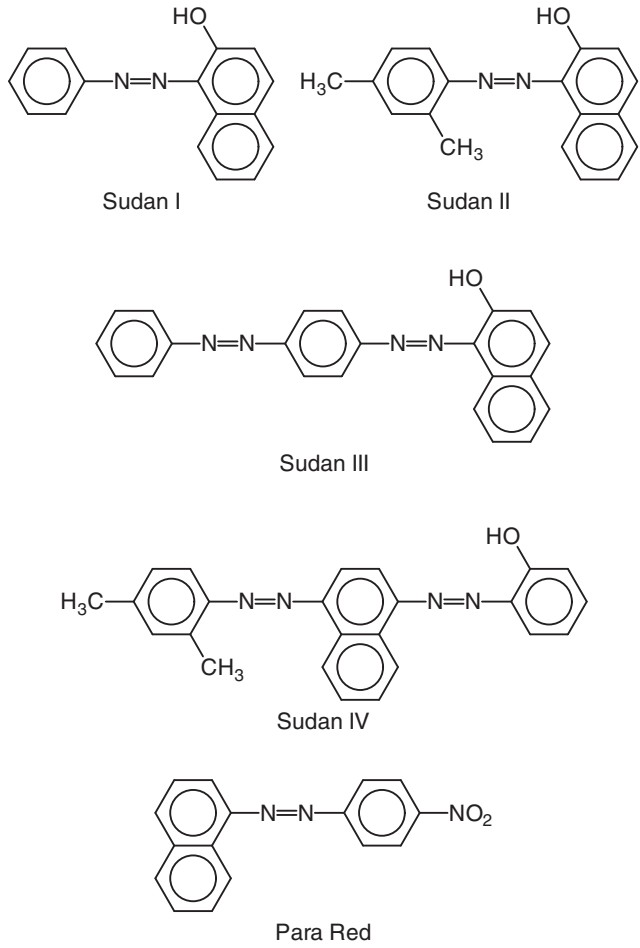

Figure 1.4 Sudans and Para Red.

Table 1.1 Chemical names of the dyes.

Short name	Chemical name
Sudan I	1-[(2,4-Dimethylphenyl)azo]-2-naphthalenol
Sudan II	1-(Phenylazo)-2-naphthol
Sudan III	1-(4-Phenylazophenylazo)-2-naphthol
Sudan IV	*o*-Tolyazo-*o*-tolylazo-*β*-naphthol
Para Red	1-*p*-Nitrobenzeneazo-2-naphthol

Two ionic liquids, i.e., 1-butyl-3-methylimidazolium hexafluorophosphate, cf. Figure 1.5, and 1-octyl-3-methylimidazolium hexafluorophosphate have been compared as extraction solvents. It was found that 1-octyl-3-methylimidazolium hexafluorophosphate showed higher recoveries for each analyte.

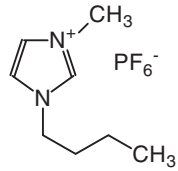

Figure 1.5 1-Butyl-3-methylimidazolium hexafluorophosphate.

Also, the conditions for the extraction of Sudan dyes and Para Red were optimized. Under optimal conditions, a good reproducibility of extraction performance was obtained, with relative standard deviation values of 2.0–3.5% (7).

The ionic liquids were prepared according to a previously reported method (8, 9). The Sudan dyes and Para Red standard solutions were obtained from Zhejiang Entry-Exit Inspection and Quarantine Bureau (Hangzhou, China).

The detection limits and the recoveries are summarized in Table 1.2.

Table 1.2 Detection limits and recoveries for Sudan dyes and Para Red (7).

Material	Detection limit $[\mu g\, kg^{-1}]$	Recovery [%]
Chili powder	7.0– 8.2	76.8–109.5
Chili oil	11.2–13.2	70.7–107.8
Food additives	11.2–13.2	70.7–107.8

Nucleotides Separation. A method for the separation of nucleotides has been developed (10). These nucleotides include 5′-monophosphate adenosine, 5′-monophosphate cytidine, 5′-monophosphate uridine, 5′-monophosphate guanosine, and

5′-monophosphate inosine. Some of these compounds are shown in Figure 1.6.

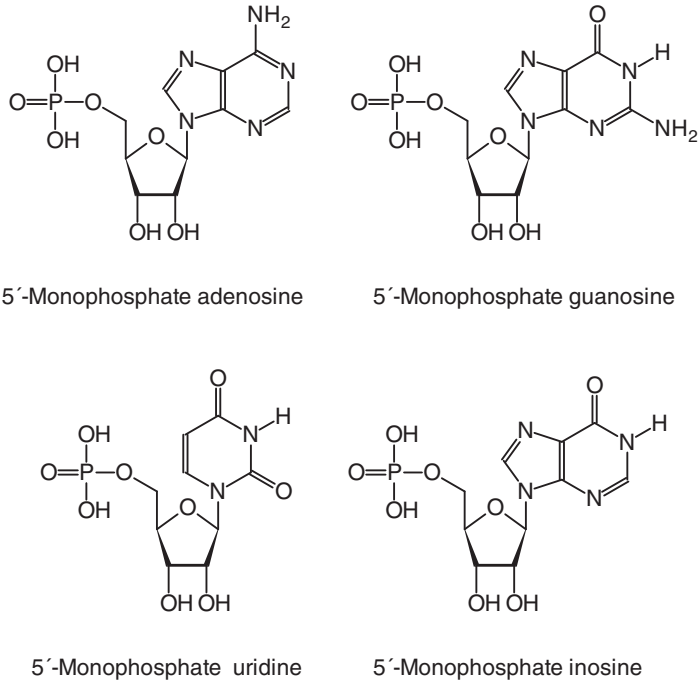

Figure 1.6 Nucleotides.

The essential feature of the method is that 1-alkyl-3-methylimidazolium salts are used as mobile phase additives, resulting in a baseline separation of nucleotides without the need for gradient elution and organic solvent addition, as usually used in reversed phase HPLC (10).

Amine Separation. By varying the lengths and branching of alkyl chains of the anionic core and the cationic precursor, it is possible to design solvents for specific applications. Because of these characteristic properties, ionic liquids are widely used as new solvent media in heterogeneous catalysis, synthesis, electrochemistry, sensors, battery applications, analysis and separation techniques (11).

Some amines, including benzidine, benzylamine, *N*-ethylaniline

and *N,N′*-dimethylaniline could be separated using ionic liquids as additives for the mobile phase in HPLC (12).

The compounds 1-ethyl-3-methylimidazolium tetrafluoroborate ([EMIm][BF4]), 1-butyl-3-methylimidazolium tetrafluoroborate ([BMIm][BF4]), 1-hexyl-3-methylimidazolium tetrafluoroborate ([HMIm][BF4]) and 1-butyl-3-methylimidazolium bromide ([BMIm][Br]) were used as ionic liquids. Some of these compounds are shown in Figure 1.7. Some properties are summarized in Table 1.3.

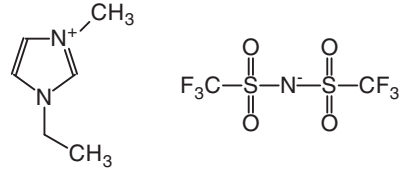

1-Ethyl-3-methylimidazolium tetrafluoroborate

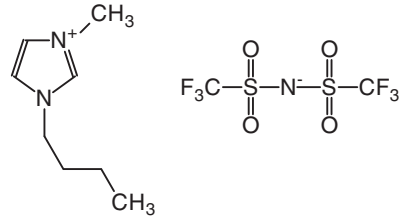

1-Butyl-3-methylimidazolium tetrafluoroborate

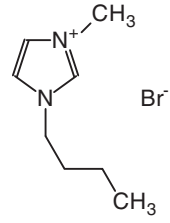

1-Butyl-3-methylimidazolium bromide

Figure 1.7 Ionic liquids.

The effects of the length of alkyl chain or counterions on different

Table 1.3 Properties of certain ionic liquids (8, 12, 13).

Compound	Melting point [°C]	Density [$g\ ml^{-1}$]
1-Ethyl-3-methylimidazolium tetrafluoroborate	6	1.29
1-Butyl-3-methylimidazolium tetrafluoroborate	−81	1.17
1-Hexyl-3-methylimidazolium tetrafluoroborate	−66	1.29
1-Butyl-3-methylimidazolium bromide	−72	1.44

ionic liquids and their concentrations on the separation of these analytes have been assessed (12).

The differences between the ionic liquids and tetrabutyl ammonium bromide on the separation of *o*-phthalic acid, *m*-phthalic acid, and *p*-phthalic acid have been compared. The results indicated that ionic liquids act as ion-pair reagents, although their hydrophobicity and hydrogen bonding also play important roles (12).

Catecholamines. The use of 1-alkyl-3-methylimidazolium salts and *N*-butyl-pyridinium salts as mobile phase additives for the separation of catecholamines in reversed phase HPLC has been reported (14). As catecholamines, norepinephrine, epinephrine and dopamine were investigated. These compounds are shown in Figure 1.8.

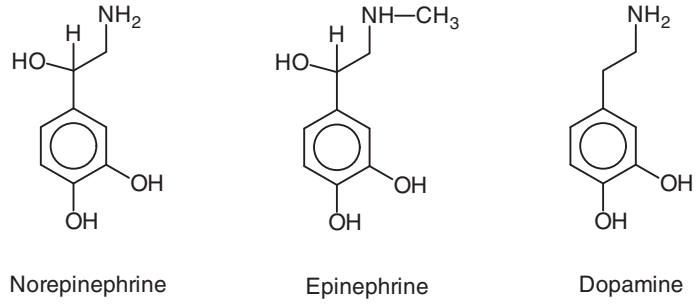

Figure 1.8 Catecholamines.

A good separation could be achieved with these additives. The effects of pH of the mobile phase, the concentration of ionic liquids, and different alkyl substituents on the cations, and different counterions of the ionic liquids were investigated. The separation occurs by molecular interactions between the ionic liquids and the catecholamines (14).

Fluoroquinolone Antibiotics. Ionic liquids differing in the length of the alkyl chain were tested as mobile phase additives for the separation using HPLC of fluoroquinolone antibiotics (15). The materials are listed in Table 1.4. Fluoroquinolone antibiotics are shown in Figure 1.9

Table 1.4 Ionic liquids and antibiotics (15).

Ionic liquids	
1-Ethyl-3-methylimidazolium tetrafluoroborate	
1-Butyl-3-methylimidazolium tetrafluoroborate	
1-Hexyl-3-methylimidazolium tetrafluoroborate	
1-Methyl-3-octylimidazolium tetrafluoroborate	
Tetraethylammonium tetrafluroborate	
Fluoroquinolone antibiotics	
Fleroxacin	Ciprofloxacin
Lomefloxacin	Danofloxacin
Enrofloxacin	Sarafloxacin
Difloxacin	

A conventional reversed phase Nova-Pak C_{18} column and fluorescence detection were used. 1-Butyl-3-methylimidazolium tetrafluoroborate enabled an effective separation of the antibiotics with a relatively low analysis time of 14 *min*. The best separation was achieved by isocratic elution at 1 $mlmin^{-1}$ with 5 $mmol\,l^{-1}$ 1-butyl-3-methylimidazolium tetrafluoroborate and 10 $mmol\,l^{-1}$ ammonium acetate at a pH of 3.0 with 13% by volume acetonitrile (15).

The use of 1-ethyl-3-methylimidazolium tetrafluoroborate as mobile phase additive has been evaluated for the analysis by HPLC with fluorescence detection for seven basic fluoroquinolone antibiotics, i.e., fleroxacin, ciprofloxacin, lomefloxacin, danofloxac-

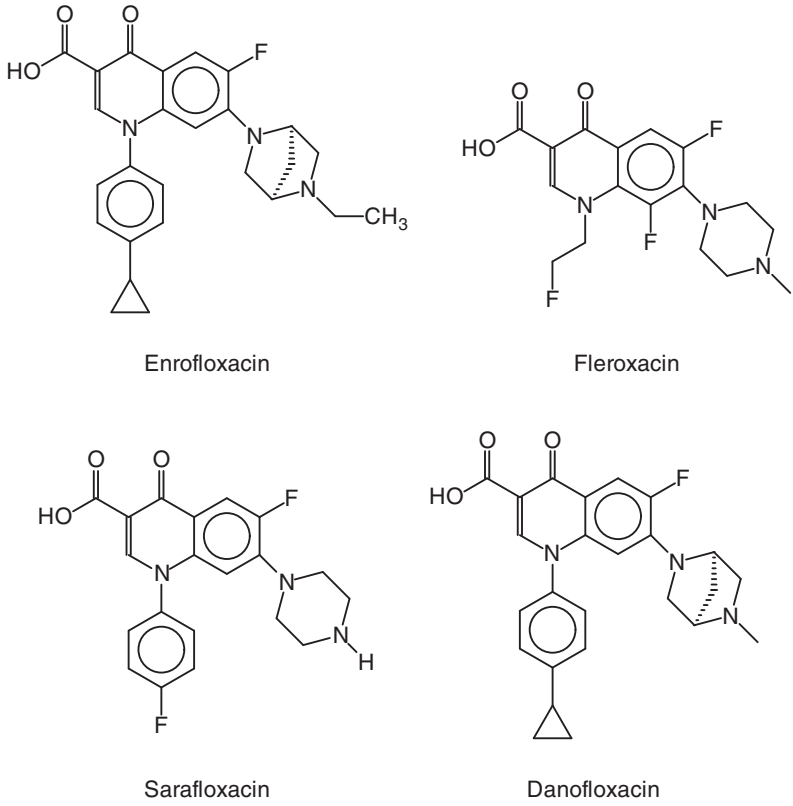

Figure 1.9 Fluoroquinolone antibiotics.

in, enrofloxacin, sarafloxacin and difloxacin, in different milk samples (16).

1-Ethyl-3-methylimidazolium tetrafluoroborate was found to be superior in comparison to 1-butyl-3-methylimidazolium tetrafluoroborate for the separation of the analytes from chromatographic interferences of the sample matrix.

The optimized method was used for the analysis of ovine, caprine and bovine milk, in the last case in either skimmed, semi-skimmed and full-cream milk, after suitable acidic deproteination followed by a solid phase extraction procedure.

Recovery values between 73% and 113% were obtained for the three types of bovine milk samples, as well as for ovine and caprine milk. The limits of detection were in the range of 0.5–8.1 $\mu g l^{-1}$ (16).

Nucleic Compounds. The chromatographic behavior of nucleic compounds, i.e., nucleobases, nucleosides, and nucleotides was investigated using reversed phase HPLC on a C18 column (17). Several different mobile phase additives were used, including 1-butyl-3-methylimidazolium tetrafluoroborate, 1-ethyl-3-methylimidazolium methylsulfate ionic liquids, ammonium formate, and potassium phosphate.

The effect of the alkyl group length, the imidazolium ring, and the counterions of the ionic liquid on the retention and the resolution of the samples were tested. The nature of the modifiers can affect the separation of ionic analytes. The two ionic liquids tested have an improved effect on the retention and resolution of nucleic compounds.

The length of the alkyl on the imidazolium ring and its counterion can also affect the resolution, because part of the ionic liquids coated on the surface of the stationary phase could suppress the free silanols of the surface. The comparison of the ionic liquids with standard mobile phase additives, such as ammonium formate, showed that the ionic liquids have advantages as silanol suppressors in HPLC (17).

1.1.1.2 Fluorescent Whitening Agents

Fluorescent whitening agents based on 4,4′-diaminostilbene-2,2′-disulfonic acid, cf. Figure 1.10, with different numbers of sulfonic acid

groups were separated by using an ionic liquid as a mobile phase additive in high performance liquid chromatography using a fluorescence detection method (18).

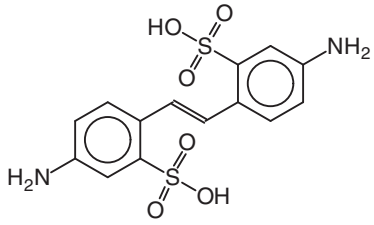

Figure 1.10 4,4′-Diaminostilbene-2,2′-disulfonic acid.

The effects of ionic liquid concentration, the pH of the mobile phase B, and the composition of mobile phase A on the separation of fluorescent whitening agents have been systematically investigated.

It was found that the ionic liquid tetrabutyl ammonium tetrafluoroborate is superior to tetrabutyl ammonium bromide for the separation of the fluorescent whitening agents. The optimal separation conditions were an ionic liquid concentration at 8 *mM* and the pH of mobile phase B at 8.5 with methanol as mobile phase A.

The established method exhibited only low limits of detection (0.04–0.07 $ng\,ml^{-1}$) and wide linearity ranges (0.30–20 $ng\,ml^{-1}$) with high linear correlation coefficients from 0.9994 to 0.9998. The optimized procedure was applied to analyze target analytes in paper samples with satisfactory results.

Eleven target analytes were quantified, and the recoveries of spiked paper samples were in the range of 85–105% with the relative standard deviations from 2.1 to 5.1%. The obtained results indicated that the method is efficient for the analysis of a series of fluorescent whitening agents (18).

1.1.2 Food Additives

1.1.2.1 Analysis of Natural Food Additives

Propyl propane thiosulfonate, cf. Figure 1.11, is an active ingredient from *Allium* spp., like onion and shallot (19). This compound has

been proposed as a natural additive for feed as an efficient alternative to antibiotics and use as growth promoter due to its efficiency of improving animal health.

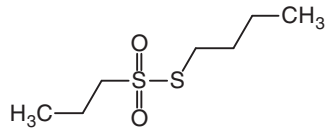

Figure 1.11 Propyl propane thiosulfonate.

A new simple analytical method for monitoring propyl propane thiosulfonate in animal feed has been developed. Reversed phase liquid chromatography with UV detection has been used and a previous sample treatment based on solid-liquid extraction has been optimized in order to extract propyl propane thiosulfonate from a feed for laying hens using acetone as extraction solvent.

The method has been characterized and limits of detection and quantification of 11.2 and 37.3 $mg\,kg^{-1}$ respectively, were obtained, which are lower than the concentrations expected in samples containing this additive (19).

1.1.2.2 Analysis of Synthetic Food Additives

An efficient and accurate analytical method was developed for the simultaneous determination of 20 synthetic food additives using HPLC with a photodiode array detector (20). These additives include sweeteners, food colorants, synthetic preservatives and caffeine.

The method allows the detection of food additives at very low concentrations of 5–150 $ng\,ml^{-1}$. The applicability was verified by the determination of food additives present in various foodstuffs (20).

1.1.2.3 Analysis of Carbohydrates

A method has been developed for the determination of large amounts of carbohydrates (glucose, lactose, maltose, mannose, sucrose, and fructose) and sweeteners (xylitol and sorbitol) by reversed

phase liquid chromatography with refractive index detection without any need of derivatization (21).

The limits of determination for glucose, fructose, and sucrose in liquid samples were 0.1 $g\,l^{-1}$, and for xylite, lactose, maltose, mannose, and sorbite, 1 $g\,l^{-1}$. In solid samples the limits of determination for glucose, fructose, and sucrose were 0.1%, and for xylite, lactose, maltose, mannose, and sorbite, 0.6%.

The method is applicable to the analysis of samples of wine, juice, honey, cookies, dairy products, and biologically active additives (21).

Boric acid. HPLC was used for the analysis of ribose, arabinose and ribulose mixtures obtained from chemical and biochemical isomerization processes (22). These processes have gained importance since the molecules can be used for the synthesis of antiviral therapeutics.

The HPLC method uses boric acid as a mobile phase additive to enhance the separation on an Aminex HPX-87K column.

By complexing with boric acid, the carbohydrates become negatively charged, thus elute faster from the column by means of ion exclusion and are separated because the complexation capacity with boric acid differs from one carbohydrate to another. An excellent separation between ribose, ribulose and arabinose was achieved with concentrations between 0.1 and 10 $g\,l^{-1}$ of discrete sugar (22).

1.1.3 Chaotropicity

1.1.3.1 Imidazolium Salts

The use of 1-butyl-3-methylimidazolium of varying anion chaotropicity as a mobile phase additive for separation and chromatographic behavior studies of acidic, basic, and amphoteric compounds in reversed phase liquid chromatography has been reported (23). Two hydrophobic columns were used: Zorbax XDB-C18 and Zorbax SB-Phenyl. Satisfactory separations could be achieved by the use of carefully optimized chromatographic systems modified with the additive.

Biogenic amines are derived from neutral or basic amino acids via decarboxylation (24). Some prominent examples of biogenic amines

include: serotonin, catecholamine neurotransmitters: epinephrine, norepinephrine and dopamine.

Highly hydrophilic compounds belonging to biogenic amines were analyzed in a reversed phase system, modified with the addition of ionic liquids: 1-Ethyl-3-methylimidazolium hexafluorophosphate and the chaotropic salt $NaPF_6$ on a Discovery HS C18 column under acidic conditions. The effect of the additives concentration and the presence of organic solvent on the analytes' chromatographic parameters, such as retention factor, tailing factor and theoretical plate numbers, were determined (24).

The effect of chaotropic salt additives to the mobile phase on the chromatographic parameters was investigated (25). A buffered acetonitrile-water mobile phase was chosen because of the significant retention of added liophilic ions due to strong dispersive π-π interactions. The addition of a salt, such as hexafluorophosphate, perchlorate or trifluoroacetate, leads to an increase in retention, efficiency and separation selectivity. The influence of added salts on increase in retention parameters increases as follows: H_2PO^{4-}, CF^3COO^-, ClO^{4-}, PF^{6-}. This order is in agreement with ability of salts to the salting-in effect according to the Hofmeister series (25). The Hofmeister series is a classification of ions in order of their ability to salt out or salt in proteins (26, 27).

It was established that the presence of an organic solvent with a low dielectric constant and ionic liquid with both chaotropic ions allows achieving a typical Langmuir shape. The investigated mobile phase additives are comparable according to their efficiency and selectivity towards the analysis of biogenic amines. However, the sensitivity was found to be better for the eluent system that was modified with the chaotropic salt (24).

1.1.3.2 Phenothiazine Derivatives

Ionogenic basic compounds belonging to phenothiazine derivatives, cf. Figure 1.12, were analyzed in a reversed phase HPLC system and were modified by the addition of three ionic liquids: 1-ethyl-3-methylimidazolium hexafluorophosphate, 1-butyl-3-methylimidazolium hexafluorophosphate, and 1-butyl-3-methylimidazolium chloride.

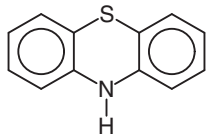

Figure 1.12 Phenothiazine.

Phenothiazines contain positively charged amine groups in a mobile phase at low pH. Therefore, they are retained in the presence of ionic liquids through the combination of electrostatic interactions and hydrophobic effects. The effects of the concentration and the type of ionic liquid on the retention of the analytes, peak symmetry, and efficiency were examined. The following trends increase the retention factor of the analytes and improve system efficiency: 1-butyl-3-methylimidazolium hexafluorophosphate > 1-ethyl-3-methylimidazolium hexafluorophosphate > 1-butyl-3-methylimidazolium chloride.

With its asymmetric cation enlarged with hydrophobic substituents and a chaotropic anion, 1-butyl-3-methylimidazolium hexafluorophosphate appeared to be the most advantageous one. The isotherm of adsorption of this reagent presents a typical Langmuir adsorption behavior.

By the application of high performance liquid chromatography, lipophilicity parameters were established for the investigated compounds. Chromatographic systems modified with these ionic liquids have been compared to buffered organic-aqueous mobile phase and eluent containing a chaotropic salt additive (28).

It could be demonstrated that the ionic liquids are useful as mobile phase additives in reversed phase chromatography of phenothiazine derivatives. A very important feature of these additives is their ability to decrease the peak width. In the absence of such strong ion-ion interaction reagents, wide peaks for cationic analytes are usually observed (28).

1.1.4 Cigarette Additives

Ultrahigh performance liquid chromatography was used for the determination of imidazole, 4-methylimidazole, and 2-methylim-

idazole in cigarette additives (29). These compounds are shown in Figure 1.13. After a solid phase extraction and filtration, the analytes were separated using isocratic elution with 5 $mmol\,l^{-1}$ acetonitrile-ammonium formate at a volume ratio of 80:20 0.5 $ml\,min^{-1}$. The quantification of these analytes was achieved with an external standard method on a diode-array detector at 215 *nm*.

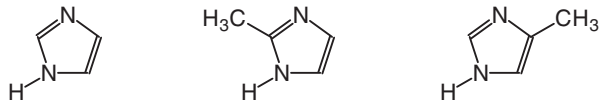

Imidazole 2-Methylimidazole 4-Methylimidazole

Figure 1.13 Imidazole compounds.

The linear dynamic ranges for imidazole, 4-methylimidazole, and 2-methylimidazole were between 0.0375 and 18.0300 $mg\,kg^{-1}$. The limits of detection for the analytes were 0.0094 $mg\,kg^{-1}$. The recoveries and the relative standard deviations at fortification levels of 0.1322–1.6220 $mg\,kg^{-1}$ were 95.20–101.93% and 0.55–2.54%, respectively.

In summary, the method offers an easy operation, rapid analysis, and accurate results, and is suitable for the determination of imidazole, 4-methylimidazole, and 2-methylimidazole in cigarette additives (29).

1.1.4.1 Additives in Insulating Mineral Oils

Often, insulating mineral oils contain additives that improve their inherent characteristics, such as oxidation stability, electrostatic charging tendency, and compatibility with other materials.

Standard test methods are available for the detection of these individual additives (30–32), but none of these test methods are suitable for the simultaneous detection of additives for different purposes (33). The simultaneous determination of antioxidants and passivators that are most frequently added to mineral insulating oils has been reported (33).

The tested compounds included three inhibitors (*N*-phenyl-1-naphthylamine, 2,6-di-*tert*-butylphenol, and 2,6-di-*tert*-but-

yl-*p*-cresol) and two passivators (benzotriazole and another tolutriazole derivative, Irgamet 39). The chemical structure of these additives is shown in Figure 1.14.

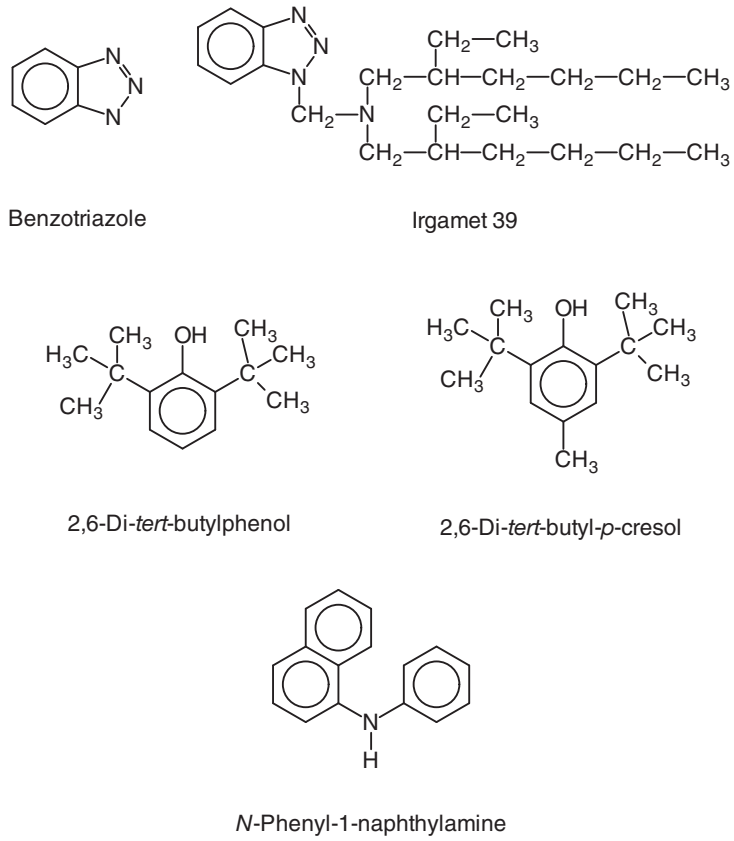

Figure 1.14 Inhibitors and passivators (33).

A solid phase extraction step for the reduction of the matrix oil components was optimized. Because of the hydrophobic characteristics of the additives, a reversed phase chromatographic separation method was used and optimized. The so developed method was used for the analysis of inhibited and passivated transformer oils (33).

1.1.4.2 Microwave-Assisted Extraction of Additives

Traditionally, the extraction of additives in polyolefins is performed as (34):

1. Three 6 *h* refluxing of chlorinated solvents under magnetic stirring.
2. Twelve 16 *h* boiling with chlorinated solvents in a Soxhlet apparatus (35).
3. Dissolution of polymer with either substituted aromatic or hydrogenated naphthalene solvents followed by coagulation with alcohol (36).
4. Extraction in aliphatic solvents using an ultrasonic technique (37).
5. Supercritical fluid extraction (38).
6. Pressurized liquid extraction (39).

It has been shown that microwave-assisted extraction for the systematic analysis of organic additives in polyolefins can be done by two processes (34):

The one-step microwave-assisted extraction is useful for additives with low-medium dipolarity, like stabilizers, flame retardant, antistatics, slip and processing agents. The two-step microwave-assisted extraction is useful for additives with either high dipolarity, like organic salts, antigasfading, antiacid, nucleating agent, or high molecular mass, such as polymeric hindered amine light stabilizers.

A method for the determination and quantification of frequently used stabilizers in polyolefins has been reported (40).

The extraction of the stabilizers from the polymeric matrix was investigated for several different solvents and solvent mixtures in a monomode microwave reaction system. The solvents tested are summarized in Table 1.5.

Among the solvents listed in Table 1.5, ethyl acetate showed the best extraction performance with respect to easy and rapid sample preparation. For this solvent, a systematic and comprehensive survey of time- and temperature-dependence of extraction efficiency was carried out.

Extractions utilizing ethyl acetate for 30 *min* at 130°C showed the best overall performance for all investigated analytes. In addition, the influence of the physical form of the polyolefin sample was

Table 1.5 Solvents tested for extraction of stabilizers (40).

Solvent	Grade
Acetonitrile	HPLC gradient grade
Ethyl acetate	Pesticide residue analysis
Toluene	Analytical reagent grade
Methanol	HPLC gradient grade
Cyclohexane	
i-Propanol	

investigated. The extraction of pellets and powder was compared and, regardless of the physical form, the reproducibility for the whole method developed for all chosen analytes was below 2% (40).

1.1.5 Chiral Separation

1.1.5.1 Atrolactic Acids

A method for the enantioseparation of atrolactic acids has been presented. HPLC is used with sulfobutyl ether-β-cyclodextrin as a chiral mobile phase additive and a C18 reversed phase column (41).

Atrolactic acid is also addressed as 2-hydroxy-2-phenylpropionic acid or α-methylmandelic acid and shown in Figure 1.15. The configuration of atrolactic acid and methods of synthesis and reactions have been described (42).

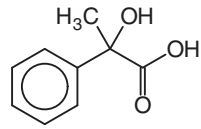

Figure 1.15 Atrolactic acid.

The influences of the different types of cyclodextrin derivatives, the concentration of chiral mobile phase additive, pH value of the mobile phase, the flow rate and column temperature on the peak resolution were investigated.

The retention times of atrolactic acids were 26.65 *min* and 28.28 *min* and a peak resolution of 1.68 could be achieved (41).

1.1.5.2 *Mandelic Acid*

The enantioseparation of ten mandelic acid derivatives was done using reverse phase HPLC with hydroxypropyl-β-cyclodextrin or sulfobutyl ether-β-cyclodextrin as chiral mobile phase additives (43). The mandelic acid derivatives are shown in Figure 1.16.

Cyclodextrins, also called cycloamyloses, are a family of compounds made up of sugar molecules bound together in a ring. So they are cyclic oligosaccharides (44). β-Cyclodextrin is a ring from seven members of amylose and also called cyclohepta amylose.

The inclusion complex formations between the cyclodextrins and the mandelic acid enantiomers were evaluated. The effects of various factors such as the composition of the mobile phase, concentration of cyclodextrins and the column temperature on the retention and the enantioselectivity were studied.

It was found that the peak resolutions and retention time of the enantiomers were strongly affected by pH, the organic modifier and the type of the β-cyclodextrin in the mobile phase. On the other hand, the concentration of the buffer solution and the temperature had a comparatively low effect on the resolution.

The enantioseparations could be successfully achieved on a Shimpack CLC-ODS column. The mobile phase was a mixture of acetonitrile and 0.10 $moll^{-1}$ of phosphate buffer at pH 2.68 containing 20 $mmoll^{-1}$ of hydroxypropyl-β-cyclodextrin or sulfobutyl ether-β-cyclodextrin (43).

1.1.5.3 *Amines*

Ethanesulfonic acid showed a beneficial effect on the chiral HPLC separation of basic compounds (45). Using a single chiral column and a starting mobile phase, more than half of a diverse set of amines was baseline separated. Changing the alcohol content and the alcohol type increased the success rate.

Methanesulfonic acid proved even more successful than ethanesulfonic acid. The mechanism of this effect seems to be a combination of ion-pair salt formation in the mobile phase and an increased binding with the chiral stationary phase arising from a localized decrease in pH (45).

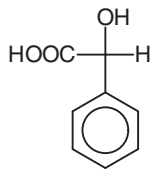

Mandelic acid

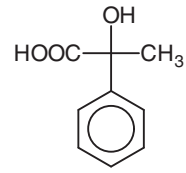

α-Methylmandelic acid

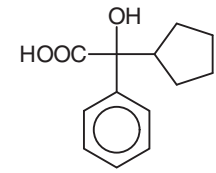

α-Cyclopentylmandelic acid

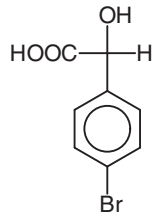

4-Bromomandelic acid

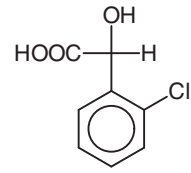

2-Chloromandelic acid

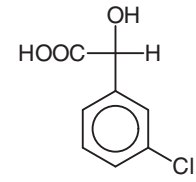

3-Chloromandelic acid

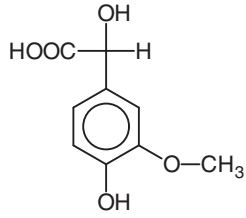

4-Hydroxy-3-methoxymandelic acid

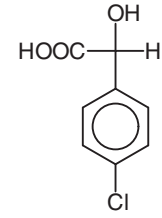

4-Chloromandelic acid

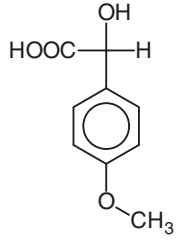

4-Methoxymandelic acid

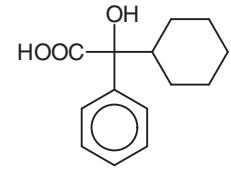

α-Cyclohexylmandelic acid

Figure 1.16 Mandelic acid derivatives.

1.1.5.4 Peptides

Seven macrocyclic antibiotics have been evaluated as chiral selectors for the enantiomeric separation of dansyl amino acids using narrow-bore HPLC (46). The dansyl amino acids are listed in Table 1.6. The antibiotics used were Vancomycin (47), A82846B,

Table 1.6 Dansyl amino acids (46).

Compound	Compound	
Glutamic acid	Leucine	Methionine
Norleucine	Norvaline	Phenylalanine
Serine	Threonine	Valine
α-Amino-*n*-butyric acid		

LY307599, LY333328, A35512B, Teicoplanin, and Actaplanin A (48). Vancomycin is shown in Figure 1.17, and Actaplanin is shown in Figure 1.18.

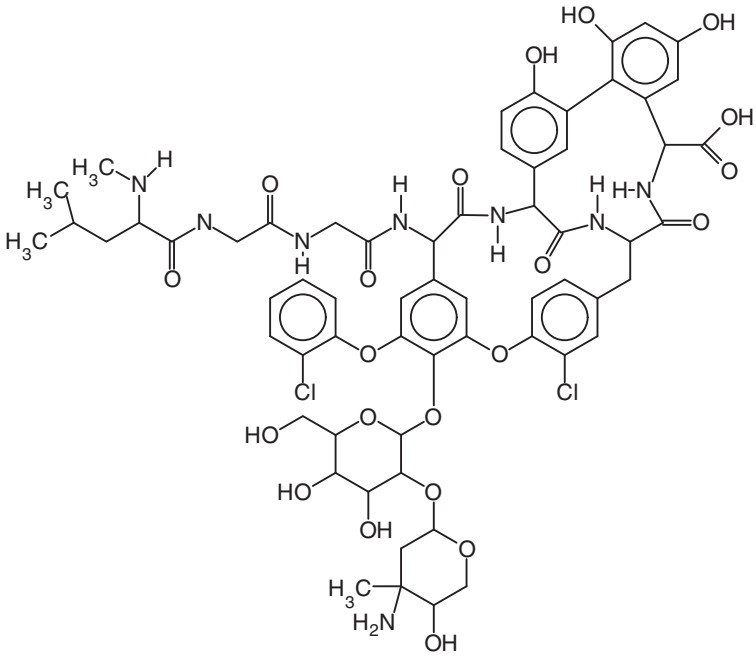

Figure 1.17 Vancomycin.

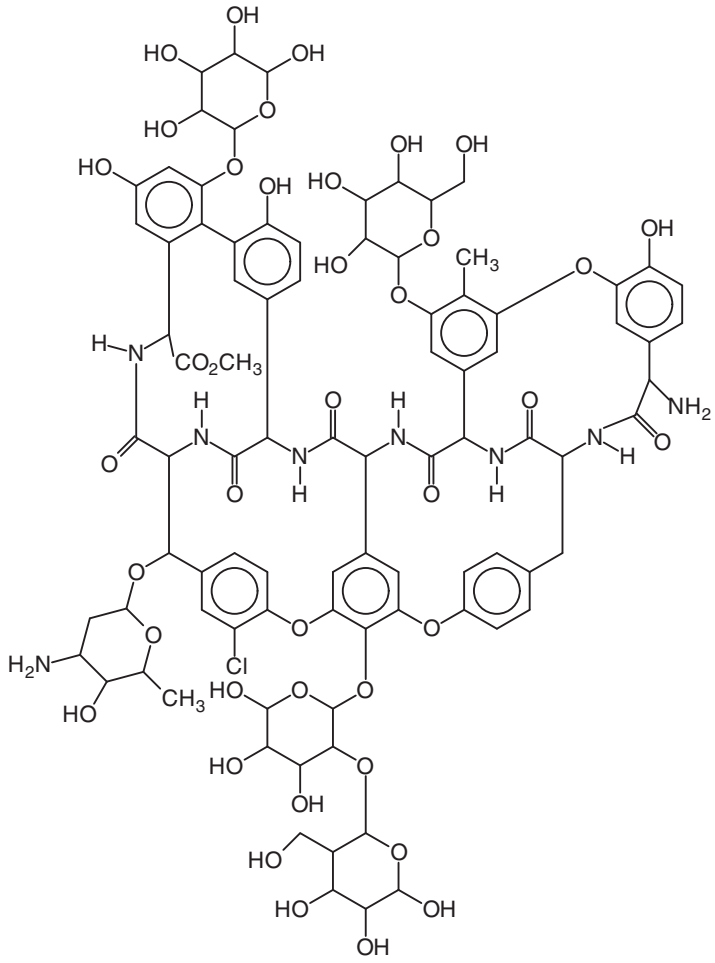

Figure 1.18 Actaplanin.

Vancomycin is a glycopeptide antibiotic used in the therapy of severe bacterial infections (49). The monitoring of vancomycin levels is recommended because of its narrow therapeutic index and toxicity. This measurement is especially appropriate for patients with unstable renal functions, who receive high doses of vancomycin or present serious bacterial infections accompanied by important sequestration of liquids when it could be difficult to achieve the optimal therapeutic dose. Most of the methods for vancomycin determination in routine practice are immunoassays. Chromatog-

raphy-based techniques in combination with UV or mass spectrometry detection provide results with greater accuracy and precision also in complicated biological matrices.

Teicoplanin is an antibiotic agent used in the prevention and the treatment of serious infections caused by gram-positive bacteria. It is a semisynthetic glycopeptide antibiotic with a spectrum of activities similar to vancomycin. Teicoplanin is marketed by Sanofi Aventis Corp. as Targocid®. The oral administration of teicoplanin is effective in the treatment of Pseudomembranous colitis and Clostridium difficile-associated diarrhoea, with a comparable efficacy to vancomycin. The effectiveness of teicoplanin and its structure effect on treatment has been reviewed (50). The effect of teicoplanin is directly related to the length of its carbon chain.

The dansyl amino acids are shown in Figure 1.19. Dansyl amino

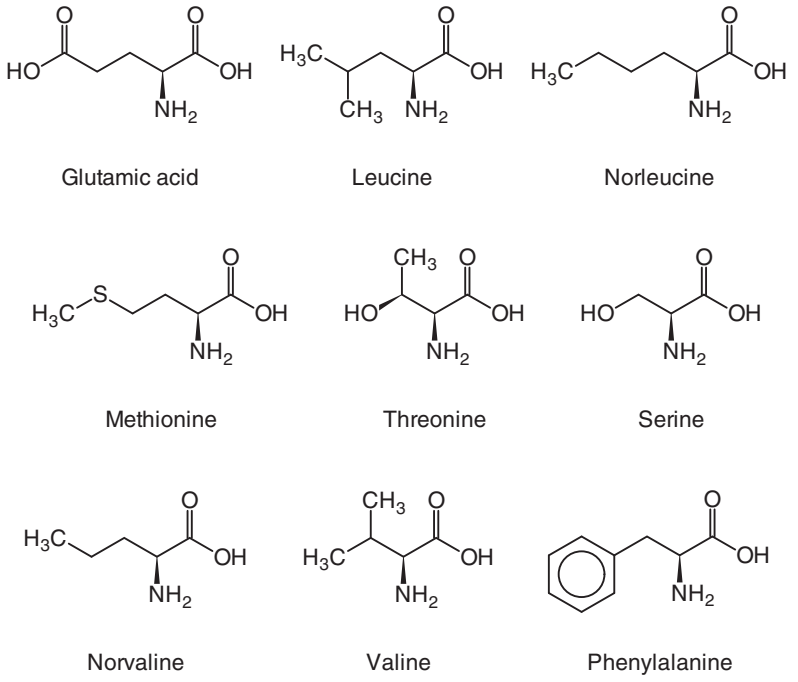

Figure 1.19 Dansyl amino acids.

acids are those primary amino acids that are reacting with dan-

syl chloride, i.e., 5-(dimethylamino)naphthalene-1-sulfonyl chloride, cf. Figure 1.20. This reagent reacts with primary amino groups in both aliphatic and aromatic amines to produce stable blue- or blue-green fluorescent sulfonamide adducts (51).

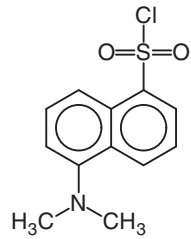

Figure 1.20 5-(Dimethylamino)naphthalene-1-sulfonyl chloride.

The macrocyclic antibiotics were incorporated as mobile phase additives to determine the enantioselective effects on the chiral analytes. The resolution and the capacity factor of each analyte were assessed by a variation of the structure of the macrocyclic antibiotic and the mobile phase buffer pH.

The selectivity of the chiral selectors was measured as a function of changes in these parameters. All of the eleven dansyl amino acids were separated by at least one of the chiral selectors (46).

The separation of the dansyl amino acid enantiomers has been shown to be highly sensitive to the macrocyclic antibiotic structure, analyte structure, and mobile phase buffer pH. Only insignificant variations in the structure can drastically alter the enantioselective capabilities of the macromolecule.

Enantioseparations achieved using compound A82846B as a chiral selector gave the largest selectivities for most analytes at both pH extremes in this study. LY333328, although not as effective as A82846B in resolving capacity for specific analytes, was more universal, separating more analytes overall. The chiral selectors best resolved dansyl amino acids containing straight chain alkyl groups adjacent to the chiral carbon.

The separation of enantiomers using macrocyclic antibiotics as chiral selectors is clearly a complex process affected not only by macromolecular and analyte structure and 3D conformation, but also the pH environment in which the enantioseparations occur (46).

1.1.5.5 Flavonoid Racemates

In order to perform a chiral separation of three flavonoid racemates, including dihydrodaidzein, equol and alpinetin, using HPLC, an effective method was developed by using sulfobutyl ether-β-cyclodextrin as a mobile phase additive (52). These compounds are shown in Figure 1.21.

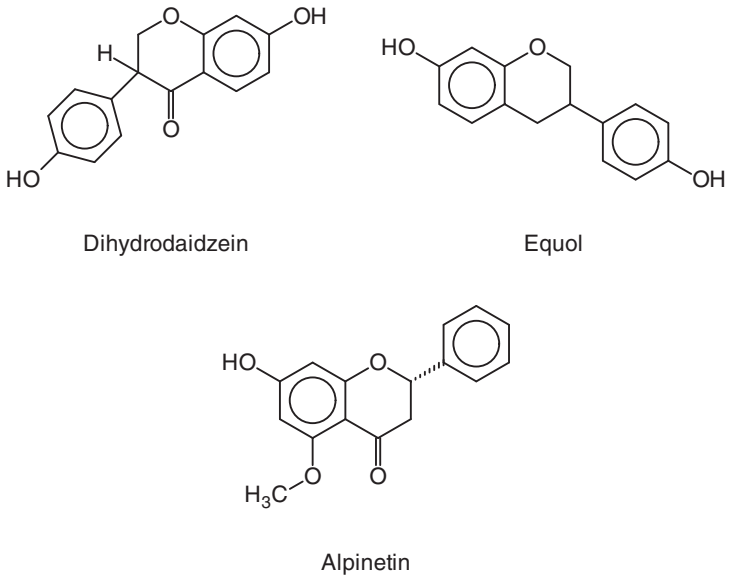

Figure 1.21 Flavonoid racemates.

The effects of different factors on the chiral separation have been investigated. These were the cyclodextrin types, the concentration, pH, the nature of the organic solvents and the phosphate buffer concentration. The mobile phase consisted of acetonitrile and 10 $mmol\,l^{-1}$ of sulfobutyl ether-β-cyclodextrin. The pH of 4.0 was adjusted with phosphoric acid. The investigated method was able to separate the three racemates (52).

Also, the analytical enantioseparation of five β-substituted 2-phenylpropionic acids using HPLC with hydroxypropyl-β-cyclodextrin as chiral mobile phase additive has been reported (53). Hydroxypropyl-β-cyclodextrin is shown in Figure 1.22

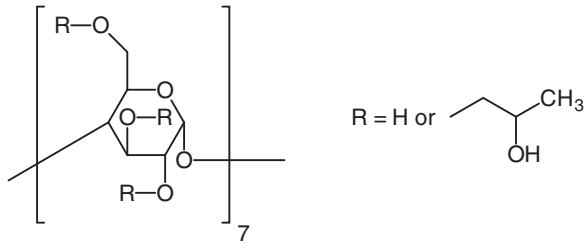

Figure 1.22 Hydroxypropyl-β-cyclodextrin.

The effects of various factors, such as the organic modifier, different ODS C18 columns and the concentration of the hydroxypropyl-β-cyclodextrin, were investigated. The chiral mobile phase was composed of methanol or acetonitrile and 0.5% triethylammonium acetate buffer at pH 3.0 added with 25 $mmol\,l^{-1}$ of hydroxypropyl-β-cyclodextrin. Triethylammonium acetate is a volatile buffering agent. It is prepared from equimolar quantities of triethylamine and acetic acid. Baseline separations could be reached for all racemates.

It was found that there was a negative correlation between the concentration of hydroxypropyl-β-cyclodextrin in the mobile phase and the retention factor at constant pH and constant column temperature (53).

1.1.5.6 Oxybutynin Enantiomers

The separation of oxybutynin enantiomers was achieved using HPLC with hydroxypropyl-β-cyclodextrin as the chiral mobile phase additive and a C18 reversed phase column as the stationary phase (54). Oxybutynin is shown in Figure 1.23.

The experiments showed that oxybutynin enantiomers could not be separated when adding β-cyclodextrin in the mobile phase, but optimal resolution was obtained when using hydroxypropyl-β-cyclodextrin as the chiral mobile phase additive.

An excellent enantioseparation could be achieved with the mobile phase composed of 30 $mmol\,l^{-1}$ KH_2PO_4-acetonitrile 80:20 by volume, mixed with 60 $mmol\,l^{-1}$ hydroxypropyl-β-cyclodextrin at a

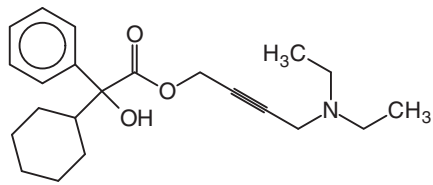

Figure 1.23 Oxybutynin.

pH of 4. Under the optimized conditions, the resolution of enantiomers was 1.54 and the limit of quantification was 1.0 *ng* (54).

1.1.5.7 Amino Alcohols

Amino alcohols, such as β-agonists and β-blockers, are chiral hydroxyl-amine-containing compounds. Most of the amino alcohols are marketed as racemic mixtures. In general, for these β-agonists, only the (R)-enantiomers are potent β-adrenoceptor stimulants with little or no activity attributed to the (S)-enantiomers (55).

For β-blockers, it has been shown that the (S)-enantiomers have been usually more potent than the (R)-enantiomers (56).

Furthermore, it has been reported that some (R)-enantiomers are toxic and present undesirable side effects (57). Therefore, the development of analytical methods for their enantiomeric resolution is advisable.

HPLC is one of the most commonly used analytical methods in chiral separations. The direct chiral separation of amino alcohols by HPLC with the chiral stationary phases has been reported in many articles (58–61).

Three amino alcohols, propranolol, clenbuterol and cycloclenbuterol, could be enantioseparated on an achiral column by reversed phase HPLC (62). These alcohols are shown in Figure 1.24.

A chiral chromatographic system was established, based on C_{18}-bonded silica gel as the support and a self-prepared di-*n*-butyl-*l*-tartrate boric acid complex as the chiral mobile phase additive.

In order to obtain better enantioseparations, the influences of di-*n*-butyl-*l*-tartrate and boric acid concentrations, the type, concentration and pH of the buffer, as well as methanol content were investigated.

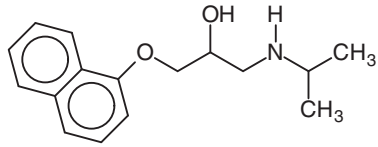

Propranolol

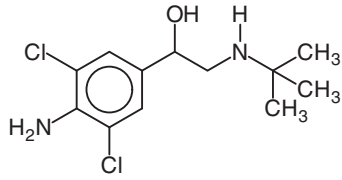

Clenbuterol

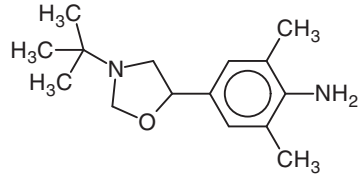

Cycloclenbuterol

Figure 1.24 Amino alcohols.

It was found that the mobile phase composition showed an important role to improve the enantioseparations and all of the enantiomers could be baseline resolved under the optimized experimental conditions. Three pairs of enantiomers, which could not be separated with only di-*n*-butyl-*l*-tartrate, obtained good chiral separations using the complex chiral selector.

The primary driving forces responsible for the chiral recognition were assumed to be the ion-pair interaction between the enantiomers and the chiral selector. The interactions between the ion-pairs above and the stationary phase also played important roles for the chiral separations in reversed phase HPLC (62).

1.1.6 Peptides and Proteins

The effect of mobile phases on the sensitivity in the analysis of peptides and proteins by HPLC coupled with electrospray mass spectrometry has been reviewed (63). The analysis of proteins and peptides using reversed phase chromatography mostly involves the use of trifluoroacetic acid as an ion-pairing agent despite this compound being a strong suppressor of the mass spectroscopic signal.

Various studies dealing with the effects of other ion-pairing agents, such as other perfluorinated acids, acetic acid, or formic acid, and buffers, such as ammonium acetate, ammonium formate, ammonium bicarbonate, and morpholine, in reversed phase chromatography of proteins and peptides did not suggest a single strong candidate that could generally replace trifluoroacetic acid (63–65). Morpholine and trifluoroacetic acid are shown in Figure 1.25.

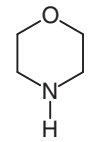

Morpholine

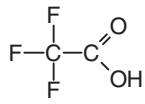

Trifluoroacetic acid

Figure 1.25 Morpholine and trifluoroacetic acid.

1.1.7 1,4-Dihydroxy-2-Naphthoic Acid

1,4-Dihydroxy-2-naphthoic acid is a bifidogenic growth stimulator from *Propionibacterium freudenreichii* (66). According to a previously described method, the peak area of 1,4-dihydroxy-2-naphthoic acid measured by HPLC gradually increases with repeated analyses of the same sample. It has been suspected that the oxidizability of 1,4-dihydroxy-2-naphthoic acid was the reason for this poor precision. Therefore, an attempt was made to develop an improved method using DL-dithiothreitol as a mobile phase additive. 1,4-Dihydroxy-2-naphthoic acid is shown in Figure 1.26.

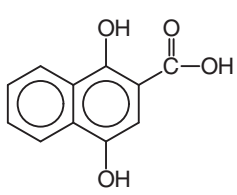

1,4-Dihydroxy-2-naphthoic acid

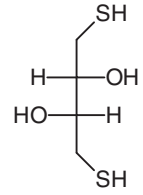

Dithiothreitol

Figure 1.26 1,4-Dihydroxy-2-naphthoic acid and Dithiothreitol.

A 1,4-dihydroxy-2-naphthoic acid standard solution of 5 $\mu g\, ml^{-1}$ was analyzed five times in a row by either the original or the improved method. The relative standard deviation of the peak area was 37.0% and 1.6%, respectively. The linearity of the improved method was confirmed in the range of 0.25–10 $\mu g\, ml^{-1}$. These data indicate that the addition of DL-dithiothreitol to the mobile phase improves the precision of the analysis of 1,4-dihydroxy-2-naphthoic acid by HPLC (66).

1.1.8 Diesel Lubricating Additives

1.1.8.1 Diesel Fuel Additives

New procedures for the analysis of cleaning additives in diesel fuel have been presented (67). Cleaning additives play an important role in the prevention of the formation of deposits in the injection system. There the temperature and pressure conditions can effect the

formation of deposits of contaminants from the fuel. As lubricating additive in diesel fuel, a mixture of oleic and linoleic acids was tested.

Cleaning additives contain straight chain and branched alcohols, solvent naphtha, a mixture of trimethylbenzene isomers and naphthalene. Two procedures were initially compared (67):

1. One-step analysis using gas chromatography (GC) with flame ionization detection or mass spectroscopy (MS), and
2. A two-step procedure in which normal-phase high performance liquid chromatography was used for the preliminary separation of the additives.

The additive fraction was collected using either a simple elution technique or eluent backflush. The final determinations were performed by GC with flame ionization detection and GC with MS.

The studies revealed that it was impossible to determine the investigated analytes by a one-step procedure. In contrast, a two-step procedure ensures reproducible results of analysis with detection limits of 1.4–2.2 *ppm* using HPLC and 9.6–24.0 *ppm* using GC with flame ionization detection (67).

1.1.8.2 Zinc Dialkyl Dithiophosphates

A series of zinc dialkyl dithiophosphates have been synthesized and their mixtures have been separated by normal-phase HPLC on a 5-μm silica column (68). The zinc dithiophosphates are listed in Table 1.7.

Dichloromethane-based or heptane-based eluents containing alkylamine in a concentration of less than 0.4% and acetic acid in a volume ratio of 2:1 and 1% methanol have been found to be suitable for the separation of the mixtures of these metal complexes in commercial lubricating oil additives.

In all the cases tested, the zinc complexes eluted from the column without decomposition and there was no evidence for ligand-exchange reactions having taken place during synthesis or on the column.

Table 1.7 Zinc dithiophosphates (68).

Compound
Ethyl zinc dithiophosphate
n-Propyl zinc dithiophosphate
Isopropyl zinc dithiophosphate
n-Butyl zinc dithiophosphate
i-Butyl zinc dithiophosphate
sec-Butyl zinc dithiophosphate
n-Pentyl zinc dithiophosphate
2-Pentyl zinc dithiophosphate
4-Methyl-2-Pentyl zinc dithiophosphate
i-Octyl zinc dithiophosphate
n-Decyl zinc dithiophosphate

1.1.9 Acidic Drugs

The role of *n*-octanol as mobile phase additive for the lipophilicity assessment of 45 structurally diverse acidic drugs both at neutral (pH 2.5) and ionized form (pH 7.4) was investigated (69). Some of the acidic drugs investigated are shown in Table 1.8 and in Figure 1.27.

The *n*-octanol/water partition coefficient *logP* in Table 1.8 was determined by the shake-flask method, as described in detail (70).

The extrapolated retention factors $logk_w$ were determined on a BDS C18 column using methanol as organic modifier and with different amounts of *n*-octanol as the mobile phase additive. For more polar compounds, the effect of *n*-octanol in retention was found to decrease as their lipophilicity was increasing. In the case of carboxylic acids and oxicams, the differentiation in retention, in presence and absence of *n*-octanol, could be attributed to the attenuation of polar interactions, concerning mainly hydrogen bonding (69).

At a pH of 2.5, the use of a *n*-octanol saturated buffer, without further addition of *n*-octanol in the mobile phase, led to an 1:1 correlation with the logarithm of *n*-octanol/water partition coefficient *logP*. At a physiological pH, an 1:1 correlation was obtained between $logD_{7.4}$ (69).

Table 1.8 Acidic drugs (69).

Compound	*logP*
Acetylsalicylic acid	1.13
2-Amino-3-methoxybenzoic acid	1.60
Benzoic acid	1.87
α-Benzoinoxim	2.59
4-Bromobenzoic acid	2.86
Captopril	1.02
4-Chlorobenzoic acid	2.06
Chlorothiazide	−0.24
Chlorthalidone	1.11
Ciglitazone	5.43
Diclofenac	4.40
Enalapril	0.71
Fenbufen	3.39
Flufenamic acid	5.25
Flurbiprofen	3.81
Gentisic acid	1.12
Hydrochorothiazide	−0.07
Hydroquinone	0.41
m-Hydroxybenzoic acid	1.50
Ibuprofen	3.87
Indomethacin	4.27
Ketoprofen	3.12
Mefenamic acid	5.12
Meloxicam	3.01
Naproxen	3.18
Netoglitazone	4.96
Nimesulide	2.38
Paracetamol	0.51
Pentobarbital	2.07
Phenobarbital	1.44
Phenytoin	2.47
Pioglitazone	3.14
Piroxicam	1.61
Rosiglitazone	2.63
Salicylic acid	2.27
Sulfamerazine	0.12
Sulfamethazine	0.25
Sulfamethoxazole	0.72
Sulfaphenazole	1.27
Tenoxicam	0.81
Theophylline	−0.02
Thiopental	2.85
Tolbutamide	2.34
Tolfenamic acid	5.17
Troglitazone	5.07

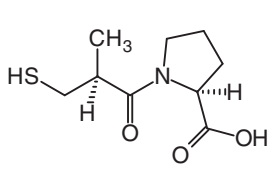

Captopril

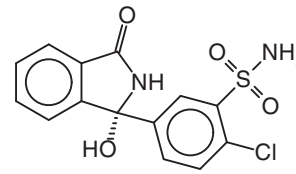

R-Chlorthalidone

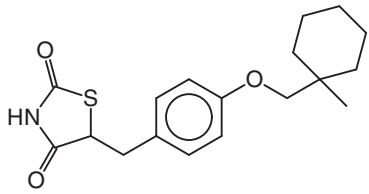

Ciglitazone

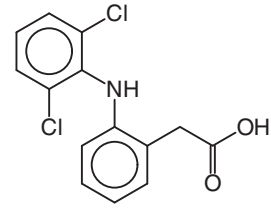

Diclofenac

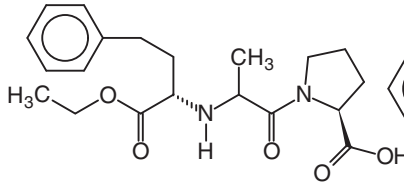

Enalapril

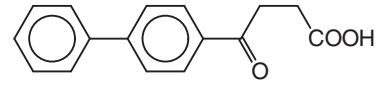

Fenbufen

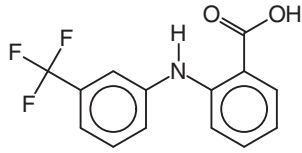

Flufenamic acid

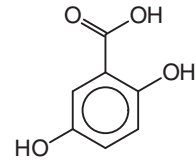

Gentisic acid

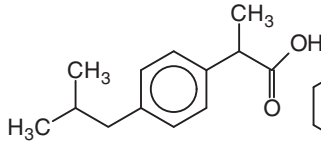

Ibuprofen

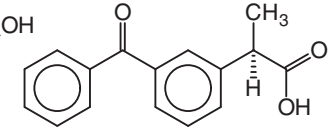

Ketoprofen

Figure 1.27 Acidic drugs.

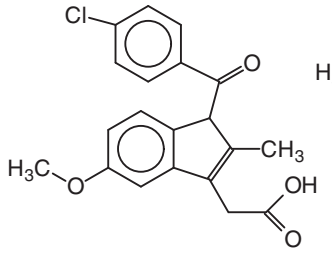

Indomethacin

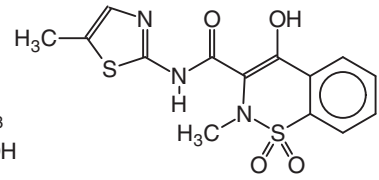

Meloxicam

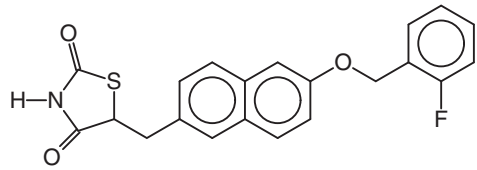

Netoglitazone

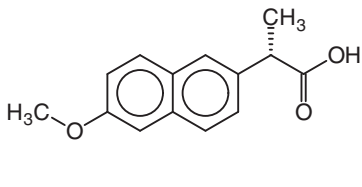

Naproxen

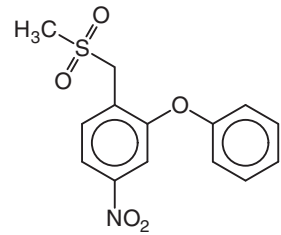

Nimesulide

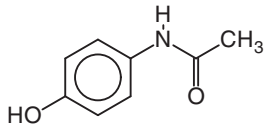

Paracetamol

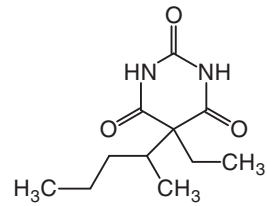

Pentobarbital

Figure 1.27 (cont.) Acidic drugs.

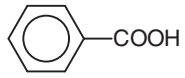

Benzoic acid

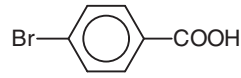

4-Bromobenzoic acid

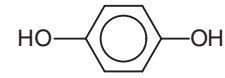

Hydroquinone

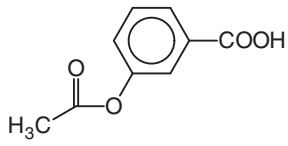

Acetylsalicylic acid

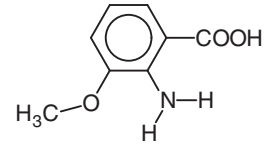

2-Amino-3-methoxybenzoic acid

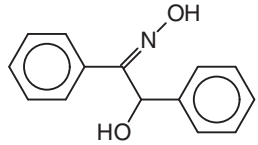

α-Benzoinoxim

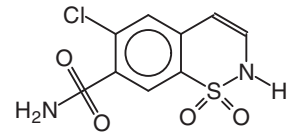

Chlorothiazide

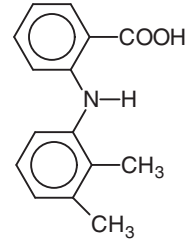

Mefenamic acid

Figure 1.27 (cont.) Acidic drugs.

1.2 Chelation Ion Chromatography

The selectivity characteristics of high performance chelation ion chromatography when separating a range of metal ions with a number of complexing eluents has been investigated (71).

The exploitation of competitive metal complexation between ligands in the eluent and surface bonded chelating groups allows a wide range of control over the retention order and the selectivity coefficients of several groups of metal ions.

Plots of $log\beta_1$ of the metal complexes of a chosen eluent ligand against the surface bonded iminodiacetic acid silica bonded metal complexes were found as useful indicators of which metals may show unusual selectivity changes during the separation process. Iminodiacetic acid is shown in Figure 1.28.

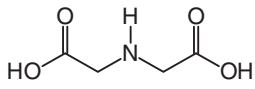

Figure 1.28 Iminodiacetic acid.

Metal separations have been tested for three complexing eluent reagents, i.e., oxalic acid, picolinic acid, and chloride, either singly or in mixtures thereof. It was found that very specific retention control could be achieved for Cu^{2+} with picolinic acid, Fe^{3+} and Fe^{2+} speciation with oxalic acid, Pb^{2+} with dipicolinic acid and Cd^{2+} with chloride (71). These compounds are shown in Figure 1.29.

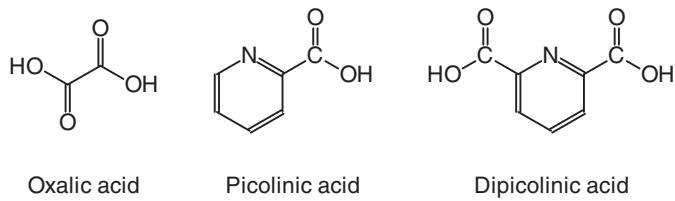

Figure 1.29 Complexing agents.

1.3 Membranes

1.3.1 Carbon Dioxide Separation

1.3.1.1 Diblock Copolymers

A series of poly(ethylene glycol)-block-poly(pentafluoropropyl acrylate) diblock copolymers have been synthesized by reversible addition-fragmentation chain transfer polymerization (72). These block copolymers were blended with up to 60% of the commercially available PEBAX® 2533. The resulting polymer mixtures were successfully spin coated onto crosslinked poly(dimethylsiloxane) gutter layers which in turn had been deposited onto a porous poly-(acrylonitrile) support, to form a thin-film composite membrane.

Gas testing of these membranes for carbon capture applications showed an enhanced CO_2 permeance up to 1830 *GPU*, without a significant drop in CO_2/N_2 selectivity at 35°C and 350 *kPa*, relative to a pure PEBAX upper layer. The impacts of temperature and pressure on membrane performance were investigated for temperatures from 25°C to 55°C and pressures from 100 *kPa* to 500 *kPa*.

Theoretical calculations indicated that in the absence of a gutter layer, the upper layer could achieve a CO_2 permeance of over 3000 *GPU* with a CO_2/N_2 selectivity of 22. These results represent a significant increase in the gas permeance (72).

1.3.1.2 Thin-Film Composite Membranes

Polymeric membranes have been investigated as a method to effectively separate CO_2 from light gases, such as N_2 and CH_4 (73–75).

With increasing improvements in membrane technologies, they offer an attractive alternative to existing solvent technologies for CO_2 separation since they have several advantages, including potentially lower operating costs, environmental friendliness, a smaller footprint and ease of operation.

However, for processes such as postcombustion removal of CO_2 from the flue gases of coal-fired power stations, improvements in membrane performance are required to make them economically viable (76).

A series of well-defined diblock copolymers consisting of poly-(ethylene glycol) (PEG) and poly(dimethyl siloxane) (PDMS) were

synthesized and blended with commercially available PEBAX 2533 to form the active layer of thin-film composite membranes, using a spin-coating technique (76).

Diblock copolymers with a PEG component ranging from 1 to 10 *kDalton* and a PDMS component ranging from 1 to 10 *kDalton* were synthesized by a facile condensation reaction of hydroxyl terminated PEG and carboxylic acid functionalized PDMS. The BCP/PEBAX 2533 blends up to 50% on crosslinked PDMS gutter layers were tested at 35°C and 350 *kPa*.

Thin-film composite membranes containing diblock copolymers of 1 *kDalton* PEG and 1–5 *kDalton* PDMS produced optimal results with CO_2 permittivities of approximately 1000 *GPU* which is an increase up to 250% of the permeance of pure PEBAX 2533 composite membranes, while maintaining a CO_2/N_2 selectivity of 21 (76). *GPU* is a measure for the permittivity and 1 *GPU* is 10^{-6} $cm^3cm^{-2}s^{-1}cmHg^{-1}$.

1.3.2 Hollow Fiber Membranes

Amphiphilic Pluronic® triblock copolymers of two blocks of poly(ethylene oxide) (PEO) and poly(propylene oxide) in between have worth as both the surface modifier and pore former in the fabrication of membranes (77). The effect of Pluronics with different molecular architectures and contents as a pore forming additive for the fabrication of poly(ethersulfone) ultrafiltration hollow fibers has been investigated.

The spun hollow fibers were characterized with regard to cross-sectional membrane morphology, membrane surface chemistry, mechanical properties, water permeation, molecular weight cut-off, and pore size distribution. It was observed that the water permeation and molecular weight cut-off of the as-spun hollow fibers are dependent on the structure of the additives.

Among all the membranes spun with 5% additives, the hollow fibers spun using Pluronic F127 and F108 as the additives possess the highest water permeation, the lowest molecular weight cut-off, and the narrowest pore size distribution.

It is suspected that the PEO brush layer formed on the internal pore surface by Pluronic F127 and F108 might reduce the appar-

ent pore size and thus improve the solute rejection of the resultant membranes.

A comparison between Pluronic and PEG as additives confirmed the importance of the presence of poly(propylene oxide) chain in Pluronic in the formation of high performance membranes. When Pluronic F127 concentration was 10%, the as-spun hollow fiber exhibited the highest water permeation of 113.8 $lm^{-2}h^{-1}bar^{-1}$ and the lowest molecular weight cut-off of 9,000 *Dalton* (77).

By introducing hydroxyapatite nanowhiskers of poly(*N*-vinyl-2-pyrrolidone) and poly(vinylidene fluoride), hollow fiber membranes were fabricated using the wet-spinning method (78). An aqueous solution containing 90% *N*-methyl-2-pyrrolidone was used as bore liquid. The effects of the two additives and the synergism on the morphologies, surface properties, permeation performances, antifouling ability and the mechanical properties of the membranes were characterized by various analytical techniques.

The addition of hydroxyapatite gradually suppresses the finger-like structure of the membranes and is replaced by a sponge-like structure. The hydrophilic behavior is evidently improved. The mechanical properties of the membranes are markedly improved with the addition of hydroxyapatite nanowhiskers. The membranes containing dual additives have a higher permeability and mechanical strength than those of the fibers containing either single additive. This suggests a synergism in improving membrane properties (78).

References

1. M.C. Garcia-Alvarez-Coque, M.J. Ruiz-Angel, A. Berthod, and S. Carda-Broch, *Analytica Chimica Acta*, Vol. 883, p. 1, 2015.
2. A. Martín-Calero, V. Pino, J.H. Ayala, V. González, and A.M. Afonso, *Talanta*, Vol. 79, p. 590, 2009.
3. X. Hu, J. Peng, Y. Huang, D. Yin, and J. Liu, *Journal of Separation Science*, Vol. 32, p. 4126, 2009.
4. G.J. Nohynek, R. Fautz, F. Benech-Kieffer, and H. Toutain, *Food and Chemical Toxicology*, Vol. 42, p. 517, 2004.
5. M.H. Habibi, A. Hassanzadeh, and S. Mahdavi, *Journal of Photochemistry and Photobiology A: Chemistry*, Vol. 172, p. 89, 2005.
6. E. Ertaş, H. Özer, and C. Alasalvar, *Food Chemistry*, Vol. 105, p. 756, 2007.

7. Y. Fan, M. Chen, C. Shentu, F. El-Sepai, K. Wang, Y. Zhu, and M. Ye, *Analytica Chimica Acta*, Vol. 650, p. 65, 2009.
8. J.G. Huddleston, A.E. Visser, W.M. Reichert, H.D. Willauer, G.A. Broker, and R.D. Rogers, *Green Chemistry*, Vol. 3, p. 156, 2001.
9. K. Shimojo and M. Goto, *Analytical Chemistry*, Vol. 76, p. 5039, 2004.
10. W.-Z. Zhang, L.-J. He, X. Liu, and S.-X. Jiang, *Chinese Journal of Chemistry*, Vol. 22, p. 549, 2004.
11. J.D. Holbrey, W.M. Reichert, R.G. Reddy, and R.D. Rogers, Ionic liquids as green solvents: Progress and prospects, in *ACS Symposium Series*, Vol. 856, pp. 121–133. American Chemical Society Washington, DC, 2003.
12. X. Xiaohua, Z. Liang, L. Xia, and J. Shengxiang, *Analytica Chimica Acta*, Vol. 519, p. 207, 2004.
13. P. Bonhôte, A.-P. Dias, N. Papageorgiou, K. Kalyanasundaram, and M. Grätzel, *Inorganic Chemistry*, Vol. 35, p. 1168, 1996.
14. W. Zhang, L. He, Y. Gu, X. Liu, and S. Jiang, *Analytical Letters*, Vol. 36, p. 827, 2003.
15. A.V. Herrera-Herrera, J. Hernández-Borges, and M.Á. Rodríguez-Delgado, *Analytical and Bioanalytical Chemistry*, Vol. 392, p. 1439, 2008.
16. A.V. Herrera-Herrera, J. Hernández-Borges, and M. Ángel Rodríguez-Delgado, *Journal of Chromatography A*, Vol. 1216, p. 7281, 2009.
17. C.H. Jin, Y.M. Koo, D.-K. Choi, and K.H. Row, *Biotechnology and Bioprocess Engineering*, Vol. 12, p. 525, 2007.
18. Q. Wang, X. Chen, B. Qiu, L. Zhou, H. Zhang, J. Xie, Y. Luo, and B. Wang, *Journal of Separation Science*, Vol. 39, p. 1242, 2016.
19. P. Abad, F.J. Lara, N. Arroyo-Manzanares, A. Baños, E. Guillamón, and A.M. García-Campaña, *Food Analytical Methods*, Vol. 8, p. 916, 2015.
20. K. Ma, Y.N. Yang, X.X. Jiang, M. Zhao, and Y.Q. Cai, *Chinese Chemical Letters*, Vol. 23, p. 492, 2012.
21. A.M. Zakharova, I.L. Grinshtein, and L.A. Kartsova, *Journal of Analytical Chemistry*, Vol. 68, p. 1081, 2013.
22. C.D. Muynck, J. Beauprez, W. Soetaert, and E.J. Vandamme, *Journal of Chromatography A*, Vol. 1101, p. 115, 2006.
23. J. Flieger and A. Czajkowska-Żelazko, *Journal of Liquid Chromatography & Related Technologies*, Vol. 34, p. 2224, 2011.
24. J. Flieger and A. Czajkowska-Żelazko, *Journal of Separation Science*, Vol. 34, p. 733, 2011.
25. J. Flieger, *Journal of Chromatography A*, Vol. 1113, p. 37, 2006.
26. F. Hofmeister, *Archiv für experimentelle Pathologie und Pharmakologie*, Vol. 25, p. 1, 1888.
27. Wikipedia, Hofmeister series — wikipedia, the free encyclopedia, 2016. [Online; accessed 17-June-2016].
28. J. Flieger, *Analytical Letters*, Vol. 42, p. 1632, 2009.

29. Y. Zhu, H. Ren, Y. Wei, Z. Bie, and L. Ji, *Analytical Letters*, Vol. 48, p. 2708, 2015.
30. International Electrotechnical Commission, Detection and determination of specified additives in mineral insulating oils, IEC Standard IEC 60666:2010, International Electrotechnical Commission, Geneva, 2010.
31. ASTM International, Standard test method for analysis of 2,6-ditertiary-butyl para-cresol and 2,6-ditertiary-butyl phenol in insulating liquids by gas chromatography, ASTM Standard ASTM D4768, ASTM International, West Conshohocken, PA, 2011.
32. ASTM International, Standard test method for 2,6-di-*tert*-butyl-*p*-cresol and 2,6-di-*tert*-butyl phenol in electrical insulating oil by infrared absorption, ASTM Standard ASTM D2668, ASTM International, West Conshohocken, PA, 2013.
33. M.C. Bruzzoniti, R. Maina, V. Tumiatti, C. Sarzanini, and R.M. De Carlo, *Journal of Liquid Chromatography & Related Technologies*, Vol. 38, p. 15, 2014.
34. B. Marcato and M. Vianello, *Journal of Chromatography A*, Vol. 869, p. 285, 2000.
35. A.M. Wims and S.J. Swarin, *Journal of Applied Polymer Science*, Vol. 19, p. 1243, 1975.
36. W. Freitag, *Fresenius' Zeitschrift für analytische Chemie*, Vol. 316, p. 495, 1983.
37. A. Caceres, F. Ysambertt, J. Lopez, and N. Marquez, *Separation Science and Technology*, Vol. 31, p. 2287, 1996.
38. T.W. Ryan, S.G. Yocklovich, J.C. Watkins, and E.J. Levy, *Journal of Chromatography A*, Vol. 505, p. 273, 1990.
39. H.J. Vandenburg, A.A. Clifford, K.D. Bartle, J. Carroll, and I.D. Newton, *Analyst*, Vol. 124, p. 397, 1999.
40. L. Sternbauer, I. Hintersteiner, W. Buchberger, A. Standler, and E. Marosits, *Polymer Testing*, Vol. 32, p. 901, 2013.
41. H. Zhang, M. Shen, S. Tong, and J. Yan, *Chinese Journal of Chromatography (Zhongguo Hua Xue Hui)*, Vol. 32, p. 612, 2014.
42. J.H. Brewster, *Journal of the American Chemical Society*, Vol. 78, p. 4061, 1956.
43. S. Tong, H. Zhang, M. Shen, Y. Ito, and J. Yan, *Journal of Chromatography B*, Vol. 962, p. 44, 2014.
44. Wikipedia, Cyclodextrin — wikipedia, the free encyclopedia, 2016. [Online; accessed 9-June-2016].
45. R.W. Stringham and Y.K. Ye, *Journal of Chromatography A*, Vol. 1101, p. 86, 2006.
46. V.S. Sharp, M.N. Letts, D.S. Risley, and J.P. Rose, *Chirality*, Vol. 16, p. 153, 2004.

47. Wikipedia, Vancomycin — wikipedia, the free encyclopedia, 2016. [Online; accessed 12-June-2016].
48. Wikipedia, Actaplanin — wikipedia, the free encyclopedia, 2015. [Online; accessed 12-June-2016].
49. L. Javorska, L.K. Krcmova, D. Solichova, P. Solich, and M. Kaska, *Journal of Separation Science*, Vol. 39, p. 6, 2016.
50. F. Khamesipour, S.M. Hashemian, P. Tabarsi, and A. Velayati, *Biomedical and Pharmacology Journal*, Vol. 8, p. 818, 2015.
51. Wikipedia, Dansyl chloride — wikipedia, the free encyclopedia, 2016. [Online; accessed 12-June-2016].
52. Y. Sun, T. Li, and C. Ma, *Chinese Journal of Chromatography*, Vol. 31, p. 447, 2013.
53. S. Tong, H. Zhang, and J. Yan, *Journal of Chromatographic Science*, Vol. 54, p. 593, 2016.
54. N. Guo, X. Gao, G. Xu, and X. Guo, *Chinese Journal of Chromatography*, Vol. 26, p. 259, 2008.
55. P.N. Patil, D.D. Miller, and U. Trendelenburg, *Pharmacological Reviews*, Vol. 26, p. 323, 1974.
56. A. Mozayani, P. Singer, and G. Jones, *Journal of Analytical Toxicology*, Vol. 19, p. 519, 1995.
57. M.I.R.M. Santoro, H.S. Cho, and E.R.M. Kedor-Hackmann, *Drug Development and Industrial Pharmacy*, Vol. 27, p. 693, 2001.
58. C.J. Welch and S.R. Perrin, *Journal of Chromatography A*, Vol. 690, p. 218, 1995.
59. Y. Agrawal and R. Patel, *Journal of Chromatography B*, Vol. 820, p. 2331, 2005.
60. S. Morante-Zarcero and I. Sierra, *Journal of Pharmaceutical and Biomedical Analysis*, Vol. 62, p. 33, 2012.
61. X. Weng, Z. Bao, H. Xing, Z. Zhang, Q. Yang, B. Su, Y. Yang, and Q. Ren, *Journal of Chromatography A*, Vol. 1321, p. 38, 2013.
62. L. Wang, X. Liu, Q. Lu, Y. Zou, Q. Liu, J. Yang, and G. Yang, *Analytical Methods*, Vol. 6, p. 4107, 2014.
63. M.C. García, *Journal of Chromatography B*, Vol. 825, p. 111, 2005.
64. R.D. Voyksner and C.A. Haney, *Analytical Chemistry*, Vol. 57, p. 991, 1985.
65. D.V. McCalley, *Journal of Chromatography A*, Vol. 1038, p. 77, 2004.
66. J. Takebayashi, J. Nagata, and K. Yamada, *Food Science and Technology Research*, Vol. 14, p. 509, 2008.
67. G. Boczkaj, M. Jaszczołt, A. Przyjazny, and M. Kamiński, *Analytical and Bioanalytical Chemistry*, Vol. 405, p. 6095, 2013.
68. N. Lambropoulos, T. Cardwell, D. Caridi, and P. Marriott, *Journal of Chromatography A*, Vol. 749, p. 87 , 1996.
69. C. Giaginis, S. Theocharis, and A. Tsantili-Kakoulidou, *Journal of Chromatography A*, Vol. 1166, p. 116, 2007.

70. D. Vrakas, A. Tsantili-Kakoulidou, and D. Hadjipavlou-Litina, *QSAR & Combinatorial Science*, Vol. 22, p. 622, 2003.
71. P. Jones and P.N. Nesterenko, *Journal of Chromatography A*, Vol. 1213, p. 45, 2008.
72. J.M.P. Scofield, P.A. Gurr, J. Kim, Q. Fu, S.E. Kentish, and G.G. Qiao, *Journal of Membrane Science*, Vol. 499, p. 191, 2016.
73. C.E. Powell and G.G. Qiao, *Journal of Membrane Science*, Vol. 279, p. 1, 2006.
74. C.A. Scholes, J. Bacus, G.Q. Chen, W.X. Tao, G. Li, A. Qader, G.W. Stevens, and S.E. Kentish, *Journal of Membrane Science*, Vol. 389, p. 470, 2012.
75. M.G. Buonomenna, W. Yave, and G. Golemme, *RSC Advances*, Vol. 2, p. 10745, 2012.
76. J.M.P. Scofield, P.A. Gurr, J. Kim, Q. Fu, A. Halim, S.E. Kentish, and G.G. Qiao, *Journal of Polymer Science Part A: Polymer Chemistry*, Vol. 53, p. 1500, 2015.
77. C.H. Loh, R. Wang, L. Shi, and A.G. Fane, *Journal of Membrane Science*, Vol. 380, p. 114, 2011.
78. X. Zhang, W.-Z. Lang, H.-P. Xu, X. Yan, and Y.-J. Guo, *RSC Advances*, Vol. 5, p. 21532, 2015.

Additives for High Performance Applications: Chemistry and Applications. Johannes Karl Fink.

2

Electrical Applications

2.1 Capacitors

2.1.1 Triethanolamine

Triethanolamine has been evaluated as an additive to a commercial electrolyte to enhance the properties of aluminum electrolytic capacitors (1). The results showed that 1–3% triethanolamine additive can prevent the pH and conductivity of the electrolytes from decreasing for 5000 *h* at 60°C.

The ability of the anodic restoration of an anode aluminum film in the electrolyte with triethanolamine additive proved to be more efficient than the electrolyte without triethanolamine additive.

The low temperature electrical characteristics of capacitors showed that the triethanolamine additive can prevent the electrolyte inside capacitors from freezing and losing electric characteristics even at −40°C.

A load life test of the capacitors impregnated with electrolytes with or without triethanolamine additive exhibited remarkable differences. The triethanolamine additive promoted 105°C load lifetime from 3019 *h* up to 5624 *h* and from 2144 *h* up to 3621 *h* for a 125°C load lifetime test (1).

2.1.2 Supercapacitors

Supercapacitors have been described in monographs (2–4). The first model for the distribution of ions near the surface of a metal electrode was invented by Helmholtz in 1874 (2). He imagined two

parallel sheets of charges of opposite sign. One of these was located on the metal surface and the other was located on the solution side, a few nanometers away, exactly as in the case of a parallel plate capacitor. The rigidity of such a model was confirmed by Gouy and Chapman. In 1947, Grahame transferred the knowledge of the structure of electrolyte solutions into the model of a metal/solution interface, by envisaging different planes of closest approach to the electrode surface depending on whether an ion is solvated or interacts directly with the solid wall.

In this way, the Gouy-Chapman-Stern-Grahame model of the electrical double layer was born (5). This model is still qualitatively accepted, although a number of additional parameters have been introduced (2).

Metal oxide-based materials, carbon materials, and conducting polymers for electrochemical supercapacitor electrodes have been reviewed in detail (6). Two important future research directions have been summarized: The development of composite and nanostructured electrochemical supercapacitor materials to overcome the problem of low energy density of electrochemical supercapacitors.

2.1.2.1 Composite Electrode

A supercapacitor composite electrode has been described (7). The composition is listed in Table 2.1.

Table 2.1 Supercapacitor electrode composition (7).

Component	%
Poly(3,4-ethylene-dioxythiophene):poly(styrenesulfonate)	81
Graphite oxide	16
Carbon nanotubes	3

Conducting polymers undergo redox reactions to store the charge in bulk material and thereby increase the energy density and reduce the self-discharge reaction.

Poly(3,4-ethylene-dioxythiophene):poly(styrenesulfonate) is a mixture of two ionomers. Poly(3,4-ethylene-dioxythiophene) is a *p*-type doped conjugated polymer, carrying positive charges. The monomer is shown in Figure 2.1.

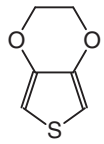

Figure 2.1 3,4-Ethylene-dioxythiophene.

The sulfonyl groups in poly(styrenesulfonate) serve as the counterions of poly(3,4-ethylene-dioxythiophene). The preparation was done by a solution casting method.

The stacking between these carbon additives having very different dimensionality provides a unique skeletal structure that allows for enlarged polymer/electrolyte interface for high capacitance and for enhanced electronic and ionic conductivities needed for high-power performance. The resulting ternary electrode exhibits nearly a ten-fold increase in energy and power performance as compared with pure conducting polymer electrode (7).

2.1.2.2 Fiber-Shaped Supercapacitors

Fiber-shaped supercapacitors have attractive applications in flexible devices. A high performance carbon nanotube (CNT)-based fiber-shaped supercapacitor has been developed by adding two redox additives simultaneously, i.e., poly(pyrrole) (PPY) to the electrodes and hydroquinone (HQ) to the electrolyte (8).

A core-shell CNT-PPY nanocomposite fiber was prepared using an electrochemical deposition method. In the fiber-shaped supercapacitor with CNT-PPY electrodes, PPY provides a pseudocapacitance due to its reversible dropping and de-dropping reactions in a poly(vinyl alcohol) (PVA)/H_2SO_4 gel electrolyte. The capacitance of the CNT-PPY fiber-shaped supercapacitor reaches 36 Fg^{-1}, which is 7 times higher than that of a pure CNT fiber-shaped supercapacitor.

By adding HQ to the PVA/H_2SO_4 gel electrolyte in the CNT-PPY fiber-shaped supercapacitor, the specific capacitance reaches 56 Fg^{-1}, which is 10 times higher than that of the pure CNT fiber-shaped supercapacitor.

Thus, HQ can enhance ion transfer of the gel electrolyte by the redox reaction of HQ and benzoquinone. Both PPY and HQ have syn-

ergistic effects on fiber-shaped supercapacitors. The fiber-shaped supercapacitors with PPY and HQ also show a high stability in the cyclic test for 2000 cycles, and good flexibility under bending, knotting, and tension (8).

2.2 Electrokinetic Micropumps

A zwitterionic additive has been tested to improve the performance of electrokinetic micropumps, which use the voltage applied across a porous matrix to generate an electroosmotic pressure and flow in microfluidic systems (9).

Modeling of electrokinetic micropump systems has predicted that the additive, i.e., trimethylammoniopropane sulfonate, cf. Figure 2.2, will result in up to a 3.3-fold increase in the pumping efficiency and up to a 2.5-fold increase in the generated pressure. The predicted values agreed well with the experimental results for flow, pressure and efficiency. Using this additive, pressures up to 156 $kPa\,V^{-1}$ and an efficiency up to 5.6% could be reached.

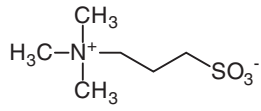

Figure 2.2 Trimethylammoniopropane sulfonate.

The improvements result in a reduction in voltage and power requirements and will facilitate the miniaturization of such systems, e.g., microfluidically driven actuators (9).

2.3 Lead-Acid Batteries

The lead-acid battery exhibits a very low energy-to-weight ratio and a low energy-to-volume ratio. However, it can supply high surge currents. Therefore, the cells have a relatively large power-to-weight ratio. These properties, along with their low cost, makes a lead-acid battery attractive for use in motor vehicles to provide the high current required in the course of starting the motor. The

lead-acid battery was invented in 1859 by French physicist Gaston Planté and therefore is the oldest type of rechargeable battery (10).

2.3.1 Activated Carbon Additives

A negative electrode of a 2 *V* cell and 12 *V* lead-acid battery was doped with activated carbon additives.

It turned out that the negative electrode that contained tens-of-micron-sized carbon particles in the negative active material exhibits a markedly increased high rate partial state of charge duty than a comparative material containing carbon particles with much smaller size of several microns or a material containing no activated carbon.

The improved performance has been attributed to the optimized negative active material microstructure and the enhanced electrode reaction kinetics by introducing appropriate activated carbon. The beneficial effects can be briefly explained as such (11):

1. The activated carbon acts as new porous-skeleton builder to increase the porosity and active surface of the negative active material, and thus facilitates the electrolyte diffusion from surface to inner plate and provides more sites for crystallization/dissolution of lead sulfate
2. The activated carbon plays the role of an electrolyte supplier to provide sufficient H_2SO_4 in the inner plate when the diffusion of H_2SO_4 from plate surface cannot keep pace with the electrode reaction.
3. The activated carbon acts as capacitive buffer to absorb excess charge current which would otherwise lead to insufficient negative active material conversion and hydrogen evolution.

2.3.2 High Performance Positive Electrode

Conventional lead-acid batteries contain a positive electrode (PbO_2 plate) and a negative electrode (Pb plate) immersed in a sulfuric acid electrolyte and having a separator interposed between each plate. Such electrodes are typically made by applying a paste containing lead oxides and lead sulfates to the surface of a battery plate and electrochemically forming the paste into an active material.

Conventional pastes for use in making automotive batteries contain lead oxide in the range of 15–30%, sulfuric acid, water and additives such as fiber and expanders. Such pastes are usually made by adding the sulfuric acid and water to a mixture of lead and lead oxides. As a result of the chemical reaction during mixing, a portion of the lead and PbO is initially converted to lead sulfate ($PbSO_4$) and the resultant positive paste becomes a heterogeneous mixture of lead, lead oxide, lead sulfate and basic lead sulfates.

In order to improve the manufacturing process of batteries, a variety of conductive additives have been proposed for incorporation into the plates. Lead dioxide has been proposed as an additive for paste mixtures containing tetrabasic lead sulfate (12). Lead dioxide enhances positive plate formation, but provides no substantial advantage in the resulting battery because it participates in the positive plate reaction. During charging of the battery, lead sulfate is converted into lead dioxide, and the reverse reaction occurs during discharge.

The use of pre-sulfated paste materials containing basic lead sulfate, e.g., tribasic and tetrabasic lead sulfates ($3PbO \times PbSO_4 \times H_2O$ and $4PbO \times PbSO_4$) made in dry form prior to forming the paste has also been proposed to improve the efficiency of the paste (13).

Also, monobasic lead sulfate has been used as a pre-sulfated paste material (14). However, positive plates prepared from such pre-sulfated paste mixes are difficult to form and must usually be cured for at least 24 hours before being formed (15). It is also known that reacting lead oxide with ozone forms improved lead oxides useful as active materials in batteries (16).

It has been shown that the surface area increase is directly related to the presence of a hydrogen bonding solvent, typically water, for ozone, and that an increase in surface area is obtained with higher ozone concentration (17,18). Several attempts have also been made to improve the conductivity of the paste through use of persulfate treatments (19).

Before the pasting operation, the grid is dipped in ammonium persulfate, sodium persulfate, or a sodium perborate solution (20). However, these methods fail to produce batteries capable of high-power outputs. In such batteries, the energy efficiency or capacity is limited to less than 50% of the theoretical value determined according to Faraday's law. This energy efficiency is even lower at

high discharge rates. An improved composition and method for preparation has been reported (21):

Preparation 2–1: A solid mix containing 44.2% tribasic lead sulfate and 5.0% potassium persulfate was prepared. To this composition 50.7% orthorhombic lead oxide and 0.1% glass fiber (0.125 *in*) were added. Water in an amount of 30% of the solid mix weight was added periodically. No acid was added to the mixture. The water and solids were thoroughly mixed until a pastable mixture was formed. The plates were then air dried. No curing procedure was used. Once dry, the plates were formed. Lead-alloy grids were used with a size of about 5.2 $cm \times 4.2\ cm \times 0.12\ cm$. The plates were cured by heating in a chamber at a temperature of about 130°F and a humidity of about 95% for approximately 24 *h*.

In particular, the battery plates prepared as described above exhibit high porosity and surface area, as well as a high efficiency of formation. Such plates have good strength and are capable of high-power outputs (21).

2.4 Lithium-Ion Batteries

There are monographs concerning the science and technology of lithium-ion batteries (22–26). The development and commercialization of Li-ion batteries during the last decades is one of the great successes of modern electrochemistry. The increasing reliability of Li-ion batteries makes them natural candidates as power sources for electric vehicles (27). However, their current energy density, which can reach an average of 200 $Wh\,kg^{-1}$ on a single cell level, limits the possible driving range of electric cars propelled by Li-ion batteries.

There is a strong interest in developing power source technologies beyond Li-ion batteries that will mark breakthroughs in energy density capabilities. Li-sulfur batteries have high theoretical energy density that can revolutionize electrochemical propulsion capability. Consequently, in recent years there has been much work throughout the world related to these systems. The scope of work on this topic justifies frequent publications of review articles that summarize recent extensive work and provide guidelines and direction for focused future work (27).

A comprehensive, systematic work related to Li-sulfur battery systems has been presented, covering the Li-anode challenges,

carbon-encapsulated sulfur cathodes, and various kinds of relevant electrolyte solutions. Several guidelines for further research and development efforts in this field have been summarized (27).

Sulfiphilic cathode materials with a strong affinity for lithium polysulfides are a promising group of candidates to control the dissolution and precipitation reactions in the cell, where the improvement of conductivity and the areal sulfur loading is an important objective. A metallic Co_9S_8 material has been described with an interconnected graphene-like nano-architecture that realizes this issue (28).

Initial calculations using spectroscopic data demonstrated a synergistic strong dual-interaction of polysulfides with the host. The three-dimensional interconnected structure with hierarchical porosity not only manifests up to a factor of 10 increase of the cycling stability with a fade of smaller than 0.045% per cycle over 1500 cycles compared to standard porous carbons, but also enables a high-loading sulfur electrode with up to 75% sulfur, and up to 4.5 $mg\,cm^{-2}$ areal sulfur loading (28).

The current energy density Li-ion batteries, which can reach an average of 200 $Wh\,kg^{-1}$ on the single cell level, limits the possible driving range of electric cars propelled by Li-ion batteries (29). On the other hand, there is a strong driving force to develop power source technologies beyond Li-ion batteries that will mark breakthroughs in energy density capabilities. Li-sulfur batteries have a high theoretical energy density that can revolutionize electrochemical propulsion capability. Therefore, there has been much work throughout the world related to these systems.

A comprehensive, systematic work related to Li-sulfur battery systems is described, beginning with the Li anode challenges, carbon-encapsulated sulfur cathodes, and various kinds of relevant electrolyte solutions (29).

Li alloying materials, such as Si and Ge nanowires, are interesting to replace the relatively low-capacity carbonaceous-based Li-ion anodes. Since the initial report of binder-free nanowire electrodes, much research has been carried out in which the performance and cycle life has significantly progressed (30).

The study of such electrodes has provided invaluable insights into the cycling behavior of Si and Ge, as the effects of repeated

lithiation and delithiation on the material can be observed without an interference from conductive additives or binders.

Some of the key developments in this area have been described. The focus was the problems encountered by Li alloying electrodes in general, e.g., pulverization, loss of contact with the current collector. Some important studies on nanowire have elucidated the consequences of the alloying and dealloying processes on the morphology of Si and Ge. In particular, the impacts that are effecting pore formation and lithium-assisted welding are influencing the performance. Also, the challenges for the practical implementation of nanowire anodes have been elucidated (30).

An efficient sulfur host has been described, i.e., hierarchical microporous–mesoporous carbonaceous nanotubes that feature a thick microporous wall and inner hollow channel (31). The electrochemical performance of these microporous–mesoporous carbonaceous nanotubes has been studied systematically at different discharge cut-off voltages and at varying sulfur content.

The cycling behavior in different voltage windows has been assessed and the highest specific capacity has been detected for microporous–mesoporous carbonaceous nanotubes-S-50 in the range of 1.4–2.8 V. These results imply that better energy densities can be achieved by controlling the discharge cut-off voltage. Moreover, it has been shown that when the sulfur loading is 50% (i.e., microporous–mesoporous carbonaceous nanotubes-S-50), the cycling and rate performance is better than that of the composite loaded with 40% sulfur (microporous–mesoporous carbonaceous nanotubes-S-40) (31).

Benefiting from the attractive hierarchical micro/mesoporous configuration, the obtained hybrid structure not only promotes electron and ion transfer during the charge and discharge processes, but also efficiently impedes the polysulfide dissolution. More specifically, the electrode can deliver a specific capacity of 558 $mA\,h\,g^{-1}$ even after 150 cycles at a high rate of 1600 $mA\,g^{-1}$ with a decay rate of only 0.13% per cycle. With regard to the beneficial structure of these carbon nanotubes, it is very feasible that these structures may also be used in other research fields, including in catalysis, as supercapacitors, in drug delivery applications, and for absorption procedures (31).

2.4.1 *Ionic Diffusion*

The behavior of battery kinetics inside the battery and the ionic diffusion during operation has been studied (32). The role of the electrolyte is to provide an ionic conduction path between the anode and the cathode. The improvement of the cyclability has been elucidated. An electrolyte containing 0.1% of a fluoro-*o*-phenylenedimaleimide-based additive was compared with an electrolyte with 0.1% *N*,*N*′-*o*-phenylenedimaleimide, cf. Figure 2.3, also without any additive.

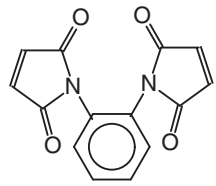

Figure 2.3 *N*,*N*′-*o*-Phenylenedimaleimide.

Electrochemical impedance spectroscopy (EIS) was used for the characterization. The results showed that a great amount of the lithium ions remains on the solid electrolyte interphase layer of the mesocarbon microbeads half cell with fluoro-*o*-phenylenedimaleimide additive, indicating that the ion moves easily because of high diffusion (32).

2.4.2 *Functional Electrolytes*

Additives have been developed to improve the cathode cyclability performance of lithium batteries (33). Benzene derivatives (biphenyl and *o*-terphenyl) and heterocyclic compounds (furan, thiophene, *N*-methylpyrrole and 3,4-ethylenedioxythiophene), which have lower oxidation potentials than those of electrolyte solvents have been tested. The functional electrolytes used are shown in Figure 2.4.

The electrochemical properties and cyclability of the additives have been investigated. The additives are found to decompose on the cathode to form a very thin film. This resulting novel-type thin surface film has been addressed as an electroconductive membrane

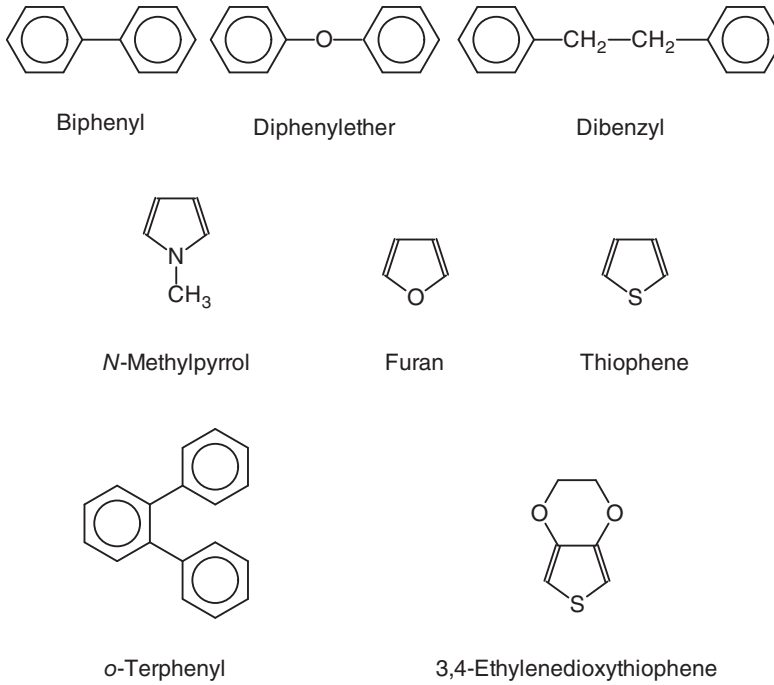

Figure 2.4 Functional electrolytes (33).

since it is different from solid electrolyte interphase by the point of its electroconductivity.

It has been concluded that these additives, which were formerly known as overcharge protection proofs, contribute to improve the cathode cyclability by forming very thin cathode surface layer in the case of slight amount of addition (33).

In contrast, in the case of 2% addition, an oxidative decomposition of the additives progresses as the cycle proceeds, which leads to an battery capacity fading, because the grown cathode film becomes thick with a high Li^+ ion resistance.

2.4.3 Synergetic Effect of Conductive Additives

Carbon black (Super P and SP) and vapor-grown carbon fibers, were used to construct an effective conducting network in the cathode of commercial $LiFePO_4$ lithium-ion batteries (34, 35). The results suggest that the lithium-ion battery with carbon black SP possesses a higher discharge capacity than that with vapor-grown carbon fibers with the same mass fraction of the additives. The high-rate capacity of lithium-ion batteries with carbon black SP is much higher than that with vapor-grown carbon fibers.

Furthermore, the lithium-ion batteries with a mixture of these two additives have an apparently improved performance in low- and high-rate discharge capacity compared with the lithium-ion batteries with only a single component additive with the same mass fraction, obviously due to a synergetic effect (34).

2.4.4 In-Situ Coating of Cathode by Electrolyte Additive

It has been demonstrated that *N*,*N*′-4,4′-diphenylmethane-bismaleimide as an electrolyte additive enhances the high-voltage performance of lithium-ion batteries by electrochemically forming an interface film on cathode surface (36).

2,2′-Bis[4-(4-maleimidophenoxy) phenyl]propane, which is more compatible with the electrolyte than *N*,*N*′-4,4′-diphenylmethane-bismaleimide, has been studied as an alternative electrolyte additive. $LiCoO_2$ has been chosen as a typical cathode material.

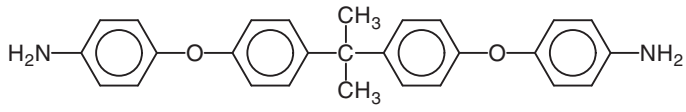

2,2´-Bis[4-(4-maleimidophenoxy) phenyl]propane

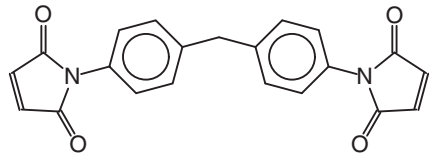

N´N´-4,4´-diphenylmethane-bismaleimide

Figure 2.5 *In-situ* coating additives.

The structure of the interface films on a $LiCoO_2$ surface has been studied using different concentrations of the 2,2′-bis[4-(4-maleimidophenoxy) phenyl]propane additive. Scanning electron microscope (SEM), transmission electron microscopy (TEM), and X-ray photoelectron spectroscopy (XPS) were used. The oxidation potential of 2,2′-bis[4-(4-maleimidophenoxy) phenyl]propane has been measured by linear sweep voltammetry (LSV) (36).

It was found that thickness-tunable interface films could be generated on the $LiCoO_2$ surface by adding different concentrations of 2,2′-bis[4-(4-maleimidophenoxy) phenyl]propane additives in the electrolyte. Also, the high-voltage cycling performance of the corresponding $LiCoO_2$/Li batteries is closely associated with the thickness of the interface film. The optimized amount of 2,2′-bis[4-(4-maleimidophenoxy) phenyl]propane additive (0.5% w/v) presents superior high-voltage cycling performance of the corresponding $LiCoO_2$/Li batteries (36).

2.4.5 Bipolar Architectures

A suitable architecture for putting electrochemical cells in series, without interfering with the mass and the volume of the resulting accumulator, is the so-called *bipolar* architecture (37). This design consists of stacking several electrochemical cells separated from

each other by a current-collecting substrate. One face of this substrate is occupied by an electrode of a cell, while the opposite face of this substrate is occupied by an electrode of the opposite sign of an adjacent cell.

This type of architecture allows a reduction in the electrical resistance of the assembly as compared with one accumulator, which would consist of a plurality of cells connected together through external connectors. The bipolar architecture also allows a limitation of unnecessary masses and volumes.

However, this type of architecture may have drawbacks in terms of charging, since the electrochemical cells, because of their positioning in the stack, have different characteristics in terms of internal resistance and capacitance, which causes different charging times for identical electrochemical materials (37).

2.4.5.1 Lithium Polysulfide

It has been discovered that by adding a specific additive into the electrolyte of the electrochemical cells of a lithium accumulator with a bipolar architecture, it is possible to find a remedy to the charging problems of this cell type. Each cell in the structure has a positive electrode and a negative electrode, separated by an electrolyte. To the electrolyte a lithium polysulfide Li_2S_6 is added. Li_2S_6 can be prepared by the reaction of lithium and sulfur in tetraethylene glycol dimethyl ether.

The lithium polysulfide ensures the role of a redox shuttle. So this additive will undergo, at a determined potential, an oxidation at one of the electrodes of the cell in order to give an oxidized form of the additive. This oxidized form in turn undergoes reduction at the electrode of the opposite sign of the same cell in order to give a reduced form. The reduced form is then capable of being oxidized at the electrode with reverse polarity.

In the case of a lithium polysulfide additive, the redox shuttle mechanism occurs at a potential located between 2.4 and 2.5 V relative to the reference pair Li^+/Li. This means that this additive is particularly suitable for electrochemical cells for which the rated cell voltage after complete charging is less than all the voltage values between 2.4 and 2.5 V. In detail, the electrolyte may contain basic components that are shown in Table 2.2.

Table 2.2 Electrolyte for bipolar architectures (37).

Organic compound	Salt	Salt
Ethylene carbonate	$LiPF_6$	$LiCF_3SO_3$
Propylene carbonate	$LiClO_4$	$LiN(CF_3SO_2)_3$
Dimethyl carbonate	$LiBF_4$	$LiN(C_2F_5SO_2)$
	$LiAsF_6$	Li_2S_6

Preferably, the liquid electrolyte contains $LiPF_6$ in a concentration of 1 mol l^{-1} in solution in a mixture of ethylene carbonate, propylene carbonate and dimethyl carbonate in respective volume proportions of 1:1:3. To this electrolyte, Li_2S_6 is added so as to obtain a concentration of this additive of 0.1 mol l^{-1} (37). Charging curves that illustrate the change in the cell voltage versus the capacity are illustrated in Figures 2.6 and 2.7.

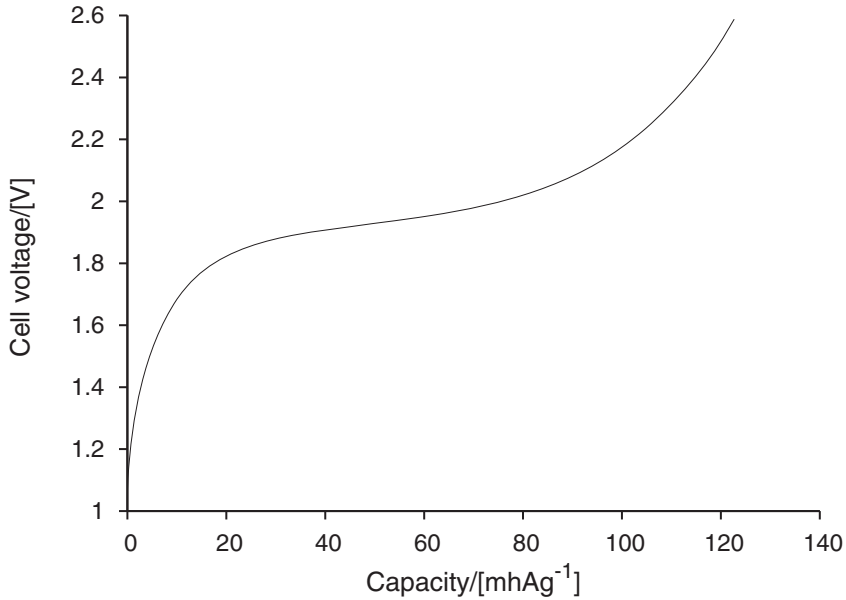

Figure 2.6 Charging curve of a device without lithium polysulfide (37).

The curve without lithium polysulfide has an ascending phase between 1 *V* and 1.8 *V* and then a plateau shape between 1.8 and 2 *V*. This is ending with an exponential ascending phase from 2.2 *V* up to 2.6 *V*.

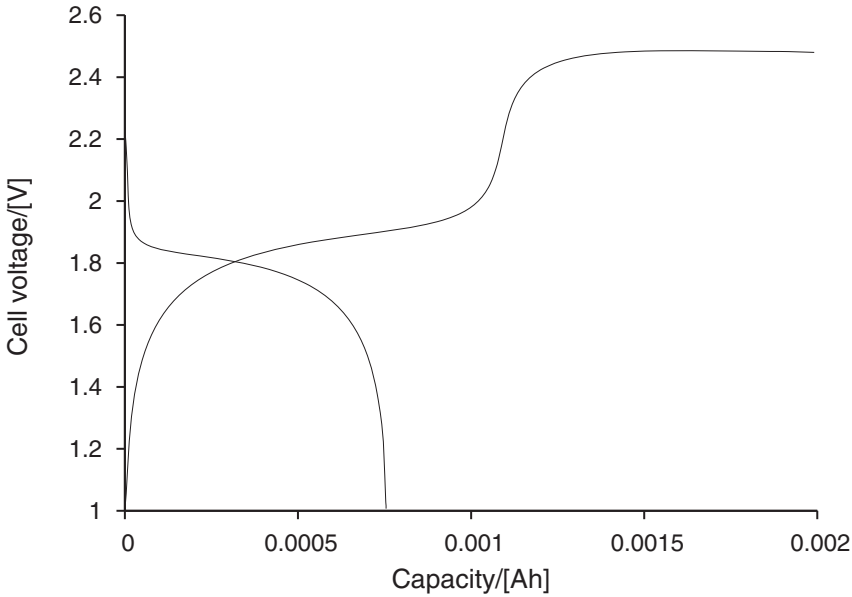

Figure 2.7 Charging and discharging curves of a device containing lithium polysulfide (37).

According to a second test, successive charging/discharging operations were carried out at C/100 at 20°C for cycling ranging from 1 to 2.6 V with an accumulator identical to the one used for the first test, only that the electrolyte in this case comprises Li_2S_6 at a concentration of 0.1 $mol\,l^{-1}$.

In a second test, Li_2S_6 in a concentration of 0.1 $mol\,l^{-1}$ was used, otherwise the same device. The charging curve has an ascending phase between 1 V and 1.8 V, then adopts a plateau shape between 1.8 V and 2 V and then shows a new ascending phase between 2 V and 2.45 V. Thus here, at the end of charging, the potential is stabilized around 2.45 V instead of increasing exponentially.

This value of 2.45 V corresponds to the potential at which an equilibrium is established between the consumption of the Li_2S_6 additive at one of the electrodes and regeneration of the consumed additive at the electrode of the opposite sign. This potential is located above the rated cell voltage after complete charging of the latter, which allows the electrochemical cell to be completely charged and also gives the possibility of avoiding the cell being subjected to too large voltages if the charging has to be maintained in order to allow the

other incompletely charged cells to continue to be subjected to this charging process (37).

2.4.6 Janus Separator

Electrochemical energy storage devices, e.g., rechargeable batteries, flow batteries, fuel cells, and supercapacitors, have been widely exploited and rapidly propelled for a low-carbon, green, and sustainable society. The separator is a crucial component of electrochemical energy storage devices and its unique functionalities are indispensable (38).

For example, separators for secondary batteries and supercapacitors separate the cathode and anode to prevent shorting, while in flow batteries and fuel cells, an ideal separator should selectively control the mass transportation in the cell.

But in newly emerging electrochemical energy storage devices with revolutionary conversion electrochemistry, such as lithium-sulfur batteries and lithium-air batteries, separators are supposed to play a crucial role in fully demonstrating superior high energy density.

A Janus separator was proposed because Janus structures can offer asymmetry and realize the emergence of properties inconceivable for homogeneous or symmetric structures (39). The name Janus was derived from the Roman god Janus.

In this Janus separator, a nanoporous poly(propylene) (PP) membrane serves as an insulating substrate in contact with lithium anode while a layer of cellular graphene framework, which has extraordinary electrical conductivity, abundant in-plane mesopores, high electrochemically active surface area, and large mesopore volume, adheres to the cathode side to reactivate the shuttling-back of the lithium polysulfides and to preserve the ion channels (39). A mesoporous material is a material containing pores with diameters between 2 and 50 *nm* (40).

The Janus separator of PP-supported cellular graphene framework separator promises the efficient utilization of sulfur cathode with high capacity and good cycling stability.

Moreover, the Janus separator, besides modifying electrode materials and electrolyte formulations, essentially opens new opportunities for facilitating the utilization of active materials that are

highly mobile in emerging high-energy-density electrochemical energy storage devices and indicates a better way to rationally adopt the superior characteristics of various novel nanostructured carbon to electrochemical energy storage devices (39). A Janus separator can be fabricated as follows (39):

Preparation 2–2: Carbonaceous materials are coated on PP substrates via facile filtration. 18 *mg* of carbon, a cellular graphene framework fabricated by a modified template chemical vapor deposition method on hydrothermally synthesized MgO templates and 2.0 *mg* of a poly(vinylidene fluoride) binder were dispersed in *N*-methyl-2-pyrrolidone, cf. Figure 2.8, by ultrasonication for 1.0 *h*. Then, 36.0 *ml* of the dispersion was filtered through a piece of a commercial PP separator (Celgard® 2400) and subsequently dried at room temperature for 24.0 *h*. The Janus separator was found with carbon loading amount of 0.3 $mg\,cm^{-2}$.

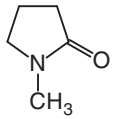

Figure 2.8 *N*-Methyl-2-pyrrolidone.

2.4.7 Synthesis of Vanadium Cathodes

Vanadium oxide hierarchical structures were controllably synthesized using a solvothermal method in water-ethylene glycol mixed media (41). A V_4O_7 *nanocross* structure has been reported. It was observed that this structure exhibits an exceptional cycling stability at 0.05 $A\,g^{-1}$ and 3.05 $A\,g^{-1}$, which could be a promising cathode candidate for lithium-ion batteries.

2.4.8 Graphite

2.4.8.1 High-Capacity Graphite Cells

The synergistic effects of $LiB(C_2O_4)_2$, $LiF_2B(C_2O_4)$, triphenylamine, and 1,4-benzodiozane-6,7-diol as functional electrolyte additives in high-energy electrochemical cells has been elucidated (42). These compounds are shown in Figure 2.9.

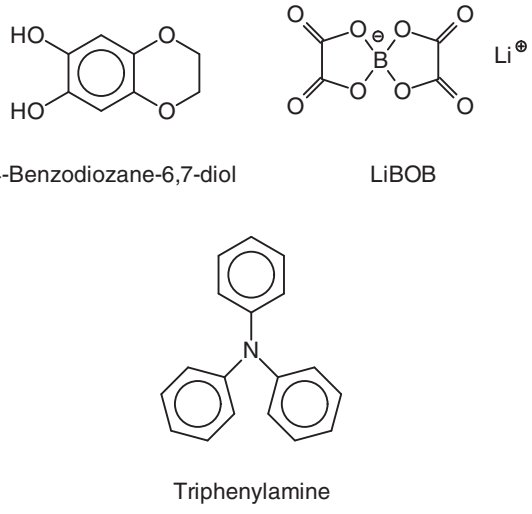

Figure 2.9 Functional electrolyte additives (42).

The influence of these additives, individually, and in different combinations, has been evaluated using galvanostatic cycling of cells containing $Li_{1.2}Ni_{0.15}Mn_{0.55}Co_{0.1}O_2$-based positive electrodes, graphite-based negative electrodes, and a $LiPF_6$-based electrolyte.

As such, $LiB(C_2O_4)_2$ is a good additive for reducing the loss of the cell capacity, but the cell impedance rise is still significant after extended cycling. Similarly, neither triphenylamine nor 1,4-benzodiozane-6,7-diol alone provide the desired improvements in cell performance.

However, cells containing $LiB(C_2O_4)_2$ in combination with $LiF_2B(C_2O_4)$, triphenylamine, or 1,4-benzodiozane-6,7-diol exhibit an enhanced capacity retention, rate capability, and cyclability. Thus, the combination of electrolyte additives that act synergistically is a practical and versatile strategy in order to improve the performance and life of lithium-ion cells (42).

2.4.8.2 Improved Cycling Performance

Lithium difluorophosphate. Lithium difluorophosphate has been used as a reducible additive to overcome the unsatisfactory rate ca-

pability and cycling instability of highly pressed graphite electrodes with a high mass loading of 8.1 $mg\,cm^{-2}$ with a vinylene carbonate derived surface film that hampers the charge transport at the graphite electrolyte interface at high rates (43).

It has been found that lithium difluorophosphate modifies the surface chemistry induced by vinylene carbonate and makes a more ionically conductive surface film on the graphite, thus ensuring a good rate capability (43).

***N*-Methyl-2-pyrrolidinone.** A lithium-ion cell is charged in such a manner that lithium is released from the positive electrode into the nonaqueous electrolytic solution, and lithium ions in the nonaqueous electrolytic solution are absorbed into the negative electrode separated from the positive electrode by a microporous separator (44). In a discharge process, the reverse phenomenon is generated to allow electrons to be extracted by an external circuit. Thus, a capacity of the lithium-ion cell is related to a quantity of ions to be absorbed and released between the positive and negative electrodes.

In the course of the charging and discharging reactions, an irreversible decomposition of the nonaqueous electrolytic solution or the lithium salt may occur on the surfaces of the negative and positive electrodes to cause consumption of lithium ions to be absorbed and released. The quantity of lithium ions consumed in the charge and discharge cycles corresponds to an irreversible capacity of the cell. Particularly, during a charge process in the first cycle, a passive film, a so-called solid electrolyte interphase, is formed on a surface of the carbon-based negative electrode, and the resulting irreversible capacity has a great impact on an energy density of the lithium-ion cell.

In order to reduce the first cycle irreversible capacity, some procedures have been proposed. A nonaqueous electrolytic solution has been developed for a lithium-ion cell having a high energy density and excellent charge and discharge cycle characteristics (44).

The composition contains an additive serving as a solvent for a fluorine resin incorporated as an adhesive in a positive electrode containing a lithium-transition metal oxide capable of absorbing and releasing lithium and a negative electrode containing a carbon material capable of absorbing and releasing lithium. Further, a nonaqueous electrolytic solution comprising a lithium salt and an

nonaqueous solvent is added with the additive for a lithium-ion cell. A negative electrode was prepared as follows (44):

Preparation 2–3: A carbon-based material serving as a negative electrode active material was dispersed in *N*-methyl-2-pyrrolidinone as a solvent for poly(vinylidene fluoride) (PVDF) serving as adhesive, and stirred. The weight ratio of the carbon-based material to the fluorine resin was 95:5. After the mixture was formed as homogenous slurry, the slurry was applied onto one surface of a copper foil serving as a collector to obtain a negative electrode sheet. This negative electrode sheet was placed on a heat plate heated at 80°C, and dried for 10 *min*. Then, the dried negative electrode sheet was stored in a dry atmosphere.

2.4.9 Silicon

Silicon can be used instead of graphite as the active anode material (45,46). It is generally believed that silicon, when used as an active anode material in a lithium-ion rechargeable cell, can provide a significantly higher capacity than the commonly used graphite.

Crystalline silicon, when converted to the compound $Li_{21}Si_5$ by the reaction with lithium in an electrochemical cell, has a maximum theoretical capacity of 4,200 $mAh\,g^{-1}$. This is considerably higher than the maximum capacity for graphite. However there are several different Li–Si alloys that can be formed by lithium insertion, depending on the temperature, crystalline state, charge voltage and charge rates (47).

For example, at room temperature it is believed that the maximum achievable capacity is close to 3,600 $mAh\,g^{-1}$ with the alloy $Li_{15}Si_4$ (48). Thus, if graphite can be replaced by silicon in a lithium rechargeable battery, a substantial increase in stored energy per unit mass and per unit volume can be achieved. Unfortunately, silicon anode material in Li-ion cells undergoe a huge volume change between the charged and the discharged states associated with the insertion and removal of lithium ions into the silicon material during the charging and discharging stages of the cells.

The volume of a fully lithiated Li–Si alloy can be 3–4 times larger than the unalloyed silicon volume. This is much larger than the volume change seen in carbon anodes. As a consequence of such expansion and contraction, which on each cycle causes mechanical degradation of the silicon material and electrical isolation of sections, the electrodes can have a short cycle life (47).

A method for treating silicon to form pillars, in particular for its use as the active anode material in Li-ion batteries, has been described (49). The process for treating silicon is done in the following steps:

1. Exposing silicon-containing material to a solution comprising 2–3 *M* HF, 0.002 to 0.2 *M* of metal ions capable of nucleating on and forming a porous layer comprising regions of elemental metal on the silicon surface,
2. Etching with 0.04–0.07 *M* of an oxidant selected from the group comprising O_2, O_3, H_2O_2, the acid HF, ammonium or alkali metal salts of NO_3^-, $S_2O_8^{2-}$, NO_2^-, $B_4O_7^{2-}$, or ClO_4^-, or a mixture thereof. The treated silicon is suitably separated from the solution after the treatment.

At the beginning of the treatment process, etching occurs preferentially along certain crystal planes and the silicon is etched into columns. The silicon is etched according to the following equation:

$$Si + 6F^- \rightarrow SiF_6^{2-} + 4e^- \tag{2.1}$$

The electrons generated by this half reaction are conducted through the silicon to the nucleated silver where the counter reaction occurs in which silver ions in the solution are reduced to elemental silver:

$$4Ag^+ + 4e^- \rightarrow 4Ag \tag{2.2}$$

A lot of details and various aspects of the above treatment reaction have been given (49). For example, detached fibers can be obtained as follows:

Preparation 2–4: First, 36 *g* of AgNO3 is added to 3 *l* of a 2 *M* HF solution. Then, 12 *g* Si powder (Elkem Silgrain® 200-800 μm) is added through a funnel at top of the container and the mass is gently stirred by hand, through the hole in the lid using a rod, for 1 *min*. This reaction mixture is allowed to stand for 60 *min*. The concentration of HF in the etching solution is monitored during the etching step and further HF is added to the solution to maintain the concentration of HF at 2 *M*. The mat of silicon plus silver forms on the surface of the etch solution in the first 1–2 *min*.

At the end of the 60 *min*, 52 *g* $NaNO_3$ (or 48 *g* NH_4NO_3) is added. The $NaNO_3$ or NH_4NO_3 is dissolved in 50 *ml* water and then added through funnel at top. The mixture is gently stirred for a further 235 *min*. Then at 295 *min* from the start of the process, when the etching is almost completed, the spent etching solution starts to be pumped into a storage chamber, which takes about 4–5 *min*, and so the total etching time is about 300 *min*. Then the mat is washed with 3–4 *l* water three times. The first two washes are such that the water is in contact for five minutes, while the third wash is a 1 *min* wash.

The wet mat, which is composed of silicon and silver, should be promptly treated with nitric acid for 5–10 *min* to remove silver. The silicon is further washed and stored wet. The washing water contains silver and may be set aside to recover the silver content.

Fibers can be harvested from the resulting particles, with pillars attached, by ultrasonic vibration by placing the particles in a beaker or any appropriate container, covering the particles with an inert liquid such as ethanol or water and subjecting them to ultrasonic agitation. It is found that within several minutes the liquid is seen to be turbid and it can be seen by electron microscope examination that at this stage the pillars have been removed from the particle.

The pillars may be removed from the particle in a two-stage process. In the first stage, the particles are washed several times in water and, if necessary, dried in a low vacuum system to remove the water. In the second stage, the particles are agitated in an ultrasonic bath to detach the pillars. These are suspended in water and then separated using a centrifuge to collect the silicon fibers.

2.4.10 Carbon Nanotubes

Due to their unique properties, CNTs have attracted considerable attention since their discovery in 1991 by Iijima (50). Their high electrical conductivity, great mechanical strength, and low percolation threshold values make them attractive as additive materials for precipitates in lithium-ion batteries (51).

Recently, high performance $LiMn_{0.8}Fe_{0.2}PO_4$ was prepared with both etched and functionalized multi-walled CNTs and ketjenblacks (52). Ketjenblack® is an electroconductive carbon black from AKZO Chemicals B.V. Corp. In detail, the preparation was done as follows (52):

Preparation 2–5: The materials were synthesized using a chemical vapor deposition process that resulted in tubes with an average diameter of 10 *nm*, a length of 10 μm, and a purity of 95%. The functionalization with

carboxyl groups was carried out using a mixture of concentrated sulfuric acid and nitric acid at a ratio of 3:1, with a 3 *M* acid concentration. The CNTs were soaked in the acid solution at 80°C for 10 *h* and then washed with distilled water until the pH value of the filtrate reached 7. Finally, the CNTs were heated at 120°C overnight, under vacuum, to remove surface-adsorbed species such as water and hydrocarbons.

The multi-walled CNTs functionalized with carboxylic groups exhibited a better affinity toward cathode materials than pristine-based nanotubes. Also, the electrochemical performance of the $LiMn_{0.8}Fe_{0.2}PO_4$ cathode materials was improved by using multi-walled CNTs shortened by vigorous mechanical mixing, in comparison to pristine long multi-walled CNTs samples.

Moreover, the use of multi-walled CNTs together with Ketjenblacks showed better electrochemical performance than when Ketjenblacks or multi-walled CNTs were used separately (52). Ketjenblacks® are electroconductive carbon black powders with high surface areas, available from AkzoNobel.

2.4.11 Carbonate Additives

2.4.11.1 Methylene Ethylene Carbonate

The preparation of methylene ethylene carbonate and the incorporation of methylene ethylene carbonate into lithium-ion batteries as an electrolyte additive have been described (53).

Methylene ethylene carbonate can be prepared in a good yield by mercury-catalyzed cyclization (54). Mercuric triflate ($Hg(OTf)_2$), also called mercury(II) trifluoromethanesulfonate, is a powerful catalyst for the cyclization of alkynyl *tert*-butylcarbonates giving rise to cyclic enol carbonates under mild conditions. The synthesis is shown in Figure 2.10.

The addition of low concentrations of methylene ethylene carbonate of 1–2% to 1 *M* $LiPF_6$ in 3:7 ethylene carbonate/ethyl methyl carbonate improves the capacity retention of lithium-ion batteries cycled at an elevated temperature of 60°C.

XPS and Fourier transform infrared spectroscopy (FTIR) measurements of the electrodes indicated the presence of poly(methylene ethylene carbonate) on the anode surface. The modification of the anode solid electrolyte interphase correlates with significant improvements in the cycling performance at 60°C (53).

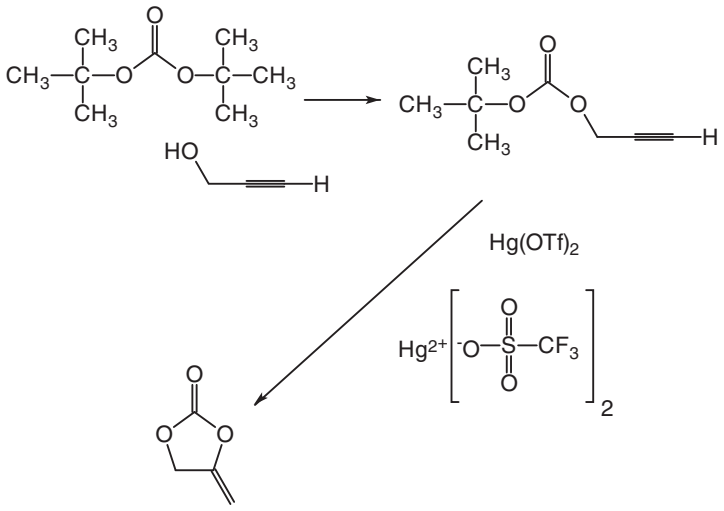

Figure 2.10 Synthesis of methylene ethylene carbonate (53).

2.4.11.2 Cyclic Carbonates

In silicone electrodes, a factor that affects the cell performance is the formation of a solid electrolyte interface layer on the silicon surface (47). Initially, the surface of the silicon material has a thin native oxide layer on it which has a low conductivity. During the first charge, this layer is replaced by a solid electrolyte interface layer of higher ionic conductivity formed from reactions with the electrolyte and reduction of the solvents.

The solid electrolyte interface can be composed of various different products, for example, Li_2CO_3, LiF, Li_2O, lithium alkyl carbonates, polymeric hydrocarbons and others. Each product will start forming at different stages of the charging process, depending on the anode potential.

A stable solid electrolyte interface layer with good ionic conductivity that can withstand the volume changes is essential to the proper working of the cells, and in this regard certain solid electrolyte interface products are much better than others.

A drawback of the solid electrolyte interface formation is that it consumes some of the lithium and electrolyte components, and ties them up in the system, preventing them from contributing to

the charge capacity of the cell. Excessive solid electrolyte interface formation will lead to an increased ionic resistance and degrade the cell performance. Therefore it is preferable to control the surface area and the surface area to volume ratio of the silicon anode material.

The solid electrolyte interface formation process can be influenced by the use of electrolyte additives. Cyclic carbonates containing a vinyl group, such as vinylene carbonate, halogenated cyclic carbonates, such as fluoroethylene carbonate, and difluoroethylene carbonate have been used as electrolyte additives. Other additives are silyl esters such as sultones, and esters of phosphoric and boric acid.

A halogenated cyclic carbonate is used as an additive which is suitably added to a base solvent comprising a mixture of a cyclic carbonate and a chain or linear carbonate. Preferably the base cyclic carbonate is ethylene carbonate and the linear carbonate is ethyl methyl carbonate or diethyl carbonate (47). Some carbonate compounds are shown in Figure 2.11.

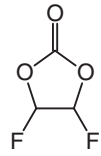

Difluoroethylene carbonate

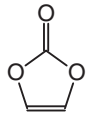

Vinylene carbonate

Figure 2.11 Cyclic carbonates.

Fluoroethylene carbonate. A method for reducing gas generation in lithium-ion batteries has been presented (55). The nonaqueous electrolyte contains 2–10% of fluoroethylene carbonate, and the electrolyte salts contain $LiBF_4$ and another electrolyte salt that is less consumed relative to $LiBF_4$ during the charge-discharge cycling, e.g., $LiPF_6$, $LiN(SO_2C_2F_5)_2$, and $LiN(SO_2CF_3)_2$.

The effects of a small amount of fluoroethylene carbonate $C_3H_3FO_3$ on the electrochemical performance of a lithium-rich layered oxide cathode have been assessed (56). When 1% or 2% by volume of $C_3H_3FO_3$ was introduced into the electrolyte, the cycling

performance and rate capability of the electrode was improved. Also, the initial irreversible capacity loss became smaller by suppressing the parasitic side reactions between the cathode and electrolyte.

However, an excess $C_3H_3FO_3$ of 5% leads to a decreased lithium transference number, large concentration polarization and a reduced discharge capacity, in particular at a high current.

Density functional calculations indicated that $C_3H_3FO_3$ enhances the antioxidation ability of the electrolyte system, and the preferential accumulation and reaction of $C_3H_3FO_3$ near cathode during charging due to the strong coordination between $C_3H_3FO_3$ and the PF_6^- anion (56).

2.4.12 Borate Additives

2.4.12.1 Lithium Bis(oxalato) Borate

Lithium bis(oxalato) borate was investigated as an additive for the stabilization of a high-voltage cathode electrolyte interface (57). It has been found that the electrochemical performance of $Li/LiNi_{0.5}Mn_{1.5}O_4$ cells with a lithium bis(oxalato) borate additive was improved at 60°C.

The effects of lithium bis(oxalato) borate on the electrolyte oxidative decomposition, the surface chemistry of separators and the cathodes cycled in electrolytes with and without a lithium bis(oxalato) borate additive were assessed using ATR-FTIR spectroscopy and XPS (57).

2.4.12.2 Trimethyl Borate and Triphenyl Borate

Alkyl-substituted and phenyl-substituted borate anion receptors have been investigated as electrolyte additives in lithium-ion batteries (58). These compounds, triphenyl borate and trimethyl borate, are shown in Figure 2.12.

As cathode $LiFePO_4$ was used and as electrolyte, 1 *M* $LiPF_6$ in a 1:1 mixture of ethylene carbonate and ethylene carbonate at 25°C and 60°C was used.

Triphenyl borate shows the formation of a thick surface/electrolyte interface which inhibits the ion flow and does not protect the electrode from degradation. Although useful at 25°C, triphenyl borate at 60°C results in only 7% capacity after 100 cycles.

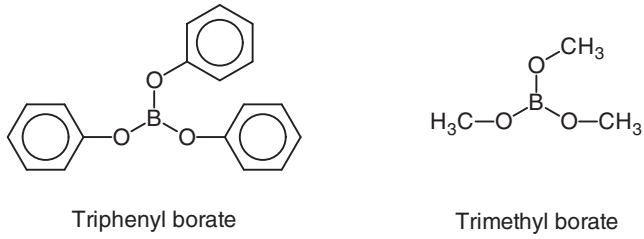

Figure 2.12 Borate-based anion receptors (58).

On the other hand, 0.1 *M* trimethyl borate results in 53% capacity. The trimethyl borate performance improves with increasing concentration. Trimethyl borate also suppresses the thermal decomposition of the electrolyte and the formation of the surface/electrolyte interface film (58).

2.4.12.3 Tris(trimethylsilyl) Borate

Tris(trimethylsilyl) borate is well known as a cathode electrolyte interphase (CEI) forming additive for improving the cycle performance of $LiCoO_2$/graphite lithium-ion batteries (59). Several borate derivatives have been tested as promising candidates for electrolyte interphase forming additives, resulting in a higher performance than tris(trimethylsilyl) borate.

This was determined via first-principles density functional calculations of the oxidation potentials, reduction potentials, and F-binding affinities. Actually, the computational screening protocol provides a faster method for the development of new electrolyte interphase forming electrolyte additives in lithium-ion batteries (59). Some properties of borates are shown in Table 2.3 and some compounds are shown in Figure 2.13.

The calculations were based on the *Kohn-Sham* density functional theory (60). This equation has become a popular method for calculating the molecular properties of organic molecules. The Kohn-Sham equation is the Schrödinger equation of a system of non-interacting particles, typically electrons (61).

Table 2.3 Highest occupied molecular orbitals (HOMO), lowest unoccupied molecular orbitals (LUMO), oxidation potentials (OP), reduction potentials (RP), and BE F^- binding affinity values in *eV*.

	HOMO	LUMO	OP	RP	BE
Boric acid	-8.78	0.96	9.00	-0.43	2.82
Trimethyl borate	-7.73	1.61	7.84	0.25	3.22
Triisopropyl borate	-7.58	1.22	7.66	0.08	3.38
Triethyl borate	-7.59	1.47	7.70	0.21	3.33
Triphenyl borate	-6.56	-0.51	6.52	0.79	4.72
Triethanolamine borate	-6.55	0.79	6.49	1.05	3.31
Tributyl borate	-7.61	1.44	7.74	0.23	3.40
Tris(trimethylsilyl) borate	-7.77	0.74	7.61	0.11	3.73
Tripropyl borate	-7.62	1.45	7.66	0.24	3.38
Tri-*tert*-butyl borate	-7.54	1.04	7.50	-0.76	3.35
Trimethylene borate	-7.30	0.91	6.81	1.02	3.94
Calcium metaborate	-8.50	-1.96	8.23	1.80	6.27
Potassium metaborate	-5.65	-1.56	7.12	1.13	2.49
Sodium borate	-6.40	-1.13	6.84	1.11	4.71
2-Aminoethoxydiphenyl borate	-6.71	-1.28	6.15	1.91	4.06
3-Pyridyltrimethylene borate	-6.79	-1.08	6.77	1.60	3.52
2-Octyl borate	-7.43	1.06	7.11	0.22	3.74
Triallyl borate	-7.17	-0.31	7.11	0.59	3.88
Tribenzyl borate	-6.76	-0.59	6.65	0.90	3.95
Trihexyl borate	-7.37	1.24	7.36	0.33	3.71
Trimethyallyl borate	-7.05	0.02	6.84	0.28	3.69
Tris(2-ethylhexyl) borate	-7.42	1.11	7.07	-0.05	3.76
Tris(3,3,5-trimethylhexyl) borate	-7.37	0.95	7.26	-0.87	3.47

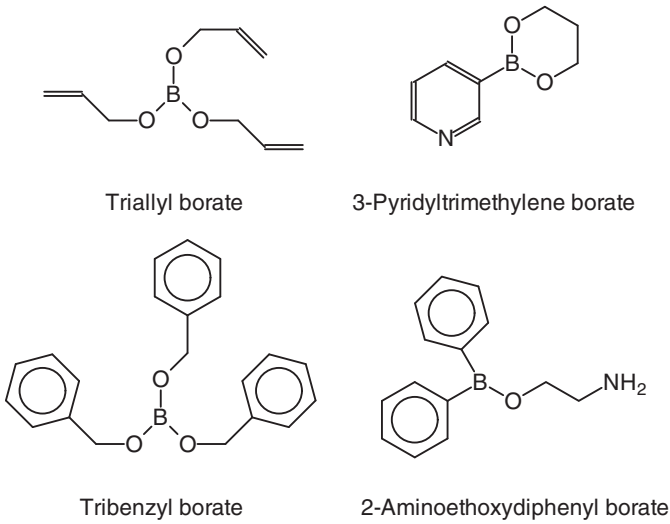

Figure 2.13 Borate compounds.

2.4.12.4 Lithium Difluoro(oxalato) Borate

Lithium difluoro(oxalato) borate was investigated as an electrolyte additive for high-voltage lithium-ion batteries in order to decrease the decomposition of the electrolyte (62).

As a typical high-voltage cathode material, $LiCoPO_4$ was tested in the lithium difluoro(oxalato) borate-containing electrolyte, exhibiting higher reversible charge/discharge capacity and better cyclic stability.

The effect of lithium difluoro(oxalato) borate on the formation of a stable interphase film was investigated through cyclic voltammetry (CV) and X-ray photoelectron spectroscopy. Lithium difluoro(oxalato) borate was helpful to form a stable interphase film and passivate the cathode surface. Therefore, the decomposition of the electrolyte could be inhibited (62).

2.4.12.5 Salicyclic Organoborate

The synthesis of a salicyclic organoborate is shown in Figure 2.14. The preparation of lithium bis[5-(2,4-difluorophenyl)salicylato-2-]-borate has been reported in detail as (63):

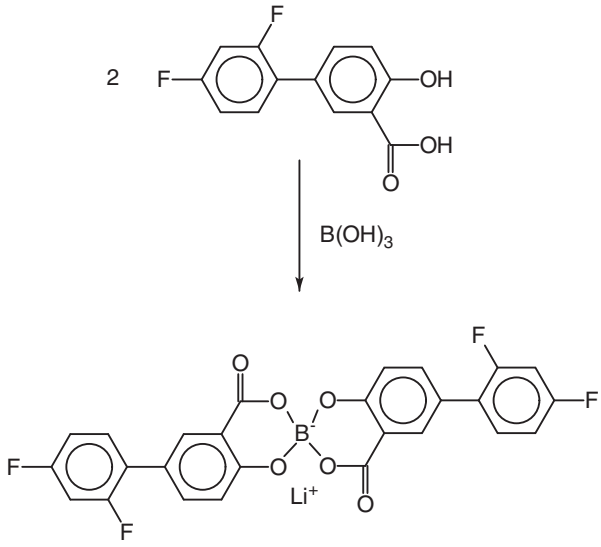

Figure 2.14 Synthesis of a salicyclic organoborate (63).

Preparation 2–6: First, 2.5 *g* (0.01 *mol*) of 5-(2,4-difluorophenyl)salicylic acid, 0.21 *g* (0.005 *mol*) of lithium hydroxide monohydrate, and 0.31 *g* (0.005 *mol*) of boric acid were put into a flask, and an acetonitrile/methanol (2:1 by volume) solvent was added thereto, preparing a mixed solution. The mixed solution was refluxed for 8 *h* and agitated at room temperature for one night. Next, the solution was concentrated down to 1/4 thereof and allowed to stand at room temperature, obtaining a white crystal. The white crystal was filtrated and recrystallized using an acetonitrile/methanol solvent. Then, the recrystallized product was dried in a 100°C vacuum oven for 24 *h*, obtaining lithium bis[5-(2,4-difluorophenyl)salicylato-2-]borate.

When lithium bis[5-(2,4-difluorophenyl)salicylato-2-]borate is added to an electrolyte, the compound may improve the electrochemical characteristics and the dissolution capability (63).

The electrolyte may further include an additive selected from lithium bis(oxalate)borate, lithium bis(salicylato)borate, and a combination thereof. These compounds improve the thermal stability of an electrolyte and the cycle life of a battery.

2.4.12.6 Trimethylboroxine

Trimethylboroxine, cf. Figure 2.15, has been tested as electrolyte additive to improve the electrode/electrolyte interface stability of $LiNi_{1/3}Co_{1/3}Mn_{1/3}O_2$ cathode for a high-voltage lithium-ion battery (64). Charge/discharge tests showed that addition of 3% trimethylboroxine is an optimal amount for these cathodes.

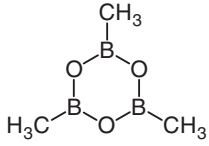

Figure 2.15 Trimethylboroxine.

After 300 cycles at 1C rate under the cut-off charge voltage of 4.5 *V*, the cathode with 3% trimethylboroxine reaches a capacity retention of 99%, in comparison to 40% of that using a standard electrolyte. It has been demonstrated that trimethylboroxine oxidizes preferentially and catalyzes the decomposition of base electrolyte subsequently, generating a thin and low impedance film on the cathode surface, which effectively stabilizes the electrode/electrolyte interface (64).

2.4.13 Tris(pentafluorophenyl) Borane

Tris(pentafluorophenyl) borane has been proposed as an electrolyte additive for silicon thin-film anodes in lithium-ion batteries (65). The introduction of tris(pentafluorophenyl) borane into the electrolyte consisting of 1 *M* lithium perchlorate ($LiClO_4$) in a mixture of ethylene carbonate and diethyl carbonate significantly enhances the capacity retention and the coulombic efficiency.

In particular, tris(pentafluorophenyl) borane enables the improvement of the properties by forming stable solid electrolyte interphase layers and suppressing a surface pulverization. The solid electrolyte interphase layers have been characterized by a variety of analytical tools, including SEM, EIS, and XPS (65).

The changes in properties, i.e., of Si thin-film cells with different

amounts of tris(pentafluorophenyl) borane during precycling, are shown in Table 2.4.

Table 2.4 Charge and discharge capacities and initial coulombic efficiencies (65).

Precycling	Tris(pentafluorophenyl) borane/[%]		
	0	2	5
Charge capacity /$mA\,h\,g^{-1}$	3125	3350	3968
Discharge capacity /$mA\,h\,g^{-1}$	1870	2003	2056
Initial coulombic efficiency /%	59.8	59.8	51.8

2.4.14 Phosphoric Additives

2.4.14.1 1-Propylphosphonic Acid

The cycling performance of graphite/$LiNi_{0.5}Co_{0.2}Mn_{0.3}O_2$ battery in the electrolyte with a different content from 0% to 2.0% of 1-propylphosphonic acid cyclic anhydride, cf. Figure 2.16, has been studied (66).

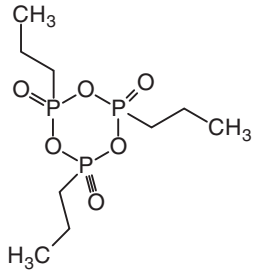

Figure 2.16 1-Propylphosphonic acid cyclic anhydride.

When 0.5% of 1-propylphosphonic acid cyclic anhydride is incorporated into the blank electrolyte, the capacity retention of graphite/$LiNi_{0.5}Co_{0.2}Mn_{0.3}O_2$ battery at high voltage after 100 cycles is increased from 79.12% to 91.84%.

EIS, X-ray diffraction (XRD), and XPS revealed a mechanism in which the surface film derived from the anhydride can decrease the

surface film impedance of the cell (from 40.63 to 16.57 Ω), stabilizing the structure of cathode material (66).

2.4.14.2 2-(Triphenylphosphoranylidene) Succinic Anhydride

The capacity of $LiMn_2O_4$/graphite-based Li-ion batteries (LIBs) at high temperatures can be improved by the addition of 2-(triphenylphosphoranylidene) succinic anhydride (67). This compound is shown in Figure 2.17.

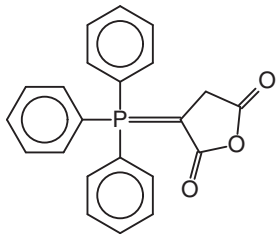

Figure 2.17 2-(Triphenylphosphoranylidene) succinic anhydride.

Unit cells with 0.1% of 2-(triphenylphosphoranylidene) succinic anhydride achieved a 43% capacity retention increase at high temperature operation, i.e., 55°C, 100 cycles, C/2 rate, in comparison to a control group without the additive, in order to understand the underlying principle of the enhanced capacity retention ability of the unit cells.

Investigation of the effect of 2-(triphenylphosphoranylidene) succinic anhydride suggested that the electrochemical decomposition of 2-(triphenylphosphoranylidene) succinic anhydride takes place on both surfaces of the $LiMn_2O_4$ and graphite during precycling, thereby reducing the decomposition reaction of the electrolyte during subsequent cycles (67).

2.4.14.3 Triphenyl Phosphate as Flame Retardant

Ever since lithium-ion batteries were first introduced on the market in 1991, their safety risks were already receiving a lot of attention (68). One of the main safety concerns is due to the usage of a highly flammable electrolyte due to the organic solvents combined with a

cell design aimed at maximizing the intrinsic high energy and power density. Abuse conditions, such as overcharge, overheating, or short circuit can lead to exothermic reactions. In the worst case a thermal runaway and fire may occur. The safety issues concerning fire risks resulted in the search for electrolytes with a reduced flammability (69).

A standard Li-ion battery electrolyte with different concentrations of the flame retardant triphenyl phosphate for high-power applications has been tested (68). The electrolyte characterization shows only a minor decrease in the electrolyte flammability for low triphenyl phosphate concentrations. The addition of triphenyl phosphate to the electrolyte leads to an increased viscosity and a decreased conductivity. The solvation of the lithium-ion charge carriers may be directly affected by the addition of triphenyl phosphate. This was found by Raman spectroscopy measurements and an increased mass transport resistivity.

Graphite/$LiFePO_4$ full cell tests showed that the energy efficiency decreased with the addition of triphenyl phosphate. Triphenyl phosphate influences the interface chemistry on both the positive and negative electrode. Higher concentrations of triphenyl phosphate lead to thicker interface layers on the $LiFePO_4$.

Even though triphenyl phosphate is not electrochemically reduced on graphite, it does participate in the formation of a solid electrolyte interphase. Thus, triphenyl phosphate cannot be considered as a suitable flame retardant for high-power applications, because there is only a minor impact of triphenyl phosphate on the flammability of the electrolyte at low concentrations of triphenyl phosphate. Further, a significant increase in polarization is observed for higher concentrations of triphenyl phosphate (68).

Phosphorous Pentasulfide. Phosphorous pentasulfide (P_2S_5) has been described as an electrolyte additive for high-energy lithium-sulfur batteries (70). P_2S_5 passivates the surface of metallic lithium anodes, promotes the dissolution of Li_2S, blocks the polysulfide shuttle, and thus enables a long battery cycle life.

An *in-situ* X-ray fluorescence microscopy combined with an X-ray absorption spectroscopy technique has been reported in order to investigate the Li_2S batteries during their electrochemical cycling (71). The evolution of morphology changes of the electrode is monitored

in real time using the X-ray fluorescence images, while the changes of the sulfur chemical state are characterized simultaneously using the X-ray absorption spectroscopy spectra.

Lithium-sulfur batteries suffer from a rapid capacity decay and low energy efficiency because of the low solubility of lithium sulfide (Li2S) in organic solvents and the intrinsic polysulfide shuttle phenomenon. Phosphorus pentasulfide (P_2S_5) in an organic electrolyte, has been shown to boost the cycling performance of lithium-sulfur batteries. The function of the additive is two-fold (72):

1. P_2S_5 promotes the dissolution of Li_2S and alleviates the loss of capacity caused by the precipitation of Li_2S, and
2. P_2S_5 passivates the surface of lithium metal and therefore eliminates the polysulfide shuttle phenomenon.

A lithium-sulfur test cell has shown a high reversible capacity of 900–1350 $mA\,h\,g^{-1}$ and a high coulombic efficiency of some 90% for at least 40 stable cycles at 0.1°C (72). It has been demonstrated to have a theoretical energy density of 2600 $Wh\,kg^{-1}$, which is about 3–5 times higher than that of the lithium-ion batteries. So Li−S batteries are promising for the next generation of high-energy batteries for large-scale energy storage (70).

Lithium-sulfur (Li_2S) batteries had been regaining tremendous interest because of their attractive attributes such as high gravimetric energy, low cost and environmental benignity (73).

However, it is still not conclusively known how polysulfide ring/chain participates in the whole cycling and whether the discharge and charge processes follow the same pathway. Herein, we demonstrate the direct observation of sulfur radicals by using *in-situ* electron paramagnetic resonance technique.

Based on the concentration changes of sulfur radicals at different potentials and the electrochemical characteristics of the cell, it has been revealed that the chemical and electrochemical reactions in Li_2S cell are driving each other to proceed through sulfur radicals, leading to two completely different reaction pathways during the discharging process and the charging process (73).

The proposed radical mechanism may provide new perspectives to investigate the interactions between sulfur species and the electrolyte, inspiring novel strategies to develop Li_2S battery technology (73).

2.4.15 Sulfur Additives

2.4.15.1 Methylene Methanedisulfonate

The capacity fading of $LiCoO_2$/graphite lithium-ion batteries that are cycled in the voltage range of 3.0–4.5 *V* can be reduced by methylene methanedisulfonate as an electrolyte additive (74). This compound is shown in Figure 2.18.

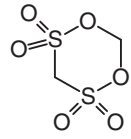

Figure 2.18 Methylene methanedisulfonate.

LSV and CV measurements indicated that methylene methanedisulfonate has a lower oxidation potential in the mixed solvents of ethylene carbonate and ethyl methyl carbonate. Further, it participates in the formation process of the CEI film.

The addition of 0.5% methylene methanedisulfonate into the electrolyte effects a significant increase of the capacity retention of the cells from 32.0% to 69.6% after 150 cycles Also, the rate capacity is improved in comparison to the cells without the methylene methanedisulfonate additive in the electrolyte.

The results of EIS, XPS and TEM indicated that the enhanced electrochemical performances of the cells can be ascribed to the modification of components of the cathode's surface layer in the presence of methylene methanedisulfonate. This results in the suppression of the electrolyte oxidized decomposition and the improvement of CEI conductivity (74).

2.4.15.2 3,3′-Sulfonyldipropionitrile

3,3′-Sulfonyldipropionitrile has been used as an electrolyte additive. It can enhance the performance of $LiNi_{1/3}Co_{1/3}Mn_{1/3}O_2$/ graphite batteries at high voltages (75).

The synthesis starts from acrylonitrile that is dimerized by sodium sulfide and in a second step the 3,3′-thiodipropionitrile is oxidized using hydrogen peroxide. The synthesis is shown in Figure 2.19.

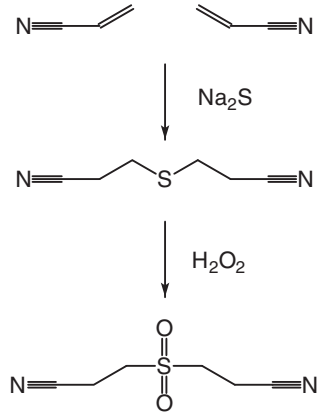

Figure 2.19 Synthesis of 3,3′-sulfonyldipropionitrile (75).

After adding 0.2% 3,3′-sulfonyldipropionitrile to the electrolytes, the capacity for a $LiNi_{1/3}Co_{1/3}Mn_{1/3}O_2$/graphite cell to retain power was significantly increased from 59.5% to 77.3% after only 100 cycles. This shows the promising application of 3,3′-sulfonyldipropionitrile at higher voltages.

It has been suggested that 3,3′-sulfonyldipropionitrile has a reduced oxidative constancy in comparison to ethylene carbonate, dimethyl carbonate and ethyl methyl carbonate. The improvement in the cycling activity could be ascribed to the thinner CEI film originated from 3,3′-sulfonyldipropionitrile electrode. This reduces the interfacial resistance at a high voltage, but also protects the decomposition of electrolytes and suppresses transition metal dissolution (75).

3,3′-Sulfonyldipropionitrile, cf. Figure 2.20, is structurally different from commonly used compounds as additives for an $LiMn_2O_4$ cathode, e.g., tris(pentafluorophenyl) borane (76), vinyl ethylene carbonate (77), fluoroethylene carbonate (78), hexamethyldisilazane (79), tris(trimethylsilyl) borate (80), or tris(trimethylsilyl) phosphate (81).

3,3′-Sulfonyldipropionitrile was studied as a film-forming additive for a $LiMn_2O_4$ cathode at elevated temperature. The retention capacity of the $LiMn_2O_4$/Li cell with the electrolyte (1.0 *M* $LiPF_6$ ethylene carbonate/dimethyl carbonate/ethyl methyl carbon-

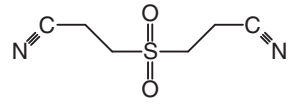

3,3´-Sulfonyldipropionitrile

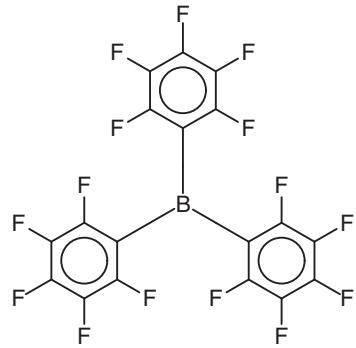

Tris(pentafluorophenyl) borane

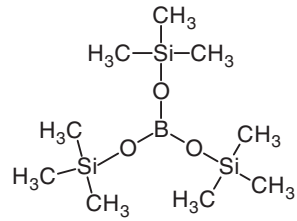

Tris(trimethylsilyl) borate

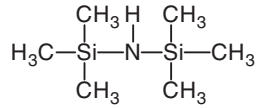

Hexamethyldisilazane

Figure 2.20 Additives for performance improvement.

ate) containing 0.5% 3,3′-sulfonyldipropionitrile cycled at 55°C and increased significantly from 56.7% to 70.3% after 200 cycles. The electrolyte solvents are shown in Figure 2.21.

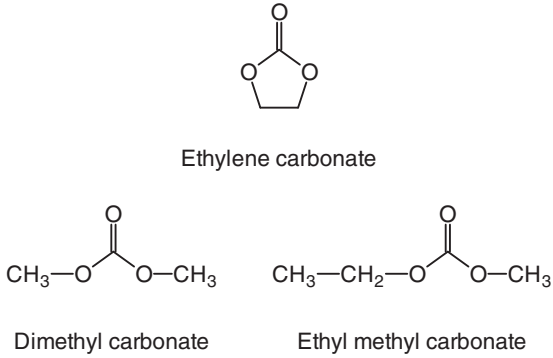

Figure 2.21 Electrolyte solvents.

The 3,3′-sulfonyldipropionitrile is more easily oxidized than the solvents, and may take part in the formation of the interface on the cathode surface (82).

The results of EIS and nuclear magnetic resonance spectroscopy show that the solid electrolyte interphase is gradually formed during cycling. XPS and TEM showed that a thinner solid electrolyte interphase with less inorganic degradation products can be formed on the surface of the $LiMn_2O_4$ cathode due to 3,3′-sulfonyldipropionitrile (82).

2.4.15.3 Sultones

Sultones are cyclic sulfonic esters. The term sultone arises from sulfonate lactone. Sultones, in particular 1,3-propane sultone, undergo alkylating reactions easily and are potential carcinogens (83–86).

Propane sultone. 1,3-Propane sultone is a versatile intermediate compound that can react with a wide variety of compounds to introduce a propane sulfonic functionality (87). 1,3-Propane sultone is shown in Figure 2.22. 1,3-Propane sultone is toxic, carcinogenic,

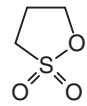

Figure 2.22 1,3-Propane sultone.

mutagenic, and teratogenic (86). The issues of synthesis and application of sultones have been reviewed (88).

The use of 1,3-propane sultone in an ethylene carbonate dimethyl carbonate electrolyte with $LiPO_4$ as a protective additive has been assessed during cathode material activation and cycling at a high potential (89).

The results showed that the presence of 1% 1,3-propane sultone ensured complete and better electrode activation during the first cycle. Capacities as high as 330 $mAhg^{-1}$ during charge and 275 $mAhg^{-1}$ during the discharge with a higher cut-off voltage of 5 V were found.

CV measurements demonstrated that activating at such a voltage enhanced the redox activity from Li_2MnO_3 activation. At the same time, the contribution of nickel and cobalt electroactivity is decreased at their regular voltage.

This feature was attributed to structural modifications occurring on the surface in the bulk of the material. Long-term cycling tests of the half-cells with 1,3-propane sultone provided a higher reversible capacity and superior capacity retention (89).

Disultones. The battery life of a lithium battery can be improved by using an organic electrolyte solution including a disultone-based additive. Disultones can be prepared as shown in Figure 2.23.

The preparation procedure has been described in detail as (90):

Preparation 2–7: A solution of 10.34 *g* (0.156 *mol*) of potassium hydroxide dissolved in 200 *ml* of ethanol was added dropwise into a solution of 50 *g* (0.154 *mol*) of pentaerythritol tribromide dissolved in 200 *ml* of ethanol, and the resulting mixture was refluxed for about 30 *min*. The resulting reaction product was cooled down to room temperature, and then filtered to remove KBr, followed by evaporating the ethanol. The residue was distilled in vacuum to obtain 28 *g* (0.115 *mol*) of 3,3-bis(bromomethyl)oxacyclobutane.

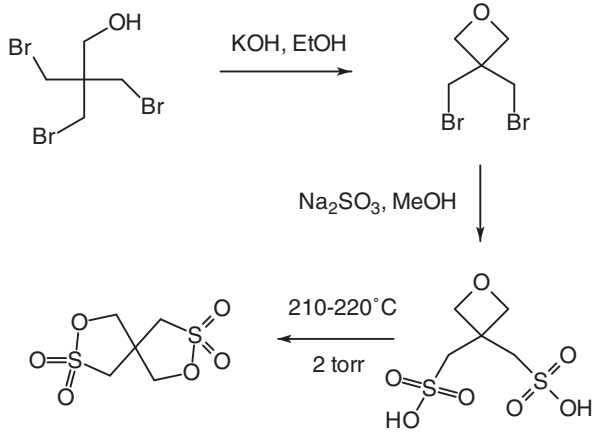

Figure 2.23 Preparation of disultones (90).

Then, 28 *g* (0.115 *mol*) of bis(bromomethyl)oxacyclobutane dissolved in a mixed solvent of 94 *ml* of methanol and 28 *ml* of water was added dropwise into a solution of 44.8 *g* (0.358 *mol*) of Na_2SO_3 dissolved in 252 *ml* of water. The resulting mixture was refluxed for about 3.5 *h*, and the solvent was removed under vacuum. The residue was treated with 200 *ml* of concentrated HCl, and filtered to remove NaCl, thereby obtaining a sulfonic acid solution, which was then evaporated in a vacuum. The resulting residue oil was heated at about 2 *torr* at about 210–220°C for about 2 *h* to obtain a black mass, which was then extracted with boiling dioxane and then filtered in the hot state. The filtrate was cooled down to crystallize 10 *g* of disultone.

Various derivates are advantageous. A sulfonate ester group may be included in the disultone-based compound shown in Figure 2.23. This group may be reduced by itself by accepting electrons from a surface of an anode during charging, or may react with a previously reduced polar solvent molecule, thereby affecting characteristics of a solid electrolyte interface layer on a surface of the anode. For instance, a disultone-based derivate may be reduced at a lower voltage than a polar solvent before the polar solvent is oxidized.

2.4.15.4 *Di(methylsulfonyl) Methane*

In order to overcome the capacity fading of $LiNi_{1/3}Co_{1/3}Mn\_1/3O_2$ graphite lithium-ion batteries cycled in the voltage range of 3.0–4.6 *V*, di(methylsulfonyl) methane, cf. Figure 2.24, has been evaluated as electrolyte additive (91).

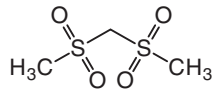

Figure 2.24 Di(methylsulfonyl) methane.

The experiments indicated that di(methylsulfonyl) methane in the electrolyte can dramatically improve the cycling performance of a $LiNi_{1/3}Co_{1/3}Mn\_1/3O_2$/graphite cell at a higher voltage operation. Due to the addition of 0.1% di(methylsulfonyl) methane into the electrolyte, the capacity loss of the $LiNi_{1/3}Co_{1/3}Mn\_1/3O_2$/graphite cell cycled at the voltage range of 3.0–4.6 *V* significantly decreased from 39.0% to 19.9% after 100 cycles. This demonstrates a promising application of di(methylsulfonyl) methane at a higher voltage.

The enhanced cycling performance has been attributed to the thinner cathode electrolyte interface film originated from di(methylsulfonyl) methane on the $LiNi_{1/3}Co_{1/3}Mn\_1/3O_2$. This not only results in a lower interfacial impedance, but also protects the decomposition of electrolyte and so prevents the cathode transition metal dissolution at high voltages (91).

2.4.15.5 *Thiophene*

It has been shown that the addition of thiophene improves the cycle life of lithium-ion cells at high voltage (92). The electrolyte solution used was 1 *M* $LiPF_6$ in ethylene carbonate and diethyl carbonate (3:7 by volume). Thiophene was added at 0.1% to the electrolyte solution. The cathode was prepared by coating an *N*-methyl-2-pyrrolidone-based slurry with $LiCoO_2$, PVDF, and conductive carbon black.

The results of EIS suggest that the addition of thiophene significantly suppresses the increase of the charge transfer resistance

that occurs during cycling up to a high voltage. Differential scanning calorimetry studies showed that the thermal stability of a fully charged $LiCoO_2$ cathode was also enhanced in the presence of thiophene (92).

2.4.16 Isothiocyanates

Additives for a rechargeable lithium battery electrolyte capable of improving charge and discharge characteristics and cycle life characteristics have been described (93). These are aromatic compounds bearing an isothiocyanate group. Suitable isothiocyanates are summarized in Table 2.5 and shown in Figure 2.25.

Table 2.5 Isothiocyanates (93).

Compound
Phenyl isothiocyanate
4-Nitrophenyl isothiocyanate
Trifluoromethyl phenyl isothiocyanate
4-Cyanophenyl isothiocyanate
4-Methoxyphenyl isothiocyanate
4-Fluorophenyl isothiocyanate
4-Methylphenyl isothiocyanate
2-Fluoro-5-(trifluoromethyl)phenyl isothiocyanate
4-Methyl-3-(trifluoromethyl)phenyl isothiocyanate
4-Fluoro-3-(trifluoromethyl)phenyl isothiocyanate
3,5-Bis(trifluoromethyl)phenyl isothiocyanate
1,4-Phenylene diisothiocyanate

The aromatic compound may be included in an amount of about 0.01–1% based on the total amount of the rechargeable lithium battery electrolyte. By including an electrolyte containing such additives, the charge and discharge characteristics and the cycle life characteristics of the rechargeable lithium battery may be improved.

The aromatic compound with an isothiocyanate group can be reduced and decomposed at the initial charge of rechargeable lithium battery to provide a stable solid electrolyte interface passivation film on the negative electrode surface. This passivation film may improve the cycle life characteristics of the lithium battery and may suppress lowering the discharge capacity at a low temperature and swelling when allowed to stand at a high temperature.

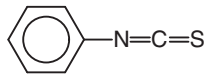

Phenyl isothiocyanate

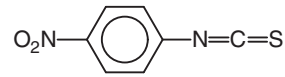

4-Nitrophenyl isothiocyanate

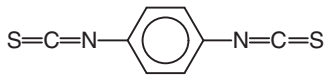

1,4-Phenylene diisothiocyanate

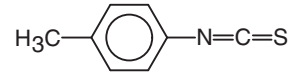

4-Methylphenyl isothiocyanate

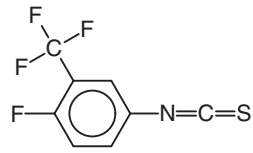

4-Fluoro-3-(trifluoromethyl)phenyl isothiocyanate

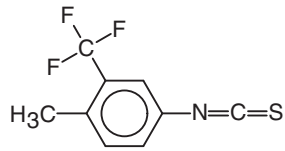

4-Methyl-3-(trifluoromethyl)phenyl isothiocyanate

Figure 2.25 Isothiocyanates.

The polymerization reaction that produces a solid electrolyte interface is shown in Figure 2.26.

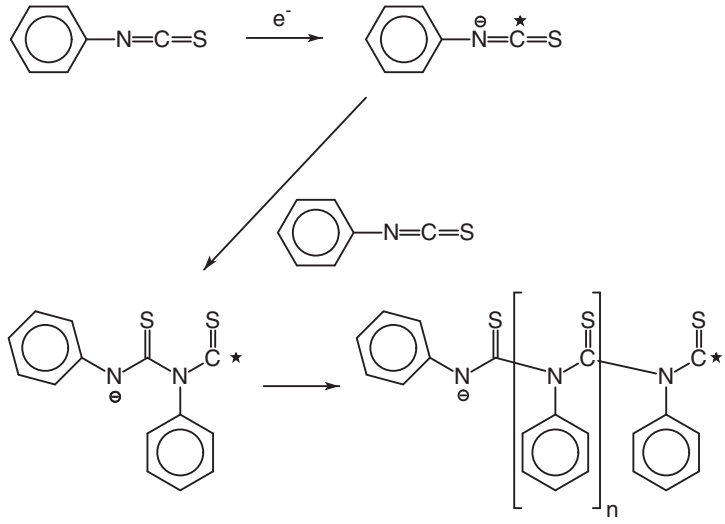

Figure 2.26 Polymerization of an isothiocyanate.

Here, the isothiocyanate containing aromatic compound receives electron on the negative electrode surface and is reduced to a radical. The thus produced radical acts as a polymerization initiator in the polymerization reaction. In addition, since the radical is continuously easily produced with the polymerization reaction, the polymerization reaction may be continuously occurring. In this way, a solid electrolyte interface film may be produced on the negative electrode surface. It has been found that the reduction potential of 4-nitrophenyl isothiocyanate was remarkably lower than the reduction potential of ethylene carbonate (93).

2.4.17 Other Additive Types

2.4.17.1 Bismaleimide

A *N*,*N*′-4,4′-diphenylmethane-bismaleimide (BMI) compound, cf. Figure 2.27, has been tested for the enhancement of the high-voltage performance of lithium-ion batteries (94).

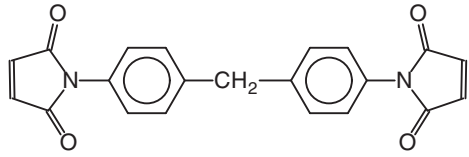

Figure 2.27 *N*,*N*′-4,4′-diphenylmethane-bismaleimide.

When only 0.1% (m/v) BMI is added into the control electrolyte, the high-voltage cycling performance of $LiCoO_2$/Li cells is improved evidently while charging the cell up to 4.5 *V* rather than the conventional 4.2 *V*.

SEM and XPS measurements showed that an interface film is formed on the cathode surface from BMI in electrolyte. AC impedance spectra and charge/discharge test were tested after incubation of the charged cell at 60°C. LSV was used to test the electrochemical stability window of the electrolyte with the addition. The results demonstrate that the improvement of high-voltage performance is attributed to the surface film on cathode.

In addition, the addition of BMI does not cause damage in conventional performance with 4.2 *V* electrochemical window. The addition of BMI to the electrolyte provides a high-voltage cycling performance with 4.5 *V* electrochemical window, suggesting the $LiCoO_2$ battery as a simple and promising system for applications with high energy density (94).

A branched oligomer from *N*-phenylmaleimide and bismaleimide was tested as additive in lithium-ion batteries in order to increase the safety performance by reducing the probability of batteries suffering an internal short circuit (95).

Several safety tests for batteries have been described (96). In the nail penetration test, a $LiCoO_2$/mesocarbon microbeads full battery with the branched oligomer showed a significant improvement in the thermal stability and was able to restrain the temperature of the battery at about 85°C. The nail penetration test was conducted according to the standard procedure described in UL1642 (97) and SBA G1101 (98). An internal short circuit occurs upon nail penetration, and the thermal runaway behavior can be observed if there is no mechanism to quench the heat or stop the chain reaction quickly.

Furthermore, it was found that the branched oligomer showed a better cycling and electrochemical performance in comparison to a battery with a bismaleimide-containing branched oligomer in the electrolyte.

This improvement could be effected by the favorable ionic conductivity, Li-ion mobility and lower resistance in the battery. So, this additive can meet the cycling performance and safety requirements for Li-ion batteries (95).

2.4.17.2 Allyloxytrimethylsilane

The commonly used $LiPF_6$ in current electrolytes is very susceptible to hydrolysis even if trace amounts of water are present in the electrolyte (99):

$$LiPF_6 + H_2O \rightarrow POF_3 + LiF + 2HF \tag{2.3}$$

The electrochemical performance of a high voltage $LiNi_{0.5}Mn_{1.5}O_4$ cell could be improved by the addition of the electrolyte additive allyloxytrimethylsilane, cf. Figure 2.28 (100).

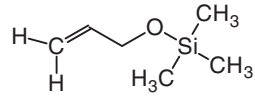

Figure 2.28 Allyloxytrimethylsilane.

In the presence of 0.5% allyloxytrimethylsilane, the discharge capacity retention of the $Li/LiNi_{0.5}Mn_{1.5}O_4$ cell is improved from 73.1% to 80.2% after 500 cycles at room temperature, and from 52.4% to 92.5% after 100 cycles at 55°C.

In addition, the $Li/LiNi_{0.5}Mn_{1.5}O_4$ cell with allyloxytrimethylsilane has a superior discharge capacity of 95.6 $mAhg^{-1}$ at a high rate of 3 C, whereas a cell without allyloxytrimethylsilane only has 76.8 $mAhg^{-1}$ discharge capacity.

Theoretical calculations and experimental results indicated that allyloxytrimethylsilane is oxidized prior to the carbonate solvents during the first charge process and then creates a less resistive and

high thermal stability of solid electrolyte interface film on the surface of $LiNi_{0.5}Mn_{1.5}O_4$ cathode. The solid electrolyte interface film from allyloxytrimethylsilane, composed of organic silicon-based species, ether moieties and reduced LiF, is responsible for the suppression of the electrolyte decomposition and dissolution of transition metal ions at high voltage, in particular at a high temperature (100).

2.4.17.3 Chitosan

Chitosan with abundant hydroxyl and amine groups as an additive for cathodes and separators has been proven to be an effective polysulfide trapping agent in lithium-sulfur batteries (101).

In comparison to common sulfur cathodes, a cathode with chitosan shows an enhanced initial discharge capacity from 950 to 1145 $mA\,h\,g^{-1}$. The reversible specific capacity after 100 cycles increases from 508 $mA\,h\,g^{-1}$ to 680 $mA\,h\,g^{-1}$ and 473 to 646 $mA\,h\,g^{-1}$ at rates of C/2 and 1 C, respectively (101).

In addition, batteries with separators that are coated with a carbon/chitosan layer can exhibit a high discharge capacity of 830 $mA\,h\,g^{-1}$ at C/2 after 100 cycles and 675 $mA\,h\,g^{-1}$ at 1 C after 200 cycles with the capacity fading to as low as 0.11% per cycle.

It has been demonstrated that chitosan is beneficial not only for lithium-sulfur batteries, but also other sulfur-based battery applications (101).

2.4.17.4 1,2-Bis(difluoromethylsilyl)ethane

In the case of graphite/$LiMn_2O_4$ lithium-ion batteries, the charge/discharge capacity retention during high temperature cycling at 60°C could be successfully improved by the addition of 1,2-bis(difluoromethylsilyl)ethane into the electrolyte (102). In addition, the additive suppresses the self-discharge in a storage test at 60°C for 7 *d*.

Surface analysis showed that a silicon and fluorine-containing thin layer is formed by the decomposition of 1,2-bis(difluoromethylsilyl)ethane, cf. Figure 2.29. This effectively protects the graphite negative electrode during the high temperature cycling and storage.

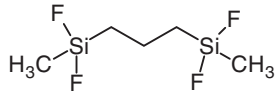

Figure 2.29 1,2-Bis(difluoromethylsilyl)ethane.

The silicon-containing and fluorine-containing surface layer suppresses the degradation of the negative electrode caused by deposition of manganese, resulting from Mn^{2+} dissolution from $LiMn_2O_4$, and so prevents the self-discharge due to an excess decomposition of the electrolyte on the surface (102).

2.4.17.5 Surface Stability Enhancers

Several types of additives have been tested to enhance the surface stability of high-Ni-content cathodes with a content greater than 60%. The additive candidates with different chemical functionalities that have been tested are shown in Table 2.6 and in Figure 2.30.

Table 2.6 Additive used for testing (103).

Compound	Functional group
Vinylene carbonate	Alkenyl group
Succinonitrile	Nitrile group
Propene sulfone	Sulfone and alkenyl groups
Propane sulfone	Sulfone group

The additives were added in amounts of 2%. All additives improved the behavior of the electrodes to a certain extent. The most effective additive was found to be propane sulfone. The cycle performance in the presence of 2% propane sulfone is highly improved at a high temperature of 60°C and 98.9% of its initial capacity is preserved. The increase in thickness is only 17.9%, thus preventing undesired swellings. Further gases are not generated in large amounts with the internal pressure being 56.4 *kPa* (103).

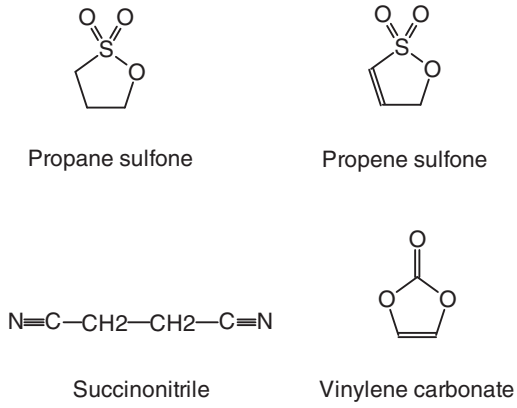

Figure 2.30 Additive used for testing (103).

2.4.17.6 Storage Stability Enhancement

An electrolyte for a rechargeable lithium battery with excellent storage stability at a high temperature has been described (104). The electrolyte for a rechargeable lithium battery includes a nonaqueous organic solvent, a lithium salt, and an additive. The additive includes vinylene carbonate, fluoroethylene carbonate, and a nitrile-based compound.

The electrolyte may include mixtures of carbonate-based solvents and aromatic hydrocarbon-based solvents. The carbonate-based solvents and the aromatic hydrocarbon-based solvents are preferably mixed together in a volume ratio of 1:1 to 30:1. Suitable carbonate-based solvents are summarized in Table 2.7.

Suitable aromatic hydrocarbon-based nonaqueous organic solvents are summarized in Table 2.8 and in Figure 2.31.

Nitrile-based compounds are summarized in Table 2.9 and shown in Figure 2.32.

When vinylene carbonate was included at an amount of 0.01–9% and fluoroethylene carbonate was included at an amount of 0.1–7%, and a nitrile-based compound, such as adiponitrile, was included in an amount of 0.005–10% to prepare an electrolyte, a cell including the electrolyte demonstrated an excellent storage stability even at a high temperature (104).

Table 2.7 Carbonate-based solvents (104).

Compound	Compound
Dimethyl carbonate	Diethyl carbonate
Dipropyl carbonate	Methylpropyl carbonate
Ethylpropyl carbonate	Methylethyl carbonate
Ethyl methyl carbonate	Ethylene carbonate
Propylene carbonate	Butylene carbonate
Methyl acetate	Ethyl acetate
Propyl acetate	Dimethyl acetate
Methyl propionate	Ethyl propionate
γ-Butyrolactone	Decanolide
Valerolactone	Caprolactone
Dibutyl ether	Tetraglyme
Diglyme	Dimethoxyethane
2-Methyltetrahydrofuran	Tetrahydrofuran
Cyclohexanone	Ethyl alcohol
Isopropyl alcohol	Dimethylformamide
1,3-Dioxolane	

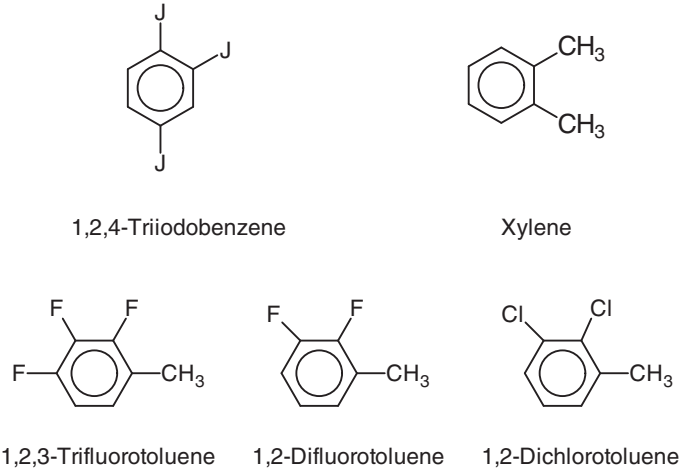

Figure 2.31 Aromatic hydrocarbon-based nonaqueous organic solvents.

Table 2.8 Aromatic nonaqueous organic solvents (104).

Compound	Compound
Benzene	Fluorobenzene
1,2-Difluorobenzene	1,3-Difluorobenzene
1,4-Difluorobenzene	1,2,3-Trifluorobenzene
1,2,4-Trifluorobenzene	Chlorobenzene
1,2-Dichlorobenzene	1,3-Dichlorobenzene
1,4-Dichlorobenzene	1,2,3-Trichlorobenzene
1,2,4-Trichlorobenzene	Iodobenzene
1,2-Diiodobenzene	1,3-Diiodobenzene
1,4-Diiodobenzene	1,2,3-Triiodobenzene
1,2,4-Triiodobenzene	Toluene
Fluorotoluene	1,2-Difluorotoluene
1,3-Difluorotoluene	1,4-Difluorotoluene
1,2,3-Trifluorotoluene	1,2,4-Trifluorotoluene
Chlorotoluene	1,2-Dichlorotoluene
1,3-Dichlorotoluene	1,4-Dichlorotoluene
1,2,3-Trichlorotoluene	1,2,4-Trichlorotoluene
Iodotoluene	1,2-Diiodotoluene
1,3-Diiodotoluene	1,4-Diiodotoluene
1,2,3-Triiodotoluene	1,2,4-Triiodotoluene
Xylene	

Table 2.9 Nitrile-based compounds (104).

Compound	Compound
Succinonitrile	Glutaronitrile
Adiponitrile	Pimelonitrile
Suberonitrile	

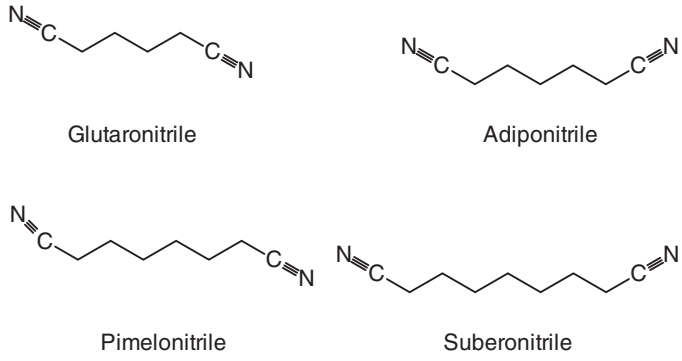

Figure 2.32 Nitrile-based compounds.

2.4.17.7 Polyalkyleneglycol Diglycidylether

It has been found that a lithium secondary battery with a noticeably improved high-temperature performance and lifespan characteristics can be fabricated by adding a polyalkyleneglycol diglycidylether to the electrolyte of the battery (105).

When a battery is stored or used at a high temperature, a decomposition reaction between an electrode and an electrolyte of the battery may be decreased. This in turn reduces considerably the gas generated thereby, so that deterioration of a cycle at elevated temperature or a capacity reduction caused by high temperature storage of the battery may be significantly decreased. In addition, thickness swelling of the battery may be inhibited. Moreover, the battery containing the electrolyte does not suffer from a performance deterioration, thus exhibiting enhanced safety. The polyalkyleneglycol diglycidylether used is shown in Figure 2.33.

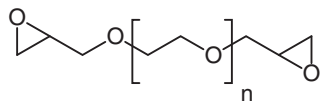

Figure 2.33 Polyalkyleneglycol diglycidylether.

If the amount of the additive is too small, the additive may have

little effect. Conversely, when the amount is too large, a viscosity of the electrolyte may be increased, while a battery manufactured using the electrolyte may exhibit high resistance, causing undesirable deterioration in performance of the battery (105).

The electrolyte may include a nonaqueous electrolyte and an aprotic organic solvent. These compounds are summarized in Table 2.10. Some compounds are shown in Figure 2.34.

Table 2.10 Nonaqueous electrolytes and aprotic organic solvents (105).

Compound	Compound
N-Methyl-2-pyrrolidinone	Propylene carbonate
Ethylene carbonate	Butylene carbonate
Dimethyl carbonate	Diethyl carbonate
Ethyl methyl carbonate	γ-Butyrolactone
1,2-Dimethoxyethane	Tetrahydrofuran
2-Methyltetrahydrofuran	Dimethylsulfoxide
1,3-Dioxolane	Formamide
Dimethylformamide	1,3-Dioxolane
Acetonitrile	Nitromethane
Methyl formate	Methyl acetate
Phosphoric acid triester	Trimethoxy methane
Sulfolane	Methyl sulfolane
1,3-Dimethyl-2-imidazolidinone	

2.5 Nickel Batteries

Large-scale electrical energy storage systems are needed to accommodate the intrinsic variability of energy supply from solar and wind resources. Such energy storage systems will store the excess energy during the periods of electricity production, and they release the energy during the periods of electricity demand. Viable energy storage systems will have to meet the following requirements (106):

- Low installation cost of smaller than 100 USD per kWh,
- A long operating life of more than 5000 cycles,
- High round-trip energy efficiency of over 80%, and
- Ease of scalability to megawatt-hour level systems.

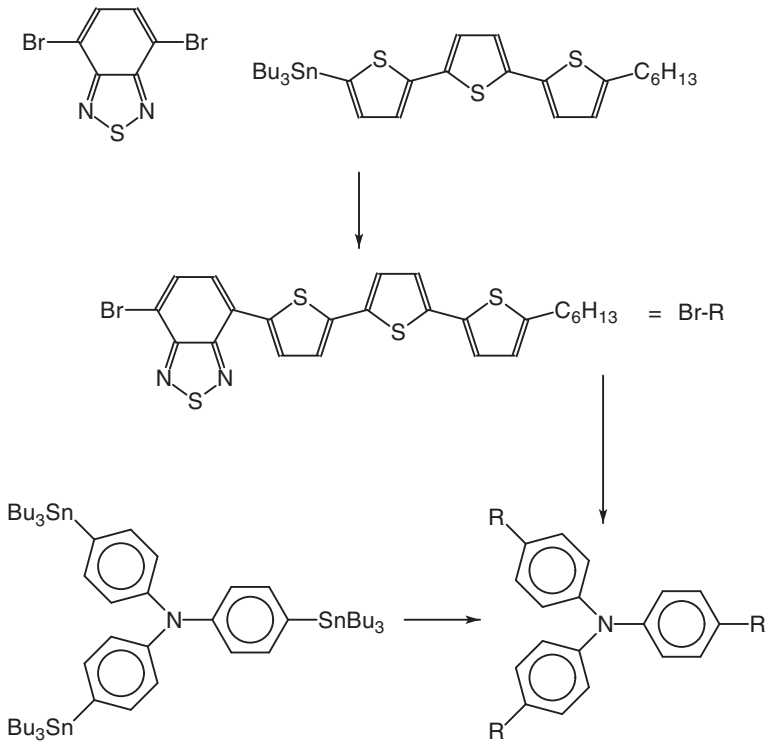

Figure 2.36 Synthesis of star molecules (121).

Rechargeable batteries are particularly suitable for such large-scale storage of electrical energy because of their high round-trip efficiency and scalability. Suitable types of rechargeable batteries are vanadium-redox, sodium-sulfur, zinc-bromine, zinc-air and lithium-ion batteries.

However, with regard to durability, cost, and large-scale implementation, the beneficial features of iron-based alkaline batteries for large-scale energy storage have been largely overlooked.

Nickel-iron batteries have been used in various stationary and mobile applications for more than 70 *y* in the USA and Europe until the 1980s. Then, the iron-based batteries were largely supplanted by sealed lead-acid batteries. Because of their high specific energy, iron-air batteries again underwent active development for electric vehicles and military applications in the 1970s, but this was discontinued after 1984 (21).

The electrochemistry of the iron electrode in alkaline batteries involves the redox process involving iron (II) hydroxide and elemental iron:

$$Fe(OH)_2 + 2e^- \rightarrow Fe + 2OH^- \qquad E^o = -0.877V \qquad (2.4)$$

Iron, the primary raw material for iron-based battery systems, is globally abundant, relatively inexpensive, can be easily recycled, and is eco-friendly.

Also, the iron electrode is well known for being robust over repeated cycles of charge and discharge. Stable performance over 3000 charge and discharge cycles has been demonstrated in nickel-iron batteries. Such robustness is extraordinary as most rechargeable battery electrodes degrade within 1000 cycles. The robustness of the iron electrode is attributed to the low solubility of the hydroxides of iron in alkaline media. The principal limitation of the iron electrode is its low charging efficiency that is in the range of 55–70%. This limitation arises from the wasteful hydrogen evolution that occurs during charging according to the following reaction:

$$2H_2O + 2e^- \rightarrow H_2 + 2OH^- \qquad E^o = -0.828V \qquad (2.5)$$

$$Fe + 2H_2O \rightarrow Fe(OH)_2 + H_2 \quad (2.6)$$

On the other hand, a self-discharge during the idle stand of the battery can occur as follows:

The hydrogen evolution reaction occurs because the electrode potential for this reaction is positive to that of the iron electrode reaction (Eq. 2.4). Therefore, these batteries will have to be overcharged by 60–100% to achieve their full capacity. The hydrogen evolution that occurs during charging is undesirable because it lowers the round-trip energy efficiency and results in loss of water from the electrolyte.

Thus, suppressing the hydrogen evolution at the iron electrode has important benefits of raising the overall energy efficiency, lowering the cost, and increasing the ease of implementation of iron-based batteries in large-scale energy storage systems.

However, suppressing hydrogen evolution and achieving an iron electrode with a charging-efficiency close to 100%, without interfering with the other performance features of the electrode, has been a formidable challenge for many years (106).

Another limitation of commercially available iron batteries is their inability to be discharged at high rates. When discharged in less than five hours (also termed the five-hour rate), the capacity realized is very small.

Grid-scale electrical energy storage requires that the battery be capable of being charged and discharged in one to two hours. The discharge rate capability of the iron electrode can be improved if the passivation by the electrically non-conductive iron (II) hydroxide can be achieved (107, 108).

Additives and formulations that can overcome the above-mentioned problems have been reported (106). In one formulation, the electrodes may include 50–99% carbonyl iron, approximately 5–50% of potassium carbonate or a similar soluble additive that creates pores when dissolved, and approximately 5–30% of a polymeric binder such as a poly(ethylene) binder. Alternatively, a portion of the carbonyl iron, such as approximately 5%, may be substituted with bismuth sulfide. The powder mixture may be spread on a metallic grid, such as a degreased nickel grid or a nickel coated steel

grid, and pressed at a temperature of about 140°C and a pressure of about 5 $kp\,cm^{-2}$.

Carbonyl iron does not contain the common impurities, such as manganese, sulfur and phosphorus, that are present in the reduced oxides. These impurities decrease the hydrogen overpotential and facilitate hydrogen evolution by increasing the ease of formation of adsorbed hydrogen species on the surface of iron.

A further decrease in the rate of hydrogen evolution has been achieved by the addition of bismuth sulfide to the carbonyl iron material. Bismuth sulfide is an electrically conducting solid, insoluble in the potassium hydroxide electrolyte. During charging, the bismuth sulfide is transformed into elemental bismuth:

$$Bi_2S_3 + 6e^- \rightarrow 2Bi + 3S^{2}- \qquad E^o = -0.818V \qquad (2.7)$$

The electrode potential for the reduction of bismuth sulfide to bismuth is more positive than that of the iron electrode reaction (Eq. 2.7) and thus the charging process conducted at $-1\ V$ facilitates the formation of elemental bismuth.

According to Eq. 2.6, iron is responsible for the hydrogen formation in the presence of water. So it can be concluded that the suppression of the hydrogen evolution reaction can be achieved by excluding water from the surface of the iron electrode.

Alkanethiols and other organo-sulfur compounds are known to form a self-assembled monolayer on various metal surfaces through the interaction of the sulfur atom of the thiol with various metals. Such self-assembled layers can be very compact and water repellent and can substantially reduce the access of reactants to the electrode solution interface. Therefore, such self-assembled monolayers of alkanethiol formed on an iron surface may inhibit the hydrogen evolution reaction.

Since the properties of self-assembled monolayers depend on chain length of the alkanethiol, the degree of suppression of the hydrogen evolution reaction will depend on the molecular structure of the alkanethiol. If the self-assembled layer is too compact, then the total exclusion of water from the surface will also inhibit all the electrochemical processes, including the desirable process of charging the battery electrode (Eq. 2.4). It is therefore important

to identify the optimal chain length of alkanethiol that can achieve inhibition but not a complete blockage of the surface reactions.

Several different organo-sulfur additives have been investigated for suppressing the hydrogen evolution during charging of the iron electrode. Oxidation resistance and suppression of hydrogen evolution is also offered by *p*-dithiane, bis(methylthio)methane, 1-octanethiol, sodium 1-propanethiolate, and hexanethiol. These compounds are listed in Table 2.11 and in Figure 2.35.

Table 2.11 Organo-sulfur compounds (106).

Additive	Additive
1,2-Ethanedithiol	Hexanethiol
Bis(methylthio)methane	2-Methyl benzene thiol
1-Octanethiol	1-Dodecanethiol
p-Dithiane	Sodium 1-propanethiolate
3,6-Dioxa-1,8-octanedithiol	2,2′-(Ethylenedioxy)diethanethiol

It was observed that 2-methyl benzene thiol suppresses the hydrogen adsorption on platinum and iron. 1,2-Ethanedithiol and 2,2′-(ethylenedioxy)diethanethiol adsorb strongly on platinum electrodes, suppress the adsorption of hydrogen from water, and also resist oxidative degradation. However, iron electrodes only show a five to ten times increase in polarization resistance and five to ten times reduction in double-layer capacitance. Therefore, 1,2-ethanedithiol and 2,2′-(ethylenedioxy)diethanethiol are considered as promising additives for improving the charge efficiency of the iron electrode (106).

2.5.1 High-Rate Discharge Performance

The effects of flaky rare earth oxide additives, including Er_2O_3, Tm_2O_3, Yb_2O_3, and Lu_2O_3, on the high temperature and high-rate discharge performance of nickel electrodes were investigated (109).

The discharge efficiency at 0.2*C* reached 96% at 60°C for electrodes using 1% flaky rare earth oxides. The high-rate discharge performance for electrodes with flaky rare earth oxides could be improved significantly. For example, the discharge efficiency at 5 *C* improved from 50% to 70%. A C-rate of 0.2*C* is also known as a five-hour discharge; 5*C* corresponds to 12 *min* discharge time (110).

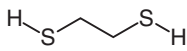

1,2-Ethanedithiol

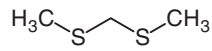

Bis(methylthio)methane

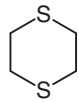

p-Dithiane

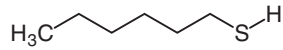

Hexanethiol

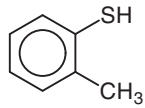

2-Methyl benzene thiol

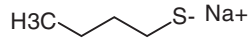

Sodium 1-propanethiolate

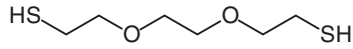

2,2´-(Ethylenedioxy)diethanethiol

Figure 2.35 Organo-sulfur compounds.

The results showed that the end charging potential of the nickel electrodes with flaky rare earth oxides were higher than that without rare earth oxide additives, but lower than that with normal rare earth oxide additives. In summary, flaky rare earth oxides increased the oxygen evolution potential and improved the reversibility of nickel electrodes (109).

2.5.2 Multiphase Nano-Nickel Hydroxide

Multiphase nano-$Ni(OH)_2$-doped with Y or La was prepared by a supersonic co-precipitation method (111). The crystal morphology, structure and particle size were characterized by TEM, XRD and particle size distribution.

Measurements of the electrochemical performance indicated that micromorphology and grain size were changed with the changing of the supersonic power, pH values and doping elements. The morphology of a Y-doped sample changed from flake-like to needle-like with the increase of supersonic power. Particles were modified from quasi-spherical particles to needle-like with an increase of the pH. The pH is very important for the formation of a crystalline phase. Lower pH value was beneficial to the formation of $Ni(OH)_2$. However, the pH values had only a slight effect on the reaction reversibility.

Complex electrodes were prepared by mixing 8% nickel hydroxides with commercial microsize spherical nickel. The discharge capacity of electrodes increased initially and then decreased with the increase of the supersonic power. When the supersonic power was 60 *W* and the pH value was 9, the sample had the largest discharge capacity of 358 $mAh\,g^{-1}$ at 0.5*C* rate, which was 122.7 and 76 $mAh\,g^{-1}$ higher than the spherical nickel electrode and the La-doped sample electrode, respectively (111).

2.5.3 Nickel-Metal Hydride Batteries

The high-temperature performance of nickel-metal hydride batteries is directly related to the behavior of the nickel hydroxide electrode materials, which determines the cell capacity. Due to oxygen evolution on the positive electrode at a temperature higher than 50°C, the charge efficiency of positive electrodes is significantly diminished when the undesirable oxygen evolution reaction occurs.

This results in a poor performance of the batteries at high temperatures (112, 113).

2.5.3.1 *Enhancement of High-Temperature Performance*

An alternative approach to improve the high-temperature performance of nickel-metal hydride batteries has been proposed by introducing a NaOH electrolyte containing $NaBO_2$ additives. The paste nickel electrodes were prepared as follows (114):

Preparation 2–8: A mixture with 90% $\beta-$CoOOH coated $\beta-Ni(OH)_2$, 5% CoO and 5% Ni powder were mixed thoroughly by milling to ensure the uniformity of the mixture. After adding a proper amount of 3% of the binders poly(tetrafluoroethylene) and sodium carboxymethyl cellulose and distilled water, a paste with adequate rheological properties was produced by a blender in the course of continuous stirring for 1 *h*. The resultant slurry was poured into a foam nickel sheet and dried at 80°C in air. Afterward, the positive electrodes were rolled into a sheet with a thickness of 0.65 *mm* and cut into small pieces with the dimensions of 90 *mm* $\times$ 41 *mm* $\times$ 0.68 *mm*.

A commercial MmNi5-type hydrogen storage alloy was used for the negative electrode material. A slurry containing 96% alloy powders, 4% nickel powder and a proper amount of binders styrene-butadiene rubber and hydroxypropyl methyl cellulose was pasted onto the nickel coated stainless steel strip substrates, and then dried and compressed to obtain the metal hydride electrode. The dimensions of the pasted metal hydride electrode plate were 125 *mm* $\times$ 42 *mm* $\times$ 0.28 *mm*.

In comparison to conventional batteries that use KOH electrolyte, the alternatively prepared batteries with these new electrolytes exhibit an enhanced discharge capacity, improved high-rate discharge ability, increased cycle stability and reduced self-discharge rate at an elevated temperature of 70°C.

The charge acceptance of these nickel-metal hydride batteries at 70°C is over 96% at a charge/discharge rate of 1°C. These performance improvements are due to the increased oxygen evolution overpotential, slower oxygen evolution rate and lower electrochemical impedance, as indicated by CV, steady-state polarization measurements and EIS (114).

2.5.3.2 *Effects of Different Electrolytes*

In order to improve the high-temperature performance of the nickel hydroxide electrodes in nickel-metal hydride batteries, sodium tungstate (Na_2WO_4) was used as an electrolyte additive (115). It was added into two types of binary electrolytes, i.e., KOH–LiOH and NaOH–LiOH.

The effects of electrolyte composition on the electrochemical performance of nickel electrodes have been systematically investigated using a combination of CV, EIS, SEM, XRD, and charge/discharge tests. It was found that by adding 1.0% Na_2WO_4, the performance of nickel electrodes is significantly improved in both KOH–LiOH and NaOH–LiOH electrolytes at 70°C.

The improved performance has been attributed to the deposition of a $WO_3 \times 2H_2O$ solid film on the surface of the nickel electrode, which is beneficial to the increase in oxygen evolution overpotential, the slow-down of oxygen evolution rate and the decrease in charge transfer resistance (115).

2.5.3.3 *Sodium Tungstate*

Sodium tungstate, (Na_2WO_4, was tested as an electrolyte additive to enhance the high-temperature performance of a nickel-metal hydride battery (116). The effects of Na_2WO_4 on nickel hydroxide electrodes have been investigated by CV, EIS, and a charge/discharge test.

It has been found that the nickel-metal hydride cell with the conventional KOH electrolyte containing 1% Na_2WO_4 additive exhibits a higher discharge retention and a better cycling performance than a cell without the Na_2WO_4 additive at 25°C and also at 70°C.

These improvements are ascribed to the enhancement of the oxygen evolution overvoltage and lower electrochemical impedance, as indicated by CV and EIS. The results suggest that the use of Na_2WO_4 may be an effective way to improve the high temperature performance of nickel-metal hydride batteries (116).

2.5.3.4 *Calcium Metaborate*

Calcium metaborate has been proposed to improve the high-temperature characteristics of the nickel electrodes for nickel-metal hydride

batteries (117).

As a soluble calcium salt, calcium metaborate can be easily and uniformly dispersed in nickel electrodes. The effects of calcium metaborate on the nickel electrode have been investigated via a combination of cyclability, capacity retention, electrochemical impedance spectroscopy, scanning electron microscope and X-ray diffraction.

In comparison to conventional nickel electrodes, an electrode with 0.5% calcium metaborate exhibited superior electrode properties, including an enhanced discharge capacity, improved high-rate discharge ability and excellent cycle stability at an elevated temperature of 70°C. The improved cell performance of the nickel electrode containing calcium metaborate additives has been attributed to the increased oxygen evolution overvoltage and slower oxygen evolution rate. Thus, in comparison to insoluble calcium salts, such as $Ca(OH)_2$, $CaCO_3$, and CaF_2, calcium metaborate is more effective as a cathode additive to improve the high-temperature performance of nickel-metal hydride batteries (117).

2.5.3.5 Ytterbium-Substituted Nickel Hydroxide

Nanosized ytterbium (Yb)-substituted α-$Ni(OH)_2$ was synthesized by ultrasonic-assisted precipitation, using nickel sulfate as nickel source and $Yb(NO_3)_3 \times 5H_2O$ as doping material (118).

The crystal structure, morphology, and particle size distribution of the sample were characterized using XRD, IR, TEM, SEM, and other methods. The results of these characterization methods indicated that the samples are anisotropic polycrystalline α-$Ni(OH)_2$ with a particle size of 50–200 *nm*, and the particle size increases with Yb-doping.

The synthesized samples were tested in a nickel-metal hydroxide battery. The specific capacity increases initially and then decreases with increasing Yb-doping ratio with the maximum discharge capacity of 295.1 $mAh\,g^{-1}$ at 0.2*C*, which is 60 $mAh\,g^{-1}$ higher than a microsized spherical nickel electrode. At the same time, the prepared material has lower charging voltage, higher discharge voltage plateau, and better cycle performance (118).

2.6 Sodium-Ion Batteries

2.6.1 Antimony-Based Intermetallic Alloy Anodes

An antimony containing intermetallic alloy compound consisting of molybdenum and antimony dispersed in an amorphous carbon matrix was developed using a high-energy mechanical milling technique (119). This material was used as the anode for a sodium-ion battery.

The structure and morphology of the as-prepared material were characterized using XRD and TEM. The *ex-situ* XRD measurement confirmed the formation of a Na_3Sb phase during the sodiation. The electrochemical performance of the so-prepared Mo_3Sb_7−C composite demonstrated a stable cyclability up to 40 cycles at a current rate of 100 $mA\ g^{-1}$.

When a fluoroethylene carbonate additive was introduced into the electrolyte, the Mo_3Sb_7−C anodes exhibited a longer cyclic life with a capacity retention of around 90% at 100 cycles, as well as a superior rate-cyclic performance corresponding to a capacity retention of more than 70% at 10,000 $mA\ g^{-1}$.

This enhanced electrochemical performance could be ascribed to the formation of a stable solid electrolyte interphase layer, smaller charge transfer resistance, and better dispersion of Mo_3Sb_7 nanoparticles in the carbon matrix (119).

2.6.1.1 High Performance Anodes

An important strategy to design suitable electrolyte systems has been shown that makes the desirable interfacial structure to allow the reversible sodiation and desodiation of Sn_4P_3 anodes (120). A remarkable improvement in the electrochemical performance of Sn_4P_3 anodes for sodium-ion batteries can be achieved by the combination of fluoroethylene carbonate with tris(trimethylsilyl) phosphite.

Unique functions of this binary additive combination have been detected that build up a protective surface film on the Sn_4P_3 anode against an undesired electrolyte decomposition and to prevent the formation of the $Na_{15}Sn_4$ phase, which is accompanied by a large volume expansion during the sodiation process (120).

2.7 Solar Cells

Organic solar cells exhibit tremendous potential in the world's energy strategy due to their predominant advantages such as low cost, light weight, and large-area fabrication on flexible substrates (121).

Small molecule semiconductors for bulk heterojunction organic solar cells are attractive because of their advantages over their polymer counterparts, which include well-defined molecular structure, definite molecular weight, and high purity without batch-to-batch variations.

2.7.1 Star-Shaped Molecules

Star-shaped molecules have been developed as an interesting class of semiconducting materials and used in organic solar cells because of a number of advantages (122).

By tailoring the functional groups in the core and the arm, star molecules can be designed to realize a low band gap, strong and broad absorption, together with high mobility, resulting in an improved performance (121,123–126)

2.7.1.1 Triphenylamine

Triphenylamine has been regarded as a promising unit for efficient photovoltaic materials due to its good electron-donating and high hole-transporting capabilities. Solution-processable triphenylamine-based small molecules have been widely investigated for application in organic solar cells with power conversion efficiencies below 3%

Benefiting from its special propeller starburst molecular structure, amorphous materials with isotropic optical and charge-transporting properties could be expected when combining triphenylamine with linear π-conjugated systems. The synthesis is shown in Figure 2.36.

The intermediate compound 4-bromo-7-[5′′-*n*-hexyl-(2,2′,5′,2′′-terthiophene)-5-yl]-benzo[c][1,2,5]thiadiazole was synthesized by a Stille coupling reaction of the compound 4,7-dibromobenzo[c]-[1,2,5]thiadiazole with 5-(*n*-hexyl)-5′′-(tributylstannyl)-2,2′,5′,2′′′-terthiophene. The terthiophene unit was used to extend the conjugated length in order to broaden the absorption spectrum (121).

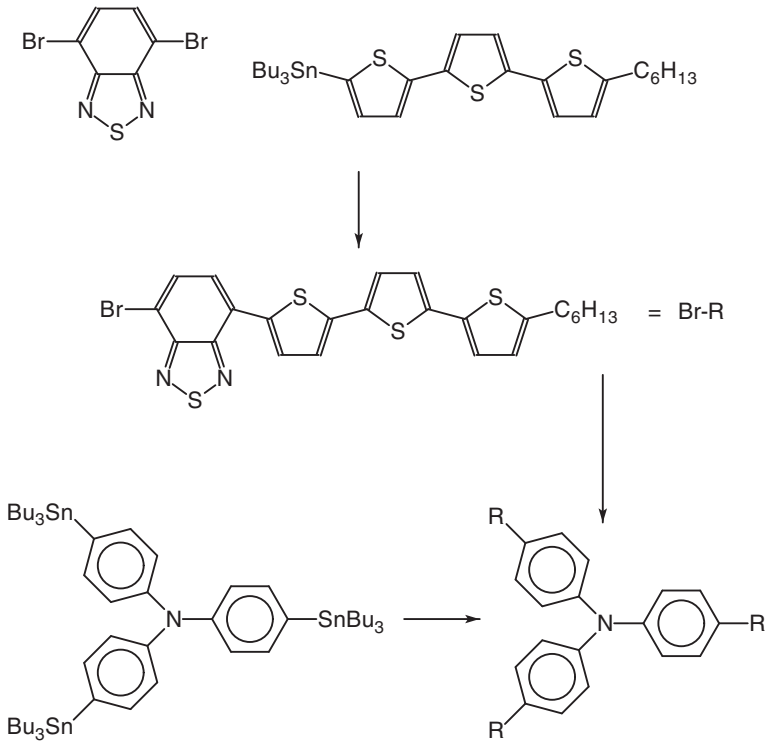

Figure 2.36 Synthesis of star molecules (121).

2.7.1.2 *Knövenagel Condensation Products*

Another method has been shown using the Knövenagel condensation reaction with a ketone precursor (127). This process is shown in Figure 2.37.

2.7.1.3 *Solution-Processable Star-Shaped Molecules*

The impact of alkyl side chain substituents on conjugated polymers on the photovoltaic properties of bulk heterojunction solar cells has been studied extensively (128). However, their impact on small molecules has not received adequate attention. In order to assess the effect of side chains, a series of star-shaped molecules based on a triphenylamine core, bithiophene, and dicyanovinyl units derivatized with various alkyl end-capping groups of methyl, ethyl, hexyl and dodecyl have been synthesized. These molecules were studied to get structure-property relationships.

UV-vis absorption and CV showed that the variation of the alkyl chain length has only little influence on the absorption and the highest occupied molecular orbital and lowest unoccupied molecular orbital levels.

However, only small changes have a pronounced impact on the morphology of bulk heterojunction thin films as well as their charge carrier separation and transportation. This in turn influences the photovoltaic properties of the small molecule-based bulk heterojunction devices. Solution-processed organic solar cells based on the molecules with the shortest methyl end groups exhibit a high short circuit current and fill factor (128).

2.7.2 *Dye-Sensitized Solar Cells*

2.7.2.1 *Pyridinyl-Functionalized Ionic Liquid*

A pyridinyl-functionalized ionic liquid, *N*-butyl-*N*′-(4-pyridylheptyl)imidazolium bromide, cf. Figure 2.38, has been synthesized and applied as an additive for dye-sensitized solar cells (129). In comparison to a volatile organic additive, 4-*tert*-butyl pyridine, the bromine-containing compound can be used at a very low concentration for high overall power conversion efficiency cells, which shows an overall power conversion efficiency of 5.67% under the simulated air

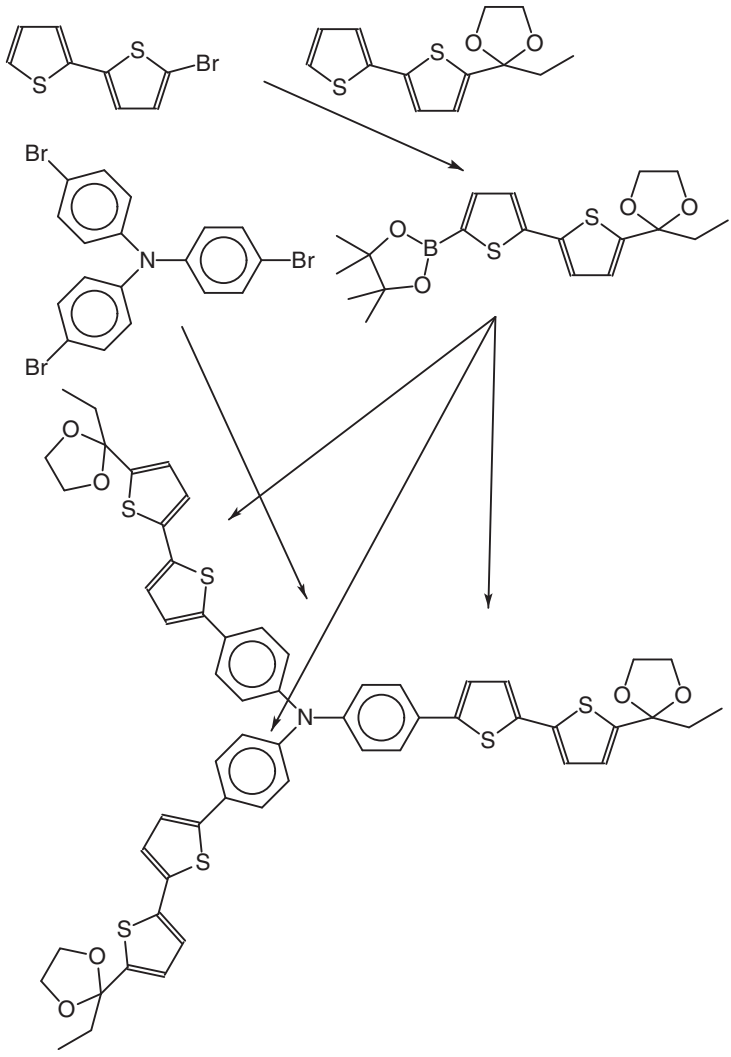

Figure 2.37 Synthesis of star molecules (127).

mass 1.5 solar spectrum illumination at 100 $mW\,cm^{-2}$ and 6.69% at 15 $mW\,cm^{-2}$, respectively.

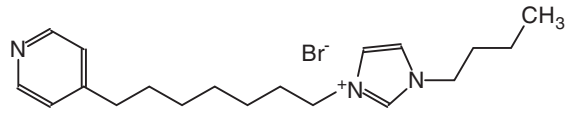

Figure 2.38 *N*-Butyl-*N*′-(4-pyridylheptyl)imidazolium bromide.

Furthermore, *N*-butyl-*N*′-(4-pyridylheptyl)imidazolium bromide cells show a better long-term stability than that of 4-*tert*-butyl pyridine-based devices. These results indicate that the dye-sensitized solar cell devices based on the pyridinyl-functionalized ionic liquid additive can overcome the drawbacks of the volatile organic additive, and offer a feasible method to fabricate dye-sensitized solar cells in future practical applications (129).

2.7.2.2 Redox Electrolyte

The influences of a redox electrolyte, additives and solvents on the photovoltaic performance of dye-sensitized solar cells containing 1-methyl-3-propyl-imidazolinium iodide as the electrolyte were investigated (130). This compound is shown in Figure 2.39.

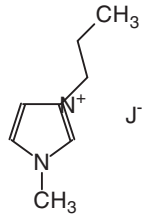

Figure 2.39 1-Methyl-3-propyl-imidazolinium iodide.

An optimum conductivity of 20.31 $mS\,cm^{-1}$ for 0.6 *M* 1-methyl-3-propyl-imidazolinium iodide in acetonitrile (AN) was found out from the measurement of the conductivity. Among the different inorganic and organic iodides as additives, the dye-sensitized solar

cells showed a high performance with lithium iodide and tetrabutyl ammonium iodide, respectively.

The performance of the dye-sensitized solar cells with different solvents was studied. It was suspected that the poor conversion efficiencies of the dye-sensitized solar cells were associated with a high charge transfer resistance (130).

2.7.2.3 Diethyl Oxalate

Diethyl oxalate has been used as an effective inexpensive additive-based iodide/triiodide electrolyte in dye-sensitized solar cells. The addition of an amount of diethyl oxalate of 1 *M* into the electrolyte shows a dramatic improvement in the short circuit current and, consequently, in the total conversion efficiency (131).

The fabricated devices based on N719 and 2-cyano-3-(4-(diphenylamino) phenyl) acrylic acid sensitizers with modified electrolyte show the efficiency of 7.33% and 2.63% at an irradiation of AM 1.5, and 37% and 22% energy conversion efficiency increments, respectively.

The boost in the photocurrent density mainly occurs due to the molecular complex formation between the diethyl oxalate and redox species in the electrolyte solution that promotes the electrochemical properties of electrolyte. Also, electrochemical impedance measurements indicate that adsorption of diethyl oxalate on the semiconductor surface leads to an incensement in the lifetime and the electron density in the conduction band of TiO_2 that shifts the Fermi level, which leads to a small enhancement in the volatile organic compound (VOC).

Adsorbing of diethyl oxalate on the titania surface retards the interfacial charge recombination that has a beneficial effect on the VOC and short circuit current. Furthermore, the effect mechanisms of diethyl oxalate and 4-*tert*-butyl pyridine additives on the cell performance by applying different electrolytes containing the additives have been compared. These compounds are shown in Figure 2.40

The results showed that 4-*tert*-butyl pyridine increases VOC, while diethyl oxalate additive has an effect on the short circuit current. Using a combination of these additives leads to a remarkable improvement. As a result, diethyl oxalate has been shown to be a

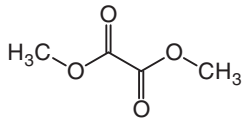

Diethyl oxalate

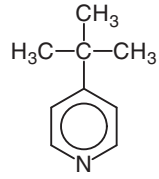

4-*tert*-Butylpyridine

Figure 2.40 Diethyl oxalate and 4-*tert*-Butyl pyridine.

promising co-additive which can be used for high efficient and low cost dye-sensitized solar cells (131).

2.7.2.4 Functionalized Ionic Liquids

Benzimidazolyl functionalized ionic liquids have been synthesized and tested as additives for dye-sensitized solar cells (132). The fabricated devices show an overall power conversion efficiency of ca. 7.79% under AM 1.5 radiation (50 $mW\,cm^{-2}$), and an excellent long-term stability.

2.7.3 Perovskite

Photovoltaic devices based on organic lead halide perovskites have several attractive features, including the ability to use solution processing, their high-power conversion efficiencies, the ease of synthesis of their active layer materials, and the capacity to use roll-to-roll production methods (133).

The film morphologies, crystallinities, and optical properties of $CH_3NH_3PbI_3{-}xCl_x$ perovskite layers can be manipulated by incorporating a small amount of ethylammonium iodide into the perovskite precursor solution. In the ethylammonium iodide modified films, higher absorbencies at higher wavelengths and higher degrees of crystallinity were found. This was associated with the higher surface coverage of the perovskite films (133).

The optimized power conversion efficiency improved from 9.4 ± 0.76 to 10.2 ± 0.58% after the addition of 0.5% by volume of ethylammonium iodide. These devices exhibit an extremely high stability,

retaining approximately 80% of their power conversion efficiencies under accelerated heating to 65°C in a dark nitrogen-filled glove box for more than 360 *h*. In contrast, the corresponding unmodified device was relatively sensitive to this temperature. It as been suggested that the presence of ethylammonium iodide suppresses the crystallization of $CH_3NH_3PbI_3{-}xCl_x$ (133).

2.7.3.1 Controllable Perovskite Crystallization

A key issue for perovskite solar cells is the stability of perovskite materials due to moisture effects under ambient conditions (134). An improved $CH_3NH_3PbI_3{-}xCl_x$ perovskite quality with good crystallization and stability by using water has been developed as an additive during the crystal perovskite growth.

Incorporating suitable water additives in *N*,*N*-dimethylformamide leads to a controllable growth of perovskites due to the lower boiling point and the higher vapor pressure of water compared with *N*,*N*-dimethylformamide (134). In addition, hydrated perovskites $CH_3NH_3PbI_3{-}xCl_x \times n\,H_2O$ can be resistant to the corrosion by water molecules to some extent. These compounds are suspected to be generated during the annealing process.

Thus, water additive-based perovskite solar cells present a high-power conversion efficiency of 16% and an improved cell stability under ambient conditions in comparison to previous materials. These findings provide a route to control the growth of crystal perovskites to improve the stability of organic-inorganic halide perovskites (134).

2.7.4 Control of Active Layer Nanomorphology

Two high boiling point solvents, i.e., 1-chloronaphthalene and 1,8-diiodooctane, cf. Figure 2.41, were utilized as co-additives in *o*-dichlorobenzene and chlorobenzene solutions for fine tuning of the donor and acceptor domains in the bulk heterojunction of poly(benzo[1,2-b:4,5-b′]dithiophene-*alt*-thieno[3,4-c]pyrrole-4,6-dione) and fullerene derivatives (135).

A power conversion efficiency of 7.1% and a fill factor up to 70% were obtained for solar cells with active area of 1 cm^2 when using

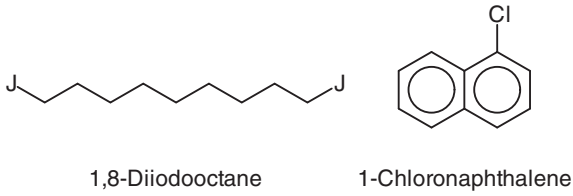

Figure 2.41 Co-additives for nanomorphology control.

[6,6]-phenyl C61-butyric acid methyl ester as acceptor, suggesting that an improved morphology could be achieved (135).

2.7.5 Phosphonium Halides as Processing Additives and Interfacial Modifiers

Organic halide salts have been introduced as a processing additive to modulate the growth kinetics of perovskite light-absorbing films. Phosphonium halides with bulky aromatic substituents are found to be the most efficient at improving perovskite film coverage and crystallinity (136).

Moreover, phosphonium halides can be used as an interfacial *n*-dopant to improve the electrical properties of cathode contacts. Perovskite solar cells incorporating organic halides as processing additives and interfacial modifiers show significant device performance improvement.

2.7.6 Polymeric Solar Cells

A photoactive polymer with two different molecular weights has been described, based on a new building block: thieno[3,2-*b*][1]-benzothiophene isoindigo (137). This compound is shown in Figure 2.42

Due to the improved crystallinity, optimal blend morphology, and higher charge mobility, solar cell devices of this high molecular weight polymer exhibit a superior performance, affording efficiencies of 9.1% without the need for additives, annealing, or additional extraction layers during device fabrication (137).

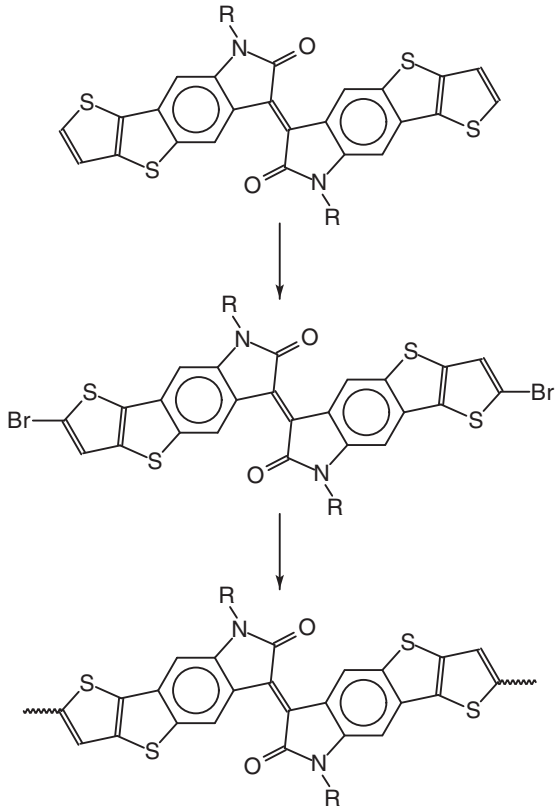

Figure 2.42 Polymer from thieno[3,2-*b*][1]benzothiophene isoindigo, R= 2-decyltetradecyl.

Also, asymmetric indenothiophene-based donor acceptor copolymers have been prepared by Stille coupling reactions between distannyl indenothiophene and brominated benzothiadiazole derivatives. The basic compounds are shown in Figure 2.43. The Stille

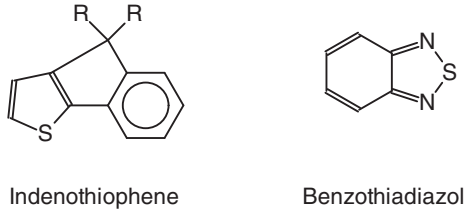

Figure 2.43 Indenothiophene and benzothiadiazole.

coupling involves the coupling of an organotin compound with a variety of organic electrophile compounds using palladium as catalyst (138, 139). The reaction can be summarized as:

$$R'-X + RSnBu_3 \rightarrow R'-R + XSnBu_3 \tag{2.8}$$

The best performing solar cell fabricated from these compounds exhibited a power conversion efficiency of 9.14%, which demonstrates the great potential of asymmetric indenothiophene for high performance copolymers (140).

2.8 Fuel Cells

There are monographs concerning fuel cells (141–144). The principle of fuel cells was observed already in 1838 (145). Soon afterwards the Grove cell was developed (146). The Grove cell consisted of a zinc anode in dilute sulfuric acid and a platinum cathode in concentrated nitric acid. The two electrodes were separated by a porous ceramic pot (147). Further aspects of the history of fuel cells have been detailed (148).

A fuel cell generates electricity and heat simultaneously through the chemical reaction of atmospheric oxygen with hydrogen produced through the reaction of water vapor with natural gas, methanol, and others and thus produces only water as a byproduct of

power generation (149). In addition to this, a high-power generation efficiency is obtained even in a low output power range, and electrical power generation is not affected by weather and thus is stable.

Fuel cells can be classified into phosphoric acid fuel cells, molten carbonate fuel cells, solid oxide full cells, polymer electrolyte membrane fuel cells, and alkaline full cells according to the type of electrolyte used (150). All these fuel cells operate on the same principle, but the type of fuel used, operating speed, the catalyst used and the electrolyte used are different. In particular, polymer electrolyte membrane fuel cells can be used in small-sized stationary power generation equipment or transportation systems due to their high reaction speed, low operating temperature, high output density, rapid startup, and variation in the requested output.

In particular, the polymer electrolyte fuel cell type has received attention in applications such as vehicle-mounted use, mobile use, and stationary use in homes (149). In a vehicle-mounted fuel cell system serving as a driving source for an automobile, pure hydrogen stored in a hydrogen tank is supplied to an anode. Further, in a power source system for mobile devices such as notebook personal computers and cellular phones, alcohol-based liquid fuel such as methanol is supplied to an anode.

When such a fuel is sufficiently supplied to an anode and contributes to power generation, an anode reaction represented by Eq. 2.9 or 2.10 occurs, and the protons move toward a cathode through an electrolyte layer (149).

$$H_2 \rightarrow 2H^+ + 2e^- \tag{2.9}$$

$$CH_3OH + H_2O \rightarrow 6H^+ + 6e^- + CO_2 \tag{2.10}$$

However, when a load is increased abruptly or when the concentration of the fuel decreases, a so-called fuel starvation occurs in which the amount of fuel required at the anode during power generation becomes insufficient. In such a case, for example, carbon in a carbon-supported catalyst medium reacts with water at the anode, and occasionally, also at the cathode, to produce protons as shown

in Eq. 2.11 and 2.12, and thus a problem arises in that the carbon is released as carbon dioxide.

$$C + H_2O \rightarrow CO + 2H^+ + 2e^- \tag{2.11}$$

$$C + H_2O \rightarrow CO_2 + 4H^+ + 4e^- \tag{2.12}$$

In addition, when the catalyst for the anode contains ruthenium, the reaction represented by Eq. 2.13 occurs.

$$Ru + 2H_2O \rightarrow RuO_2 + 4H^+ + 4e^- \tag{2.13}$$

Thus a problem arises in that the ruthenium is oxidized and dissolved as ruthenium oxide (RuO_2). When the carbon in the carbon-supported catalyst medium is released, the catalyst is no longer supported, and thus the amount of the catalyst in the anode decreases. Also, when the ruthenium is oxidized and dissolved, a problem arises in that CO resistance is reduced.

2.8.1 Porosity Additive

An oxygen reduction electrode in a fuel cell has been described (150). The catalyst layer of the oxygen reduction electrode contains a metalloporphyrin derivative as an additive. Accordingly, the oxygen reduction electrode can increase oxygen concentration and can easily form a triple phase boundary by reducing a flooding phenomenon caused by an electrolyte. The metalloporphyrin derivative may be a hemin compound. This is shown in Figure 2.44.

Since the hemin compound has a substituent having a double bond and a terminal carboxyl group is in β position, the double bond can be reduced by a catalyst, such as Pt, thus enabling the hemin compound to bind chemically onto the surface of the catalyst. The combined hemin compound increases the hydrophobicity in the chemical atmosphere around the catalyst, thus preventing a deterioration of efficiency caused by a flooding phenomenon of the catalyst particles. Also, the increased hydrophobicity maintains a path where oxygen flows into the catalyst layer. As a result, the

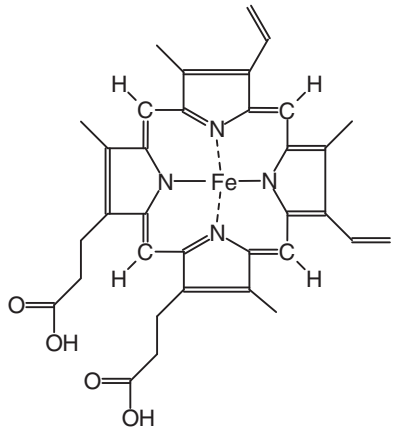

Figure 2.44 Hemin.

oxygen concentration around the catalyst layer can be maintained at a high level, due to the prevention of flooding in the catalyst layer (150).

2.8.2 Electrolyte Membranes

Electrochemical fuel cells convert fuel and oxidant streams, to generate electric power and reaction products. Fuel cells typically oxidize fuels to produce electrons and protons, at a catalyst layer disposed on an electrically conductive material, serving as the anode.

The electrons are conducted through the anode, and produce electrical energy. The protons flow from the anode through an electrolytic medium, often supported by a membrane, to a catalyst layer disposed on the cathode, where they are recombined with electrons to reduce an oxidant. In the case of hydrogen fuel cells, molecular hydrogen is oxidized into electrons and protons at the anode. The electrons so produced are transported through the electrically conductive anode, whereas the protons migrate through a polymer-electrolyte membrane (PEM). The PEM comprises a polymeric scaffold supporting a proton conductive electrolyte phase that enables the conduction of protons through the PEM, to the cathode where they recombine with electrons to reduce an oxidant, in general oxygen.

To produce a structure capable of performing the above-mentioned electrochemical task, an anode and cathode, each containing catalyst particles, are adhered to opposite sides of the PEM to form a layered composite structure. This composite structure is responsible for the electrochemical conversions and directed flow of fuel, byproducts, ions, electrolytes and electrons requisite for the electrochemical functioning of a fuel cell. This layered composite structure is also referred to as a membrane electrode assembly (MEA).

Generally, PEMs may exhibit phase separated morphologies, wherein an electrolyte phase is dispersed within a continuous polymeric phase that provides mechanical stability. Both electrolyte and polymer phases can impact the permeation of protons through the PEM. On a molecular level, the chemical characteristics of the electrolyte desirable for proton conduction include molecular topology, mobility, and acidity.

An increased electrolyte concentration within the membrane may enhance accessibility and improve rates of proton sorption and permeation though the membrane. Maintenance of constant electrolyte concentration may be desirable for obtaining stable proton conductivity, and replenishment of vaporized or leached electrolyte may be continuously performed during operation. On a morphological level, dynamic fluctuations between electrolyte domains may provide conductive pathways through the polymeric continuous phase. Thus, the ability of the polymeric phase to mechanically comply with the anodic proton flux may enable proton percolation though the membrane and enhance conductivity.

It is also desirable that the membrane be mechanically robust during operation, and serve as a dielectric and mechanical barrier to the electrical and electrochemical processes within the membrane electrode assembly, while simultaneously conducting protons. Thus typical polymers for PEMs possess oligomeric regions that are non-interactive with the electrolyte, but rather, are involved in intermolecular associations to provide a mechanically robust, continuous phase. In addition, these polymers have regions compatible with the chosen electrolyte; and these regions generally contain acidic or basic residues.

PEMs of particular interest contain acid-functional polymers, such as acid-functional fluoropolymers, and electrolytes, such as water. Suitable examples of acid-functional fluoropolymers include

electrolyte noninteractive (or hydrophobic) oligo(perfluoroethylene) blocks, and electrolyte interactive fluorosulfonic acid residues pendant to the polymer chain.

The ability of the PEM to separate electrochemical processes by selectively restricting permeation of fuel, oxidant and byproducts is also desirable. This process is often referred to as crossover. Thus, in order to improve efficiencies, it may be desirable to have a PEM with low fuel crossover.

When water is used as an electrolyte, the conductivity of the PEM may suffer at temperatures greater than 80°C. This is a result of evaporative depletion of the electrolyte phase in the PEM. Humidification of the membrane thus improves performance of the fuel cell over extended periods. However, the cell performance may further degrade at higher temperatures, particularly over 100°C, where there is reduced water absorption. As the vapor pressure of water increases rapidly with temperature, it becomes necessary to operate the fuel cell at higher pressures, which increases system design complexity and cost. Thus, there is a need to operate under low relative humidity conditions, even at normal operating temperatures.

Therefore, there is a need for PEM configurations that improve electrochemical performance when operated under low humidity and/or high temperature conditions. Further, it may be desirable to have such PEM configurations suitable for use within the fuel cell environment.

2.8.2.1 Cycloaliphatic Additives

A special PEM has been developed (151). This membrane contains an acid-functional polymer, and an additive incorporated in at least a portion of the membrane. The additive is a fluorinated cycloaliphatic additive, or a hydrophobic cycloaliphatic additive. The additive should have a boiling point greater than about 120°C (151). Suitable additives of this type are collected in Table 2.12.

It is believed that the use of the cycloaliphatic additives may result in a reduced leaching of the additive from the membrane, when compared to the hydrophilic linear additives, e.g., linear alkanes or amines. The cycloaliphatic additives, due to their increased steric size and lower water solubility, are expected to have a reduced mobility in the membrane environment, thus resulting in reduced

Table 2.12 Fluorinated cycloaliphatic additives (151).

Compound	Compound
trans-Perfluorodecalin	*cis*-Perfluorodecalin
Perfluoro(1-methyldecalin)	Perfluoro(2-methyldecalin)
Perfluoro(isopentyl-tetrahydro-pyran)	Perfluorobicyclohexane
Perfluorohydrophenanthrene	Perfluorotetradecahydroanthracene
Perfluoro(2-(cyclohexylmethyl) decalin	Perfluoro(*N*-methyldecahydroisoquinoline)
Perfluoro-(1,2-ethanediylbis(morpholine))	Perfluoro(*N*-cyclohexylmorpholine)
Perfluoro(dimethyl-adamantane)	Perfluorotri-methylbicyclo(3.3.1) nonane
Perfluoro methyldecalin	Perfluoro(isopropylcyclohexane)
Perfluoro(*n*-propylcyclohexane)	Perfluoro(1,4-diethylcyclohexane)
Perfluoro(1,3-diethylcyclohexane	Perfluoro(1,2-diethylcyclohexane)
Perfluoro(1H-fluorene)	Perfluorobutylcyclohexane
Perfluorophenanthrene	Perfluorobicyclohexyl

leaching. The leaching of the additives out of the membrane during prolonged use of the fuel cell may result in a performance degradation over time. Thus the cycloaliphatic additives may be beneficial for long-term use of the fuel cell (151).

2.8.2.2 Ionic Liquid Doped Poly(benzimidazole) Membranes

The use of the ionic liquid 1-*H*-3-methylimidazolium bis(trifluoromethanesulfonyl)imide as conductive filler has been chosen for a tailor-made porous, poly(benzimidazole) (PBI) support as proton conductive membrane for high temperature (>100°C) fuel cell applications (152). PBI has been selected because of its excellent thermal and mechanical stability, while the choice for the ionic liquid has been based on its high proton conductivity, low water sorption, thermal stability and low viscosity.

The morphology of the porous PBI support is especially tailored for this application using a delayed immersion precipitation process. The macrovoid-free porous structure has a volume porosity of 65% and a pore size of approximately 0.5 μm.

Pores filling with ionic liquid by direct immersion of the PBI support into the molten ionic liquid at 50°C introduced the membrane proton conductivity. After impregnation the proton conductivity of this PBI ionic liquid membrane reached a value of 1.86 $mS\,cm^{-1}$ at 190°C.

It has been shown that the fuel cell performance of these membranes clearly exceeds that of Nafion® 117 at temperatures above 90°C. A power density of 0.039 $W\,cm^{-2}$ is obtained at the intended operation temperature of 150°C, which proves that the such developed membrane can be considered as a serious candidate for high temperature fuel cell applications (152).

2.8.3 Molybdenum Oxide

In order to circumvent the above-mentioned problems a special fuel cell has been developed. The fuel cell comprises (149):

1. An electrolyte layer,
2. A first electrode which is provided on one surface of the electrolyte layer and to which fuel is supplied, and
3. A second electrode which is provided on the other surface of the electrolyte layer and to which an oxidant is supplied.

The first electrode contains an additive having an oxidation-reduction potential which is higher than a potential of formation reaction for forming a proton from the fuel and which is lower than an oxidation potential of a component contained in the first electrode (149).

As additive, molybdenum oxide can be used. Molybdenum oxides have excellent electrical conductivity and are insoluble in water and in dilute acid. In particular, MoO_2 and MoO_3 are readily available. The carbon-supported catalyst is platinum-supporting carbon.

Examples of the fuel include pure hydrogen and a reformed gas which is produced by reforming city gas, liquefied natural gas that contains approximately 80% of hydrogen. In addition to this, when the fuel cell is of a type to which organic fuel, such as methanol, is directly supplied, the organic fuel itself, an aqueous solution thereof, can be used as the fuel.

It has been stated that even when fuel starvation occurs at the anodes of the cell, the reaction represented by Eq. 2.13 does not

occur. Thus, the problem of oxidation and dissolution of Ru as Ru^{2+} can be avoided. The CO resistance of the anodes is prevented from being reduced (149).

2.8.4 Nano-Metal Oxides

A fuel cell has been described that contains a first layer comprising a first ionomer and an additive. The additive is a metal oxide from Ce, Mn, V, Pt, Ru, Zr, Ni, Cr, W, Co, Mo, or Sn. This additive is present in an amount of at least 0.1% of the ionomer. The metal oxide essentially consists of nanoparticles (153).

So, the particles have at least one dimension that is less than 200 *nm*. The use of nanoparticles was found to improve the performance of the membrane assemblies compared to assemblies using macroparticles. As ionomers, perfluorosulfonic acid polymers, e.g., poly-(tetrafluoroethylene-perfluorosulfonyl fluoride), can be used (153).

2.8.5 Coolant Additive

In a fuel cell vehicle, the temperature of fuel cells rises due to the exothermic reaction of the fuel cells and thus, while the fuel cells are cooled by a coolant, a radiator installed in a cooling system radiates heat of the coolant to maintain the operating temperature of the fuel cells at an optimum value, e.g., 80°C (154).

The coolant of fuel cells flows through a fuel cell stack and there is a danger of a short circuit of cells or a leakage of current if electrical conductivity of the coolant is high. Thus, ion exchanged water with an electrical conductivity of 1 $mS\,m^{-1}$ or less, or a low-conductive antifreeze, is used as coolant.

A fuel cell vehicle is supposed to be used in an environment in which the temperature falls to zero or below and thus, the use of ion exchanged water, which may be frozen, is not preferable. Therefore, glycols often used as a freezing point depressant of an antifreeze for vehicle are preferably used as a coolant of fuel cells. However, glycols are known to generate corrosive substances such as organic acids due to heat degradation and to corrode metal components. Thus, when glycols are used as a coolant, an inhibitor such as an anticorrosion agent and an antioxidant must typically be added to the coolant.

The coolant also poses the problem of the electrical conductivity of the coolant being high because of ionization of products of such organic acids or the like caused by heat degradation or elution of ions from component materials, such as rubber and metal, in the cooling system (154).

Thus, low electrical conductivity of the coolant must be maintained by installing an ion exchange resin in the cooling system of fuel cells to remove ions. A mixed bed ion exchange resin in which both a cation exchange resin and an anion exchange resin are mixed can be used as ion exchange resin.

A fuel cell system has been developed that includes the fuel cells, a circulation channel of a coolant to cool the fuel cells, and an ion exchange resin provided on the circulation channel to maintain electrical conductivity of the coolant. Further, the coolant contains an additive, and the ion exchange resin is prepared so that adsorption of the additive on the ion exchange resin is in a saturated state (154).

Examples of the additive are an anticorrosive agent and an antioxidant. A coolant is thermally degraded or oxidized due to repeated use thereof and generates corrosive substances. The inhibitor can suppress corrosion of metal due to the corrosive substances and generation of corrosive substances.

Specific examples of the inhibitor are summarized in Table 2.13.

Table 2.13 Inhibitor additives for fuel cells (154, 155).

Compound	Compound
Benzotriazole	Methyl benzotriazole
Cyclobenzotriazole	4-Phenyl-1,2,3-triazole
Imidazoline	Imidazole
Mercaptoimidazoline	Mercaptoimidazole
Benzimidazoline	Methylimidazole
Mercaptobenzothiazole	Benzothiazole

As another additive, a surface active agent can be added to improve the dispersability. Examples of the surface active agents include an anionic surface active agent, cationic surface active agent, and nonionic surface active agent. Furthermore, as an additive, an antifoaming agent can be added to suppress the generation of foam

in the coolant. An example of the antifoaming agent is a silicon-based antifoaming agent (154).

2.8.6 Membrane Exchange Humidifier

A microporous polymer membrane with a hydrophilic additive or filler has been used in an improved membrane exchange humidifier (156). Such membranes may be competitive with regard to water transmission rate and be dimensionally stable, and bondable by the use of adhesives or via melt bonding. The use of membranes with such properties allows a simpler configuration of a membrane exchange humidifier.

An improved humidification is useful for a membrane exchange apparatus in situations where gaseous wet and dry streams are occurring. In such a membrane exchange apparatus, a suitable water permeable membrane is employed, and a first fluid stream is directed across one major surface of the water permeable membrane and the second fluid stream is directed across the opposing major surface.

The water permeable membrane should contain sufficient amounts of a hydrophilic additive to render it wettable to water. Thus, when the second fluid stream contains liquid water, the membrane may become wetted and saturated with liquid water. This may effectively seal the membrane sufficiently so as to hinder the unwanted transfer of other gases across it. The second fluid stream comprises liquid water when the dewpoint temperature of the second fluid stream is greater than its actual temperature. Suitable hydrophilic additives include silica or alumina, in fiber or powder forms.

Such water permeable membranes are characterized by pore structures in which the total porosity is greater than about 50%. Further, the average pore size may be from about 0.025 μm to about 0.1 μm. Such a humidifier is particularly suitable for use in humidifying a reactant gas supply stream for a solid polymer fuel cell. The fuel cell has a reactant gas inlet port and a reactant gas exhaust port (156).

2.8.7 Poly(vinyl alcohol)/Titanium Dioxide Nanocomposites

The fabrication of PVA/titanium dioxide nanocomposites with different titanium dioxide (TiO_2) loading by using ultrasound irradiation has been described (157). For an improvement of the dispersion of the nanoparticles and for increasing possible interactions between nanoparticles and PVA, the surface of TiO_2 nanoparticles was modified by γ-aminopropyltriethoxy silane.

The so-prepared nanocomposites were characterized by spectroscopic, thermogravimetric analysis and electron microscopy methods. The results demonstrated that nanoparticles dispersed homogeneously within the PVA matrix in a nanoscale range could be assigned to the hydrogen and covalent bonds formed between PVA and the nanoparticles. The results indicated that the heat stability of nanocomposites was improved in the presence of modified TiO_2 nanoparticles. The mechanism of surface modification and a possible mechanism of ultrasonic induced interaction between the polymer and the nanoparticles have been analyzed.

Then, these nanocomposites have been used as a novel electrolyte additive in an alkaline half cell to improve the electrical efficiency of a direct methanol fuel cell. Finally, the electrochemical characteristics of the half cell of direct methanol fuel cell which employ the PVA/TiO_2 nanocomposites were investigated. The results revealed that the introduction of nanocomposites within the electrolyte can modify the electronic property of the Pt surface and improve the electrocatalytic activity of TiO_2 in methanol oxidation and prevents the catalyst from more poisoning by intermediate products of the methanol oxidation (157).

Tradenames appearing in the references are shown in Table 2.14.

Table 2.14 Tradenames in References.

Tradename Description	Supplier
Amberjet® UP 6040 Ion exchanger (155)	Evonik Rohm & Haas
Aquivion® Acid-functional polymer (151)	Solvay SA Corp.
Celgard™ Porous polyethylene separation membrane (105)	Celanese Corp.
Flemion® Fluoropolymer ion-exchange membrane (151)	Asahi Glass Comp.
GORE-TEX Clothing ware (156)	W. L. Gore & Associates, Inc. Corp.
Nafion® Sulfonated PTFE, for membrane applications (149,151,153,156)	DuPont
Osmonics® Fluid separation system (156)	GE Osmonics, Inc.
PALL® Polyether sulfone (156)	Pall Corp. N.Y
Puranal® Chemicals used for analytical purposes (49)	Riedel-De Haen AG
Silgrain® Silicon (47,49)	Elkem of Norway
Teslin.RTM Synthetic membrane (156)	PPG Industries Ohio, Inc.

References

1. K.-L. Wang and R.-F. Chang, *Journal of Power Sources*, Vol. 162, p. 1455, 2006.
2. B.E. Conway, *Electrochemical Supercapacitors Scientific Fundamentals and Technological Applications*, Springer US, Boston, MA, 1999.
3. F. Béguin and E. Frackowiak, eds., *Supercapacitors: Materials, Systems, and Applications*, Materials for Sustainable Energy and Development Series, Wiley-VCH, Weinheim, 2013.
4. A. Yu, V. Chabot, and J. Zhang, *Electrochemical Supercapacitors for Energy Storage and Delivery. Fundamentals and Applications*, Electrochemical Energy Storage and Conversion Series, CRC Press, Boca Raton, FL, 2013.
5. Wikipedia, Double layer (surface science) — wikipedia, the free encyclopedia, 2016. [Online; accessed 21-June-2016].
6. G. Wang, L. Zhang, and J. Zhang, *Chemical Society Reviews*, Vol. 41, p. 797, 2012.
7. Y.-T. Weng and N.-L. Wu, *Journal of Power Sources*, Vol. 238, p. 69, 2013.
8. R. Xu, F. Guo, X. Cui, L. Zhang, K. Wang, and J. Wei, *Journal of Materials Chemistry A*, Vol. 3, p. 22353, 2015.
9. D.S. Reichmuth, G.S. Chirica, and B.J. Kirby, *Sensors and Actuators B: Chemical*, Vol. 92, p. 37 , 2003.
10. Wikipedia, Lead-acid battery — wikipedia, the free encyclopedia, 2016. [Online; accessed 21-June-2016].
11. J. Xiang, P. Ding, H. Zhang, X. Wu, J. Chen, and Y. Yang, *Journal of Power Sources*, Vol. 241, p. 150, 2013.
12. G.N. Reich, Forming of tetrabasic lead sulfate battery electrodes, US Patent 4 415 410, assigned to Allied Corporation (Morristown, NJ), November 15, 1983.
13. J.P. Malloy, Method of manufacturing storage battery electrode active material, US Patent 3 194 685, assigned to Electric Storage Battery Co., July 13, 1965.
14. R.V. Biagetti and M.C. Weeks, *Bell System Technical Journal*, Vol. 49, p. 1305, 1970.
15. C.F. Yarnell and M.C. Weeks, *Journal of the Electrochemical Society*, Vol. 126, p. 7, 1979.
16. B.K. Mahato and W.C. Delaney, Formation efficiency of positive plates of a lead-acid battery, US Patent 4 656 706, assigned to Globe-Union, Inc. (Milwaukee, WI), April 14, 1987.
17. P.C.S. Hayfield, Electrode material, electrode and electrochemical cell, US Patent 4 422 917, assigned to IMI Marston Limited (Wolverhampton, GB2), December 27, 1983.

18. J.J. Rowlette, T.J. Clough, J.Y. Josefowicz, and J.W. Sibert, Unitary plate electrode, US Patent 4 547 443, assigned to Atlantic-Richfield Company (Los Angeles, CA) California Institute of Technology (Pasadena, CA), October 15, 1985.
19. A. Reid, Electric storage battery plate and a method of treating such plate, US Patent 2 159 226, assigned to US L Battery Corp., May 23, 1939.
20. S.C. Barnes and J. Armstrong, Battery plates, US Patent 3 398 024, assigned to Lucas Industries Ltd, August 20, 1968.
21. W.-H. Kao, N.K. Bullock, and R.A. Petersen, High performance positive electrode for a lead-acid battery, US Patent 5 302 476, assigned to Globe-Union Inc. (Milwaukee, WI), April 12, 1994.
22. M. Yoshio, R.J. Brodd, and A. Kozawa, eds., *Lithium-ion Batteries: Science and Technologies*, Springer, New York, NY, 2009.
23. X. Yuan, H. Liu, and J. Zhang, eds., *Lithium-ion Batteries: Advanced Materials and Technologies*, Green Chemistry and Chemical Engineering Series, CRC Press, Boca Raton, FL, 2012.
24. K. Ozawa, ed., *Lithium Ion Rechargeable Batteries*, John Wiley and Sons, Hoboken, 2012.
25. J. Jiang and C. Zhang, *Fundamentals and Applications of Lithium-ion Batteries in Electric Drive Vehicles*, John Wiley & Sons Inc, Singapore, 2015.
26. A. Chagnes and J. Swiatowska, eds., *Lithium Process Chemistry: Resources, Extraction, Batteries, and Recycling*, Elsevier, Amsterdam, 2015.
27. A. Rosenman, E. Markevich, G. Salitra, D. Aurbach, A. Garsuch, and F.F. Chesneau, *Advanced Energy Materials*, Vol. 5, 2015.
28. Q. Pang, D. Kundu, and L.F. Nazar, *Materials Horizons*, Vol. 3, p. 130, 2016.
29. L. Qie, C. Zu, and A. Manthiram, *Advanced Energy Materials*, Vol. 6, 2016.
30. T. Kennedy, M. Brandon, and K.M. Ryan, *Advanced Materials*, 2016.
31. K. Mi, Y. Jiang, J. Feng, Y. Qian, and S. Xiong, *Advanced Functional Materials*, Vol. 26, p. 1571, 2016.
32. N.L. Hamidah, G. Nugroho, and F.M. Wang, *Ionics*, Vol. 22, p. 33, 2016.
33. K. Abe, Y. Ushigoe, H. Yoshitake, and M. Yoshio, *Journal of Power Sources*, Vol. 153, p. 328, 2006.
34. Q. Wang, F.-Y. Su, Z.-Y. Tang, G.-W. Ling, and Q.-H. Yang, *New Carbon Materials*, Vol. 27, p. 427, 2012.
35. Q. Wang, F.-Y. Su, Z.-Y. Tang, G.-W. Ling, and Q.-H. Yang, *Carbon*, Vol. 55, p. 376, 2013.
36. J. Yang, Y. Zhang, P. Zhao, Y. Shang, L. Wang, X. He, and J. Wang, *Electrochimica Acta*, Vol. 158, p. 202, 2015.

37. C. Barchasz, M. Chami, and S. Patoux, Electrochemical lithium accumulator with a bipolar architecture comprising a specific electrolyte additive, US Patent 9 337 508, assigned to Commissariat a l'Energie atomique et aux energies alternatives (Paris, FR), May 10, 2016.
38. H. Lee, M. Yanilmaz, O. Toprakci, K. Fu, and X. Zhang, *Energy & Environmental Science*, Vol. 7, p. 3857, 2014.
39. H.-J. Peng, D.-W. Wang, J.-Q. Huang, X.-B. Cheng, Z. Yuan, F. Wei, and Q. Zhang, *Advanced Science*, Vol. 3, p. n/a, 2016.
40. Wikipedia, Mesoporous material — wikipedia, the free encyclopedia, 2016. [Online; accessed 25-July-2016].
41. X. Wang, S. Zheng, X. Mu, Y. Zhang, and H. Du, *Chemical Communications*, Vol. 50, p. 6775, 2014.
42. Y. Zhu, Y. Li, M. Bettge, and D.P. Abraham, *Electrochimica Acta*, Vol. 110, p. 191, 2013.
43. K.-E. Kim, J.Y. Jang, I. Park, M.-H. Woo, M.-H. Jeong, W.C. Shin, M. Ue, and N.-S. Choi, *Electrochemistry Communications*, Vol. 61, p. 121, 2015.
44. X. Wang, Y. Sone, and S. Kuwajima, Non-aqueous electrolytic solution containing additive for increasing capacity of lithium-ion cell and lithium-ion cell using same, US Patent 8 580 440, assigned to Japan Aerospace Exploration Agency (Tokyo, JP), November 12, 2013.
45. M. Winter, J.O. Besenhard, M.E. Spahr, and P. Novák, *Advanced Materials*, Vol. 10, p. 725, 1998.
46. U. Kasavajjula, C. Wang, and A.J. Appleby, *Journal of Power Sources*, Vol. 163, p. 1003 , 2007.
47. F. Coowar, M.E. Abdelsalam, and M.J. Lain, Additive for lithium ion rechargeable battery cells, US Patent 9 368 836, assigned to Nexeon Ltd. (Oxfordshire, GB), June 14, 2016.
48. M.N. Obrovac and L. Christensen, *Electrochemical and Solid State Letters*, Vol. 7, p. A93, 2004.
49. M. Green, F.-M. Liu, Y. Jiang, V.E.D. Stevens, and B.O. Mills-Lamptey, Method of fabricating structured particles composed of silicon or silicon-based material and their use in lithium rechargeable batteries, US Patent 8 772 174, assigned to Nexeon Ltd. (Oxfordshire, GB), July 8, 2014.
50. S. Iijima, *Nature*, Vol. 354, p. 56, 1991.
51. B.J. Landi, M.J. Ganter, C.D. Cress, R.A. DiLeo, and R.P. Raffaelle, *Energy & Environmental Science*, Vol. 2, p. 638, 2009.
52. H.C. Shim, S. Bang, D.-M. Yoon, Y. Kong, and T. Yu, *Journal of Alloys and Compounds*, Vol. 649, p. 1315, 2015.
53. D. Chalasani, J. Li, N.M. Jackson, M. Payne, and B.L. Lucht, *Journal of Power Sources*, Vol. 208, p. 67, 2012.

54. H. Yamamoto, M. Nishiyama, H. Imagawa, and M. Nishizawa, *Tetrahedron Letters*, Vol. 47, p. 8369, 2006.
55. H. Yamamoto and K. Saisho, Non-aqueous electrolyte secondary battery, US Patent Application 20 070 072 074, March 29, 2007.
56. Y. Li, F. Lian, L. Ma, C. Liu, L. Yang, X. Sun, and K. Chou, *Electrochimica Acta*, Vol. 168, p. 261, 2015.
57. S.-Y. Ha, J.-G. Han, Y.-M. Song, M.-J. Chun, S.-I. Han, W.-C. Shin, and N.-S. Choi, *Electrochimica Acta*, Vol. 104, p. 170, 2013.
58. C.-C. Chang, K.-Y. Lee, H.-Y. Lee, Y.-H. Su, and L.-J. Her, *Journal of Power Sources*, Vol. 217, p. 524, 2012.
59. Y.-K. Han, K. Lee, J. Yoo, and Y.S. Huh, *Theoretical Chemistry Accounts*, Vol. 133, 2014.
60. W. Kohn and L.J. Sham, *Physical Review*, Vol. 140, p. A1133, 1965.
61. Wikipedia, Kohn-Sham equations — wikipedia, the free encyclopedia, 2016. [Online; accessed 16-May-2016].
62. M. Hu, J. Wei, L. Xing, and Z. Zhou, *Journal of Applied Electrochemistry*, Vol. 42, p. 291, 2012.
63. V. Egorov, W.-C. Shin, D. Chernyshov, M. Khasanov, P. Shatunov, and A. Tereshchenko, Electrolyte additive and electrolyte including same and rechargeable lithium battery including electrolyte, US Patent 9 127 023, assigned to Samsung SDI Co., Ltd. (Giheung-Gu, Yongin-Si, Gyeonggi-Do, KR), September 8, 2015.
64. Q. Yu, Z. Chen, L. Xing, D. Chen, H. Rong, Q. Liu, and W. Li, *Electrochimica Acta*, Vol. 176, p. 919, 2015.
65. G.-B. Han, J.-N. Lee, J.W. Choi, and J.-K. Park, *Electrochimica Acta*, Vol. 56, p. 8997, 2011.
66. G. Yan, X. Li, Z. Wang, H. Guo, J. Wang, W. Peng, and Q. Hu, *Electrochimica Acta*, Vol. 166, p. 190, 2015.
67. M.-H. Ryou, J.-N. Lee, D.J. Lee, W.-K. Kim, J.W. Choi, J.-K. Park, and Y.M. Lee, *Electrochimica Acta*, Vol. 102, p. 97 , 2013.
68. K.C. Högström, H. Lundgren, S. Wilken, T.G. Zavalis, M. Behm, K. Edström, P. Jacobsson, P. Johansson, and G. Lindbergh, *Journal of Power Sources*, Vol. 256, p. 430, 2014.
69. S.S. Zhang, *Journal of Power Sources*, Vol. 162, p. 1379, 2006.
70. Z. Lin, Z. Liu, W. Fu, N.J. Dudney, and C. Liang, *Advanced Functional Materials*, Vol. 23, p. 918, 2013.
71. X. Yu, H. Pan, Y. Zhou, P. Northrup, J. Xiao, S. Bak, M. Liu, K.-W. Nam, D. Qu, J. Liu, T. Wu, and X.-Q. Yang, *Advanced Energy Materials*, Vol. 5, 2015.
72. Z. Lin, Z. Liu, W. Fu, N.J. Dudney, and C. Liang, *Advanced Functional Materials*, Vol. 23, p. 1064, 2012.
73. Q. Wang, J. Zheng, E. Walter, H. Pan, D. Lv, P. Zuo, H. Chen, Z.D. Deng, B.Y. Liaw, and X. Yu, *Journal of the Electrochemical Society*, Vol. 162, p. A474, 2015.

74. X. Zuo, C. Fan, X. Xiao, J. Liu, and J. Nan, *Journal of Power Sources*, Vol. 219, p. 94, 2012.
75. X. Zheng, T. Huang, Y. Pan, W. Wang, G. Fang, K. Ding, and M. Wu, *Journal of Power Sources*, Vol. 319, p. 116, 2016.
76. X. Sun, H.S. Lee, X.-Q. Yang, and J. McBreen, *Electrochemical and Solid-State Letters*, Vol. 5, p. A248, 2002.
77. J. Li, W. Yao, Y.S. Meng, and Y. Yang, *The Journal of Physical Chemistry C*, Vol. 112, p. 12550, 2008.
78. M.-H. Ryou, G.-B. Han, Y.M. Lee, J.-N. Lee, D.J. Lee, Y.O. Yoon, and J.-K. Park, *Electrochimica Acta*, Vol. 55, p. 2073, 2010.
79. Y. Li, R. Zhang, J. Liu, and C. Yang, *Journal of Power Sources*, Vol. 189, p. 685, 2009.
80. Z. Cai, Y. Liu, J. Zhao, L. Li, Y. Zhang, and J. Zhang, *Journal of Power Sources*, Vol. 202, p. 341, 2012.
81. G. Yan, X. Li, Z. Wang, H. Guo, and C. Wang, *Journal of Power Sources*, Vol. 248, p. 1306, 2014.
82. T. Huang, X. Zheng, Y. Pan, W. Wang, G. Fang, and M. Wu, *Electrochimica Acta*, Vol. 156, p. 328, 2015.
83. H. Druckrey, H. Kruse, and R. Preussmann, *Naturwissenschaften*, Vol. 55, p. 449, 1968.
84. B. Ulland, M. Finkelstein, E.K. Eisburger, J.M. Rice, and J.H. Weisburger, *Nature*, Vol. 230, p. 460, 1971.
85. BAuA, Hazardous substances ordinance, Federal law 13, Federal Institute for Occupational Safety and Health, Berlin (DE), 2010.
86. Wikipedia, 1,3-propane sultone — wikipedia, the free encyclopedia, 2015. [Online; accessed 13-June-2016].
87. R.F. Fischer, *Industrial & Engineering Chemistry*, Vol. 56, p. 41, 1964.
88. S. Mondal, *Chemical Reviews*, Vol. 112, p. 5339, 2012.
89. J. Pires, L. Timperman, A. Castets, J.S. Peña, E. Dumont, S. Levasseur, R. Dedryvère, C. Tessier, and M. Anouti, *RSC Advances*, Vol. 5, p. 42088, 2015.
90. K. Makhmut, S.-H. Kim, H.-R. Lee, P.A. Shatunov, I.-H. Cho, and W.-C. Shin, Additive for electrolyte of lithium battery, organic electrolyte solution comprising the same, and lithium battery using the organic electrolyte solution, US Patent 9 263 766, assigned to Samsung SDI Co., Ltd. (Yongin-Si, KR), February 16, 2016.
91. X. Zheng, T. Huang, Y. Pan, W. Wang, G. Fang, and M. Wu, *Journal of Power Sources*, Vol. 293, p. 196, 2015.
92. K.-S. Lee, Y.-K. Sun, J. Noh, K.S. Song, and D.-W. Kim, *Electrochemistry Communications*, Vol. 11, p. 1900, 2009.
93. M. Khasanov, W.-C. Shin, D. Chernyshov, A. Tereshchenko, V. Egorov, and P. Shatunov, Electrolyte additive and electrolyte and lithium rechargeable battery including same, US Patent 8 940 434,

assigned to Samsung SDI Co., Ltd. (Yongin-Si, Gyeonggi-Do, KR), January 27, 2015.
94. J. Yang, P. Zhao, Y. Shang, L. Wang, X. He, M. Fang, and J. Wang, *Electrochimica Acta*, Vol. 121, p. 264, 2014.
95. Y.-H. Li, M.-L. Lee, F.-M. Wang, C.-R. Yang, P.P. Chu, S.-L. Yau, and J.-P. Pan, *Applied Surface Science*, Vol. 261, p. 306, 2012.
96. K. Kitoh and H. Nemoto, *Journal of Power Sources*, Vol. 81-82, p. 887, 1999.
97. Underwriters Laboratories, Standard for lithium batteries, UL Standard UL 1642, Underwriters Laboratories Inc., Northbrook, Illinois, 2015.
98. Storage Battery Association, Guideline for safety evaluation on secondary lithium cells, SBA Standard SBA G1101, The Battery Association of Japan, 1997.
99. S. Lux, I. Lucas, E. Pollak, S. Passerini, M. Winter, and R. Kostecki, *Electrochemistry Communications*, Vol. 14, p. 47, 2012.
100. J. Chen, H. Zhang, M. Wang, J. Liu, C. Li, and P. Zhang, *Journal of Power Sources*, Vol. 303, p. 41, 2016.
101. Y. Chen, N. Liu, H. Shao, W. Wang, M. Gao, C. Li, H. Zhang, A. Wang, and Y. Huang, *Journal of Materials Chemistry A*, Vol. 3, p. 15235, 2015.
102. K. Yamagiwa, D. Morita, N. Yabuuchi, T. Tanaka, M. Fukunishi, T. Taki, H. Watanabe, T. Otsuka, T. Yano, J.-Y. Son, Y.-T. Cui, H. Oji, and S. Komaba, *Electrochimica Acta*, Vol. 160, p. 347, 2015.
103. K.S. Kang, S. Choi, J. Song, S.-G. Woo, Y.N. Jo, J. Choi, T. Yim, J.-S. Yu, and Y.-J. Kim, *Journal of Power Sources*, Vol. 253, p. 48, 2014.
104. E.-Y. Jung, D.-C. Hwang, J.-H. Lee, I.-T. Mun, S.-W. Roh, S.-H. Hur, Y.-C. Park, J.-S. Kim, and J.-Y. Ryu, Electrolyte including an additive for rechargeable lithium battery and rechargeable lithium battery including same, US Patent 8 906 559, assigned to Samsung SDI Co., Ltd. (Yongin-Si, KR), December 9, 2014.
105. S. Ryu, D. Kim, and E.Y. Kim, Lithium secondary battery containing additive for improved high-temperature characteristics, US Patent 8 758 944, assigned to LG Chem, Ltd. (Seoul, KR), June 24, 2014.
106. S.R. Narayan, G.K.S. Prakash, R. Aniszfeld, A. Manohar, S. Malkhandi, and B. Yang, High efficiency iron electrode and additives for use in rechargeable iron-based batteries, US Patent Application 20 130 149 615, assigned to University of Southern California, Los Angeles (CA), June 13, 2013.
107. K. Vijayamohanan, A.K. Shukia, and S. Sathyanarayana, *Journal of Electroanalytical Chemistry and Interfacial Electrochemistry*, Vol. 289, p. 55, 1990.
108. T.S. Balasubramanian, K. Vijayamohanan, and A.K. Shukla, *Journal of Applied Electrochemistry*, Vol. 23, p. 947, 1993.

109. Q. Fang, Y. Cheng, X. Jian, L. Zhu, H. Yu, Z. Wang, and L. Jiang, *Journal of Rare Earths*, Vol. 28, p. 72, 2010.
110. Battery University, Bu-402: What is c-rate?, [electronic:] http://batteryuniversity.com/learn/article/what_is_the_c_rate, 2016.
111. X. Ye, Y. Zhu, S. Wu, Z. Zhang, Z. Zhou, H. Zheng, and X. Lin, *Journal of Rare Earths*, Vol. 29, p. 787, 2011.
112. S.N. Begum, V. Muralidharan, and C.A. Basha, *International Journal of Hydrogen Energy*, Vol. 34, p. 1548, 2009.
113. W. Zhang, W. Jiang, L. Yu, Z. Fu, W. Xia, and M. Yang, *International Journal of Hydrogen Energy*, Vol. 34, p. 473, 2009.
114. E. Shangguan, J. Wang, J. Li, G. Dan, Z. Chang, X.-Z. Yuan, and H. Wang, *International Journal of Hydrogen Energy*, Vol. 38, p. 10616, 2013.
115. E. Shangguan, J. Li, D. Guo, Z. Chang, X.-Z. Yuan, and H. Wang, *International Journal of Hydrogen Energy*, Vol. 39, p. 3412, 2014.
116. E. Shangguan, J. Li, Z. Chang, H. Tang, B. Li, X.-Z. Yuan, and H. Wang, *International Journal of Hydrogen Energy*, Vol. 38, p. 5133, 2013.
117. J. Li, E. Shangguan, D. Guo, Q. Li, Z. Chang, X.-Z. Yuan, and H. Wang, *Journal of Power Sources*, Vol. 263, p. 110, 2014.
118. Q. Xu, Y. Zhu, Q. Han, R. Zhao, Y. Zhuang, Y. Liu, S. Zhang, and C. Miao, *Journal of Alloys and Compounds*, Vol. 584, p. 1, 2014.
119. J. Hur and I.T. Kim, *Bulletin of the Korean Chemical Society*, Vol. 36, p. 1625, 2015.
120. J.Y. Jang, Y. Lee, Y. Kim, J. Lee, S.-M. Lee, K.T. Lee, and N.-S. Choi, *Journal of Materials Chemistry A*, Vol. 3, p. 8332, 2015.
121. H. Shang, H. Fan, Y. Liu, W. Hu, Y. Li, and X. Zhan, *Advanced Materials*, Vol. 23, p. 1554, 2011.
122. S.A. Ponomarenko, E.A. Tatarinova, A.M. Muzafarov, S. Kirchmeyer, L. Brassat, A. Mourran, M. Moeller, S. Setayesh, and D. de Leeuw, *Chemistry of Materials*, Vol. 18, p. 4101, 2006.
123. S. Roquet, A. Cravino, P. Leriche, O. Alévêque, P. Frère, and J. Roncali, *Journal of the American Chemical Society*, Vol. 128, p. 3459, 2006.
124. J. Zhang, D. Deng, C. He, Y. He, M. Zhang, Z.-G. Zhang, Z. Zhang, and Y. Li, *Chemistry of Materials*, Vol. 23, p. 817, 2011.
125. E. Ripaud, T. Rousseau, P. Leriche, and J. Roncali, *Advanced Energy Materials*, Vol. 1, p. 540, 2011.
126. H. Shang, H. Fan, Y. Liu, W. Hu, Y. Li, and X. Zhan, *Journal of Materials Chemistry*, Vol. 21, p. 9667, 2011.
127. J. Min, Y.N. Luponosov, T. Ameri, A. Elschner, S.M. Peregudova, D. Baran, T. Heumüller, N. Li, F. Machui, and S. Ponomarenko, *Organic Electronics*, Vol. 14, p. 219, 2013.

128. J. Min, Y.N. Luponosov, A. Gerl, M.S. Polinskaya, S.M. Peregudova, P.V. Dmitryakov, A.V. Bakirov, M.A. Shcherbina, S.N. Chvalun, S. Grigorian, N. Kaush-Busies, S.A. Ponomarenko, T. Ameri, and C.J. Brabec, *Advanced Energy Materials*, Vol. 4, 2014.
129. D. Xu, X. Chen, L. Wang, L. Qiu, H. Zhang, and F. Yan, *Electrochimica Acta*, Vol. 106, p. 181, 2013.
130. V. Suryanarayanan, K.-M. Lee, J.-G. Chen, and K.-C. Ho, *Journal of Electroanalytical Chemistry*, Vol. 633, p. 146, 2009.
131. M. Afrooz and H. Dehghani, *Electrochimica Acta*, Vol. 174, p. 521, 2015.
132. J. Zhao, F. Yan, L. Qiu, Y. Zhang, X. Chen, and B. Sun, *Chemical Communications*, Vol. 47, p. 11516, 2011.
133. H.-L. Hsu, C.-C. Chang, C.-P. Chen, B.-H. Jiang, R.-J. Jeng, and C.-H. Cheng, *Journal of Materials Chemistry A*, Vol. 3, p. 9271, 2015.
134. X. Gong, M. Li, X.-B. Shi, H. Ma, Z.-K. Wang, and L.-S. Liao, *Advanced Functional Materials*, Vol. 25, p. 6671, 2015.
135. B.R. Aïch, J. Lu, S. Beaupré, M. Leclerc, and Y. Tao, *Organic Electronics*, Vol. 13, p. 1736, 2012.
136. C. Sun, Q. Xue, Z. Hu, Z. Chen, F. Huang, H.-L. Yip, and Y. Cao, *Small*, Vol. 11, p. 3343, 2015.
137. W. Yue, R.S. Ashraf, C.B. Nielsen, E. Collado-Fregoso, M.R. Niazi, S.A. Yousaf, M. Kirkus, H.-Y. Chen, A. Amassian, J.R. Durrant, and I. McCulloch, *Advanced Materials*, Vol. 27, p. 4702, 2015.
138. Wikipedia, Stille reaction — wikipedia, the free encyclopedia, 2016. [Online; accessed 9-June-2016].
139. J.K. Stille, *Angewandte Chemie International Edition in English*, Vol. 25, p. 508, 1986.
140. M. Wang, D. Cai, Z. Yin, S.-C. Chen, C.-F. Du, and Q. Zheng, *Advanced Materials*, Vol. 28, p. 3359, 2016.
141. L.M.J.M. Blomen and M.N. Mugerva, eds., *Fuel Cell Systems*, Springer Science + Business Media, New York, 1993.
142. R. Busby, *Hydrogen and Fuel Cells: A Comprehensive Guide*, PennWell Corp., Tulsa, Oklahoma, 2005.
143. B. Sørensen, *Hydrogen and Fuel Cells Emerging Technologies and Applications*, Academic Press, Oxford Burlington, MA, 2012.
144. F. Barbir, *PEM Fuel Cells Theory and Practice*, Academic Press, London, 2013.
145. C.F. Schönbein, *Annalen der Physik*, Vol. 123, p. 101, 1839.
146. W.R. Grove, *Philosophical Magazine Series 3*, Vol. 14, p. 127, 1839.
147. Wikipedia, Grove cell — wikipedia, the free encyclopedia, 2016. [Online; accessed 11-July-2016].
148. J.A.A. Ketelaar, "History," in L.M.J.M. Blomen and M.N. Mugerva, eds., *Fuel Cell Systems*, chapter 1, pp. 19–36. Springer Science + Business Media, New York, 1993.

149. K. Matsuoka and T. Taniguchi, Fuel cell, US Patent 7 771 859, assigned to Sanyo Electric Co., Ltd. (Osaka, JP), August 10, 2010.
150. W.-S. Jeon, S.-H. Suh, and S.-G. Hong, Oxygen reduction electrode and fuel cell including the same, US Patent 8 632 929, assigned to Samsung SDI Co., Ltd. (Yongin-Si, KR), January 21, 2014.
151. L. Krishnan, G.W. Yeager, and G.L. Soloveichik, Polymer-electrolyte membrane, electrochemical fuel cell, and related method, US Patent 8 906 572, assigned to General Electric Company (Niskayuna, NY), December 9, 2014.
152. E. van de Ven, A. Chairuna, G. Merle, S.P. Benito, Z. Borneman, and K. Nijmeijer, *Journal of Power Sources*, Vol. 222, p. 202, 2013.
153. T.J. Fuller, M.R. Schoeneweiss, T. Xie, F. Coms, S.M. MacKinnon, and G.W. Fly, Additives for fuel cell layers, US Patent 9 083 049, assigned to GM Global Technology Operations LLC (Detroit, MI), July 14, 2015.
154. K. Sato, M. Yasukawa, A. Sagasaki, T. Wada, and Y. Kato, Fuel cell system including coolant additive and ion exchange resin and fuel-cell vehicle, US Patent 8 951 689, assigned to Suzuki Motor Corporation (JP) Showa Water Industries Co., Ltd. (JP), February 10, 2015.
155. B. Wenderoth, S. Dambach, L. Meszaros, and U. Fidorra, Coolant comprising azole derivatives for cooling systems in fuel-cell drives, US Patent 7 419 617, assigned to BASF Aktiengesellschaft (Ludwigshafen, DE), September 2, 2008.
156. A.D. Mossman, Membrane exchange humidifier for a fuel cell, US Patent 6 864 005, assigned to Ballard Power Systems Inc. (Burnaby, CA), March 8, 2005.
157. S. Mallakpour, M. Zhiani, A. Barati, and H. Rostami, *International Journal of Hydrogen Energy*, Vol. 38, p. 12418, 2013.

Additives for High Performance Applications: Chemistry and Applications. Johannes Karl Fink.
2017 Scrivener Publishing LLC. Published 2017 by John Wiley & Sons, Inc.

3

Medical Uses

3.1 High Performance Additive Manufactured Scaffolds

The advances by additive manufacturing have significantly improved the control over the microarchitecture of scaffolds for tissue engineering (1). The optimization of additive manufactured scaffolds microarchitecture with regard to conflicting requirements, e.g., mechanical stiffness and porosity level, have been assessed.

The integration of additive manufacturing with other scaffold fabrication methods, i.e., combined additive manufacturing, is an interesting trend. This results in hybrid architectures with complementary structural features.

Even when this innovative approach is still at its beginning, significant results have been achieved with regard to an improved biological response to the scaffold, in particular to the regeneration of complex tissues. The state of the art in the field of combined additive manufacturing has been reviewed in detail (1,2).

3.1.1 Nanotechnology

The field of nanotechnology has a definite potential to significantly advance the field of bone tissue engineering (3). The current limitations in regenerative strategies include impaired cellular proliferation and differentiation, insufficient mechanical strength of scaffolds, and inadequate production of extrinsic factors necessary for efficient osteogenesis.

Some major areas of research in nanotechnology with potential implications in bone regeneration have been reviewed (3):

1. Nanoparticle-based methods for delivery of bioactive molecules, growth factors, and genetic material,
2. Nanoparticle-mediated cell labeling and targeting, and
3. Nano-based scaffold construction and modification to enhance physicochemical interactions, biocompatibility, mechanical stability, and cellular attachment.

At the moment, as these technologies continue to evolve, ultimate translation to the clinical environment may allow for improved therapeutic results for patients with large bone deficits and osteodegenerative diseases (3).

3.1.2 Poly(caprolactone) Tricalcium Phosphate Scaffolds

The feasibility of additive manufactured poly(caprolactone) (PCL) silanized tricalcium phosphate scaffolds coated with carbonated hydroxyapatite-gelatin composite for bone tissue engineering has been tested (4). In order to reinforce the scaffolds to match the mechanical properties of cancellous bone, tricalcium phosphate has been modified with γ-glycidoxypropyltrimethoxysilane and incorporated into PCL to synthesize a PCL/silanized tricalcium phosphate composite. γ-Glycidoxypropyltrimethoxysilane is shown in Figure 3.1.

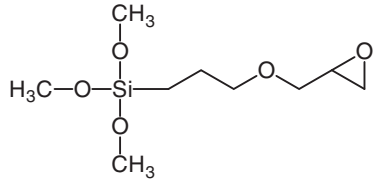

Figure 3.1 γ-Glycidoxypropyltrimethoxysilane.

The successful modification has been confirmed by X-ray photoelectron spectroscopy (XPS) and Fourier transform infrared spectroscopy analysis. Additive manufactured PCL/silanized tricalcium phosphate scaffolds have been fabricated using a screw extrusion system. Testing mechanical properties have demonstrated that both

the compressive modulus and compressive yield strength of the developed PCL/silanized tricalcium phosphate scaffolds fall within the lower ranges of mechanical properties for a cancellous bone, with a compressive modulus and compressive yield strength of 6.0 times and 2.3 times of those of PCL/tricalcium phosphate scaffolds, respectively.

In order to enhance the osteoconductive property of the developed PCL/silanized tricalcium phosphate scaffolds, a carbonated hydroxyapatite-gelatin composite has been coated onto the scaffolds using a biomimetic co-precipitation process, which has been characterized by scanning electron microscope (SEM) and XPS. Confocal laser microscopy and SEM images revealed a most uniform distribution of porcine bone marrow stromal cells and cell-sheet accumulation on the carbonated hydroxyapatite-gelatin composite coated PCL/silanized tricalcium phosphate scaffolds (4).

The proliferation rate of bone marrow stromal cells on the carbonated hydroxyapatite-gelatin composite coated PCL/silanized tricalcium phosphate scaffolds is 2.0 and 1.4 times higher compared to PCL/silanized tricalcium phosphate and carbonated hydroxyapatite coated PCL/silanized tricalcium phosphate scaffolds, respectively, at the 10th day.

Furthermore, the reverse transcription polymerase chain reaction and western blot analysis revealed that carbonated hydroxyapatite-gelatin composite coated PCL/silanized tricalcium phosphate scaffolds stimulate an osteogenic differentiation of bone marrow stromal cells the most in comparison to the other scaffolds. *In-vitro* results of SEM, confocal microscopy and proliferation rate also showed that there is no detrimental effect of the modification on biocompatibility of the scaffolds (4).

3.1.3 Silk Fibroin Nanofibers

Fibroin is an insoluble protein present in silk created by silkworms and spiders. Its primary structure mainly consists of the recurrent amino acid sequence of glycine-serine-glycine-alanine-glycine-alanine (5).

As stated above, silk fibroin is a natural polymer and has thus established a good reputation for bone tissue engineering applications due to its many unique properties, including exceptional

biocompatibility, biodegradability, mechanical behavior, and ease of processability. The recent advances in the design and application of silk fibroin-based scaffolds for bone regeneration have been reviewed (6,7).

3.1.3.1 Electrospun Silk Fibroin Scaffolds

Electrospinning is a technique used for the production of polymer nanofiber meshes. The use of biodegradable and biocompatible polymers to produce nanofibers that closely mimic the extracellular matrix of different tissues has opened a wide range of possibilities for the application of electrospinning in tissue engineering (8). Functional materials formed by the electrospinning technology are of interest for many bioactive applications. The issues of this topic have been reviewed (9).

Electrospun silk fibroin scaffolds exhibit a large surface area, high porosity, and interconnection for cell adhesion and proliferation. They may replace collagen for many tissue engineering applications (10).

Despite such advantages, electrospun silk fibroin scaffolds are still limited as bone tissue replacement due to their low mechanical strengths. The enhancement of the mechanical strength has been demonstrated by incorporating inorganic ceramics into polymers.

However, electrospinning of a mixture of silk fibroin and inorganic ceramics, such as hydroxyapatite, is still a challenging task. The mechanical properties of electrospun silk fibroin scaffolds can be enhanced by uniformly dispersing hydroxyapatite nanoparticles within silk fibroin nanofibers. Hydroxyapatite nanoparticles were modified by γ-glycidoxypropyltrimethoxysilane for uniform dispersion and enhanced interfacial bonding between hydroxyapatite and silk fibroin fibers.

Optimal conditions for electrospinning of silk fibroin and γ-glycidoxypropyltrimethoxysilane modified hydroxyapatite nanoparticles to achieve beadless nanofibers without any aggregation of hydroxyapatite nanoparticles could be identified.

MTT tests (11) and SEM analysis of the osteoblasts-cultured scaffolds could confirm the biocompatibility of the composite scaffolds.

When cells are populated in fibrous scaffolds, the mechanical strength of the individual nanofibers has a significant influence on

the cell behavior, such as, cell attachment, proliferation, differentiation, and protein expressions. Silk fibroin has been frequently utilized in a form of nanofibers as a promising tissue scaffolding material. The mechanical properties of the composite scaffolds were analyzed by tensile tests for the scaffolds using varying contents of hydroxyapatite within the silk fibroin fibers.

The mechanical moduli and dependency on the content of the hydroxyapatite nanoparticles could be analyzed using three point bending with a tipless atomic force microscopy cantilever (12). An increase of the hydroxyapatite content up to 20% increased the mechanical properties of the composite scaffolds. But a further increase above 20% disrupted the polymer chain networks within silk fibroin nanofibers and weakened the mechanical strength (10).

3.1.3.2 Chitosan Silk Fibroin Scaffolds

Electrospinning of inorganic-organic composites into nanofibers has emerged as a new approach for the fabrication of scaffolds for biomimetically engineered bone tissues. Biomimetic nanocomposite nanofibers are composed of mesoporous silica nanoparticles and chitosan, cf. Figure 3.2. The materials were prepared by electrospinning. Increasing the content of the mesoporous silica nanoparticles to 10% enhanced the mechanical properties of the composite scaffolds (13).

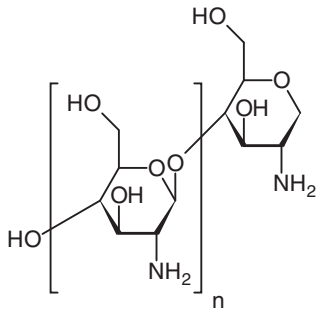

Figure 3.2 Chitosan.

The incorporation of nanohydroxyapatite into a chitosan/silk fibroin nanofibrous membrane scaffold may provide a favorable mi-

croenvironment that more closely mimics the natural bone tissue physiology and facilitates an enhanced osteogensis of the implanted cell population (14).

A pristine chitosan/silk fibroin nanofibrous membrane scaffold composite membrane scaffold with intrafibrillar nanohydroxyapatite was prepared by *in-situ* blending of 10% or 30% nanohydroxyapatite before the electrospinning step. There was a deposition of nanohydroxyapatite through alternative soaking surface mineralization.

The effect of the incorporation of HAP nanoparticles on the physicochemical properties of the nanofibrous membrane scaffold was investigated. The presence of ca. 30 *nm* nanohydroxyapatite in the composite nanofibrous membranes was confirmed by thermogravimetry, X-ray diffraction, and SEM. It was found that the alternative soaking surface mineralization method drastically influenced the mechanical properties of the nanofibrous membrane scaffold with a 88% and 94% drop in Young's modulus and ultimate maximum stress (14).

The effects of nanohydroxyapatite content and location on proliferation and osteogenic differentiation of human bone marrow mesenchymal stem cells were investigated by *in-vitro* cell culture experiments. The proliferation of the human bone marrow mesenchymal stem cells showed no significant difference among pristine and composite nanofibrous membrane scaffold.

In-vivo experiments were carried out with human bone marrow mesenchymal stem cells seeded in chitosan/silk fibroin/30% nanohydroxyapatite nanofibrous membrane scaffold prepared by *in-situ* blending and subcutaneous implantation in nude mice. Micro-computed tomography images and histological and immunohistochemical analysis of the retrieved membrane scaffold construct after 1 and 2 months of implantation indicated that nanofibrous membrane scaffold showed the potential for bone regeneration and thus can be suggested as a promising scaffold for bone tissue engineering (14).

3.1.3.3 Hydroxyapatite-Tussah Silk Fibroin Scaffolds

The bone is a composite of inorganic and organic materials and possesses a complex hierarchical architecture consisting of mineralized

fibrils formed by collagen molecules and coated with oriented hydroxyapatite (15). In order to regenerate bone tissue, it is necessary to provide a scaffold that mimics the architecture of the extracellular matrix in the native bone.

A scaffold was described which is a nanostructured composite with a core made of a composite of hydroxyapatite and tussah silk fibroin (15). The core is encased in a shell of tussah silk fibroin. The composite fibers were fabricated by coaxial electrospinning using green water solvent.

In comparison to nanofibers of pure tussah silk, the composite notably improved the mechanical properties, with a higher initial modulus and breaking stress. It was found that the fiber scaffold supported both the cell adhesion and the proliferation, and also functionally promoted alkaline phosphatase and mineral deposition relevant for biomineralization. The composites are more biocompatible than pure tussah silk fibroin or cover slip (15).

3.1.3.4 Silk Fibroin Microneedles

Thermal drawing is a versatile rapid prototyping method that can freely form microneedle structures with an ultrahigh aspect ratio without relying on any complex and expensive processes (16). However, thermal drawing is only applicable to thermoplastic materials and most natural biomaterials are incompatible with this method.

For this reason, it has been proposed to use thermal drawing for the fabrication of master molds with high aspect ratios and replicate the shape by micromolding. Microneedles with various body profiles could be fabricated using thermal drawing and could be replicated multiple times to silk fibroin microneedles using micromolding. The original microneedle shape was precisely copied to the silk fibroin microneedles.

A methanol treatment enhanced the mechanical strength of silk fibroin microneedles up to about 113%. It has been demonstrated that the methanol exposure time could effectively control the drug release rates from the silk fibroin microneedles (16).

3.1.4 Calcium Phosphate, Hydroxyapatite, and Poly(d,l-lactic acid)

Because of their outstanding bioactivity and biocompatibility, calcium phosphate-based materials have been widely investigated for applications in the biomedical fields (17). Amorphous calcium phosphate nanospheres and hydroxyapatite nanorods have been prepared and hybridized with poly(*d*,*l*-lactic acid) in order to fabricate composite nanofibers using an electrospinning technique.

The so-prepared composite nanofibers exhibit favorable mineralization behaviors in a simulated body fluid. In the mineralization process, the calcium phosphate nanospheres and the hydroxyapatite nanorods play an important role in the formation of hydroxyapatite nanosheets on the surface of composite nanofibers. The composite nanofibers exhibit a high biocompatibility (17).

3.1.5 Propylene Fumarate Lactic Acid Copolymer

Scaffolds with intrinsically interconnected porous structures are highly desirable in tissue engineering and regenerative medicine. Three-dimensional polymer scaffolds with highly interconnected porous structures could be fabricated by thermally induced phase separation using novel synthesized biodegradable poly(propylene fumarate)-*co*-poly(*l*-lactic acid) in a dioxane/water binary system (18).

Porous scaffolds could be achieved by optimizing the conditions to get interconnected porous structures. The effect of phase separation parameters on scaffold morphology was investigated, including polymer concentration, quenching time, the ratio of dioxane to water, and the freeze temperature.

Interesting pore morphologies were created by adjustment of the processing parameters, e.g., a flower-shaped, a spherulite-like, and a bead-like morphology. The change of the phase separation conditions also resulted in remarkable differences in porosities of the scaffold and their thermal properties.

Scaffolds with various mechanical strength, degradation rates, and protein adsorption capabilities could be fabricated using the phase separation method (18).

3.1.6 Thermosensitive Composite Gel

A thermosensitive composite gel for use as a bone graft substitute has been designed (19). The gel can provide a more suitable microenvironment by using an amphiphilic triblock copolymer consisting of methoxy poly(ethylene glycol), and poly(lactic-*co*-glycolic acid).

By aqueous dispersion of the triblock copolymer mixed with different ratios of hydroxyapatite/tricalcium phosphate, a composite gel underwent a sol-gel-sol transition when the temperature was increased from 4°C to 70°C. The particle size and critical micellization concentration were increased by adding the ceramic materials.

In the course of the *in-vitro* degradation process, the composite gels demonstrated a slight decrease in pH value, a slower degradation rate, less toxicity, and a higher cell survival rate. The biocompatibility of the composite gels was validated by a hemolysis test. *In-vivo* studies with animals demonstrated both radiographic and gross bone union when the ratio of hydroxyapatite to tricalcium phosphate was 7:3 (19).

3.1.7 Biomimetic Wet-Stable Fibers

One of the limitations of electrospun collagen as bone-like fibrous structure is the potential collagen triple helix denaturation in the fiber state and the corresponding inadequate wet stability even after crosslinking (20).

The feasibility of fabrication of wet-stable fibers by wet-spinning and diacid-based crosslinking of collagen triple helices has been demonstrated (20). The fibers can also act as a bone-mimicking mineralization system. Circular dichroism experiments demonstrated a nearly complete triple helix retention in resulting wet-spun fibers, and the corresponding chemically crosslinked fibers successfully preserved their fibrous morphology following a one week incubation in phosphate buffer solution. The diacid-based crosslinking route imparted a superior tensile modulus and strength into the resulting fibers.

To mimic the constituents of natural bone extracellular matrix, the crosslinked fibers were coated with carbonated hydroxyapatite through a biomimetic precipitation, resulting in an attractive bio-

material for guided bone regeneration, e.g., in bony defects of the maxillofacial region (20).

3.1.8 Poly(ester urea) from l-Leucine

Electrospun scaffolds from an amino acid containing poly(ester urea) have been developed for use in tissue engineering applications (21). The selected poly(ester urea) was obtained with a high yield and molecular weight by reaction of phosgene with a bis(α-aminoacyl)-α,ω-diol-diester monomer. The polymer with *l*-leucine, 1,6-hexanediol and carbonic acid units showed a semicrystalline character and a comparatively high glass transition temperature and high melting temperature. poly(ester urea) is highly soluble in most organic solvents. This facilitates the electrospinning process and the effective incorporation of drugs with bactericidal activity, e.g., biguanide derivatives such as clorhexidine and poly(hexamethylenebiguanide) and enzymes, e.g., α-chymotrypsin, that accelerated the degradation process. Clorhexidine is shown in Figure 3.3.

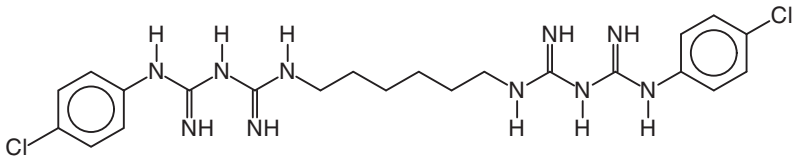

Figure 3.3 Clorhexidine.

The poly(ester urea) compounds were found to be degradable in media containing lipases and proteinases, but the degradation rate was highly dependent on the surface area, being specifically greater for scaffolds with respect to films. The scaffolds were found to be biocompatible, as demonstrated by adhesion and proliferation assays performed with fibroblast and epithelial cells (21).

3.1.9 Static Cell Seeding Versus Vacuum Cell Seeding

An adequate cell seeding technique is essential for effective bone regeneration on cell-seeded constructs of porous tricalcium phos-

phates (22). In the past, dynamic cell seeding, in which an external force is applied to seed cells on a biomaterial, resulted in more homogeneous cell seeding in low porosity scaffolds than static seeding. However, the optimal cell seeding technique for high porosity scaffolds has not yet been fixed.

Human mesenchymal stem cells were isolated from bone marrow and characterized (22). The cells were seeded on low porosity (45%) and high porosity (90%) tricalcium phosphate scaffolds using a static and a vacuum seeding technique. LIVE/DEAD® staining of the cell-scaffold complexes followed by confocal laser scanning microscopy was used to measure cell proliferation, cell distribution and cell viability one, three and seven days after seeding.

The cell proliferation was also quantified using a deoxyribonucleic acid quantification assay. Neither static nor vacuum seeding resulted in homogeneous cell seeding on both low and high porosity scaffolds. The cell density was lower on the inside than on the outside of the scaffolds. On low porosity scaffolds, the vacuum method yielded the highest numbers of cells compared to the static method. Low porosity scaffolds were seeded most homogeneously using the static seeding method.

Seven days after seeding, the numbers of the adherent cells were comparable for both scaffold types and independent of the applied cell seeding technique. In summary, on high porosity scaffolds, static seeding results in more homogeneous cell seeding and this method is easier to use than a vacuum seeding technique (22).

3.1.10 Controlled Drug Release

The generation of porous topographic substrates by mimicking the native extracellular matrix to promote the regeneration of damaged bone tissues, is a rather challenging process (23).

Scaffolds that have been developed for bone tissue regeneration support bone cell growth and induce bone-forming cells by natural proteins and growth factors. Several issues of these materials are improper scaffold stability, insufficient cell adhesion, proliferation, and differentiation. For these reasons, the use of engineered nanoparticles is of interest in bone tissue engineering applications.

Electrospraying is advantageous in comparison to other methods, as it generates nanomaterials of particle sizes in the microscale

range and nanoscale range. The size and the charge of the particles can be controlled by regulating the polymer solution flow rate and the electric voltage. Nanoparticles show unique properties such as large surface area to volume ratio, small size, and higher reactivity. These properties make them promising candidates in the field of biomedical engineering.

These nanomaterials can be extensively used as therapeutic agents and for drug delivery. The controlled and sustained release of encapsulated drugs, proteins, vaccines, growth factors, cells, and nucleotides from nanoparticles has been well developed in the field of nanomedicine. These topics have been reviewed (23).

References

1. S.M. Giannitelli, P. Mozetic, M. Trombetta, and A. Rainer, *Acta Biomaterialia*, Vol. 24, p. 1, 2015.
2. M. Tarik Arafat, I. Gibson, and X. Li, *Rapid Prototyping Journal*, Vol. 20, p. 13, 2014.
3. G.G. Walmsley, A. McArdle, R. Tevlin, A. Momeni, D. Atashroo, M.S. Hu, A.H. Feroze, V.W. Wong, P.H. Lorenz, M.T. Longaker, and D.C. Wan, *Nanomedicine: Nanotechnology, Biology and Medicine*, Vol. 11, p. 1253, 2015.
4. M. Tarik Arafat, C.X.F. Lam, A.K. Ekaputra, S.Y. Wong, C. He, D.W. Hutmacher, X. Li, and I. Gibson, *Soft Matter*, Vol. 7, p. 8013, 2011.
5. Wikipedia, Fibroin — wikipedia, the free encyclopedia, 2015. [Online; accessed 24-June-2016].
6. F. Mottaghitalab, H. Hosseinkhani, M.A. Shokrgozar, C. Mao, M. Yang, and M. Farokhi, *Journal of Controlled Release*, Vol. 215, p. 112, 2015.
7. J. Melke, S. Midha, S. Ghosh, K. Ito, and S. Hofmann, *Acta Biomaterialia*, Vol. 31, p. 1, 2016.
8. J.V. Araujo, P.P. Carvalho, and S.M. Best, "Electrospinning of bioinspired polymer scaffolds," in E.L. Bertassoni and G.P. Coelho, eds., *Engineering Mineralized and Load Bearing Tissues*, pp. 33–53. Springer International Publishing, Cham, 2015.
9. S. Torres-Giner, R. Pérez-Masiá, and J.M. Lagaron, *Polymer Engineering & Science*, Vol. 56, p. 500, 2016.
10. H. Kim, L. Che, Y. Ha, and W. Ryu, *Materials Science and Engineering: C*, Vol. 40, p. 324, 2014.
11. Wikipedia, Mtt assay — wikipedia, the free encyclopedia, 2016. [Online; accessed 23-June-2016].

12. D. Yang, H. Kim, J. Lee, H. Jeon, and W. Ryu, *Composites Science and Technology*, Vol. 122, p. 113, 2016.
13. K. Li, H. Sun, H. Sui, Y. Zhang, H. Liang, X. Wu, and Q. Zhao, *RSC Advances*, Vol. 5, p. 17541, 2015.
14. J.-P. Chen, G.-J. Lai, and K.T. Shalumon, *International Journal of Nanomedicine*, p. 567, 2015.
15. W. Shao, J. He, F. Sang, B. Ding, L. Chen, S. Cui, K. Li, Q. Han, and W. Tan, *Materials Science and Engineering: C*, Vol. 58, p. 342, 2016.
16. J. Lee, S.H. Park, I.H. Seo, K.J. Lee, and W. Ryu, *European Journal of Pharmaceutics and Biopharmaceutics*, Vol. 94, p. 11, 2015.
17. H. Zhang, Q.-W. Fu, T.-W. Sun, F. Chen, C. Qi, J. Wu, Z.-Y. Cai, Q.-R. Qian, and Y.-J. Zhu, *Colloids and Surfaces B: Biointerfaces*, Vol. 136, p. 27, 2015.
18. X. Liu, A.L. Miller II, B.E. Waletzki, M.J. Yaszemski, and L. Lu, *RSC Advances*, Vol. 5, p. 21301, 2015.
19. P.-L. Lai, C.T.-Y. Lin, D.-W. Hong, S.-R. Yang, Y.-H. Chang, L.-H. Chen, W.-J. Chen, and I.-M. Chu, *Chemical Engineering Science*, Vol. 89, p. 133, 2013.
20. M.T. Arafat, G. Tronci, J. Yin, D.J. Wood, and S.J. Russell, *Polymer*, Vol. 77, p. 102, 2015.
21. A. Diaz, L.J. del Valle, D. Tugushi, R. Katsarava, and J. Puiggali, *Materials Science and Engineering: C*, Vol. 46, p. 450, 2015.
22. A.T. Buizer, A.G. Veldhuizen, S.K. Bulstra, and R. Kuijer, *Journal of Biomaterials Applications*, Vol. 29, p. 3, 2014.
23. P. Jayaraman, C. Gandhimathi, J.R. Venugopal, D.L. Becker, S. Ramakrishna, and D.K. Srinivasan, *Advanced Drug Delivery Reviews*, Vol. 94, p. 77, 2015.

Additives for High Performance Applications: Chemistry and Applications. Johannes Karl Fink.
2017 Scrivener Publishing LLC. Published 2017 by John Wiley & Sons, Inc.

4

Lubricants

4.1 Fuels

4.1.1 Graphene Oxide

Graphene oxide is a layered material bearing a variety of oxygen-containing functional groups on its basal planes and edges, which allow it as a substrate to conduct a variety of chemical transformations.

Graphene oxide can be readily manipulated by chemical modification because it has various oxygen-containing functional groups identified as hydroxyl and epoxy groups on the basal planes, and smaller amounts of carboxy, carbonyl, phenol, lactone, and quinone at the sheet edges (1,2). These polar oxygen-containing groups allow graphene oxide to be modified or restored by some organic solvents for improving its dispersion and stability.

Modified graphene oxide was prepared using alkyl imidazolium ionic liquids (1-butyl-3-methylimidazolium tetrafluoroborate, 1-butyl-3-methylimidazolium hexafluorophosphate and 1-hexyl-3-methylimidazolium bis(trifluoromethylsulfonyl) amide via an epoxide ring-opening reaction, cation-p stacking, or van der Waals interactions, with modified graphene exfoliated from a graphite rod by a moderate electrochemical method as a a comparative material (3).

The stability and tribological properties of modified graphene oxide and modified graphene as multialkylated cyclopentanes (MACs) additives were investigated in detail. The results show that the graphene oxide is converted into graphene through the chemical

modification using imidazolium ionic liquids, and modified graphene oxide with good dispersion and stability in multialkylated cyclopentanes significantly improves the tribological performance.

Friction and wear were reduced about 27% and 74% with pure multialkylated cyclopentanes. The excellent tribological properties are attributed to the formation of imidazolium ionic liquids containing graphene-rich tribofilm on the sliding surfaces, which as the third body can prevent the sliding surfaces from straight asperity contact and improve friction reducing and anti-wear behaviors (3).

4.1.2 Deposit Control

Additives for gasoline used in vehicles have been used for many years to improve the performance of the vehicle, reduce the emissions from the combustion of the fuel, and modify the physical and chemical properties of the fuel (4).

One additive that has been used for many years is ethanol. However, the use of ethanol in a gasoline combusted in an internal combustion engine is well known to create harmful and undesirable deposits on the fuel intake valves of the engine.

In fact, ethanol fuel mixtures can reduce the formation of these intake valve deposits, but such a remediation typically shifts the problem to the combustion chamber, where unacceptable combustion chamber deposits are then formed. Therefore, an additive is needed which upon combustion will effect in the engine a significant reduction in the intake valve deposits and simultaneously effect a reduction of the combustion chamber deposits in the engine.

A method for reducing all the engine deposits in the course of combusting a fuel having a high concentration of an oxygenate and a detergent-containing fuel additive has been developed (4).

The oxygenate in the fuel is ethanol, and the detergent is Mannich-based, a poly(isobutylene) cresol detergent, e.g., HiTEC™ 6421 from Ethyl Corporation. Increasing the amount of oxygenate increases the conductivity of the fuel. The increase in conductivity in combination with the addition of a detergent, more effectively reduces engine deposits. Good results are obtained when the conductivity of the fuel is more than 1 $mS\,m^{-3}$.

It has been found that the ethanol and the Mannich-base detergent work synergistically to control the formation of deposits, without

a negative impact on combustion chamber deposits. The intake valve deposits are reduced and combustion chamber deposits are not increased when the Mannich-base detergent additive is used with ethanol in a concentration of more than 5% by volume in the fuel (4).

4.2 Lubricant Additives

Lubricants comprise a variety of compounds selected for desirable characteristics such as anti-wear and anti-friction properties (5, 6). Lubricant additives can enhance the lubricity of the lubricant base or may provide anti-wear characteristics. Often commercial lubricants are compositions containing a lubricant base such as a hydrocarbon oil or grease, to which is added numerous lubricant additives selected for additional desirable properties. Lubricant additives may enhance the lubricity of the lubricant base or may provide anti-wear or other desirable characteristics.

Lubricants are used in enormous quantities. For example, more than four billion quarts of crankcase oil are used in the United States per year. However, many lubricants currently in use also have undesirable characteristics. Currently available crankcase oils generally include the anti-wear additive zinc dialkyldithiophosphate, which contains phosphorous and sulfur. Phosphorous and sulfur poison catalytic converters cause increased automotive emissions. It is expected that the EPA eventually will mandate the total elimination of zinc dialkyldithiophosphate or will allow only extremely low levels of zinc dialkyldithiophosphate in crankcase oil. However, no acceptable anti-wear additives to replace zinc dialkyldithiophosphate in engine oils are currently available.

Additionally, lubricant bases used in conventional lubricants usually have lubricant additives added to them to improve lubricity. Many of these lubricant additives do not provide sufficient additional lubricity or possess additional undesirable characteristics (6).

4.2.1 GL Ratings

Gear lubricant compositions are classified by the American Petroleum Institute (API) using the so-called GL ratings (7, 8). These classifications are subdivided into six classes. The lowest rating,

API GL-1, classifies oils used for light conditions, which consist of base oils without additives. The highest rating, API GL-6, classifies oils for very heavy conditions, such as high speeds of sliding and significant shock loading, and which contain up to 10% high performance antiscuffing additives. However, class API GL-6 is not applied any more as it is considered that class API GL-5 will meet most severe requirements. Lubricant compositions classified meeting API GL-5 performance requirements are generally applied, for example, in hypoid gears having significant displacement of axles.

4.2.2 Organophosphates

Methods for preparing lubricant additives and lubricants by mixing or reacting together organophosphates such as zinc dialkyldithiophosphate and organofluorine compounds such as poly(tetrafluoroethylene) (PTFE) have been described. The PTFE used comprise more than 40 carbon atoms. The synergistic effect between the dialkyldithiophosphate and functionalized, irradiated PTFE may occur either as a mixture of zinc dialkyldithiophosphate and the irradiated PTFE, or as a reaction product between both compounds. Also, a synergistic effect between fluorinated zinc dialkyldithiophosphate and sulfurized additives has been observed (5).

4.2.3 Crankcase Oils

Conventional crankcase oils contain, as anti-wear additive, zinc dialkyldithiophosphate, which contains phosphorous and sulfur. However, phosphorous and sulfur poison catalytic converters, thus causing increased automotive emissions.

A lubricant additive has been produced by mixing a zinc dialkyldithiophosphate and a low molecular weight PTFE compound and reacting these compounds (6, 9). Irradiated PTFE is particularly suited for its use with reaction mixtures comprising organophosphates and metal halides, as it interacts strongly with such compounds, resulting in reaction products that are usable as high performance lubricant additives.

For example, molybendum disulfide can enhance the lubricant properties of lubricant additives by the formation of molybendum

disulfide complexes with the reaction products formed by the organophosphate and organofluoride reactants (6).

4.2.4 Low Sulfur and Low Metal Additive Formulations

The types of additives used for a formulation and the ranges are listed in Table 4.1.

Table 4.1 Types of additives (10).

Additive	Range/[%]
Anti-wear	35–45
Anti-rust	8–12
Metal Passivator	2–4
Antioxidant	12–17
Friction Modifier	15–26
Defoamant	4–8

The anti-wear additive has at least two components, i.e., a phosphate ester and an amine phosphate. The antioxidant is an aryl amine. The anti-rust additive is an amide carboxylate. The metal passivator is preferably a amine phosphate. The demulsifier is a low molecular weight extreme pressure or EO-PO polymer. The defoamant is a two component system consisting of poly(siloxane) and poly(methyl methacrylate). In addition, an oleyl phosphate as anti-wear friction reducer can be added. Preferably the additives should have low levels or zero levels of metal and sulfur (10).

The lubrication of industrial equipment including gears and enclosed gearboxes has become increasingly more difficult. This difficulty is partially caused by machinery builders continually shrinking equipment and driving more power through a given speed reducer. Generally, gear oil consists of base oil more viscous than typical engine oils, and an additive package which is formulated to enhance various performance features.

These additive features include: protection against wear, resistance to thickening by the use of antioxidants, rust protection, copper-metal passivation, demulsification, air release and foam control, among others. Industrial gear oils have to achieve the following requirements: excellent resistance to aging and oxidation, low foam-

ing tendency, good load-carrying capacity, neutrality toward the materials involved (ferrous and nonferrous metals, seals, paints), suitability for high and/or low temperatures, and good viscosity-temperature behavior.

The most important performance feature that additives impart is anti-wear protection. The most prevalent anti-wear additive systems in gear lubricating oils contain combinations of sulfur-containing hydrocarbons with various amine-phosphates, and/or phosphates. The key downside of these sulfur-containing additives is that while they protect against wear, they rapidly hydrolyze in the presence of acidic contaminates. This reaction produces sulfuric acid, causing excessive corrosive damage. It is then very desirable to develop gear oil which is capable of delivering all the previously mentioned features while being sulfur free or at least low sulfur.

Oil operating temperature and efficiencies are very important to the designers, builders, and users of equipment which employ worm gearing. On a relative basis, a higher percentage efficiency rating for a lubricant results in more power (torque) being transmitted through a subject gearbox. Since more power is being transferred through a piece of equipment using a more efficient lubricant, less power is being wasted on friction or heat. It is desirable for a lubricant to be optimized for maximum power throughput and to therefore allow for lower operating temperatures. Lower operating temperatures in gearboxes give rise to several benefits which include: lower energy consumption, longer machine life, and longer seal life. Seal failures are one of the principle reasons for repair and downtime in rotating equipment. A decrease of 10°C of operating temperature can double seal life and therefore decrease overall costs of operation and ownership.

A Small Worm Gear Rig measures both dynamic operating temperature and efficiency of power throughput simultaneously. In this SWGR gear rig, a splash lubricated bronze on steel worm gear set is the gearbox design employed. The subject worm drive gearbox with a 1.75 inch centerline distance, 20:1 reduction ratio, was mounted in an L-shaped test rig with high precision torque meters on both the input and output shafts of the gearbox to measure power throughput efficiency performance based on control of output torque. The output torque was controlled to 100% of the rated load with a ser-

vice factor of 1.0. Also, gearbox sump oil temperature was carefully monitored during operation using four thermocouples.

All torque and temperature data were logged every 10 seconds for a period of 12 *h* after thermal stability was attained. The efficiency was calculated by establishing the ratio of output torque to input torque. The resulting efficiency and operational temperatures compare experimental blends against reference oils.

In addition to temperature and efficiency, air entrainment is another issue in lubricating oils. All lubricating oil systems contain some air. It can be found in four phases: free air, dissolved air, entrained air and foam. Free air is trapped in a system, such as an air pocket in a hydraulic line. Dissolved air is in solution with the oil and is not visible to the naked eye. Foam is a collection of closely packed bubbles surrounded by thin films of oil that collect on the surface of the oil.

Air entrainment is a small amount of air in the form of extremely small bubbles (generally less than 1 *mm* in diameter) dispersed throughout the bulk of the oil. Agitation of lubricating oil with air in equipment, such as bearings, couplings, gears, pumps, and oil return lines, may produce a dispersion of finely divided air bubbles in the oil. If the residence time in the reservoir is too short to allow the air bubbles to rise to the oil surface, a mixture of air and oil will circulate through the lubricating oil system. This may result in an inability to maintain oil pressure (particularly with centrifugal pumps), incomplete oil films in bearings and gears, and poor hydraulic system performance or failure. Air entrainment is treated differently than foam, and is most often a completely separate problem. A partial list of potential effects of air entrainment include: pump cavitation, spongy, erratic operation of hydraulics, loss of precision control, vibrations, oil oxidation, component wear due to reduced lubricant viscosity, equipment shut down when low oil pressure switches trip, *micro-dieseling* due to ignition of the bubble sheath at the high temperatures generated by compressed air bubbles, safety problems in turbines if overspeed devices do not react quickly enough, and loss of head in centrifugal pumps.

Antifoamants, including silicone additives, help produce smaller bubbles in the bulk of the oil. In stagnant systems, the combination of smaller bubbles and greater sheath density can cause serious air entrainment problems. Turbine oil systems with quiescent

reservoirs of several thousand gallons may have air entrainment problems with as little as a half a part per million silicone.

One widely used method to test air release properties of petroleum oils is ASTM D3427 (11). This test method measures the time for the entrained air content to fall to the relatively low value of 0.2% under a standardized set of test conditions and hence permits the comparison of the ability of oils to separate entrained air under conditions where a separation time is available. The significance of this test method has not been fully established. However, entrained air can cause sponginess and lack of sensitivity of the control of turbine and hydraulic systems. This test may not be suitable for ranking oils in applications where residence times are short and gas contents are high.

In the ASTM D3427 method (11), compressed air is blown through the test oil, which has been heated to a temperature of 25, 50, or 75°C. After the air flow is stopped, the time required for the air entrained in the oil to reduce in volume to 0.2% is usually recorded as the air release time.

A universal industrial oil lubricant with low sulfur and low metals and providing favorable performance properties is not commercially available. Accordingly, there is a need for an additive package and lubricant formulation that provides a consistent favorable operating temperature and power efficiency along with air release properties using high viscosity base stock blends. A novel combination of additives that gives the desired performance has been published (10).

Amine type antioxidants are summarized in Table 4.2 and some are shown in Figure 4.1. Examples of phenol type antioxidants are summarized in Table 4.3 and some are shown in Figure 4.2. Examples of anti-rust additives are summarized in Table 4.4. Some of these compounds are shown in Figure 4.3.

4.2.5 Lithium Soaps

Lithium soaps are the most common thickeners used in the formulation of lubricating greases. Lithium soaps used for grease-making are classified into two types: Simple soap and complex soap.

The main performance difference between the two is the greater

Table 4.2 Amine type antioxidants (10).

Compound	Compound
4,4′-Dibutyl diphenylamine	4,4′-Dipentyl diphenylamine
4,4′-Dihexyl diphenylamine	4,4′-Diheptyl diphenylamine
4,4′-Dioctyl diphenylamine	4,4′-Dinonyl diphenylamine
Tetrabutyl diphenylamine	Tetrahexyl diphenylamine
Tetraoctyl diphenylamine	Tetranonyl diphenylamine
1-Naphthylamine	*N*-Phenyl-1-naphthylamine
Butylphenyl-1-naphthylamine	Pentylphenyl-1-naphthylamine
Hexylphenyl-1-naphthylamine	Heptylphenyl-1-naphthylamine
Octylphenyl-1-naphthylamine	Nonylphenyl-1-naphthylamine

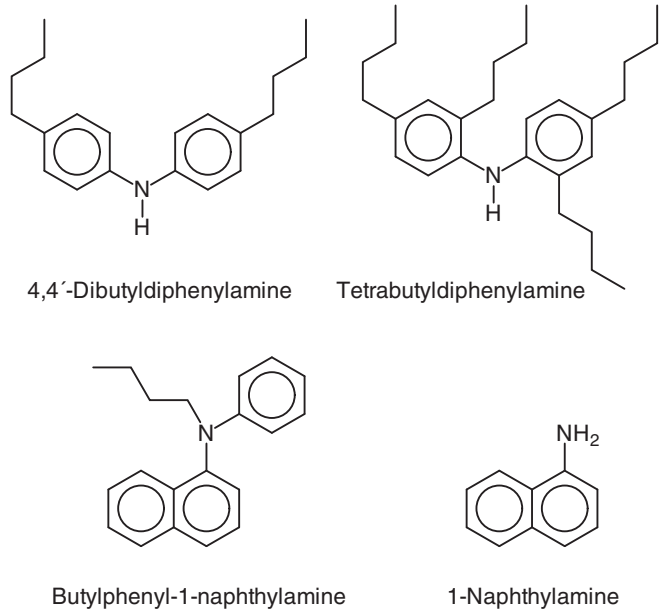

Figure 4.1 Amine type antioxidants.

Table 4.3 Phenol type antioxidants (10).

Compound	Compound
2-*tert*-Butylphenol	2-*tert*-butyl-4-methylphenol
2-*tert*-Butyl-5-methylphenol	2,4-Di-*tert*-butylphenol
2,4-Dimethyl-6-*tert*-butylphenol	2-*tert*-Butyl-4-methoxyphenol
3-*tert*-Butyl-4-methoxyphenol	2,5-Di-*tert*-butylhydroquinone
2,6-Di-*tert*-butylphenol	2,6-Di-*tert*-butyl-4-methylphenol
2,6-Di-*tert*-butyl-4-ethylphenol	2,6-Di-*tert*-butyl-4-methoxyphenol
2,6-Di-*tert*-butyl-4-ethoxyphenol	3,5-Di-*tert*-butyl-4-hydroxybenzylmercaptooctyl-1 acetate
n-Octyl-3-(3,5-di-*tert*-butyl-4-hydroxyphenyl)propionate	
n-Dodecyl-3-(3,5-di-*tert*-butyl-4-hydroxyphenyl)propionate	
2′-Ethylhexyl-3-(3,5-di-*tert*-butyl-4-hydroxyphenyl)propionate	
2,6-Di-*tert*-butyl-α-dimethylamino-*p*-cresol	
2,2′-Methylenebis(4-methyl-6-*tert*-butylphenol)	
2,2′-Methylenebis(4-ethyl-6-*tert*-butylphenol)	
4,4′-Butylidenebis(3-methyl-6-*tert*-butylphenol)	
4,4′-Methylenebis(2,6-di-*tert*-butylphenol)	
4,4′-Bis(2,6-di-*tert*-butylphenol)	
2,2-Di-*p*-hydroxyphenyl)propane	
2,2-Bis(3,5-di-*tert*-butyl-4-hydroxyphenyl)propane	
4,4′-Cyclohexylidenebis(2,6-di-*tert*-butylphenol) Hexamethylene glycol bis[3,(3,5-di-*tert*-butyl-4-hydroxyphenyl)propionate]	
Triethylene glycol bis[3-(3-*tert*-butyl-4-hydroxy-5-methylphenyl)propionate]	
2,2′-Thio[diethyl-3-(3,5-di-*tert*-butyl-4-hydroxyphenyl)propionate]	
3,9-Bis1,1-dimethyl-2-[3-(3-*tert*-butyl-4-hydroxy-5-methylphenyl)-propionyloxy]ethyl-2,4,8,10-tetraoxaspiro[5,5]undecane	
1,1,3-Tris(2-methyl-4-hydroxy-5-*tert*-butylphenyl)butane	
1,3,5-Trimethyl-2,4,6-tris(3,5-di-*tert*-butyl-4-hydroxybenzyl)benzene	
Bis[3,3′-bis(4′-hydroxy-3′-*tert*-butylphenyl)butyric acid] glycol ester	
2-(3′,5′-di-*tert*-butyl-4-hydroxyphenyl)-methyl-4-(2,4-di-*tert*-butyl-3-hydroxyphenyl)methyl-6-*tert*-butylphenol	
2,6-Bis(2′-hydroxy-3′-*tert*-butyl-5′-methylbenzyl)-4-methylphenol	

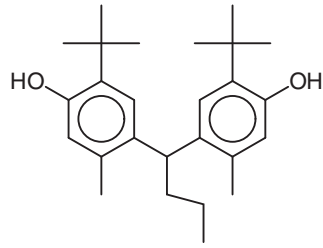

4,4'-Butylidenebis(3-methyl-6-*tert*-butyl-phenol)

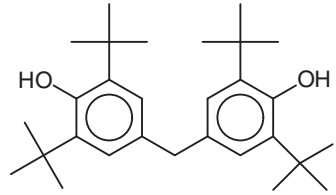

4,4'-Methylenebis(2,6-di-*tert*-butylphenol)

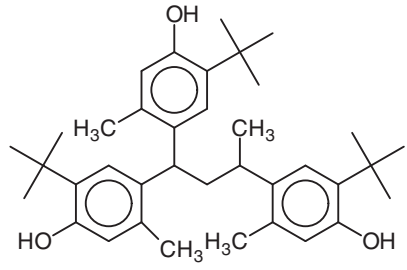

1,1,3-Tris(2-methyl-4-hydroxy-5-*tert*-butylphenyl)butane

Figure 4.2 Phenol type antioxidants.

Table 4.4 Anti-rust additives (10).

Compound	Compound
Laurylamine	Coconut amine
n-Tridecylamine	Myristylamine
n-Pentadecylamine	Palmitylamine
n-Heptadecylamine	Stearylamine
n-Nonadecylamine	*n*-Eicosylamine
n-Heneicosylamine	*n*-Docosylamine
n-Tricosylamine	*n*-Pentacosylamine
Oleylamine	Beef tallow amine
Hydrogenated beef tallow amine	Soy bean amine
Dilaurylamine	Di-coconut amine
Di-*n*-tridecylamine	Dimyristylamine
Di-*n*-pentadecylamine	Dipalmitylamine
Di-*n*-pentadecylamine	Distearylamine
Di-*n*-nonadecylamine	Di-*n*-eicosylamine
Di-*n*-heneicosylamine	Di-*n*-docosylamine
Di-*n*-tricosylamine	Di-*n*-pentacosylamine
Dioleylamine	Di-beef tallow amine
Di-hydrogenated beef tallow amine	Di-soy bean amine

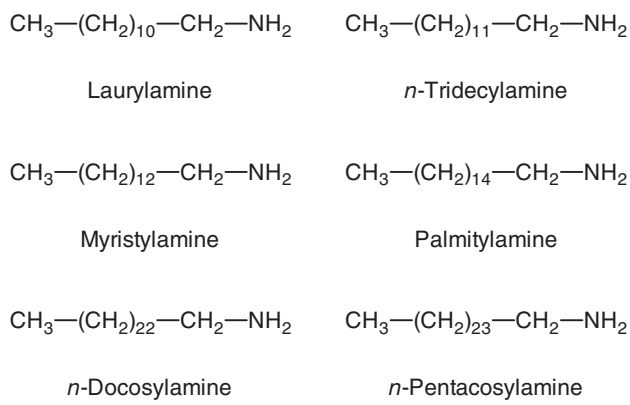

Figure 4.3 Anti-rust additives.

thermal stability of the lithium complex greases as seen in the dropping point as given in the ASTM D566 standard (12).

Both soap types contain the lithium salt of a fatty acid. Lithium complex soaps contain an additional lithium salt, or complexing agent, most commonly a dilithium salt of a low molecular weight dibasic organic acid or dibasic ester (13).

Lithium greases can be manufactured by continuous process in a heated tube reactor. This process is convenient and problem-free for simple lithium soap thickened greases. However, lithium complex greases having much higher thickener concentrations resulted in increased difficulties during the continuous production. These difficulties include wide fluctuations in flow rates, cessation of flow and resultant downtime, and greatly reduced unit production capacity.

A continuous process for the production of high dropping point lithium complex greases has been developed (13). Here, the conventional dibasic acid salt or the dibasic ester component is no longer used. These conventional components are substituted with a borated additive fed into the reactor downstream of the thickener formation zone. This substitution and process modification results in a significantly less problematic process and a substantial increase in production throughput (13).

The thus obtained saponification products are especially suitable for use in a subsequent grease-making procedure because they accept additional base oil. Also, shorter soap conditioning periods are required. The different physical conditions of these products are shown by the fact that they form grease-like products immediately upon cooling when the saponification mixture contains base oil, differently from saponification products obtained under different conditions.

4.2.6 Titanium Complex Grease Composition

A lubricating grease composition has been described. The composition is based on titanium complex soap thickeners. Several additives are added and described in the Tables 4.5 to 4.9 and shown in Figure 4.4. Zinc di-*n*-butyldithiocarbamate is shown in Figure 4.5.

These performance additives have been added in the grease composition as single component or more in combination to get synergis-

Table 4.5 Antioxidants (14).

Compound
Amino-4-hydroxy benzyl phosphoro dithioate
2,6-Di-*tert*-butyl phenyl borates
4-Dihydrocarbyl-α-cyanomethyl phenols
Bis-2,6-*tert*-butylphenol
Phenyl-1-naphthylamine
N,*N*′-dimethyl tetralone-hydrazone
N,*N*′,*N*′′-tri substituted bis (*p*-aminobenzyl) anilines
(Aminoxy) alkylamines
4-(phenyl ethyl)-2-hydroxydiphenyl amine
p,*p*′dioctyl diphenylamine
N-substituted 4-hydroxyphenylthiomethyl amine or urides
Octylated diphenyl amines
Zn dialkyl dithiophosphates
Reaction product of dithiophosphoric acid ester and aldehyde
S-(hydroxylphenyl) thiophosphates
Bis(dialkyl dithiophosphate) alkylene polyamine
N-*tert*-Octyl benzotriazole
1-(Di(2-ethylhexyl) amino methyl) benzotriazole
Benzothiazoline thione derivatives
Benzotriazole
Alkyl resorcinol phosphite
Thiobis (alkyl phenol)/dithiobis (alkyl phenol)
2-(3,5-di-*tert*-butyl-4-hydroxyphenyl)-3-benzyl-4-thiozolidinone
Butoxy carbonyl phenyl animo methyl thiobenzo thiazole Phenothiazine
Trimethyldihydroquinoline oligomers

Table 4.6 Extreme pressure and anti-wear additives (14).

Compound
Thiirane derivatives with thiophosphate and thiocarbamates
Dithiobis(thiadiazole thiol)
Benzothiazoline thione
Substituted dimercapto-thiadiazole
Imidazolidine dimethylene bis phosphoro dithioate
Derivatives of pyridine, pyrazine, pyrimidine and pyridazine and their fused ring derivatives
Triaryl phosphates
Triphenyl phosphate
Tritolyl phosphate
Trixylyl phosphates and mixed aryl phosphates
Zn and Mo dithiophosphate
Soluble Mo type additives
Zn diisopropyl dithiophosphate
Zn dipropylglycolate dithiophosphate } Product of tallow, diethanolamine and ammonium molybdate
Mo oxysulfide dithiocarbamate
Sulfurized oxy Mo organo phosphorothioate
Lead diamyl dithiocarbamate
Organo Pb–S additive
Antimony dialkyl dithiocarbamate
Ba petroleum sulfonate/synthetic barium dinonylnaphthalene sulfonate
Triphenyl phosphorothionate

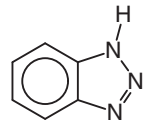

Benzotriazole

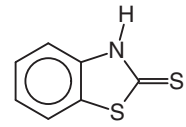

Benzothiazoline thione

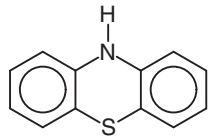

Phenothiazine

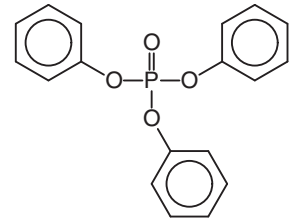

Triphenyl phosphate

Figure 4.4 Additives for greases.

Table 4.7 Friction modifiers (14).

Compound
Mo-dithiophosphates and Mo-dithiocarbamates
Reaction product of sulfurized dodecyl phenol and alkylbenzene sulfonic acid
Overbased Mo-alkylene earth metal sulfonates
2,6-Di-*tert*-butyl-4-methyl phenyl-borate
Borated polyhydroxy-alkyl sulfides
Borated *N*-hydrocarbyl alkylene triamines
Product of boric acid and cocosyl sarcosene
Product of 1,2-hexadecanediol, C_{15}–C_{19} alcohols and boric acid
Zinc salts of partially borated and partially phosphosulfurized penta or dipentaerythritol
N-Oleylglycolamide
N-Alkoxylakylene diamine diamide
N-Cocoformamide
Dialkoxylated alkylpolyoxy alkylamine
Product of 4,4′-thiodiphenol, formaldehyde and cocoamines
Reaction products of hydroxyl-methyl imidazoline and acyl sarcosine
Salts of imidazolines

Table 4.8 Rust and corrosion inhibitors (14).

Compound
Benzotriazole derivatives containing more than one benzotriazole nuclei
Nonyl-phenoxy-acetic acid
N-acyl derivatives of sarcosine (*N*-methyl glycine)
High molecular weight substituted imidazoline
Disodium salt of an aliphatic dicarboxylic acid
Diesters of sebacic acid
Zinc di-*n*-butyldithiocarbamate
Sodium mercapto benzothioazole
Zinc dinonyldithiocarbamate
Barium petroleum sulfonate
Sodium dinonylnaphthalene sulfonate
Zinc dinonylnaphthalene sulfonate
Lithium dinonylnaphthalene sulfonate

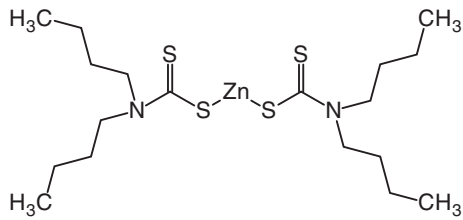

Figure 4.5 Zinc di-*n*-butyldithiocarbamate.

Table 4.9 Structure modifiers (14).

Compound
Linear isobutylene polymer
Methacrylic polymer/functionalized methacrylate copolymer
Methacrylate-styrene copolymer
Ethylene-propylene vinyl alkyl ketone polymer
Ethylene-propylene copolymers grafted with glycidyl methacrylates
Styrene-diene copolymers
Ester modified styrene-diene polymers

tic or antagonistic effects. The effect of these additives on lubricating grease properties has been systematically studied by suitable evaluation techniques as per ASTM/IP test methods as described in Table 4.10. The total quantity of these additives alone or in combination ranges from 0.01 to 50%.

Table 4.10 Standards used for the evaluation (14).

Standard	Description
ASTM D217	Cone penetration of lubricating greases (15)
ASTM D566	Drop point of lubricating greases (12)
ASTM D2265	Drop point of lubricating greases (16)
ASTM D3527	Life performance of automotive wheel bearing grease (17)
ASTM D1743	Corrosion preventive properties of lubricating greases (18)
IP 239	Determination of extreme pressure and anti-wear properties of lubricants
ASTM D2266	Wear preventive characteristics of lubricating greases. Four ball method (19)
ASTM D942	Oxidation stability of lubricating by the oxygen bomb method (20)
IP 112	Determination of corrosiveness to copper of lubricating grease strip method

4.2.7 Improving the Wetting Properties of Ionic Liquids

It has been found that additives which have formerly been employed exclusively in aqueous systems achieve the object of controlling the wetting and spreading behavior of ionic liquids.

These are nonionic organic surfactants, cationic surfactants, amphoteric surfactants, perfluorinated surfactants, and gemini surfactants (21). A wide variety of examples have been given. Some are listed in Table 4.11 and shown in Figure 4.6.

Table 4.11 Surfactants for ionic liquids (21).

Compound
Polyethylene glycol cocosamine
Polyethylene glycol stearylamine
Octyl-*β*-*D*-thioglucopyranoside
Poly(propylene glycol) myristyl ether
Sorbitan monolaurate
Sorbitan trioleate
Cetyltrimethylammonium bromide
Cetylpyridinium chloride
N,*N*-bis(hydrotallowamidoethyl)-*N*-polyethoxy-*N*-methylammonium methylsulfate
N,*N*-bis(oleylamidoethyl)-*N*-polyethoxy-*N*-methylammonium methylsulfate
N,*N*-bis(tallowamidoethyl)-*N*-polypropoxy-*N*-methylammonium methylsulfate]
N-Methyl-*N*,*N*-bis(2-hydroxyethyl)-*N*-cocoammonium chloride
Dimethylalkyl(C12-C16)benzylammonium chloride
Dimethylstearylbenzylammonium chloride
3-[*N*,*N*-dimethyl(3-myristoylaminopropyl)ammonio]propanesulfonate (Amidosulfobetaine-14)
1-(3-Sulfopropyl)pyridinium betaine
3-Dodecyldimethylammoniopropane-1-sulfonate
3-[(3-cholamidopropyl)dimethylammonio]-1-propanesulfonate
Lauryl betaine
Cocamidopropyl betaine
n-dodecyl-*N*,*N*-dimethylglycine
Tallowglycine
Perfluorooctanesulfonate
Perfluorinated carboxylic acids
Perfluorooctanoic acid
Fluorinated telomere alcohols
Acetylene diols
Acetylene diol alkoxylates
Acetylene glycols
Alkanedicarboxylic acids and esters
1,4-bis(*α*-octylpyridinio)butane dibromide
1,4-Bis(dodecylpyridinium)butane dichloride

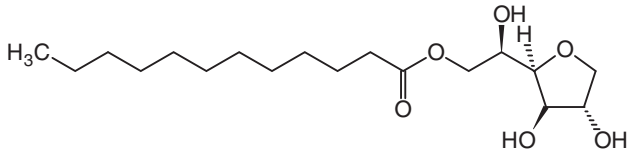

Sorbitan monolaurate

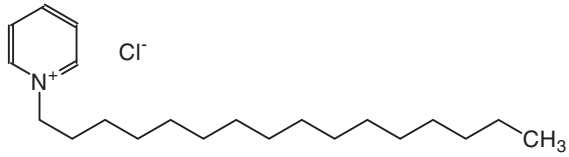

Cetylpyridinium chloride

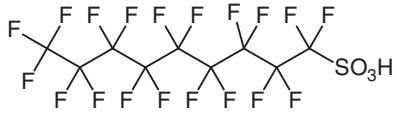

Perfluorooctanesulfonate

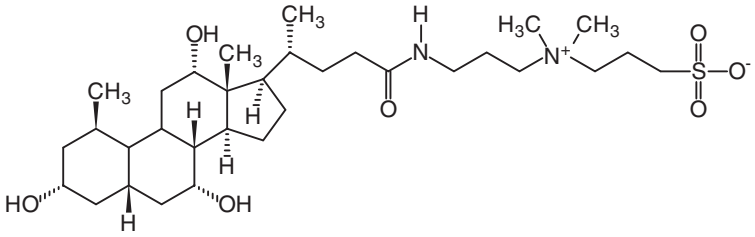

3-[(3-Cholamidopropyl)dimethylammonio]-1-propanesulfonate

Figure 4.6 Surfactants for ionic liquids.

4.3 Anti-Wear Additives

4.3.1 Ionic Liquids

Bisimidazolium-based ionic liquids with different anions have been evaluated as the anti-wear additives in poly(ethylene glycol) at room temperature (22). The results showed that bisimidazolium-based ionic liquids could effectively reduce the friction and wear of sliding pairs.

The excellent tribological properties of these additives were attributed to the formation of high-quality physical adsorption films and tribochemical products during the friction and the good miscibility of ionic liquids with the base oil (22).

4.3.2 Castor Oil Tris(diphenyl phosphate)

Castor oil tris(diphenyl phosphate) was synthesized using an environmentally friendly and renewable resource, i.e., castor oil (23).

The tribological properties of this compound were evaluated in lithium 12-hydroxystearate greases and lithium complex greases at 150°C. The tribological behaviors of the additive for lithium 12-hydroxystearate greases and lithium complex greases application in steel/steel contacts were evaluated using an Optimol SRV-IV oscillating reciprocating friction and wear tester and also a MS-10J four-ball tester. The worn steel surface was analyzed by a scanning electron microscope (SEM) and a multifunctional X-ray photoelectron spectrometer.

The results indicated that castor oil tris(diphenyl phosphate) as the additive could effectively reduce the friction and wear of sliding pairs in the two base greases. The tribological performances were also better than the commonly used zinc dialkyldithiophosphate-based additive package in lithium 12-hydroxystearate greases and also in lithium complex greases.

It was found that boundary lubrication films composed of Fe(OH)O, Fe_3O_4, $FePO_4$ and compounds containing P–O bonds were formed on the worn surface, which resulted in an excellent friction reduction and also anti-wear performance (23).

4.3.3 *Bifunctional Hairy Silica Nanoparticles*

Bifunctional hairy silica nanoparticles are silica nanoparticles covered with alkyl and amino organic chains (24). These nanoparticles were prepared as high performance additives for lubricants.

In comparison to hairy silica nanoparticles covered only with a single type of an organic chain, binary hairy silica nanoparticles exhibit the advantage of both types of organic chains, which show an excellent compatibility with lubricants and adsorption behavior to metal surfaces.

Nanoparticles with different ratios of amino and alkyl ligands were investigated. In comparison to an untreated lubricant, bifunctional hairy silica nanoparticles reduce the friction coefficient and wear scar diameter by 40% and 60%, respectively. The wear mechanism of bifunctional hairy silica nanoparticles was investigated. The protective and filling effect of the nanoparticles was improved because of a collaboration of the amino and the alkyl ligands (24).

4.3.4 *Boron Thiophosphite*

A water soluble boron-containing thiophosphite derivative was synthesized, and its tribological, anticorrosion, and anti-rust properties as an additive for the base liquid of water-glycol hydraulic fluid were evaluated in detail (25). The compound is shown in Figure 4.7.

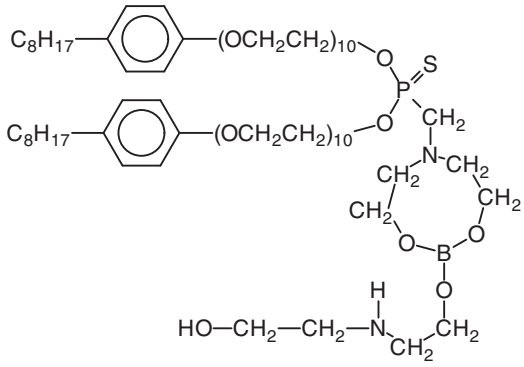

Figure 4.7 Thiophosphite derivative.

The compound was synthesized from Triton X-100, diethyl phosphite, boric acid, diethanolamine, and formaldehyde. The method of synthesis has been described in detail (26).

The results of the tests demonstrated that the boron-containing thiophosphite derivative is in fact a high performance and multifunctional water soluble lubricant additive that was able to remarkably improve the extreme pressure, friction reduction, anti-wear, anticorrosion, and the rust inhibiting properties of the base liquid when added at a low concentration, smaller than 3%.

Based on a performance comparison of boron-containing thiophosphite derivative and thiophosphite, whose chemical structure is similar to that of boron-containing thiophosphite derivative but without boron, several conclusions were drawn:

The boron element existing as alkanolamine borate group could greatly improve the extreme pressure, anti-wear, and anti-rust performance of boron-containing thiophosphite derivative, especially the anti-rust performance, but only a small effect on the friction reducing and anticorrosion properties were shown.

Based on the characterization and analysis of the worn surfaces, it has been proposed that the anti-wear mechanism consists of the prepared compound boron-containing thiophosphite derivative reacting with the steel surface during the friction process to generate a protective film mainly composed of phosphate, sulfide, sulfate, organic amine, and B_2O_3 (25).

4.3.5 Hydroxyaromatic Compounds

Both conventional poly(isobutylene) (PIB) and high vinylidene PIB are commercially available as starting materials to alkylate hydroxyaromatic compounds such as phenols. The alkylated hydroxyaromatic compounds can be used as functional additives and as intermediates to functional additives for various applications (27).

Conventional PIBs are generally prepared by polymerizing isobutylene or an isobutylene-containing composition from a petroleum catalytic cracker, with an active acidic polymerization catalyst such as $AlCl_3$.

The resulting conventional PIB contains mainly 60–70 *mol*% of a trisubstituted double bond isomer, $-CH_2C(CH_3)=CHCH_3$ and lesser amounts of 20–25 *mol*% of a tetrasubstituted double bond

isomer $-CH(CH_3)-C(CH_3)=C(CH_3)_2$ and about 5–20 *mol*% of α- and/or β-vinylidene double bond isomers.

High vinylidene poly(isobutylene)s are usually prepared by the polymerization of isobutylene or an isobutylene containing composition with a milder acidic polymerization catalyst such as BF_3. The resulting high vinylidene PIB can contain about 90 *mol*% or greater of vinylidene double bond isomers. Also, a minor amount of a tetra-substituted double bond isomer is found. High vinylidene PIBs are thought to be more reactive in comparison to conventional PIBs (27).

A Mannich reaction product has been synthesized that shows a good detergency performance in hydrocarbon fuels. The Mannich reaction product is prepared from a PIB-substituted phenol, an aldehyde and ethylenediamine, where the PIB has at least 70% vinylidene double bond isomer (28).

It has been found that a derivative of an alkylated hydroxyaromatic compound derived from a conventional PIB and a high vinylidene PIB is equally effective and may be more effective as a fuel additive than a derivative of an alkylated hydroxyaromatic compound derived from a high vinylidene PIB. The preparation of a PIB alkylated phenol and the Mannich reaction runs as follows (27):

Preparation 4–1: Molten phenol and toluene are charged to a reactor and mixed with constant stirring at ambient temperature under a nitrogen purge. A BF_3-phenol complex is then charged to the reactor. A solution of a high vinylidene PIB is then charged to the reactor over 5 *h*, while maintaining the temperature of the reaction mixture below 30°C. The reaction mixture was held for 4 *h*. Then the reaction is quenched by charging $Ca(OH)_2$ into the reactor. The quenched reaction mixture was filtered through diatomaceous earth. The filtrate was gradually distilled under vacuum to 205°C to remove toluene and unreacted phenol.

For the Mannich reaction, the PIB alkylated phenol in an aromatic solvent is charged into the reactor. Formalin was charged to the reactor at 48°C and dimethylamine in water solution was charged to the reactor over 2 *h* at 48°C. Then, the mixture was heated to 99°C to attain full reflux. Afterwards, the mixture was gradually heated to 130°C and held at 130°C for 2 *h*. Finally, the mixture was vacuum distilled at 130°C to remove the remaining water. The resultant mixture was filtered through diatomaceous earth to give the Mannich reaction product.

4.4 Fluid Loss Control Additives

4.4.1 Graphene Oxide

Graphene oxide is a good filtration additive in water-based drilling fluids at concentrations as low as 0.2% by carbon content (29). Standard American Petroleum Institute (API) filtration tests were done with pH-adjusted, aqueous dispersions of graphene oxide and xanthan gum.

It was found that a combination of large-flake graphene oxide and powdered graphene oxide in a ratio of 3:1 performed best in the API tests, allowing an average fluid loss of 6.1 *ml* over 30 *min* and leaving a filter cake of ca. 20 μm thickness.

In comparison, a standard suspension of 12 $g\,l^{-1}$ of clays and polymers, as used in the oil industry, showed an average fluid loss of 7.2 *ml* and a filter cake ca. 280 μm thick.

SEM imaging showed an extreme pliability of well-exfoliated graphene oxide, as the pressure due to filtration crumpled single graphene oxide sheets, forcing them to slide through pores with diameters much smaller than the flattened size of the flake. Graphene oxide suspensions also exhibited a greater shear thinning and higher temperature stability in comparison to clay-based fluid loss additives. This demonstrates a potential for well applications at high temperatures (29).

4.4.2 Montmorillonite

The modification of montmorillonite (MMT) by the nonionic surfactant sorbitan monooleate and the cationic surfactant cetyltrimethylammonium bromide has been examined (30). This compound can be used as a fluid loss control additive for preventing the fluid invasion into a porous pristine formation and avoiding the collapse of borehole wall in oil-drilling excavation.

Transmission electron microscopy imaging revealed that modified MMT with a small particle size displays a high dispersibility in comparison to that of pristine MMT in white oil.

Small-angle X-ray diffraction, Fourier transform infrared spectroscopy (FTIR), and SEM measurements showed that a bilayer of cetyltrimethylammonium bromide and sorbitan monooleate was intercalated into the interlayer space of the MMT (30).

The synthesized organo-clays as a fluid loss control additive performed well in oil phase. The organo-clays modified with 2.0 cation exchange capacity cetyltrimethylammonium bromide and 2.0 cation exchange capacity sorbitan monooleate yielded 100% colloid fraction in colloid fraction tests, showed low filtration loss of 5.7 *ml*, and left a filter cake approximately 68 μm thick in American Petroleum Institute filtration tests (31). This indicates that the synthesized organo-clays can be potentially used as fluid loss control additive in oil-drilling excavation (30).

4.5 Warm Mix Asphalt Additives

In particular, due to energy reductions and environmental benefits, warm asphalt has increased in popularity in recent years (32). A laboratory investigation was done concerning the rheological properties of non-foaming warm mix asphalt additives at high performance temperatures. Conventional testing procedures, such as viscosity, performance grade, creep and creep recovery, amplitude sweep, frequency sweep and FTIR, were performed to determine the influences of non-foaming additives on asphalt binders.

The PG system is based on project climate. The standard notation for PG binder is PG XX-YY where XX is the average seven-day maximum pavement design temperature and YY is the minimum pavement design temperature (33).

Several PG asphalt binders were used in combination with non-foaming warm mix asphalt additives, i.e., Cecabase®, Evotherm®, Rediset®, and Sasobit®.

The test results showed that non-foaming warm mix asphalt additives can slightly reduce the viscosity of the asphalt binder and thus decrease the mixing and compaction temperatures of the mixture. The binders containing a non-foam additive have a slight increase in high failure temperatures in comparison to a conventional binder and improve the rutting resistance of the mixtures. Further, creep recovery, amplitude and frequency sweep tests showed that the binders that contain Sasobit have a slightly higher complex modulus but exhibit a lower creep compliance and phase angle than the binder containing other warm mix asphalt additives, regardless of the asphalt type. FTIR showed that the binder type plays a key

role in determining the rheological properties of warm mix asphalt binders (32).

Tradenames appearing in the references are shown in Table 4.12.

Table 4.12 Tradenames in References.

Tradename Description	Supplier
Alfol® (Series) Fatty alcohols (10)	Continental Oil Corp.
Duraphos DBHP™ di-*n*-butyl hydrogen phosphite (10)	Albright and Wilson
Duraphos® Phosphate ester (10)	Rhodia Inc. Corp.
Glissopal® 1000 Poly(isobutene) (28)	BASF AG
Irgalube TPPT™ Triphenylthiophosphate (10)	Ciba Specialty Chemicals
Nanoflon™ Irradiated PTFE (5,6,9)	Shamrock Technologies, Inc.
Neodol® (Series) Alkyl alkoxylated surfactants (10)	Shell
Surfam® (Series) Ether amines (10)	Mars Chemical Company, Atlanta, Ga.
Surfam® P14B Decyloxypropylamine (10)	Mars Chemical Company, Atlanta, Ga.
Surfam® P17B Tridecyloxypropylamine (10)	Mars Chemical Company, Atlanta, Ga.
Ultravis® Poly(butene) based additives (28)	British Petroleum Comp.

References

1. S. Park, K.-S. Lee, G. Bozoklu, W. Cai, S.T. Nguyen, and R.S. Ruoff, *ACS Nano*, Vol. 2, p. 572, 2008.
2. G. Eda and M. Chhowalla, *Advanced Materials*, Vol. 22, p. 2392, 2010.
3. X. Fan and L. Wang, *Journal of Colloid and Interface Science*, Vol. 452, p. 98, 2015.

4. A.A. Aradi, W.J. Colucci, K. Copley, and T.L. Zahalka, Use of detergent additives in high-ethanol fuels for deposit control, US Patent Application 20 050 034 360, February 17, 2005.
5. P.B. Aswath, H. Shaub, R. Mourhatch, K. Patel, D.P. Owen, and R.L. Eisenbaumer, High performance lubricants and lubricant additives for crankcase oils, greases, gear oils and transmission oils, US Patent 7 754 662, July 13, 2010.
6. K. Patel, P.B. Aswath, H. Shaub, and R.L. Elsenbaumer, High performance lubricant additives, US Patent 7 879 776, February 1, 2011.
7. V. Balasubramaniam, M. Witschger, and U. Forster, High viscosity lubricant compositions meeting low temperature performance requirements, US Patent Application 20 120 289 445, assigned to Cognis IP Management Gmbh, Dusseldorf (DE), November 15, 2012.
8. Wikipedia, Gear oil — wikipedia, the free encyclopedia, 2016. [Online; accessed 2-June-2016].
9. P.B. Aswath, H. Shaub, R. Mourhatch, K. Patel, D.P. Owen, and R.L. Elsenbaumer, High-performance lubricants and lubricant additives for crankcase oils, greases, gear oils and transmission oils, US Patent 8 227 389, July 24, 2012.
10. J.T. Carey, A.S. Galiano-Roth, M.M. Wu, and H.M. Haigh, Low sulfur and low metal additive formulations for high performance industrial oils, US Patent 8 394 746, assigned to ExxonMobil Research and Engineering Company (Annandale, NJ), March 12, 2013.
11. ASTM International, Standard test method for air release properties of hydrocarbon based oils, ASTM Standard ASTM D3427-15, ASTM International, West Conshohocken, PA, 2015.
12. ASTM International, Standard test method for dropping point of lubricating grease, ASTM Standard ASTM D566-16, ASTM International, West Conshohocken, PA, 2016.
13. G.L. Fagan, Continuous lithium complex grease manufacturing process with a borated additive, US Patent 9 157 045, assigned to Chevron U.S.A. Inc. (San Ramon, CA), October 13, 2015.
14. A. Kumar, S.C. Nagar, K.P. Naithani, M.M. Rai, and A.K. Bhatnagar, Titanium complex grease composition including performance additives and process for preparation thereof, US Patent 6 172 012, assigned to Indian Oil Corporation Limited (Mumbai, IN), January 9, 2001.
15. ASTM International, Standard test methods for cone penetration of lubricating grease, ASTM Standard ASTM D0217-10, ASTM International, West Conshohocken, PA, 2010.
16. ASTM International, Standard test method for dropping point of lubricating grease over wide temperature range, ASTM Standard ASTM D2265-15, ASTM International, West Conshohocken, PA, 2015.

17. ASTM International, Standard test method for life performance of automotive wheel bearing grease, ASTM Standard ASTM D3527-15, ASTM International, West Conshohocken, PA, 2015.
18. ASTM International, Standard test method for determining corrosion preventive properties of lubricating greases, ASTM Standard ASTM D1743-13, ASTM International, West Conshohocken, PA, 2013.
19. ASTM International, Standard test method for wear preventive characteristics of lubricating grease (four-ball method), ASTM Standard ASTM D2266-01, ASTM International, West Conshohocken, PA, 2015.
20. ASTM International, Standard test method for oxidation stability of lubricating greases by the oxygen pressure vessel method, ASTM Standard ASTM D942-15, ASTM International, West Conshohocken, PA, 2015.
21. P. Schwab, S. Kempka, M. Seiler, and B. Gloeckler, Performance additives for improving the wetting properties of ionic liquids on solid surfaces, US Patent Application 20 100 029 519, February 4, 2010.
22. M. Yao, Y. Liang, Y. Xia, and F. Zhou, *ACS Applied Materials & Interfaces*, Vol. 1, p. 467, 2009.
23. X. Wu, Q. Zhao, M. Zhang, W. Li, G. Zhao, and X. Wang, *RSC Advances*, Vol. 4, p. 54760, 2014.
24. T. Sui, B. Song, Y.-h. Wen, and F. Zhang, *Scientific Reports*, Vol. 6, 2016.
25. J. Wang, J. Wang, C. Li, G. Zhao, and X. Wang, *Tribology Letters*, Vol. 43, p. 235, 2011.
26. J. Trautmann, A.I. Suarez, P. Tongcharoensirikul, G.W. Muth, and C.M. Thompson, *Phosphorus, Sulfur, and Silicon and the Related Elements*, Vol. 177, p. 471, 2002.
27. M.M. Jackson, J.G. Dietz, and M. Davies, Alkylated hydroxyaromatic compound from conventional and high vinylidene polyisobutylenes and compositions and processes thereof, US Patent Application 20 070 068 070, assigned to The Lubrizol Corporation, 29400 Lakeland Blvd., Wickliffe OH, 44092, March 29, 2007.
28. D.J. Moreton, Detergents for hydrocarbon fuels, US Patent 5 876 468, assigned to Lubrizol Adibis Holdings (UK) Limited (Merseyside, GB), March 2, 1999.
29. D.V. Kosynkin, G. Ceriotti, K.C. Wilson, J.R. Lomeda, J.T. Scorsone, A.D. Patel, J.E. Friedheim, and J.M. Tour, *ACS Applied Materials & Interfaces*, Vol. 4, p. 222, 2012.
30. J. Fan, H. Zhu, R. Li, and N. Chen, *Journal of Dispersion Science and Technology*, Vol. 36, p. 569, 2015.
31. API, Recommended practice for field testing of oil-based drilling fluids, API Standard API RP 13B-2, American Petroleum Institute, Washington, DC, 2005.
32. F. Xiao, V.S. Punith, and S.N. Amirkhanian, *Fuel*, Vol. 94, p. 144, 2012.

33. H. Vergara, What is a PG system?, California Department of Transportation, 2006.

Additives for High Performance Applications: Chemistry and Applications. Johannes Karl Fink.
2017 Scrivener Publishing LLC. Published 2017 by John Wiley & Sons, Inc.

5

Concrete Additives

Concrete is a combination of cement and an aggregate to form a strong building material. Cement is the binder material. There are monographs concerning the chemistry of cement and concrete (1–4). Conventional concrete, as a construction material, suffers from a number of inherent deficiencies (5). The primary drawbacks relate to its lack of ductility, low tensile strength, and a tendency to undergo significant shrinkage during curing. The brittle nature of concrete has had a direct effect on the specifications and guidelines used in the design of concrete structures.

Industrial performance products for concrete and admixtures have been presented (6). Also, the common types of cement additives for use in oil well applications have been reviewed (7). The cement additives selected for cementing operations are an integral part of sound well design, construction and well integrity.

5.1 Properties of Concrete

Since the ultimate goal in the design of any structure is generally safety, there are a number of precautions that needed to be taken when formulating the design approaches used today. Chief among these is the avoidance of brittle failure modes.

If a structure were to fail in service, people inside that structure would be at great risk if they had insufficient warning to vacate the premises before collapse. If such a failure occurred instantaneously, as in brittle behavior, there would be no warning. Alternatively, if there was a large amount of deformation, movement and noise

produced by the structure before failure (ductile), people would have time to get out. Current design codes recognize this dilemma and base their criteria around ductile failures. The question becomes how to force a brittle material (concrete) to fail in a ductile manner (5).

The behavior of typical concrete beam to which a uniform load is added is well known. When the load is applied, the beam deflects. This causes a shortening of the upper surface of the beam, resulting in compressive stresses in this region of the member as the material of the beam, i.e., concrete, tries to resist the change in shape. The bottom surface, on the other hand, is lengthened or stretched, resulting in an induced tensile stress as the concrete tries to resist elongation.

Concrete is relatively strong in compression but very weak in tension (5). If the beam were to be made entirely from concrete, it would fail at the bottom surface under a very low load, possibly even its own weight, and that failure would be very brittle in nature. Thus, something must be done to the lower portion of the beam to prevent the tensile stresses from failing the concrete.

This logic is the foundation for conventional reinforced concrete beam design. Generally, reinforcing bars are placed within the concrete beam, near the bottom, to carry tensile loads and alleviate the tensile stresses otherwise applied to the concrete. Steel, being much stronger than concrete in tension, is well suited for this application. In addition, steel fails in a very ductile manner, with very large amounts of elongation before failure. If this occurs within the concrete, a great deal of deformation and noise is generated, thus providing the warning necessary to save lives.

The basic theory behind conventional reinforced concrete beam design is well known. Essentially, steel reinforcement is placed near the bottom of the beam and is used to carry the tensile stresses while the concrete at the top of the beam carries the compressive stresses. To avoid failure of this concrete in compression, the steel is actually underdesigned so that it will fail first. Thus, the concrete never reaches its ultimate capacity (5).

Furthermore, the concrete in the bottom portion of the beam is not even considered in the design since its strength is very low in tension relative to the steel. Its job is simply to protect the steel from the surrounding environment by acting as a barrier to deleterious

substances (e.g., seawater). Seawater will not significantly affect the concrete itself but can cause corrosion of the steel reinforcement, resulting in overall degradation of the structure. The effectiveness of this approach depends upon the inherent permeability of the concrete, which is directly dependant upon the presence and size of cracks. These cracks can and do occur because of such issues as shrinkage, overloading, fatigue loading, impact, and other durability mechanisms.

5.1.1 Pozzolans

Pozzolanic materials are alumino-siliceous materials which react with calcium hydroxide in the presence of water to form compounds possessing cementitious properties at room temperature, producing calcium-silicate-hydrate. The end result is a significant reduction in porosity and permeability, accompanied by a corresponding increase in strength. Common pozzolans in use today include fly ash, silica fume, blast furnace slag, and high reactivity metakaolin.

Typical effects of commonly used pozzolanic materials on the amount of calcium hydroxide in concrete are shown in Figure 5.1.

Among the large number of clay types available, either natural or man-made, the polymerization of Montmorillonite has been the most actively studied. There are three or four main groups of clays: kaolinite, montmorillonite-smectite, illite, and chlorite.

Chlorite is not always considered a part of the clays and is sometimes classified as a separate group within the phyllosilicates. Phyllosilicates are sheet silicate minerals, which are formed by parallel sheets of silicate tetrahedra.

There are about thirty different types of pure clays in these categories but most natural clays are mixtures of these different types, along with other weathered minerals (5).

5.1.2 Calcium Aluminate Cement

The first calcium aluminate cement, containing iron and manufactured in a smelting process, the *Ciment Fondu Lafarge* was first sold in 1918. Due to its considerably high aluminate content in comparison to Portland cement, this cement type was initially referred to as high alumina cement (8).

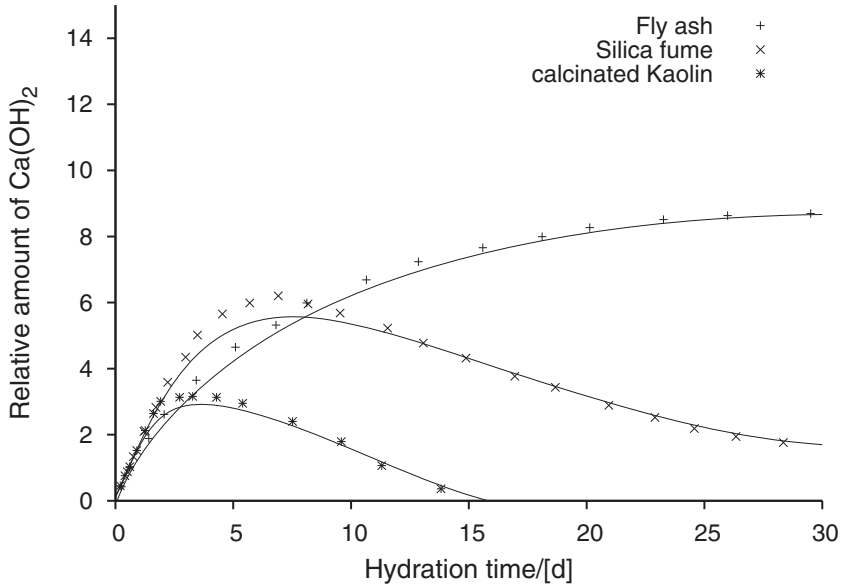

Figure 5.1 Effects of commonly used pozzolanic materials on the amount of calcium hydroxide (5).

Typical calcium aluminate cements that are rich in iron are produced by means of the smelting process and have a grey to black-grey color. Calcium aluminate cements that are low in iron are colored beige to grey. The components are listed in Table 5.1.

Table 5.1 Components in calcium aluminate cement (8).

Compound	Iron rich [%]	Iron poor [%]	Iron free [%]
Al_2O_3	36 –42	50 –55	68 –85
SiO_2	2 – 6	2 – 6	<1
Fe_2O_3	14 –19	1 – 3	<0.5
CaO	37 –40	37 –40	26 –31
MgO	<1.5	<1.5	
SO_3	<0.4	<0.4	

Additives for calcium aluminate cement formulations have been described. Additives with primarily retarding and accelerating effects are tartaric acid, sodium carbonate, and lithium carbonate.

Additives that primarily affect the consistency of the composition

are calcium hydroxide, polycarboxylic ether, cellulose ether, and the defoaming agent Agitan® P 801 (8).

5.1.3 Rutting of Bituminous Concrete

Under the traffic action, pavement crumbling may occur rapidly, which leads to severe impairments that are reflected on the surface layers (9): Rutting, cracking, substances rejection, polishing and pulling out the aggregates on surface. This situation often needs a renovation of the surface layers.

The use of local materials for pavement design has been assessed. Recycling of bituminous substances is one of the relevant solutions. This method has the advantage of reusing building materials by mixing them with a proportion of refined ones to achieve the required performance (9).

5.2 Set Retarders

A set retarder can be added to a cement composition in order to help to increase the thickening time of the cement composition such that the cement composition remains pumpable for a desired time at a specific temperature (10). The thickening time is proportional to the setting time, i.e., the longer the thickening time, the longer the setting time will be. Therefore, a set retarder can be added to a cement composition to help increase the setting time of the cement composition.

Some retarders also have an effect on the viscosity of the slurry compositions. Lignin derivatives and organic acids reduce the viscosity, whereas cellulose derivates increase the viscosity

Other examples of set retarders are ethylenediamine tetraacetic acid and nitrilotriacetic acid, or a combination of these compounds (11). Still another example of a set retarder for Portland cement is a copolymer formed from a monomer of 2-acrylamido-2-methyl-1-propane sulfonic acid. Examples of set retarders for calcium aluminate cements are polymeric phosphate salts such as sodium tripolyphosphate (12).

5.2.1 Superplasticizers

A polymer from 2-hydroxyethyl methacrylate (HEMA) has initially been described for its use for contact lenses (13). It is a macroporous hyperhydroxy polymer with a very high water-holding capability. The polymer has a crosslinked skeleton with a pore size of at least 90 Å and a high ratio of free water to solid when hydrated. In particular, water contents of 95–99.75% are possible while sufficient integrity of structure is maintained. HEMA is shown in Figure 5.2.

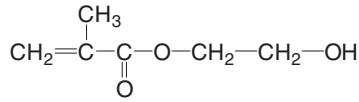

Figure 5.2 2-Hydroxyethyl methacrylate.

Another use of such polymer types as concrete additives has been described (14). The polymer can be used to retard the curing process and to incorporate specific elements that enhance the overall performance of the concrete. For example, the polymers may be used as admixtures to chelate specific elements. This chelation ability may be usable in order to ensure the uptake and distribution of a desired element throughout the concrete mixture.

The performance enhancement may be as a result of the curing process, the strength or other characteristics of the concrete or the ability of the concrete to adhere to incorporated reinforcement materials (14).

5.3 Accelerators

An accelerator is a chemical additive that is used to speed up the normal rate of the reaction between cement and water (7). This shortens the time of thickening of the cement. Further, an accelerator increases the early strength of cement. Accelerators do not increase the ultimate compressive strength of cement but promote a rapid strength development. However, in a higher concentration the accelerator may act as a retarder. Accelerators may also interact with other additives, such as dispersants.

Calcium chloride and sodium chloride are the most commonly used accelerators. Other types of accelerators are sodium metasilicate, potassium chloride and gypsum. Calcium chloride is the most efficient and economical accelerator. Anhydrous calcium chloride is more preferred because it absorbs moisture less readily and is easier to maintain in storage.

Sodium chloride is a slight accelerator at low concentrations and becomes a retarder at higher concentrations. Since seawater contains sodium chloride, it can be readily used in offshore oil well applications.

5.3.1 Aqueous Dispersions of Silica

It has also long been known, that an acceleration of setting can be achieved by the addition of a finely divided amorphous silica to cementitious preparations (15). However, this additive was not used since initially the processability of the fresh concrete was greatly limited thereby.

Recently, these problems could be overcome, and an aqueous dispersion has been described that contains water, precipitated silica, silicate, and a superplasticizer (16). The superplasticizer is a water soluble poly(carboxylate ether). The dispersion is free of binders.

Precipitated silicas differ from pyrogenic silicas, which are also referred to as aerosils. The most preferred suitable plasticizers are lignosulfonate, sulfonated naphthalene-formaldehyde polycondensates, sulfonated melamine-formaldehyde polycondensates, and poly(carboxylate ether)s (16).

5.3.2 Non-Chloride Cement Accelerators

Electric arc furnace dust is a byproduct of the electric steelmaking industry and is produced in large quantities around the world (17). The safe disposal of such a byproduct is expensive and continues to be a serious concern in many countries throughout the world. A cement composition has been disclosed comprising (17,18):

1. Cement,
2. Electric arc furnace dust, and
3. A non-chloride cement accelerator.

Exemplary non-chloride accelerators have been described. These are calcium nitrite and calcium formate (17). Calcium nitrite and calcium formate appear to provide additional sources of Ca^{2+} and may thus reduce the time required to achieve supersaturation of the solution with respect to $Ca(OH)_2$. Calcium nitrite can decompose into calcium oxide and a mixture of nitrogen dioxides according to following equation (17):

$$Ca(NO_2)_2 \rightarrow CaO + NO + NO_2 \tag{5.1}$$

The cement compositions containing electric arc furnace dust are capable of exhibiting an improved early compressive strength and workability (17).

5.4 Dispersants and Thinners

5.4.1 Xylonic Acid

Xylonic acid, cf. Figure 5.3, is a sugar acid that can be obtained by the complete oxidation of xylose. It has been attempted to utilize xylose by converting it to an aldonic acid (19). Xylose was converted to xylonic acid by using commercial glucose oxidase enzyme, palladium catalysis, and microbial bioconversion.

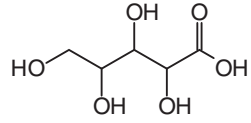

Figure 5.3 Xylonic acid.

The enzyme conversion was successfully done using a commercial glucose oxidase. The microbial conversion with *Gluconobactor oxydans* proceeded even with the presence of a large amount of lignosulfonate.

The so-obtained xylonic acid products were evaluated as a cement dispersing agent in cement and concrete tests. It was found that xylonic acid is approximately twice as effective as lignosulfonate.

Xylonic acid can be effectively utilized for concrete water reducing applications (19).

5.4.2 Thixotropy

5.4.2.1 Microfibrillar Cellulose

In concrete technology an important field of interest is a self-compacting concrete, which flows and compacts itself due to gravity (20). Therefore, no external vibration or other compaction is needed. It is possible to produce a very high performance concrete as self-compacting concrete. Because compacting work is not needed, the noise level during construction is lowered remarkably.

A problem with the self-compacting concrete is the segregation and the sensitivity of the concrete to variations on the raw materials (20). Segregation usually results in a concrete with unacceptable properties. In water segregation the water phase is separating when the cement particles are settling with time. Aggregate segregation occurs faster when aggregates are settling in the paste phase.

There have been attempts to solve these problems using viscosity-enhancing agents, for example, with water soluble polysaccharides such as welan gum or cellulose derivates (21). Cellulose fibers have been used in concrete materials in order to improve the mechanical properties of materials (22).

Microfibrillar cellulose refers to isolated cellulose microfibrils or microfibril bundles that are derived from a cellulose raw material. Microfibrils typically have a high aspect ratio. The number average diameter is typically below 200 *nm*. The smallest microfibrils are similar to so-called elementary fibrils, which are typically 2–12 *nm* in diameter.

The dimensions of the fibrils are dependent on the raw material and the method or disintegration. Microfibrillar cellulose may also contain some hemicelluloses. The amount is dependent on the plant source. Mechanical disintegration of microfibrillar cellulose from a cellulose raw material, cellulose pulp, or refined pulp is carried out by using a refiner, grinder, homogenizer, colloider, friction grinder, ultrasound sonicator, or a fluidizer-type homogenizer.

In addition, microfibrillar cellulose can also be directly isolated from certain fermentation processes. Cellulose producing micro-

organisms may be of the genus *Acetobacter xylinum* or *Acetobacter pasteurianus*. Microfibrillar cellulose also may be chemically or physically modified, for example, by carboxymethylation, oxidation, esterification, or etherification. The modification can also be realized by the physical adsorption of ionic substances.

The addition of microfibrillar cellulose increases the paste thixotropy both with and without plasticizer. Microfibrillar cellulose helps to make a self-compacting concrete more robust. Water bleeding and aggregate settlement are diminished and thus concrete durability properties are increased. Water bleeding is effectively prevented with the finest fibril additives. The aggregate settlement is also drastically decreased with microfibrillar cellulose (20).

The cementitious composition is manufactured by (20):

1. Mixing a cementitious binder, aggregate material, water, and
2. Optionally adding a plasticizer or a dispersing agent.

5.4.3 Flowability

In a typical concrete mixing process, a large amount of water is added to increase flowability of the concrete (23). However, a water overdose lowers concrete compression strength and adversely affects other properties. In contrast, a lack of water causes concrete slump and deterioration, which is harmful to a construction process. Many chemical additives have been described to improve the concrete flowability without the need for increasing the amount of water.

Traditional concrete water reducers are formed by mixing lignin as main component with naphthalene sulfonic acid sodium salt. Although the cost of such kind of additives is relatively low, they cannot provide desirable concrete water reduction when the effective content in the concrete is low. For example, when a type F water reducer, which consists mainly of naphthalene-based compounds, is used, rapid concrete slump will result.

5.4.3.1 Carboxylic Type Additives

Copolymers of acrylic acid or maleic anhydride and alkenyl ethers have been found to improve the flowability of a concrete admixture.

Also, copolymers of maleic acid and its salt and ester derivatives and hydroxy-terminated allyl ether and copolymers of maleic acid and partially esterified styrene are known to enhance concrete admixture flowability (24,25).

Such chemical reagents are classified as carboxylic type additives (23). But those concrete additives still cannot provide all the required properties. For example, although esterified acrylic acid copolymers provide a good concrete admixture flowability, they also prolong the hardening time.

5.4.3.2 Norbornene and Maleic Anhydride Copolymers

An improved family of concrete admixture additives has been developed (23). An example for the preparation has been shown in detail.

Preparation 5–1: First, 5 units of norbornene, 25 units of maleic anhydride and 0.5 unit of 2,2′-azobisisobutyronitrile are placed in a reaction flask. Then, 200 *ml* of benzene as solvent is added. The mixture is agitated for 10 *min*, followed by a slow heating. Then, at 80°C, the mixture is allowed to react for 2 *h*. After filtration, a white solid compound can be obtained. This product is a copolymer of norbornene and maleic anhydride, with an average molecular weight of 4500 *Dalton*.

In a similar way, norbornene, styrene, and maleic anhydride have been polymerized. Also, certain copolymers can be added as such. Several examples of fabrication have been detailed (23). Water reduction tests were conducted according to the ASTM C494 standard test method (26).

These additives, even at a relatively low additive level, can provide an improved water reduction, increase concrete flowability, reduce concrete slump and enhance compression strength (23).

5.5 Defoamers

Defoamers with a high hydrophobicity have limited solubility in water and are not easily incorporated into aqueous solutions, which, for the most part, comprise the water reducing admixture compositions (27). This hydrophobicity tends to destabilize the aqueous product and fosters separation of components. It requires that

the water reducing cement dispersant and defoamer be constantly stirred to prevent separation, or that they be stored in separate tanks and mixed just before use.

5.5.1 Ethoxylated Fatty Alcohol Acrylates

Ethoxylated or propoxylated fatty alcohol acrylate or methacrylate compounds are useful as defoamers for concrete compositions (28). It has been observed that a special balance between the chain length of the fatty alcohol and the distribution of the ethoxy or propoxy units results in an ester with improved defoaming properties. These products are particularly efficient in removing occluded air bubbles and foams formed during concrete processing operations. This is unusual, since the structures miss polymeric backbones.

The products are prepared by the alkoxylation of cetyl alcohol or stearyl alcohol using ethylene oxide or propylene oxide. In the second step, the intermediate is reacted with acrylic acid, methacrylic acid or a mixture from these acids. When the esterification is completed, the unreacted acid is distilled off from the product under high vacuum. An additional purification of the ester is not necessary (28). The reaction is shown in Figure 5.4.

A detailed example of preparation is as follows (28):

Preparation 5–2: First, 1 *mol* acrylic acid and 0.3 *mol* Cetylstearyl+3EO+5PO methacrylate (Agnique® DFM 250, Cognis GmbH) are placed in a 250 *ml* polymerization flask at room temperature. The mixture is diluted with 58.6 *ml* water and set under nitrogen bubbling in order to remove all traces of oxygen. Then the mixture is heated to about 80°C and 1.4 *g* ammonium persulfate as radical initiator is added. Since the polymerization is an exothermic reaction, the flask must be cooled in order to maintain a reaction temperature of 80–90° C. Once the polymerization is finished, the product is cooled to room temperature and treated with an aqueous sodium hydroxide solution to neutralize the acidic groups in the polymer and diluted with water to adjust a polymer content of 30%.

5.5.2 Hydroxyl Alkyl Acrylate

A cost-effective and environmentally friendly defoamer formulation which does not contain oil, ethylene bis-stearamide or free silicone for use in various industrial applications (29). The defoamer formulation is a mixture of a polymer containing acrylic acid, methacrylic

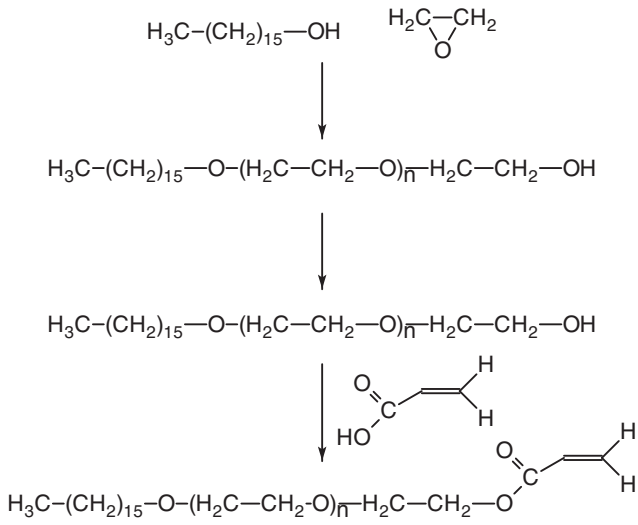

Figure 5.4 Synthesis of an ethoxylated fatty alcohol acrylate.

acid, or a combination, either in a suitable diluent, an organic carrier, an additive, or a surfactant.

A polymer containing 10–30% hydroxyl alkyl acrylate and 70–90% alkyl acrylate by weight percent was prepared as follows (29):

Preparation 5–3: First, 250 *g* of diisooctyl adipate was placed into a reaction flask. A vacuum was applied for 20 *min* to remove dissolved air. Then the diisooctyl adipate was sparged with nitrogen while being heated to 79–82°C with mixing. Once at temperature and with the nitrogen sparge and constant mixing, a free radical generating compound was added and allowed to dissolve over a 5 *min* period. Meanwhile, the acrylate monomers were premixed in a beaker. The monomer mixture was added to the diisooctyl adipate diluent through an addition funnel at a rate of approximately 1.5 $g\,min^{-1}$, making sure to maintain a temperature of approximately 79-82°C. After the monomer blend addition, 48 *g* of diisooctyl adipate were used to rinse the monomer blend container and addition funnel, and the diisooctyl adipate rinse was added to the reaction flask. Another 0.5 *g* of free radical generating compound was added, and the mixture was held at 79–82°C with mixing and nitrogen for 2 *h*. The mixture was then air cooled to room temperature.

The defoamer formulation is useful in the cement industry in

order to efficiently decrease the foam production during the preparation of cement slurries. As such, air entrainment in the cement slurry is minimized, thus leading to increased flow properties in the cement. The minimization of air entrainment in the cement slurry also results in a more structurally sound cement lattice (29).

5.5.3 Tributyl Phosphate

Tributyl phosphate has been used as defoaming agent for concretes for pavement applications that contain nanoparticles (30).

5.5.4 Silicone Oils

Silicone oils are also used as defoaming agents and have been found to be extremely effective materials. However, the silicone oils suffer from a major drawback in that they tend to remain on the surface of the parts being cleaned, which can adversely affect post-process operations such as painting, plating, welding, or bonding (31).

5.5.5 Other Additives

Defoamers may comprise an ethoxylated or propoxylated alcohol, fatty alcohol, alkylamine, alkyl polyamine or fatty carboxylic acid (27).

A mixture of three defoaming agents has been proposed, composed from a (31):

1. Hydrophilic, fumed, particulate silica,
2. Ethylene oxide-propylene oxide block copolymer, and
3. Linear alcohol alkoxylate mixture of poly(oxyethylene/oxypropylene) mono-C_6, C_8, and C_{10} alkyl ethers.

5.6 Shrinkage Compensation

Conventional concrete tends to shrink during drying and curing (32). This shrinkage occurs with a loss of water. The drying shrinkage creates tensile stresses in the concrete. Since concrete generally has a low tensile strength, shrinkage stresses often cause cracking.

In order to reduce cracking caused by shrinkage, various expansive concretes have been developed. The expansive cement generally is a hydraulic cement with an expansive component that expands during hydration (33, 34). The expansive cement causes the concrete to expand slightly as it dries, which helps to offset or compensate for the shrinkage associated with drying. As a result, shrinkage and resulting tensile stresses in the concrete are reduced or eliminated, along with the cracking resulting from those stresses.

Recently, a shrinkage-compensating concrete has been developed, in which the expansive forces developed during hydration compensate for shrinkage of the concrete, thus obviating the need for any added internal or external restraint element. With such formulations, substantially crack-free slabs may be built without using restraining steel bars, fibers, or other separate restraining elements.

Calcium sulfoaluminate or any other oxide or sulfate that expands upon hydration is used as additive (32).

5.7 Permeability

In the 1990s, fires in concrete-lined tunnels created a situation of rapidly rising temperature (35–37). This rapid rise in temperature led to explosive spalling of large areas of concrete. Large falling concrete chunks proved to be almost as dangerous to trapped motorists as the smoke and fumes from the fires. More recently, the increased heat of vertical take-off and landing aircraft (F-35 and Osprey) have caused great concern that explosive spalling might endanger both crew and aircraft.

The process of heat-induced spalling is relatively simple. When concrete is exposed to temperatures above the boiling point of water, moisture in the concrete turns to steam. If the temperature rises more rapidly than the steam can escape, rising pressure causes the concrete to spall. The heat from jet exhaust or vehicle fires is typically much greater, in the range of 930°C to 1100°C, causing potentially explosive spalling.

Accordingly, there is a need for concrete having improved spalling resistance. There is also a need for concrete having improved compressive and flexural strength, as these properties control how much concrete must be used to support a given design load.

Furthermore, given the present interest in reducing the carbon footprint of various manufacturing processes, there is a need for concrete formulations that reduce the production of carbon dioxide during cement making.

5.7.1 Expanded Perlite

A concrete additive consists of an expanded perlite with a volume weighted mean particle size of approximately 10–100 μm. The perlite further includes at least one additional component to improve workability and compensate for the natural tendency of expanded perlite to absorb water from the concrete mix. The additional component may include: water, a superplasticizer such as polycarboxylates, naphthalene sulfonate, and melamine sulfonate, or a hydrophobic compound such as salts of fatty acids, fatty acids, silanes, and siloxanes.

The additive can be made in the form of a flowable powder or a flowable slurry. Concrete containing this additive displays superior properties to conventional concrete, including extremely high thermal resistance and high strength, low chloride ion permeability, and good early strength. The expanded perlite is a readily available raw material and the finished concrete is extremely cost-effective for applications where a high strength structural concrete must withstand high temperatures (36).

5.7.2 Pozzolanic Materials

One method of improving both of these drawbacks, i.e., brittle failure mode and high permeability, is to provide a reinforcement of the concrete matrix at a smaller scale than the steel bars. This is often done through the use of short fibers mixed into the concrete during batching. Fibers have the ability to improve durability by resisting crack opening and provide strength after initial cracking, thus improving the ductility of the concrete (5).

The permeability can also be improved by altering the concrete microstructure to produce a denser, less porous, arrangement of components. The most common approach to achieving this goal is the inclusion of a pozzolanic material in the concrete mix design.

Concrete is well known to be made up of two primary components; stone and sand aggregates surrounded by a hydrated cement paste matrix. It is the latter which acts as the glue that binds the aggregates together. It is also the hydrated cement paste that is the dominant factor when it comes to permeability, since the aggregates typically used in concrete tend to be far less permeable than the surrounding matrix.

Examining the hydrated cement paste matrix reveals that there are two primary building blocks that make up its microstructure; calcium-silicate-hydrate (C–S–H) and calcium hydroxide. The C–S–H takes the form of very small crystals packed closely together to form a very dense structure. The calcium hydroxide, on the other hand, forms much larger, layered, plate-like crystals. These crystals do not pack well and tend to exhibit weakness between layers due to poor bonding. Ultimately, it is the calcium hydroxide that represents the weak link in both strength and permeability of the hydrated cement paste.

5.7.3 Cracking Catalyst

The hydration of cement paste was investigated as a function of the addition of spent catalyst for catalytic cracking in fluidized bed, in comparison with similar uses of microsilica and fly ashes (38).

The kinetics of the hydration process was studied by thermogravimetry (TG), differential scanning calorimetry, and spectroscopic methods. The time of setting of freshly prepared pastes and the compressive and bending strengths of sample beams after the 7th day and the 28th day of setting were determined.

The contents of $Ca(OH)_2$ in the pastes at various times of hydration were determined from the results of the TG studies. Also, the pozzolana nature of the additives has been found out. The ability of combining with $Ca(OH)_2$ was similar in the spent catalyst and the microsilica. In the presence of the spent catalyst, the hydration process was strongly exothermic, which promoted the rapid setting of the cement paste. Calcium carbonate aluminates that are formed in the system, favorably affect the strength of the concrete materials (38).

5.8 Air Entraining Agents

Air entraining is the intentional creation of tiny air bubbles in concrete (39). The bubbles are introduced by adding to the mix an air entraining agent and a surfactant. The air bubbles are created during the mixing of the fresh concrete. Most of them survive to be part of the hardened concrete. The purpose of an air entrainment is to lengthen the durability of the hardened concrete.

Entrained air dramatically improves the durability of concrete exposed to moisture during freeze-thaw cycles and greatly improves the resistance of the concrete to surface scaling caused by chemical deicers. Also, it is intended to increase workability of the concrete while it is in the plastic state.

Concrete mixtures may contain an air entraining agent (40). Air entraining agents are compounds that entrain microscopic air bubbles in cementitious compositions, which then harden into concrete having microscopic air voids. Air entraining agents can reduce the surface tension of a fresh cementitious composition at low concentration. Air entrainment can also increase the workability of fresh concrete and reduce segregation and bleeding. Examples of suitable air entraining agents are collected in Table 5.2.

Table 5.2 Air entraining agents (40).

Compound	Compound
Wood resin	Sulfonated lignin
Petroleum acids	Proteinaceous material
Fatty acids	Resinous acids
Alkylbenzene sulfonates	Sulfonated hydrocarbons
Vinsol resin	Anionic surfactants
Cationic surfactants	Nonionic surfactants
Natural rosin	Synthetic rosin

The air entraining agents are added in an amount to yield a desired level of air in a cementitious composition. Generally, the amount of air entraining agent in a cementitious composition ranges from about 0.001% to about 0.3%, based on the weight of the dry cementitious material. The particular amount used will depend on materials, mix proportion, temperature, and mixing action (40).

5.8.1 Fluorochemical Surfactants

Air entraining agents that may also be used include foams formed *ex-situ*, including stabilized foams from water and a fluorochemical surfactant (41). Fluorochemical foam stabilizing surfactants are well known in the art of fire fighting foams.

5.8.2 Superabsorbent Polymers

Superabsorbent polymers are an alternative to air entrainment agents in order to increase the frost resistance of the concrete (42).

A texture composition with a superabsorbent polymer showed a desirable water retention property but is significantly less susceptible to air entrainment than conventional formulations containing a cellulosic thickener (43).

The texture composition consists essentially of calcium carbonate in an amount of 30–95% of the dry composition, starch, and a superabsorbent polymer that can absorb at least about 50 times its mass and having a particle size of less than about 250 μm. The superabsorbent polymer is added in an amount of 0.02–5% of the dry composition. Superabsorbent polymers that have been disclosed are shown in Table 5.3.

Table 5.3 Superabsorbent polymers (43).

Polymer compound
Poly(acrylamide) copolymer
Ethylene maleic anhydride copolymer
Crosslinked carboxy-methylcellulose
Poly(vinyl alcohol) copolymers
Crosslinked poly(ethylene oxide)
Starch grafted poly(acrylonitrile) copolymer
Starch grafted poly(acrylamide)
Starch grafted poly(2-propenamide-*co*-2-propenoic acid)
Poly(2-propenamide-*co*-2-propenoic acid) sodium salt

Because of the reduction in air entrainment, unwanted pinholes in the applied product are greatly reduced or eliminated. Furthermore, it has been found that a superabsorbent polymer allows for a much more workable composition with reduced mobility since the composition is less apt to be runny or to drip. In addition,

texture compositions with a superabsorbent polymer are easier to handle, since the material is less sticky and easier to wash off from hands and tools, especially in comparison to conventional formulations including a cellulosic thickener (43). Formulations containing a superabsorbent polymer are shown in Table 5.4.

Table 5.4 Formulations with a superabsorbent polymer (43).

Material	Manufacturer	Amount/[%]
Calcium carbonate	Dolocron 4512A-Specialty Minerals	44.022
Calcium carbonate	Picqua P-100-Picqua	44.022
Kaolin clay	ASP 600-BASF Corporation	2.501
Mica	GIM Mica-Georgia Industrial Minerals	5.003
Attapulgite clay	Minugel FG-Active Minerals International, LLC	2.501
Superabsorbent polymer	Water Lock ® SAP C-200-Grain Processing Corporation	0.150
Wheat starch	Genvis 200D-Archer Daniels Midland	1.501
Guar gum	Galactasol 60H3FD-S-Ashland Chemicals	0.250
Preservative biocide	Vancide MZ-96-RT Vanderbilt	0.050

5.8.3 Rubber Crumb

The optimum quantity of rubber crumb as an air entraining admixture in concrete, thus providing maximum freeze-thaw protection and maximum strength, has been assessed (44).

Microscopic and chemical analysis was done with rubber samples to investigate how a rubber crumb entrains air and reacts with

the surrounding concrete. An optimum addition of rubber crumb to a concrete mix was found to be 0.6% of concrete. A freeze-thaw test was carried out with three separate batches of concrete containing washed rubber crumb, unwashed rubber crumb and plain concrete, respectively. It was found that rubber crumb was effective in providing freeze/thaw protection (44).

5.8.4 Autoclaved Aerated Concrete

Enclosures that have been built from elements of autoclaved aerated concrete often are covered with plasters (45). Certain adhesion problems between plasters and surface exist during the mechanized covering of surfaces of the enclosures with the plaster. Some dispersible additives, such as a vinyl acetate polymer or derivatives of acrylic acid esters, are used to improve the adhesion.

Another problem is the increased water absorption of the autoclaved aerated concrete elements, therefore water retarding additives, e.g., cellulose esters, are used in the mixture of plasters. Due to an insufficient amount of water in the mixture of plasters, the hydration of the cement minerals slows down. The influence of natural zeolite and clinoptilolite on the properties of plaster has been investigated (45). Clinoptilolite is a natural zeolite comprising a microporous arrangement of silica and alumina tetrahedra (46). It commonly occurs as a devitrification product of volcanic glass shards in tuff and as vesicle fillings in basalts, andesites and rhyolites.

It was found that this additive effectively absorbs water and ensures an adequate hydration of the cement minerals (45). In the mixture of plaster, when the sand is changed by clinoptilolite in an amount of 15% the structure becomes slightly compact and the compressive and flexural strength of the hardened plaster increase by 47% and 12%, respectively. Further, the adhesion to a surface of the autoclaved aerated concrete element increases by 44%. In contrast, the drying shrinkage, the water vapor resistance factor and the coefficient of capillary absorption do not change (45).

5.9 Corrosion Protection

5.9.1 Modified Hydrotalcites

Hydrotalcite is a natural mineral that was discovered in 1842 in Norway (47). Hydrotalcites are also known as a member of a large mineral group of naturally occurring layered double hydroxides.

There are a number of techniques that have been successfully applied to synthesize modified hydrotalcites (48). The most commonly method used is the co-precipitation of two metal salts in alkaline solution at a constant pH value of about 10. Another method uses the classical ion exchange process in which the guest anions are exchanged with the anions in the interlayer spaces of preformed layered double hydroxides to produce specific anion intercalated modified hydrotalcites. Still another method is a lattice reconstruction after heating, i.e., calcination, which is based on the structural memory effect of these materials, due to which the original structure is reproduced after rehydration.

Modified hydrotalcites are technologically promising materials for their addition to concrete in order to improve its durability in aggressive environments, owing to their low cost, relative simplicity of preparation, and plenty of unique composition variables that may be adopted (48).

Only a few studies have been focused on cementitious materials concerning their potential applications in corrosion protection of reinforced concrete structures. The mechanism of corrosion in reinforced concrete and concrete properties that affect corrosion of reinforcement have been briefly detailed. The existing knowledge concerning the synthesis and characterization methods of modified hydrotalcites, ion exchange within the modified hydrotalcite structure as well as the application of modified hydrotalcites in the cementitious materials have been reviewed. It is expected that modified hydrotalcites can improve the durability of reinforced concrete materials (48).

5.9.2 Chloride Ion Scavenging

The chloride-induced corrosion of reinforcement materials in concrete influences the durability of the reinforced concrete structures (49). Waste residues of the production of bioethanol have been

tested as additives for concrete in order to catch the chloride ions. A significant portion of lignin is left from the bioethanol production.

The lignin is obtained from the biomass by a two-step hydrolysis with phosphoric acid, followed by an enzymatic hydrolysis in order to remove the polysaccharides. The nitrogen in the lignin can be increased by a Mannich reaction, thus increasing the ionic capacity. It has been found that cationic lignin is suitable to catch chloride ions in concrete (49).

5.9.3 Dopamelanin

Melanins are a group of natural pigments found in many organisms. A lack of melanin results in albinism. Melanin is produced by the oxidation of the amino acid tyrosine, followed by polymerization. These compounds are shown in Figure 5.5.

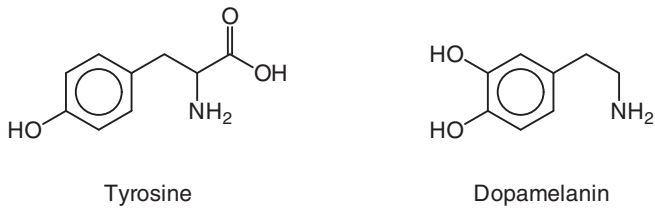

Figure 5.5 Melanin and tyrosine.

Melanin shows extraordinary properties, as in the presence of light, it can dissociate water. It has also been proposed to use these properties in industrial applications. For example, a photoelectrochemical method has been developed for the conversion of water into hydrogen and oxygen (50).

The use of dopamelanin or its precursors as an additive of a cement mixture substitutes the capillary water proportion in the cement mixture (51). The use of dopamelanin in an aqueous solution, in less than 3%, as a concrete setting and curing agent significantly increases the ductility and scouring resistance of the cement mixture.

Also, the cement mixture improves the physicochemical and bacteriological properties of the concrete, the notable increment related to compression resistance and ductility or relative displacements being of special interest, and suffers less damage in comparison with

the mixture containing water. Also, it intensifies its scouring resistance, which is advantageous for the metallic elements immersed in its interior (51).

5.10 Superabsorbent Polymers

A comprehensive overview of the properties of superabsorbent polymers, specific water absorption and desorption behavior of superabsorbent polymers in fresh and hardening concrete, the effects of the superabsorbent polymers addition on the rheological properties of fresh concrete, the changes of cement paste microstructure and mechanical properties of concrete have been reviewed (42).

In addition, the key advantages of using superabsorbent polymers have been described in detail. This material has the ability to act as an internal curing agent to mitigate autogenous shrinkage of high performance concrete, the possibility to use superabsorbent polymers as an alternative to air entrainment agents in order to increase the frost resistance of concrete, and also the benefit of steering the rheology of fresh cement-based materials (42).

5.11 Fibers

5.11.1 Poly(oxymethylene) Fibers

Polymeric additives for concrete have been described (52). These are fabricated from a poly(oxymethylene) (POM) copolymer. POM copolymers can be utilized to form fibrous additives for concrete, i.e., microfibers or macrofibers. The POM copolymers can also include chemical groups, e.g., end groups or pendant groups that can increase the polarity of the POM and thus increase the hydrophilicity of the formed fibers, which can improve miscibility of the fibers in wet concrete. The chemical groups of the POM copolymers can bond with components of the concrete or can hydrolyze to form groups that are bonding with some components of the concrete.

A POM copolymer can be manufactured by the copolymerization of trioxane and a cyclic acetal. POM fibers can be formed from monomeric reactants as follows (52):

1. Polymerization of trioxane with 1,3-dioxolane utilizing a BF_3 initiator and a methylal chain transfer agent-designated POM.
2. Polymerization of trioxane with 1,3-dioxolane utilizing a BF_3 initiator and an ethylene glycol chain transfer agent-designated POM-OH.
3. Polymerization of trioxane with glycerol formal formate utilizing a BF_3 initiator and an ethylene glycol chain transfer agent-designated lateral OH-POM.

The monomers can contain terminal groups that are much less reactive during polymerization in comparison to the formal group itself or the trioxane, e.g., an ester group, a formate group, or an acetate group. Accordingly, the terminal group can remain unreacted during the polymerization reaction to form an essentially linear polymer with a side chain functionality. This side chain functionality can be suitable for use as is or, alternatively, it can be hydrolyzed after the polymerization to result in pendant hydroxyl functional groups. Hydrolysis following the polymerization reaction can also remove unstable hemiacetal end groups and improve the stability of the resulting copolymers.

In particular, a POM copolymer can be formed by the copolymerization of trioxane with 0.2–6 parts glycerol formal formate per 100 parts trioxane or 0.2 to 6 parts of a combination of 1,3-dioxolane and glycerol formal formate per 100 parts trioxane, using ethylene glycol as a chain transfer agent. This copolymer, after hydrolysis, can have about 80% or higher of $-C_2OH$ end groups and up to 20 to 30 pendant −OH groups per chain. This copolymer is addressed as a lateral−OH POM.

The fibers can be formed by melt spinning. An apparatus for melt spinning is shown in Figure 5.6. The extruder apparatus can include a mixing manifold in which the POM composition can be mixed and heated to form a molten composition. After the formation of the molten mixture, the mixture can be conveyed under pressure to the spinneret of the extruder apparatus, where it can be extruded through an orifice to form the fiber. The spinneret can generally be heated to a temperature that can allow for the extrusion of the molten polymer while preventing the breakage of the fiber during its formation. Then, the fiber is quenched in a liquid bath and directed

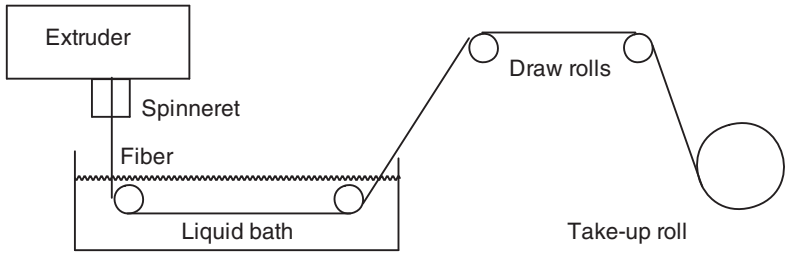

Figure 5.6 Melt spinning apparatus (53).

by the rolls. Further, the fiber is drawn while applying heat. A series of draw rolls are used to draw the fiber. After the drawing step, the drawn fiber is cooled and is wound on a take-up roll (53).

Fibers formed from the POM copolymers may exhibit an increased hydrophilicity as compared to fibers formed of more traditional polymers such as poly(propylene) (PP).

For instance, a trioxane/cyclic acetal POM copolymer formed with a methylal chain transfer agent can have a water contact angle of less than about 30°. On the other hand, PP generally has a water contact angle of greater than 35°. The increased hydrophilicity of the POM copolymer can improve the mixing between POM polymeric fibers and the wet concrete and can also prevent blooming of the fibers to the surface of the concrete during the curing procedure. Further, terminal hydroxyl groups can provide an electrostatic binding with the components of the concrete binder. (52).

5.12 Additives from Wastes

5.12.1 Waste Rubber

Waste tires are a significant health and environmental concern if they are not recycled or discarded properly. Over the years, recycling waste tires into civil engineering applications, especially into asphalt paving mixtures and Portland cement concrete, has been gaining more and more interest (54).

The use of crumb rubber in asphalt paving mixture has long been proven successful due to good compatibility and interaction

between rubber particles and asphalt binder, leading to various improved properties and performance of asphalt mixtures.

In comparison with its use in asphalt paving mixtures, the recycling of waste rubber in Portland cement concrete has not been so successful due to two factors (54):

1. Incompatibility in chemical property between rubber and cement paste, and
2. The significant difference in stiffness, resulting in stress concentrations.

Various methods have been proposed to overcome the barriers to improve the performance of rubberized Portland cement concrete, some of which have shown promise (54).

For resource reutilization, scrap tires have been investigated for a long time as an additive to concrete to form *Rubcrete* for various applications and have shown promising results (55). However, the addition of rubber particles leads to a degradation of physical properties, in particular, the compressive strength of the concrete.

A theoretical model has been proposed for the mechanisms of the decrease of the compressive strength due to the addition of rubber particles, as well as the improvement in compressive strength by the modification of the surface of the particles (55). It has been suggested in previous studies that the compressive strength can be improved by soaking the rubber particles in an alkaline solution to increase the interphase bonding between the rubber particles and cement. However, it was discovered that the loss in compressive strength is due to local imperfections in the hydration of the cement. This is induced by the addition of heterogeneous and hydrophobic rubber particles.

Microscopic studies showed that the rubber particles disturbed the water transfer to create channels, which were prone to cracking and led to a loss in the compressive strength. However, no cracking was found along the surfaces of the rubber particles. This indicates that the bonding strength between the rubber particles and cement phases is not a critical factor in determining the compressive strength. For this reason, a theoretical model was developed to describe the water transfer in rubcrete specimens to explain the experimental data (55).

By maximizing the quantity hydration, the compressive strength could be improved. Thus, the compressive strength of rubcrete could be improved by increasing the Hamaker constant of the system. The Hamaker constant A can be defined for a van der Waals body-body interaction as (56,57):

$$A = \pi^2 C \rho_1 \rho_2 \tag{5.2}$$

Here, ρ_1 and ρ_1 are the number of atoms per unit volume in two interacting bodies and C is the coefficient in the particle-particle pair interaction.

The increase was achieved by increasing the refractive indices of the solids. The refractive indices of materials increase with increases in functional groups, such as OH and SH on the surface.

So, the model provided a possible mechanism for the efficacy of treating rubber particles with NaOH in improving the compressive strength. By using an NaOH solution treatment, an oxygen-containing OH group was formed on the rubber surface to increase the Hamaker constant of the system, leading to a higher compressive strength.

Based on this mechanism, another new method for the modification of the rubber particles has also been proposed. In this model, the rubber particles should be partially oxidized with hot air or steam in a fluidized bed reactor to produce hydrophilic groups on the surface of the particles (55).

5.12.2 Nanomodified Concrete Additive

A reinforced concrete composite may consist of a a cement matrix, an exfoliated clay, and preferably can include an oligomer or polymer (5). The oligomer or polymer can link at least a portion of the exfoliated silicate platelets provided by the clay and can provide improved ductility and essentially eliminates shrinkage.

Preferred clays include sodium or calcium montmorillonite or phosphatic clays, including phosphatic waste clay, or mixtures thereof. Optionally, the concrete composite can include a dispersion agent that helps keep the clay in a dispersed state when stored as an additive to prevent, or at least limit, clumping of the clay.

Polymers or oligomers from poly(vinyl alcohol) (PVA) together with exfoliated clays can form stable admixtures. When these admixtures are added to a cement matrix they form high strength, high ductility concrete results.

The PVA in the concrete reacts with the hydroxy groups in the cement matrix, and thus participates in the hydration process, forming a bond with the cement paste. The use of an exfoliated clay as a pozzolan has been found to provide a significant advantage since 2% of the clay has been found to provide a strength increase in concrete that is equivalent to about 8% of conventional silica fumes.

Moreover, applied to concrete, the silicate platelets provided by the clay, being pozzolanic in nature, react with the calcium hydroxide crystals in the concrete matrix to produce C−S−H units, providing all of the associated benefits, i.e., increased strength, reduced permeability. Additionally, these new C−S−H crystals form around the polymer chains, resulting in what is essentially a fiber reinforced concrete, though the reinforcing is at a scale and consistency never before achieved. The result of this latter effect is an increase in ductility of the concrete during failure (5).

Tradenames appearing in the references are shown in Table 5.5.

Table 5.5 Tradenames in References.

Tradename Description	Supplier
Aerosil® Fumed Silica (27)	Degussa AG
BYK® 028 Poly(siloxane) based defoamer (27)	BYK Additives and Instruments
CFR™ (Series) Water-soluble polymer dispersants (11)	Halliburton Energy Services, Inc.
Daravair® 1000 Air-entraining agent (27)	Grace Construction Products
Diacel® LWL Fluid-Loss/Retarder additive (11)	Chevron Philips Chemical Company LP
GasStop™ HT Tannin grafted with acrylamide and 2-acrylamido-2-methylpropane sulfonic acid (11)	Halliburton Energy Services, Inc.
HR™ (Series) Hydroxycarboxy acid, retarder (11)	Halliburton Energy Services, Inc.
Lodyne® Fluorochemical surfactant (41)	Ciba-Geigy AG
Ludox® (Series) Silicon colloid (27)	DuPont
Micro Matrix™ Set retarder composition with a phosphonic acid derivative (11)	Halliburton Energy Services, Inc.
MicroMax® 90 90 Weighting material (10, 11)	Elkem Materials, Inc.
Micromax® Weighting agents (11)	Halliburton Energy Services, Inc.
Miracon® Foaming concentrate with a fluorochemical surfactant (41)	Miracon Technologies, Inc.
Narlex® Styrene sulfonic acid maleic anhydride copolymer (11)	Akzo Nobel Surface Chemistry LLC.
NexSil™ Colloidal dispersions of inorganic oxides (27)	Nyacol Nano Technologies, Inc.
Nyacol® Colloidal dispersions of inorganic oxides (27)	Nyacol Nano Technologies, Inc.
Sartomer Ricon® 130-MA-13 Butadiene-maleic anhydride copolymer (23)	Cray Valley

Table 5.5 (cont.) Tradenames in References.

Tradename Description	Supplier
Sartomer® SMA EF-30 Styrene-maleic anhydride copolymer (23)	Cray Valley
SCR™ -100 Copolymer of 2-acrylamide-2-methylpropane sulfonic acid and acrylic acid (11)	Halliburton Energy Services, Inc.
SCR™ -500 Copolymer of 2-acrylamido-2-methylpropane sulfonic acid and itaconic acid (11)	Halliburton Energy Services, Inc.
Snowtex® Colloidal silica nano-particles (27)	Nissan Chemical America Corp.
Thermalock™ Cement for corrosive environments (10)	Halliburton Energy Services, Inc.
Thermopel™ EP product (36,37)	CenterStar
TRU® Self-leveling hydraulic cement (32)	CTS Cement Manufacturing Co.
Visco-Corder® Dynamic viscosimeter (43)	Brabender Instruments, Inc.
Water Lock ® SAP C-200 Super absorbent polymer (43)	Grain Processing Corp.

References

1. S.N. Ghosh, *Advances in Cement Technology: Chemistry, Manufacture and Testing*, TBI, New Delhi, India, 2002.
2. P.C. Hewlett, *Lea's Chemistry of Cement and Concrete*, Elsevier Butterworth-Heinmann, Oxford, 2004.
3. P. Taylor, *Curing Concrete*, CRC Press, Taylor & Francis Group, Boca Raton, 2014.
4. W. Kurdowski, *Cement and Concrete Chemistry*, Springer, Dordrecht, 2014.
5. B. Birgisson and C.L. Beatty, Nanomodified concrete additive and high performance cement past and concrete therefrom, US Patent 7 786 192, assigned to University of Florida Research Foundation, Inc. (Gainsville, FL), August 31, 2010.
6. Evonik, Performance products for concrete and admixtures, Technical information, Evonik Corporation, Richmond, VA, 2015.
7. E. Broni-Bediako, O.F. Joel, and G. Ofori-Sarpong, *Oil & Gas Research*, 2016.
8. D. Ostrander and M. Schmid, Calcium aluminate cement, US Patent 9 193 626, assigned to Calucem Gmbh (Mannheim, DE), November 24, 2015.
9. B. Abdelhak, H.-C. Abdelmadjid, G. Mohamed, and G. Hamza, *Arabian Journal for Science and Engineering*, pp. 1–7, 2016.
10. B.R. Reddy, D. Gaugler, and R. Fitzgerald, Methods for cementing in a subterranean formation using a cement composition containing a set retarder of a polyester, US Patent 9 150 774, assigned to Halliburton Energy Sevices, Inc. (Houston, TX), October 6, 2015.
11. J. Chatterji, J.F. Heathman, D.W. Gray, and B.K. Waugh, Set retarder compositions, cement compositions, and associated methods, US Patent 7 004 256, assigned to Halliburton Energy Services, Inc. (Duncan, OK), February 28, 2006.
12. C.L. Keys and L.E. Brothers, Wellbore servicing compositions comprising a set retarding agent and methods of making and using same, US Patent 7 863 224, assigned to Halliburton Energy Services Inc. (Duncan, OK), January 4, 2011.
13. J.T. Carter, Macroporous hyperhydroxy polymer and articles made therefrom, US Patent 6 201 089, March 13, 2001.
14. P.W. Schmalzl and R.L. Warren, Polymeric concrete admixture containing a new class of superplasticizer polymers, US Patent Application 20 160 075 602, assigned to Polymerium, LLC, Cheyenne (WY), March 17, 2016.
15. J.E. Madden and W.J. Newell, Cement plaster, US Patent 3 135 617, assigned to Madden, James E. and Newell, W. J., June 2, 1964.

16. U. Fischer, P. Wieland, C. Hübsch, H. Grassl, K. Becher, S. Scheul, and E. Jetzlsperger, Aqueous dispersions of silica for increasing early strength in cementitious preparations, US Patent 8 835 535, assigned to Evonik Degussa GmbH (Essen, DE) Construction Research & Technology GmbH (Trostberg, DE), September 16, 2014.
17. F.M. Al-Mutlaq, Use of non-chloride cement accelerator and electric arc furnace dust in cement, US Patent 9 278 888, assigned to Saudi Basic Industries Corporation (Riyadh, SA), March 8, 2016.
18. F.M. Al-Mutlaq, Use of a cement accelerator and electric arc furnace dust in cement, US Patent 9 346 713, assigned to Saudi Basic Industries Corporation (Riyadh, SA), May 24, 2016.
19. B.-W. Chun, B. Dair, P.J. Macuch, D. Wiebe, C. Porteneuve, and A. Jeknavorian, "The development of cement and concrete additive," in J.D. McMillan, W.S. Adney, J.R. Mielenz, and K.T. Klasson, eds., *Twenty-Seventh Symposium on Biotechnology for Fuels and Chemicals*, pp. 645–658. Humana Press, Totowa, NJ, 2006.
20. A. Laukkanen, J.-E. Teirfolk, M. Leivo, H. Kuosa, K. Kataja, and A. Nurmi, Material to be used as a concrete additive, US Patent 9 174 873, assigned to UPM-Kymmene Corp. (Helsinki, FI), November 3, 2015.
21. I. Gibb and P. Griffin, Admixture for cementitious compositions and process for preparation thereof, EP Patent 1 419 121, assigned to RMC Group P.L.C., May 19, 2004.
22. H. Nanko and K.E. Kurtis, Fiber reinforced mineral-based materials and methods of making the same, US Patent 6 933 038, assigned to Institute of Paper Science and Technology, Inc. (Atlanta, GA), August 23, 2005.
23. T. Tsai, Concrete admixture additive, US Patent 7 390 855, assigned to Taiwan Gwan Chian Industrial Co., Ltd. (Simwu Township, Taoyuan County, TW), June 24, 2008.
24. T. Tsubakimoto, M. Hosoido, and H. Tahara, Copolymer and method for manufacture thereof, US Patent 4 471 100, assigned to Nippon Shokubai Kagaku Kogyo Co., Ltd. (Osaka, JP), September 11, 1984.
25. S. Valenti, Chemically treated anhydride copolymers and cementitious mixtures containing the copolymers, US Patent 5 158 996, assigned to Sandoz Ltd. (Basel, CH), October 27, 1992.
26. ASTM International, Standard specification for chemical admixtures for concrete, ASTM Standard ASTM C494, ASTM International, West Conshohocken, PA, 2015.
27. Y. Chen, L.L. Kuo, and A.A. Jeknavorian, Stabilized defoamers for cementitious compositions, US Patent 8 759 423, assigned to W. R. Grace & Co.-Conn. (Columbia, MD), June 24, 2014.

28. F. Andrioletti, S. Merlet, J. Lapere, M.d.S. Marques, B. Abribat, and W. Lamarca, Defoamers, US Patent Application 20 110 226 164, assigned to Cognis IP Management Gmbh, Dusseldorf (DE), September 22, 2011.
29. J. Martin, R. Wilson, S. Rosencrance, and D. Previs, Polymeric defoamer additive, US Patent 8 507 597, assigned to Kemira Chemicals, Inc. (Atlanta, GA), August 13, 2013.
30. H. Li, M.-H. Zhang, and J.-P. Ou, *International Journal of Fatigue*, Vol. 29, p. 1292, 2007.
31. M.S. Lunski and S.A. Bolkan, Stabilized triple defoamer composition, US Patent 5 858 279, assigned to Church & Dwight Co., Inc. (Princeton, NJ), January 12, 1999.
32. E.K. Rice, Shrinkage-compensating concrete, US Patent 9 359 258, assigned to PKL Corporation (Los Angeles, CA), June 7, 2016.
33. E.K. Rice, Expansive cement, US Patent 4 419 136, December 6, 1983.
34. E.K. Rice, Shrinkage-compensating concrete, US Patent 5 846 316, assigned to Edward Rice, December 8, 1998.
35. T.L. Anderson, J.A. Coleman, and N.S. Berke, Processed mineral additive for reducing concrete permeability and increasing strength, US Patent 8 568 527, October 29, 2013.
36. T.L. Anderson and N.S. Berke, Processed mineral additive for reducing concrete permeability and increasing strength, US Patent 8 758 503, assigned to CenterStar, Inc. (Santa Rosa Beach, FL), June 24, 2014.
37. T.L. Anderson and N.S. Berke, Processed mineral additive for reducing concrete permeability and increasing strength, US Patent 8 821 631, assigned to CenterStar, Inc. (Santa Rosa Beach, FL), September 2, 2014.
38. B. Pacewska, I. Wilińska, and J. Kubissa, *Thermochimica Acta*, Vol. 322, p. 175, 1998.
39. Wikipedia, Air entrainment — wikipedia, the free encyclopedia, 2015. [Online; accessed 3-July-2016].
40. L.J. Gray, Concrete mixtures including carbon encapsulating admixture, US Patent 8 871 021, assigned to Staker & Parson Companies (West Haven, UT), October 28, 2014.
41. L.J. Gray, Concrete mixtures having stabilized foam admixture, US Patent 8 167 997, assigned to Jack B. Parson Companies (Salt Lake City, UT), May 1, 2012.
42. V. Mechtcherine and H.W. Reinhardt, eds., *Application of Super Absorbent Polymers (SAP) in Concrete Construction: State-of-the-Art Report Prepared by Technical Committee 225-SAP*, Springer, Dordrecht New York, 2012.
43. J.F. Grussing, Composition comprising superabsorbent polymer, US Patent 8 932 678, assigned to United States Gypsum Company (Washington, DC), January 13, 2015.

44. A.E. Richardson, K.A. Coventry, and G. Ward, *Journal of Cleaner Production*, Vol. 23, p. 96, 2012.
45. G. Sezemanas, M. Sinica, P. Zacharčenko, N. Pivenj, D. Mikulskis, and M. Kligys, *Materials Science*, Vol. 19, 2013.
46. Wikipedia, Clinoptilolite — wikipedia, the free encyclopedia, 2016. [Online; accessed 27-June-2016].
47. Wikipedia, Hydrotalcite — wikipedia, the free encyclopedia, 2016. [Online; accessed 27-June-2016].
48. Z. Yang, H. Fischer, and R. Polder, *Materials and Corrosion*, Vol. 64, p. 1066, 2013.
49. T. Elena, Y. Tsui, L. Dempere, and W. Vermerris, *Microscopy and Microanalysis*, Vol. 20, p. 1956, 2014.
50. A. Solis Herrera, Device for performing a photoelectrochemical method of separating water into hydrogen and oxygen, US Patent 8 920 990, December 30, 2014.
51. A. Solis Herrera, Cement mixture with significantly improved physicochemical and bacteriological properties that contains dopamelanin, precursors thereof, analogues thereof or derivatives thereof, as an additive, US Patent 8 691 891, April 8, 2014.
52. S. Bassetti, R.M. Gronner, T. Heyer, H. Hueckstaedt, and A. Karandikar, Polyoxymethylene fibers in concrete, US Patent 9 284 664, assigned to Ticona LLC (Florence, KY), March 15, 2016.
53. S. Bassetti, R.M. Gronner, T. Heyer, H. Hueckstaedt, and A. Karandikar, Polyoxymethylene fibers in concrete, US Patent 8 785 526, assigned to Ticona LLC (Florence, KY), July 22, 2014.
54. X. Shu and B. Huang, *Construction and Building Materials Part B*, Vol. 67, p. 217, 2014. 1. Special Issue of KIFA-6 2. Utilization of Crumb Rubber in Asphalt Mixtures.
55. L.H. Chou, C.-K. Lu, J.-R. Chang, and M.T. Lee, *Waste Management & Research*, Vol. 25, p. 68, 2007.
56. H.C. Hamaker, *Physica*, Vol. 4, p. 1058, 1937.
57. Wikipedia, Hamaker constant — wikipedia, the free encyclopedia, 2016. [Online; accessed 26-June-2016].

Additives for High Performance Applications: Chemistry and Applications. Johannes Karl Fink.
2017 Scrivener Publishing LLC. Published 2017 by John Wiley & Sons, Inc.

6

Other Uses

6.1 High Performance Additive for Powder Coatings

Powder coatings are applied electrostatically and are then heat cured to allow them to flow and form a coating. Finally, they have a hard surface finish that is much tougher than a conventional paint, which results in excellent chemical and environmental resistance (1,2).

Fumed metal oxide products may help to improve the color performance, processing, application and mechanical properties of powder coatings (1,2).

In particular, fumed alumina and fumed silica products provide tribo-charging, free-flow, fluidization and anti-blocking in powder coating applications. Typically, fumed alumina is used for tribo coating processes and either fumed silica or hexamethyldisilazane treated fumed alumina is selected for corona coating processes (3).

6.1.1 Antimicrobial Powder Coatings

An improved method of preparing powder coatings with microparticles of a solid heat absorbing material has been presented (4). An antimicrobial prepolymer for powder coatings has been described.

The heat absorbing additive is selected from colorants, inorganic viscosity modifiers, fillers, flame retardants, catalysts, antimicrobial agents, or sequestering agents.

Antimicrobial ceramic particles include zeolites, hydroxyapatite, zirconium phosphates and other ion exchange ceramics. The ion

exchange antimicrobial agents may also incorporate antimicrobial metal ions, e.g., silver ions or silver ions in combination with zinc or copper ions. The ion exchange type antimicrobial agents may also have incorporated therein ion exchanged ammonium ion for an improved color stability.

The method or preparation involves heating the prepolymer and the polymer powder particles and the microparticles of the solid material to temperatures whereby when the two are in intimate contact with one another, they will fuse to each other, but not to themselves.

Preferably, the prepolymer and the polymer powder coating particles are heated to at least their Vicat temperature while the solid, heat absorbing microparticles are heated to a temperature of 50°C above the temperature at which the prepolymer or polymer becomes tacky or begins to manifest adherent properties (4).

6.2 Radiation Shielding

Nanostructured additives can improve the shielding capabilities of high performance polymers without significantly affecting the thermal and mechanical properties of the polymers (5).

Nanoparticles or nanostructured materials can be prepared by evaporation, sol-gel processing, directed self-assembly, oxidation or reduction of suitable precursors, or electrochemical synthesis.

A nanostructured material can be prepared by mixing a hydrogen-rich, high performance polymer with metal or metal oxide nanoparticles or a metal-ligand cluster.

For example, nanostructured boron, borohydrides or boron carbides and other additives can be mixed in a poly(amic acid) solution before imidization to form a poly(imide) (PI) (5). Piperidine-modified boron nanoparticles can be used with hydrogen-rich PIs. The poly(amic acid) is made from various combinations of dianhydrides and diamines displaying significant hydrogen content. Bisphenols may also be used after they are converted to diamines. These combinations may include both dianhydrides and two of the diamines to prepare a copolymer that may have more suitable solubility characteristics than either of the two corresponding homopolymers.

PIs prepared with 4,4′-oxydianiline (ODA) and 3,3′,4,4′-benzophenone tetracarboxylic dianhydride (BTDA) monomers, cf. Figure 6.1, can be loaded with 10 and 15 wt% tungsten nanoparticles that are treated with benzyl mercaptan. The 3,3′,4,4′-benzophenone tetracarboxylic dianhydride and ODA monomers are reacted to form PI films that are flexible to the point of being creaseable. The nanocomposite films are effective as an electromagnetic radiation shield (5).

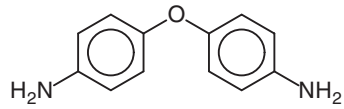

4,4´-Oxydianiline

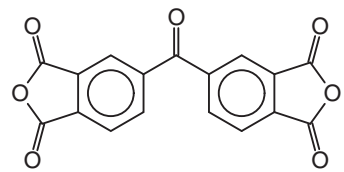

3,3´,4,4´-Benzophenone tetracarboxylic dianhydride

Figure 6.1 Aniline and anhydride monomers.

3-Aminopropyltrimethoxysilane is used to encapsulate hybrid gadolinium-oxide nanoparticles within a polysiloxane shell (6). Phenyltrimethoxysilane can be used to make the inorganic nanoparticles more compatible with aromatic organic polymers. The compounds are shown in Figure 6.2. Unmodified samarium-oxide and gadolinium-oxide nanoparticles aggregate and settle within organic solvents such as chloroform. So, such modifications make the gadolinium-oxide nanoparticles more compatible with an organic solvent or polymer.

Also, thiols or mercaptans, and amines can be used to modify the surface of metallic nanoparticles, thus increasing the compatibility between the inorganic nanoparticle additive and the organic polymer. In particular, such agents include benzyl mercaptan, thiophenol, aniline, benzylamine, pyridine and piperidine (5). These compounds are shown in Figure 6.3.

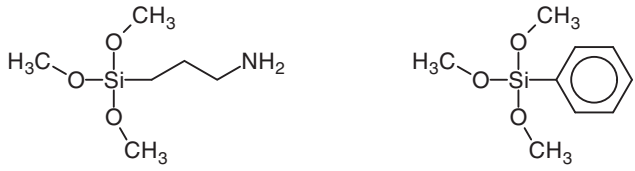

Figure 6.2 Silane compounds.

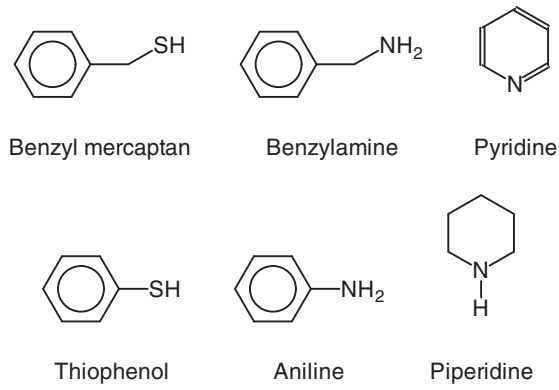

Figure 6.3 Compatibility increasers.

6.3 Superabsorbent Polymers

Superabsorbent polymers (SAPs) can be employed in various applications, such as in disposable sanitary products (i.e., diapers, incontinence articles, feminine hygiene products, and absorbent dressings), airlaids, household articles, sealing materials, humectants, i.e., agricultural products for soil conditioning, mining and oil drilling, anti-condensation coatings, water-storing materials (for use in fields as diverse as agriculture, horticulture and forestry), absorbent paper products, surgical absorbents, pet litter, bandages, wound dressings, chemical absorbents, polymeric gels for cosmetics and pharmaceuticals, artificial snow, in fire fighting techniques, and in applications related to the transportation of fresh food or seafood, as well as in food packaging applications.

The largest use of SAPs, however, is in disposable personal hygiene products. These products include, in the order of volume of superabsorbent materials used, diapers, training pants, adult incontinence products and feminine hygiene products.

Natural-based SAPs can be selected from gelling polysaccharides, gelling proteins and their mixtures.

Synthetic SAPs can be made by the polymerization of ethylenically unsaturated hydrophilic monomers. Examples are collected in Table 6.1.

SAPs and fluff cellulose pulp are usually mixed uniformly in diapers and incontinence products. This mixture of fluff and superabsorbents is formed in absorbent structures called absorbent cores. Unfortunately, physiological fluids are excreted and absorbed over only a small area of these absorbent cores. The superabsorbent performance of these absorbent cores is therefore not optimal.

Fluid acquisition or fluid distribution layers have been added to diapers and incontinence garments for some time (7).

These nonwoven textiles increase liquid diffusion along the length and width of absorbent structures, and in this way increase the amount of superabsorbents that is placed in contact with fluids. However, nonwoven textiles do not enhance the performance of superabsorbents. Nonwoven textiles can only be placed at the surface of absorbent structures, and this minimizes their impact on liquid penetration through the absorbent structures. Furthermore, they are usually very expensive. Due to their high cost, fluid distribution

Table 6.1 Materials for superabsorbent polymers (8).

Synthetic	Natural
Acrylic acid	Galactomannans
Acrylate salts	Glucomannans
Acrylic ester	Carboxyalkyl polysaccharides
Acrylic anhydride	Crosslinked polysaccharides
Methacrylic acid	Amylopectin networks
Methacrylate salts	Polysaccharide nanocomposites
Methacrylic esters	Guanidinated polysaccharides
Methacrylic anhydride	Modified proteins
Maleic anhydride	
Maleic salts	
Maleate esters	
Acrylamide	
Acrylonitrile	
Vinyl pyrrolidone	
Vinyl acetate	
Vinyl guanidine	
Aspartic acid	

layers are usually placed over a small area in absorbent structures and thus have only a limited effect on liquid diffusion.

SAPs can be mixed with inorganic additives, such as clays, zeolites or silicates. Several additives have been mixed with SAPs or in hygiene products for odor control purposes (9,10).

However, not all of these additives were reported to improve superabsorbent performance in diapers or incontinence garments.

Absorbent polymer compositions made from melt bound particles of SAPs and additives have been described (11–13).

The additives are either polysaccharides or clays. Matrix forming binder components fill entire pore spaces, and therefore drastically reduce porosity and accessible surface area. High specific surface areas and porosity provide higher driving forces for fluid transport through the absorbent structure (14).

Superabsorbent material was also reported to play a role as a matrix material or binder. Superabsorbent particles can occlude odor control additives, such as zeolites (15).

Composites made from fibers, swollen absorbent polymers and water insoluble inorganic materials, such as alumina, silica, zeolite

and clays have been described (16, 17). The absorbent materials will therefore fill pore spaces, drastically reducing accessible surface area. Further, agglomerated particles have been reported that have been made from silicates and fine superabsorbent particles (18, 19).

Agglomerated particles have been made from metal oxides and fine superabsorbent particles (20) and also from clays and fine superabsorbent particles (21, 22).

Water-agglomerated superabsorbent fine particles dissociate upon contact or swelling with an aqueous solution. This results in a concentration of swollen free fine particles that will contribute to an increased gel blocking.

Biodegradability issues have been gaining importance. It has been proposed to reduce the SAP content in hygiene articles. However, this strategy does not necessarily involve a SAP optimization (8).

As alternatives, absorbent compositions made from biodegradable and renewable feedstocks have been proposed (23). The use of starch as an additive for superabsorbent polymers has been proposed (24, 25). Examples of additives to improve the performance of SAP formulations are shown in Table 6.2.

Table 6.2 Additives for superabsorbent polymers (8).

Compound	Compound
Bentonite	Zeolite
Celite	Gypsum
Smectite	Hectorite
Montmorillonites	Laponite®
Illite	Magnesium silicate

A discrete composite particle can be formed by making a melt. This includes combining the starch component and the inert inorganic components, cf. Table 6.2, in an extruder and extruding the melt from the extruder. The agglomeration is done by pressure agglomeration, tumble growth agglomeration, or by matrix melt formation (8).

6.4 Laser Additive Manufacturing of High Performance Materials

A monograph is available about laser additive manufacturing of high performance materials (26). It covers the specific aspects of laser additive manufacturing of high performance new materials components based on unconventional materials. Incremental manufacturing philosophy, materials design and preparation, process control and optimization, and the theories of physical and chemical metallurgy have been reviewed. The capabilities of the development of metallic materials components by laser additive manufacturing process are described, including nanostructured materials, *in-situ* composite materials, and particle reinforced metal matrix composites.

A comprehensive analysis of the literature pertaining to surface texture metrology for metal additive manufacturing has been performed (27). The review addresses specific areas of interest: Industrial domain, additive manufacturing processes and materials, types of surface investigated, surface measurement technology and surface texture characterization.

Possible optimizations of the methods are suggested and the areas that may have significant potential for future research are highlighted (27).

6.4.1 Laser Metal Deposition Additive Manufacturing

Laser metal deposition additive manufacturing was used to deposit Inconel 625 matrix composites reinforced with nano TiC particles (28, 29). The effects of laser energy input per unit length on the densification level, microstructural features, mircohardness, and wear property were investigated.

The relatively low laser energy input induced insufficient liquid with higher viscosity, thus inhibiting the melted liquid from spreading out smoothly. As a result, a large number of micropores and reduced densification level of laser metal deposition-processed parts were obtained. A laser energy input of 100 $kJ\,m^{-1}$ properly settled. The obtainable densification level generally approached 98.8%. The TiC reinforcements experienced successive microstructural changes

from agglomeration to uniform distribution with coarsening grain, as the applied laser energy increased (28).

An *in-situ* TiO_2 reinforced Ti−Ni composite coating on carbon steel was successfully prepared by laser metal deposition using Ti−Ni as-mixed powder in an atomic ratio of 60:40 (30). With the aim of the *in-situ* reaction design during the laser metal deposition processing, a trace of oxygen mixed with the shielding gas was introduced.

TiO_2 particles with a unique flower-like structure were formed when the applied laser energy was 96 $kJ\,m^{-1}$, while the apparent oxidation of grain boundaries was observed when the energy increased to 120 $kJ\,m^{-1}$.

At the optimized laser energy of 96 $kJ\,m^{-1}$, the laser metal deposition-processed layer showed the highest densification degree and was free of any pores and cracks. Also, a relatively high microhardness and significantly improved tribological properties were found (30).

6.4.2 Hybrid Processes

Laser melting deposition and selective laser melting are two major metal additive manufacturing technologies that explore the near-net shaping of large components and net shaping of small complex structures (31). In order to achieve subscale complex structures, laser melting deposition and selective laser melting hybrid manufacturing processes have been proposed. Ti_6Al_4V is an α-β dual phase moderate strength titanium alloy that is widely used in the fields of medicine, aeronautics, and astronautics.

Thin horizontal, vertical selective laser melting plates and rolled plates of 1.5–2.5 *mm* have been used as substrate materials for a laser melting deposition process to analyze the tensile properties, microhardness, microstructure, and internal defects.

The results showed that the laser melting deposition process forms a hybrid with the aforementioned plates. The relative density of hybrid-forming area can reach 99.5%, because of the existence of the pores with diameter $< 20\ \mu m$. The tensile strength and the elongation of the hybrid produced in this way can reach 918 *MPa* and 11%, respectively. Fractures are located in the laser melting deposition zone. An internal layer fracture of the laser melting

deposition zone increases the elongation, whereas a layer interface fracture decreases it.

The laser deposition process epitaxially generates coarse columnar crystals, and laser remelting reduces the microhardness of the selective laser melting substrate in the 2 *mm* to 3 *mm* thick grain increased heat affected zone (31).

6.5 High Temperature Cooling Application

Capric and lauric acid mixtures with organic additives were tested and screened for cold storage in high temperature cooling application (32). The organic additives are listed in Table 6.3.

Table 6.3 Organic additives for cold storage (32).

Compound	Phase change temperature/[°C]	Density /[$kg\,m^{-3}$]
Caproic acid	−3.4	926
Ethyl benzoate	−34.6	1044
Methyl salicylate	−8.3	1180
Oleic acid	16.3	870
Tetradecane	6	762.8
Hexadecane	18.17	770.1

The phase transition behavior and heat transfer characteristics of a fabricated cold storage ball filled with the self-developed phase change material were investigated.

It was shown that the capric and lauric acid eutectic mixture in the presence of oleic acid offered an appropriate phase change temperature of 14.97°C and a high latent heat of transition of 115.1 $kJ\,kg^{-1}$. The charging and discharging time of the cold storage ball were 340 *min* and 230 *min* with a charging and discharging capacity of 113,291 $kJ\,m^{-3}$ and 106,844 $kJ\,m^{-3}$, respectively. The charging time can be reduced either by decreasing the heat transfer fluid temperature, the diameter and thickness of the spherical shell, or by increasing the thermal conductivity of the spherical shell (32).

Tradenames appearing in the references are shown in Table 6.4.

Table 6.4 Tradenames in References.

Tradename Description	Supplier
Aquastore® Copolymer of acrylamide and sodium acrylate (17)	Kemira Oyj Public Limited
Carnation® White mineral oil (22)	Sonneborn Refined Products
Drytech® 2035 Superabsorbent material (22)	Dow Chemical Comp.
Ethenier™ -F-UHV Lignocellulosic pulp (17)	Rayonier, Performance Fibers
Favor® 953 Crosslinked, partially neutralized sodium poly(acrylate) (12)	Stockhausen GmbH
Flexan® (Series) Poly(styrene sulfonate) (22)	National Starch
Lexan® Poly(carbonate) (22)	General Electric
Plexiglas® Poly(methyl methacrylate) (22)	Rohm & Haas
Premium WT-200 bentonite Bentonite (8)	Bentonite Performance Minerals
Rayfloc® -J Lignocellulosic pulp (17)	Rayonier, Performance Fibers
Readco® Mixer (13)	Readco Industries Inc.
Sulfatate™ -H-J Lignocellulosic pulp (17)	Rayonier, Performance Fibers
Superfloc® A-110 Poly(acrylamide) copolymer (17)	Cytec Industries
Tween® 20 Sorbitan monolaurate (22)	Uniqema
World's Best® Cat Litter Ground grain (13)	Grain Processing Corp.

References

1. Anonymous, *Anti-Corrosion Methods and Materials*, Vol. 52, 2005.
2. Anonymous, *Focus on Powder Coatings*, Vol. 2005, p. 6, 2005.
3. Cabot, Powder coatings, 2014.
4. J.A. Trogolo and E.K. Welch, II, Antimicrobial powder coatings and method, US Patent 8 063 116, assigned to Sciessent LLC (Wakefield, MA), November 22, 2011.
5. R.J. Churhill, E.C. Aquino, R. Orwoll, R. Kiefer, and H.P. Groger, Nanostructured additives to high-performance polymers for use in radiation shielding, protection against atomic oxygen and in structural applications, US Patent Application 20 130 161 564, assigned to International Scientific Technologies, Inc., Dublin (VA), June 27, 2013.
6. J.-L. Bridot, A.-C. Faure, S. Laurent, C. Rivière, C. Billotey, B. Hiba, M. Janier, V. Josserand, J.-L. Coll, L.V. Elst, R. Muller, S. Roux, P. Perriat, and O. Tillement, *Journal of the American Chemical Society*, Vol. 129, p. 5076, 2007.
7. H.K. Barnes, R.F. Cook, C.H. Everhart, A.L. McCormack, F.R. Radwanski, P.M. Rosch, and A.J. Trevisan, Hydraulically needled nonwoven pulp fiber web, US Patent 5 137 600, assigned to Kimberley-Clark Corporation (Neenah, WI), August 11, 1992.
8. S. Chevigny, S. Dong, A.-C. Couffin-Hoarau, I. Bolduc, M. Berrada, and C. Thibodeau, Polysaccharide-inorganic composite particles as performance additives for super-absorbent polymers, US Patent 8 563 466, assigned to Archer Daniels Midland Company (Decatur, IL), October 22, 2013.
9. R.W. Schone, Bentonite as odor control material, US Patent 6 175 055, assigned to The Procter & Gamble Company (Cincinnati, OH), January 16, 2001.
10. M. Guarracino and A. Gagliardini, Absorbent articles having an odor control system consisting of absorbent gelling material and silica, US Patent 6 225 524, assigned to The Procter & Gamble Company (Cincinnati, OH), May 1, 2001.
11. H. Brehm, Process for the agglomeration of water-swellable polymers by means of sinter granulation, US Patent 5 248 709, assigned to Chemische Fabrik Stockhausen GmbH (Krefeld, DE), September 28, 1993.
12. H. Klimmek, U. Gunther, and H. Bruggemann, Polymer composition, absorbent composition, their production and use, US Patent 5 847 031, assigned to Chemische Fabrik Stockhausen GmbH (DE), December 8, 1998.
13. V.Y. Wong, L.E. Small, A.M. Ward, and R.J. Sackenheim, Absorbent composition and extended use pet litter, US Patent 7 475 655, assigned to The Iams Company (Dayton, OH), January 13, 2009.

14. D.C. Roe, Absorbent structures containing specific particle size distributions of superabsorbent hydrogel-forming materials mixed with inorganic powders, US Patent 5 419 956, assigned to The Procter & Gamble Company (Cincinnati, OH), May 30, 1995.
15. I. Hiroki, N. Ishikawa, N. Ohba, S. Mukaida, T. Mori, and K. Tanaka, Deodorant resin composition and process for production thereof, US Patent 5 980 879, assigned to Uni-Charm Corporation (Ehima, JP), November 9, 1999.
16. T. Kobayashi, Y. Nakano, Z. Meiwa, M. Nakanishi, and T. Matsui, Absorbent composite, US Patent 5 489 469, assigned to Kao Corporation (Tokyo, JP), February 6, 1996.
17. K.D. Sears, Lignocellulose fiber composite with soil conditioners, US Patent 6 855 182, assigned to Rayonier Products and Financial Services Company (Fernandina Beach, FL), February 15, 2005.
18. S. Obayashi, M. Nakamura, T. Yamamoto, H. Tanaka, Y. Sakamoto, and Y. Shimada, Process for granulating a water-absorbent resin employing (a) water (b) inorganic powder & (c) surfactant in an inert solvent, US Patent 4 732 968, assigned to Seitetsu Kagaku Co., Ltd. (Hyogo, JP), March 22, 1988.
19. G.T. Woodrum, Pellets of clay and superabsorbent polymer, US Patent 4 914 066, assigned to Hoechst Celanese Corporation (Somerville, NJ), April 3, 1990.
20. H. Takai, T. Yuki, S. Mukaida, D. Tagawa, K. Tanaka, K. Tanaka, S. Tamabuchi, and Y. Iwasaki, Absorbent compositions, methods for producing thereof and absorbent products, US Patent 6 284 362, assigned to Sanyo Chemical Industries, Ltd. (Kyoto, JP), September 4, 2001.
21. C.J. Berg, F.H. Lahrman, and D.C. Roe, Particulate, absorbent, polymeric compositions containing interparticle crosslinked aggregates, US Patent 5 300 565, assigned to The Procter & Gamble Company (Cincinnati, OH), April 5, 1994.
22. W.G. Reeves, E.C. Damay, W.L. Hamilton, P.A. Hansen, J.N. Lindon, and H.A. Sorebo, Superabsorbent-containing composites, US Patent 6 387 495, assigned to Kimberly-Clark Worldwide, Inc. (Neenah, WI), May 14, 2002.
23. M. Berrada, S. Chevigny, and C. Thibodeau, Polysaccharide phyllosilicate absorbent or superabsorbent nanocomposite materials, CA Patent 2 483 049, assigned to Le Groupe Lysac Inc., September 10, 2013.
24. W.R. Spence, High absorption body powder, US Patent 4 272 514, assigned to Spenco Medical Corporation (Waco, TX), June 9, 1981.
25. E. Richman and M.A. Thorn, Absorbent composition of matter, process for preparing same and article prepared therefrom, US Patent 4 454 055, assigned to National Starch and Chemical Corporation (Bridgewater, NJ), June 12, 1984.

26. D. Gu, *Laser Additive Manufacturing of High-Performance Materials*, Springer, Berlin, 2015.
27. A. Townsend, N. Senin, L. Blunt, R.K. Leach, and J.S. Taylor, *Precision Engineering*, 2016. in press.
28. S. Cao and D. Gu, *Journal of Materials Research*, Vol. 30, p. 3616, 2015.
29. D. Dai, W. Chen, and H. Chen, *Journal of Manufacturing Science and Engineering*, Vol. 138, p. 1, 2016.
30. C. Ma, D. Gu, C. Hong, B. He, K. Chang, and Q. Shi, *Surface and Coatings Technology*, Vol. 291, p. 43, 2016.
31. Q. Liu, Y. Wang, H. Zheng, K. Tang, L. Ding, H. Li, and S. Gong, *Materials Science and Engineering: A*, Vol. 660, p. 24, 2016.
32. X.L. Wang, X.Q. Zhai, T. Wang, H.X. Wang, and Y.L. Yin, *Applied Thermal Engineering*, Vol. 58, p. 252, 2013.

Additives for High Performance Applications: Chemistry and Applications. Johannes Karl Fink.
2017 Scrivener Publishing LLC. Published 2017 by John Wiley & Sons, Inc.

Also of Interest

Check out these other books by the author published by Scrivener Publishing

Metallized and Magnetic Polymers
By Johannes Karl Fink
Published 2016. ISBN 9781119242321

Marine, Waterborne, and Water-Resistant Polymers
Chemistry and Applications
By Johannes Karl Fink
Published 2015. ISBN 978-1-119-018486-7

The Chemistry of Printing Inks and Their Electronics and Medical Applications
By Johannes Karl Fink
Published 2015. ISBN 978-1-119-04130-6

The Chemistry of Bio-based Polymers
By Johannes Karl Fink
Published 2014. ISBN 978-1-118-83725-2

Polymeric Sensors and Actuators
By Johannes Karl Fink
Published 2012. ISBN 978-1-118-41408-8

Handbook of Engineering and Specialty Thermoplastics
Part 1: Polyolefins and Styrenics
By Johannes Karl Fink
Published 2010. ISBN 978-0-470-62483-5

Handbook of Engineering and Specialty Thermoplastics
Part 2: Water Soluble Polymers
By Johannes Karl Fink
Published 2011. ISBN 978-1-118-06275-3

A Concise Introduction to Additives for Thermoplastic Polymers
by Johannes Karl Fink.
Published 2010. ISBN 978-0-470-60955-2

Additives for High Performance Applications: Chemistry and Applications. Johannes Karl Fink.
2017 Scrivener Publishing LLC. Published 2017 by John Wiley & Sons, Inc.

Index

Tradenames

Acronyms

Chemicals

Boldface numbers refer to Figures

General Index